Surface functionalization of heterogeneous gold / silica substrates for the selective anchoring of biomolecules and colloids onto LSPR biosensors

Francisco Palazon

ÉCOLE CENTRALELYON

N° ordre : 2014-21

Thèse de l'Université de Lyon

délivrée par l'École Centrale de Lyon

soutenue publiquement le 18 septembre 2014
par

M. Francisco PALAZON

préparée à l'Institut des Nanotechnologies de Lyon (INL)

Titre :

Fonctionnalisation de surfaces hétérogènes or/silice pour l'ancrage sélectif de biomolécules et colloïdes sur biocapteurs LSPR

-

Surface functionalization of heterogeneous gold/silica substrates for the selective anchoring of biomolecules and colloids onto LSPR biosensors

École Doctorale Matériaux de Lyon

Composition du jury :

M. Didier LÉONARD, en qualité de président
M. Michael CANVA, en qualité d'examinateur
Mme. Éliane SOUTEYRAND, en qualité d'examinatrice
M. Stéphane COLLIN, en qualité d'examinateur
M. Luc VELLUTINI, en qualité de rapporteur
M. Giacomo CECCONE, en qualité de rapporteur
M. Yann CHEVOLOT, en qualité de co-directeur
M. Jean-Pierre CLOAREC, en qualité de directeur

Para Elisa.

Acknowledgements

First of all, I would like to thank all the committee members for their time and consideration, especially Dr. Luc Vellutini and Dr. Giacomo Ceccone for the evaluation of this dissertation.

Second, the French ministry of higher education and research (Ministère de l'enseignement supérieur et de la recherche) and the French national research agency (ANR) are greatly acknowledged for financial support : the former for employing me through Ecole Centrale de Lyon and the latter for funding Piranex Project (ANR P2N, ANR-12-NANO-0016).

Third, I thank Dr. Catherine Bru-Chevallier and Dr. Christian Seassal, director and vice director of Institut des Nanotechnologies de Lyon, as well as Éliane Souteyrand, director of the Chemistry and Nanobiotechnology group. I also thank Dr. Jean-Yves Buffière, director of École Doctorale Matériaux de Lyon.

Fourth, I thank my PhD supervisors : Jean-Pierre Cloarec and Yann Chevolot. It has been a pleasure to work under their supervision. From the first day they have trusted me to make my own decisions while always being there when I have asked for guidance. Even when we could not be physically close, their prompt responses by e-mail or telephone have been remarkable.

Fifth, it has been a pleasure to work together with my colleagues at the chemistry and nanobiotechnology group and in a broader sense, all colleagues at Institut des Nanotechnologies de Lyon and Ecole Centrale de Lyon. Though I have obviously not had the same degree of collaboration with all of them, I will avoid giving names. The ones that have played a key role in the work that is presented in this manuscript know already who they are and how thankful I am for that.

Sixth, scientific collaborators from other laboratories have also played an important role in the work presented hereafter. Among them I would like to thank Michael Canva and all Piranex project partners at LCFIO, IEF, CSPBAT, AgroParisTech and Horiba ; Didier Léonard and Thierry Le Mogne from ISA and LTDS respectively for ToF-SIMS and XPS analysis and Céline Chevalier from UMI-LN2 for providing nano-antenna arrays.

Seventh, I thank all my friends and family for their support, kindness, friendship and love.

Last but most important, I thank my wife for every single moment I can spend with her.

Niño soy tan preguntero,
tan comilón del acervo,
que marchito si le pierdo
una contesta a mi pecho.
Si saber no es un derecho,
seguro será un izquierdo.

- Silvio Rodriguez, El Escaramujo -

Foreword : The invisible work

The main text of this manuscript presents a (hopefully logical and clear) synthesis of the *most relevant part* of the work conducted during the 3 years that I have spent as a PhD student. Upon reading (or quickly browsing through) these pages, one might get the impression that they are a direct reflection of the work and results obtained throughout this time.

Nothing could be further from the truth.

In making this synthesis I have picked only the work that I found most interesting. This filtering, made for the sake of presenting a "clear story", intentionally ignores many months of work devoted to alternative ideas or side-projects which ended up in a lack of significant results.

If you are interested in knowing about "all the things that did not work (well enough)", I invite you to read appendix D.

Contents

Introduction Générale

Le développement actuel des nanotechnologies implique de plus en plus des surfaces nanostructurées avec différents matériaux. Les biocapteurs plasmoniques, notamment, longtemps basés sur l'exaltation de plasmons de surface (SPR, de l'anglais Surface Plasmon Resonance) propagatifs sur une couche mince métallique approchent leur limite de sensibilité[1] qui reste en deça des performances nécessaires pour certaines applications (détection de traces de contaminants ou marqueurs biologiques). De ce fait, ces capteurs sont en train de connaître actuellement le passage d'une structuration 1D (couche mince continue ; « SPR classique ») à des structurations 2D et 3D avec des « points chauds » nanométriques provenant de l'excitation de plasmons localisées (LSPR ; voir Fig. 1).

Si ces nanostructures semblent prometteuses pour une transduction localisée et davantage exaltée, une telle architecture n'a de sens que si les biomolécules ciblées sont effectivement localisées sur ces « points chauds ». En effet, toute molécule adsorbée ailleurs sur la surface ne contribue pas au signal et donc représente une baisse de sensibilité effective du capteur (voir Fig. 2).

Parallèlement, la synthèse de nano-objets colloïdaux de différentes géométries (sphères, bâtonnets, tubes) et matériaux (organique, semi-conducteur, métallique, hybrides) est très prometteuse tant ces nano-objets ont démontré des propriétés physico-chimiques intéressantes (par exemple : supraconductivité des nanotubes de carbone ou superparamagnétisme et fonctionnalités de surface des latex magnétiques). Cependant, encore une fois, l'intégration de ces nano-objets dans des systèmes complexes nécessite souvent de les placer à des endroits précis d'une surface nano-structurée (eg : nanotube conducteur placé entre deux microélectrodes ou particule fluorescente placé sur nano-antenne) (voir Fig. 3).

Ces deux exemples (biocapteurs plasmoniques et placement de nano-objets colloïdaux) montrent que la localisation précise de « cibles » (allant de la petite molécule -quelques nm- à la particule colloïdale -jusqu'à quelques microns-) provenant d'une phase continue complexe (milieu biologique, dispersion colloïdale) vers des zones nanométriques prédéfinies sur un substrat plan hétérogène représente un défi majeur dans l'évolution des nanotechnologies. S'il existe différentes méthodes pour répondre à ce défi, notamment pour les « gros » objets colloïdaux (méthodes physiques telles que l'assemblage par forces capillaires, diélectrophorèse ou pinces optiques entre autres), la fonctionnalisation chimique de surface apparaît comme une méthode spécialement adaptée qui peut par ailleurs se combiner aux méthodes « physiques » susdites. La fonctionnalisation chimique de surface consiste à modifier les groupements chimiques des différents matériaux présents à la surface pour permettre l'ancrage sélectif des « cibles » sur des zones spécifiques. [1] Cette modification peut se faire de différentes manières, que nous avons détaillées ailleurs :[2]

1. Le terme de « cible » dans le domaine des biocapteurs désigne en général une biomolécule à détecter qui vient intéragir avec une biomolécule « sonde » greffée à la surface. Nous faisons ici un usage plus général de ce terme, tel que c'est expliqué dans le texte.

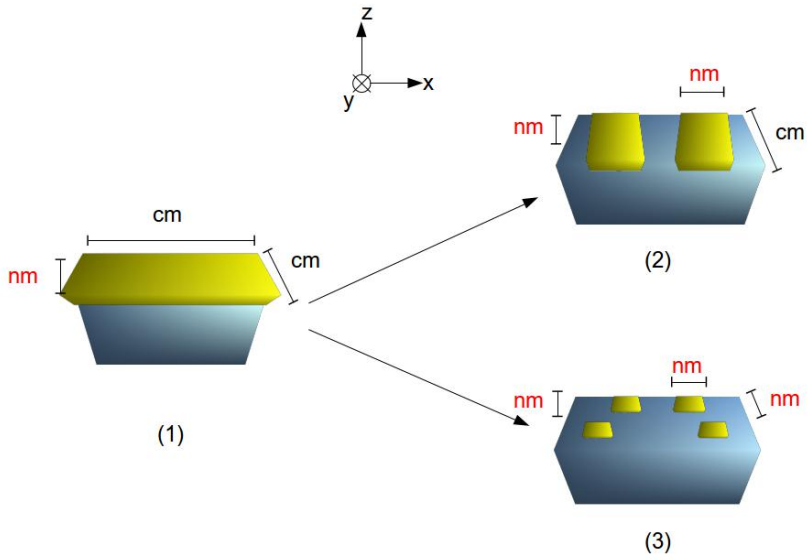

FIGURE 1 – Un capteur SPR classique (1) utilise une couche mince métallique continue, présentant des plasmons de surface. Ces plasmons sont des champs électriques évanescents dans la direction z et dont les caractéristiques varient avec les molécules présentes à la surface. Ceci explique leur utilisation comme transducteur dans les biocapteurs. Les plasmons de surface sont propagatifs dans les directions x et y. Cette architecture a démontré son utilité dans les biocapteurs mais les limites théoriques de détection s'avèrent insuffisantes dans certaines applications. De ce fait, des structurations 2D (2) et 3D (3) sont développées pour permettre l'exaltation de plasmons localisés qui permettent à priori une sensibilité accrue.

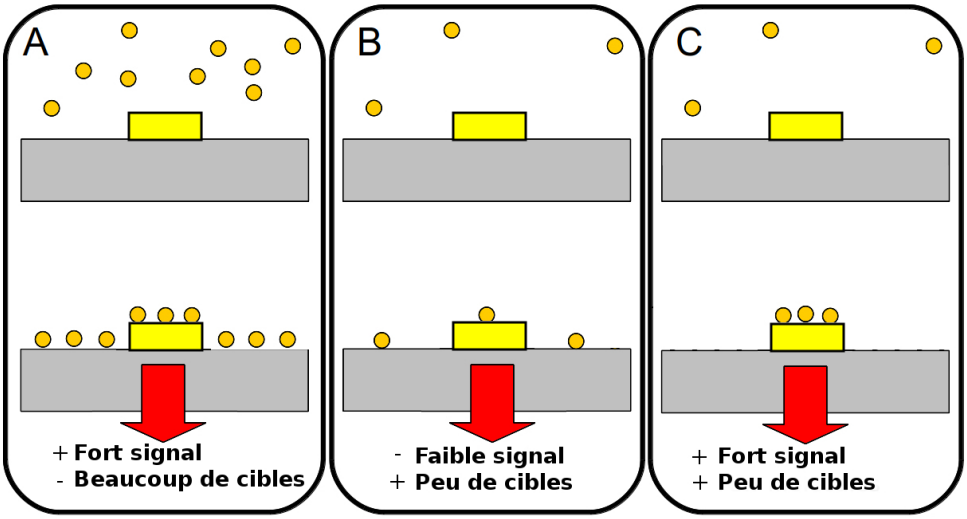

FIGURE 2 – Schéma d'une surface nanostructurée où la transduction n'a lieu que sur la nanostructure. Si les cibles ne se fixent pas de manière spécifique sur la nanostructure, le signal est proportionnel au nombre total de cibles (cas A et B). Par contre, si les cibles sont dirigées vers la nanostructure, la sensibilité est accrue.

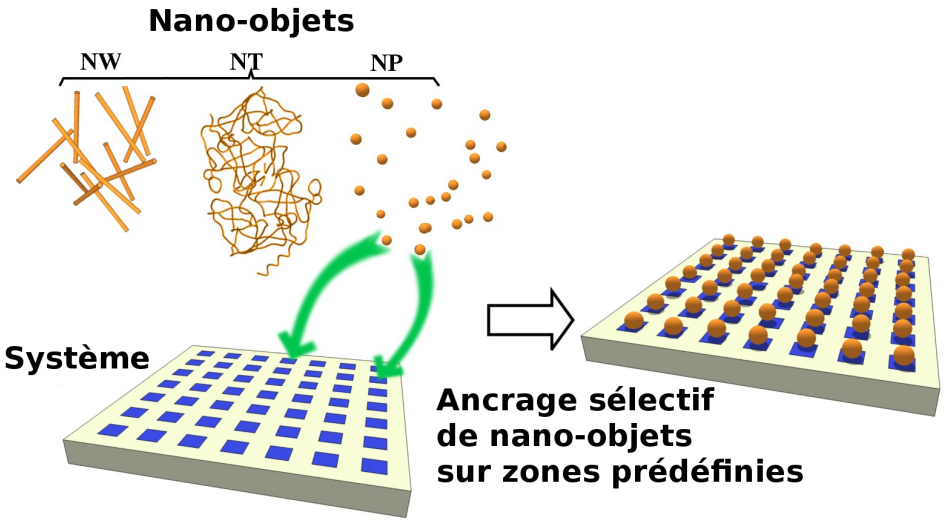

FIGURE 3 – Localisation de nano-objets colloïdaux sur un système ayant une surface nano-structurée.[2]

1. En utilisant directement les groupements chimiques disponibles en surface (ex : silanols sur une surface de silice), modifiés par le biais d'un flux d'électrons ou d'ions par exemple.[3]
2. En adsorbant différents polymères ou autres macromolécules (« fonctionnalisation 3D »).[4–6]
3. En greffant de manière covalente des -petites- molécules dont une extrémité se lie au substrat et l'autre peut être choisie pour fixer ou repousser sélectivement une cible. Ces molécules peuvent recouvrir plus ou moins la surface et acquérir une organisation plus ou moins cristalline par interactions de Van der Waals entre les chaînes adjacentes. Dans certains cas (par exemple, alkylthiols sur Au(111) monocristallin) ces molécules forment une monocouche auto-assemblée (SAM, de l'anglais Self-Assembled Monolayer) avec une organisation pseudo-cristalline bien définie. [2]

Cette troisième méthode présente certains avantages par rapport aux deux autres en termes de :

- Versatilité : l'extrémité disponible ou fonctionnelle peut être choisie parmi un grand nombre de groupements chimiques (théoriquement infini), contrairement à la première méthode qui est très limitée aux possibilités du substrat.
- Taille : Pour des applications biocapteurs à ondes évanescentes notamment, il peut être intéressant de limiter l'épaisseur de la couche d'accroche afin que la biomolécule à détecter soit au plus près de la surface métallique, c'est à dire du maximum de champ électrique. De ce fait une monocouche moléculaire de quelques nanomètres peut être préférable à l'emploi de polymères ou autres macromolécules de quelques dizaines de nanomètres.

2. Le terme de SAM est souvent employé et pourra l'être dans le cours de ce manuscrit par simplicité ou abus de langage pour d'autres systèmes où les molécules ne forment pas forcément une monocouche et les degrès d'auto-assemblage sont probablement moindres (par exemple, poly(ethyelene glycol)-trialkoxysilanes sur silice amorphe). En outre, la relation entre l'organisation de la couche organique et sa réactivité est un sujet de recherche complexe. Nous ne l'aborderons pas en détail ici mais il convient de signaler que le cas « idéal » de la monocouche auto-assemblée parfaitement cristalline ne semble pas être forcément optimum pour la réactivité globale de la surface.

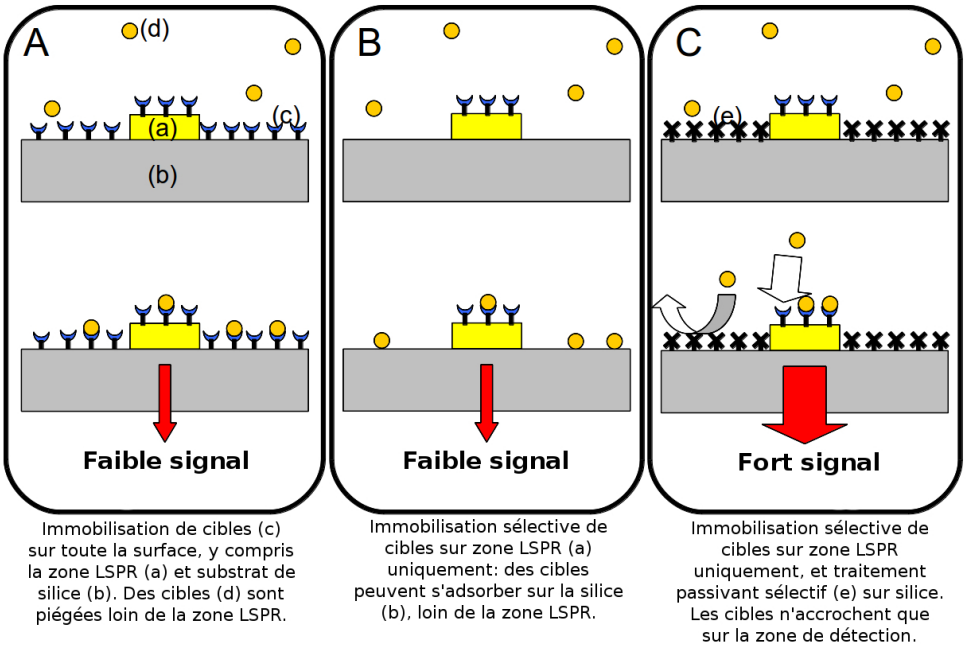

FIGURE 4 – Schéma montrant comment la fonctionnalisation chimique orthogonale peut permettre la localisation de cibles et ainsi accroître la sensibilité d'un biocapteur plasmonique (signal accru à nombre de molécules constant).

– Séléctivité : Par rapport à l'adsorption plus ou moins spécifique de polymères, le greffage covalent de certains groupements chimiques sur des surfaces avec lesquelles ils ont une grande affinité (par exemple : thiols sur or ou silanes sur silice) assure une meilleure sélectivité de la fonctionnalisation

Nous avons choisi d'utiliser le greffage covalent de petites molécules (quelques nanomètres) avec une terminaison fonctionnelle pour le ciblage précis de biomolécules et colloïdes sur des zones prédéfinies d'un substrat hétérogène. Sauf mention contraire, dans la suite de ce travail, les termes « fonctionnalisation », « fonctionnalisation de surface » ou « fonctionnalisation chimique de surface » feront référence à la modification d'une surface par le greffage covalent de petites molécules. Comme expliqué précedemment, par simplicité et à défaut d'un meilleur terme nous parlerons alors de la formation d'une *SAM*, bien qu'il soit important de garder à l'esprit que les couches organiques ainsi formées ne soient ni forcément complètes (remplissage sub-monocouche) ou uniques (multi-couches) ni forcément cristallines (orientation des chaînes adjacentes plus ou moins déterminée).

Une fonctionnalisation orthogonale des différents matériaux, c'est à dire l'élaboration de deux SAMs complémentaires, l'une assurant l'ancrage des cibles sur un des matériaux et l'autre repoussant celles-ci de la surface environnante, permet ce ciblage précis qui peut être utilisé pour améliorer effectivement la sensibilité d'un biocapteur plasmonique (voir Fig 4) ou pour le placement de nano-objets sur un microsystème (voir Fig. 3). Ce travail se concentre sur des surfaces hétérogènes or/silice, notamment des micro et nanostructures d'or sur un substrat de silice (ou verre). Ce choix de matériaux correspond à la vaste majorité des transducteurs plasmoniques. Il est cependant envisageable d'étendre ce travail à d'autres matériaux, notamment d'autres couples métal / oxyde.

Ce manuscrit présente d'abord un état de l'art sur le sujet traitant d'une manière générale la question du ciblage sur surfaces planes hétérogènes par voies physiques et chimiques, puis plus précisément des fonctionnalisations d'or, de silice et de surfaces mixtes or/silice, avec une emphase particulière sur les méthodes de caractérisation chimique. Ensuite, l'ensemble des matériels et méthodes utilisés ont été regroupées dans un deuxième chapitre où le lecteur pourra trouver précisément toutes les informations pour reproduire les résultats présentés dans le chapitre suivant. Ces résultats traiteront à la fois des questions plus fondamentales de fonctionnalisation de surface sur or, sur silice et sur surfaces mixtes ainsi que des applications au placement de colloïdes et à la détection de biomolécules. Enfin, une conclusion générale permettra de faire la synthèse de ces résultats et de les replacer dans le contexte scientifique et technologique actuel pour proposer différentes évolutions possibles.

General Introduction

The current evolution of nanotechnology stresses the importance of patterned surfaces with different materials. Plasmonic biosensors for instance, long based on the resonant excitation of surface plasmons (SPR) of a continuous metallic thin film are approaching their theoretical limits of detection[1] which remain too high for some practical applications. Thus, such sensors are turning from a 1D structuration (homogeneous thin film ; "classic SPR") to different 2D and 3D patternings with nanometric "hot spots" emerging from the excitation of localized surface plasmons (LSRP ; see Fig. 5).

However, in order to take full advantage of such nanopatterned transducers, it is crucial to selectively place the target biomolecules onto the different "hot spots". Otherwise, any target molecule adsorbed elsewhere will not contribute to the final signal and will thus skew the overall sensitivity of the biosensor (see Fig. 6).

Simultaneously, nanofabrication has evolved into the synthesis of colloidal nano-objects with different geometries (spheres, rods, tubes) and materials (organic, semi-conducting, metallic, hybrid). These nano-objects are very promising for their unprecedented physico-chemical properties (e.g : supraconductivity of carbon nanotubes -CNTs- or superparamagnetism and surface functionalities of magnetic latexes). However, again, the integration of such nano-objects onto complex systems implies their precise placement onto a patterned surface (e.g : nanotube bridging two microelectrodes or fluorescent bead onto a plasmonic nano-antenna) (see Fig. 7).

These two examples (LSPR biosensors and localization of colloidal nano-objects) show how the precise placement of "targets" (going from small molecules -few nanometers- to colloïds -up to few microns-) coming from a complex phase (biological medium, colloidal dispersion) onto predefined nanometric regions of a heterogeneous planar substrate constitutes a major challenge on the evolution of nanotechnology. There are different methods to answer this challenge, specially for the *bigger* colloidal objects (physical methods such as capillary force assembly, dielectrophoresis or optical tweezers can be used). Nonetheless, surface chemical functionalization (which can be used in conjunction with the aforementioned physical methods) appears as a specially appropriate manner to overcome this technological bottleneck. Surface chemical functionalization consists in modifying the chemical surface groups of different materials to allow the selective binding of "targets" onto specific regions. [3] Such modification can be done in several ways that we have detailed elsewhere :[2]

1. Chemical groups present at the surface (e.g : silanols on a silica surface) can be readily modified by an electron or ion beam.[3]

3. The term "target" is used in the field of biosensors to designate at biomolecule that needs to be detected, this biomolecule interacting with a "probe" biomolecule grafted on the surface. We make a more general use of this term here, as explained in the text.

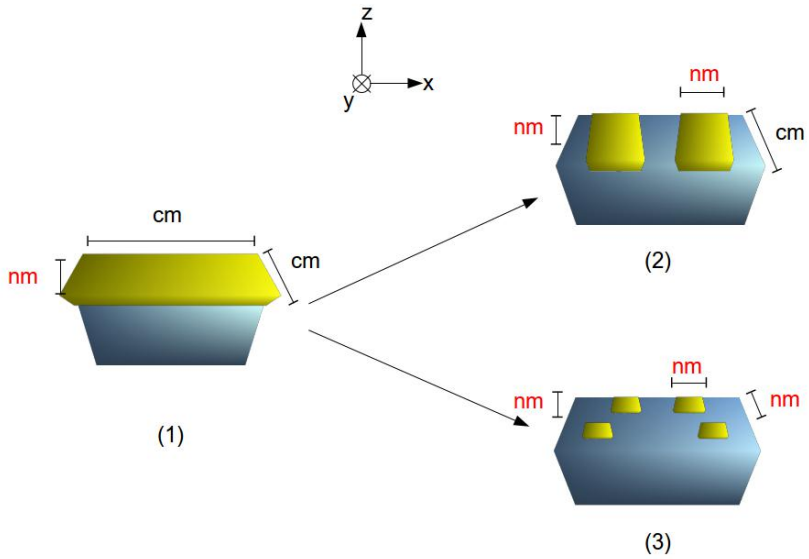

Figure 5 – A classic SPR sensor (1) uses a homogeneous thin metal layer supporting surface plasmons. These plasmons are intense electric fields, evanescent in the z direction, whose properties vary with the presence of molecules at the surface. This explain their use as a biosensor transducer. In this configuration plasmons are propagative waves in the x and y directions. Novel architectures present 2D (2) and 3D (3) patternings allowing the excitation of localized surface plasmons. These architectures should lead to an increase in sensitivity.

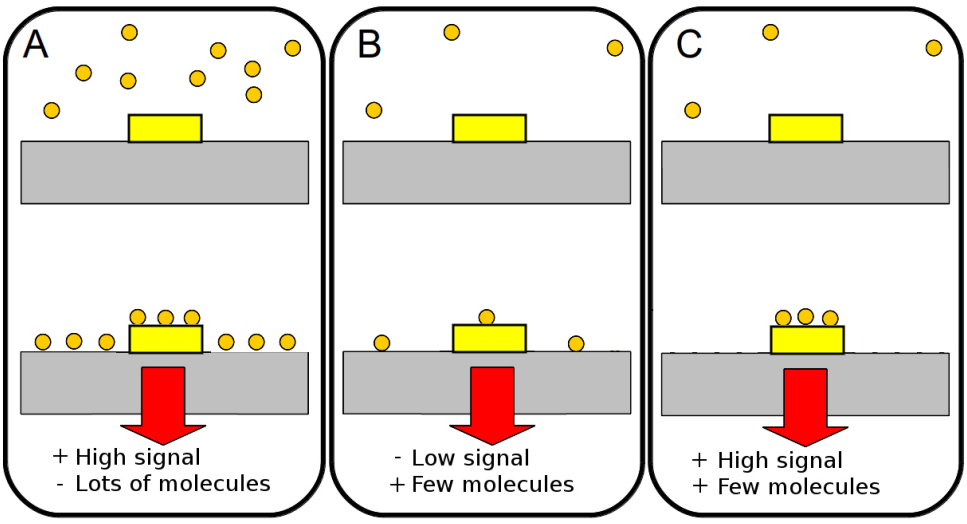

Figure 6 – Schematic representation of a nanopatterned surface where the transduction only happens on the yellow nanostructure. If the targets do not specifically bind onto the nanostructure the total signal is proportional to the amount of molecules (A and B). However, if the targets are made to bind only on top of the nanostructure, the sensibility is enhanced.

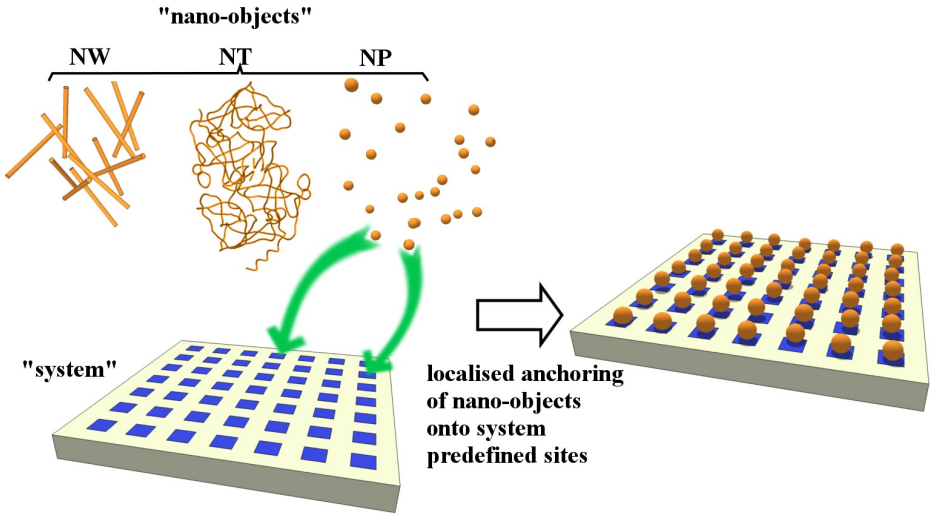

FIGURE 7 – Precise localization of colloidal nano-objets onto a nano-patterned surface.[2]

2. Polymers and other macromolecules can be adsorbed at the surface ("3D functionalization").[4–6]

3. Eventually, small molecules (ca. 1-2 nm) can be covalently grafted on the surface by one of their terminal headgroups, while using the available headgroup to allow specific coupling or repelling with the target. These molecules can form organic layers of different compacities and ordering on the surface. In some cases (e.g : alkylthiols on monocrystalline Au(111)) they adopt a well-defined crystalline structure and form a so-called Self-Assembled Monolayer (SAM). [4]

This third method has some advantages over the former, such as :

– Versatility : The available headgroup can be chosen among a wide range of chemical groups (theoretically infinite), as opposed to the first method which is limited to the substrate's intrinsic possibilities.
– Size : Specially for plasmonic biosensors, based on evanescent waves, it may be interesting to limit the thickness of the anchoring layer. Indeed, if the target molecule is located closer to the metallic surface, it will be in a position of higher field intensity and thus give a stronger signal. Therefore, a molecular monolayer of few nanometers may be preferable to the use of polymers and other macromolecules (tens of nanometers).
– Specificity : Covalent grafting through high affinity of different chemical groups towards different materials (eg : thiols on gold, silanes on silica) allow highly specific surface functionalization, whereas the adsorption of polymers may be highly non-specific leading to lower reproducibility on the final applications.

4. The word SAM is often used for simplicity's sake to refer to any "small" organic layer covalently bond onto a surface, disregarding the fact that the coverage may be sub-monolayer or multi-layer and have different degrees of ordering (eg : poly(ethylene glycol)-trialkoxysilanes on amourphous silica). Furthermore, the link between the organic layer structure and its' reactivity is a complex matter. We will not discuss it in detail but we should note that the "ideal" case of a perfectly crystalline SAM is not necessarily the optimum case for surface's reactivity.

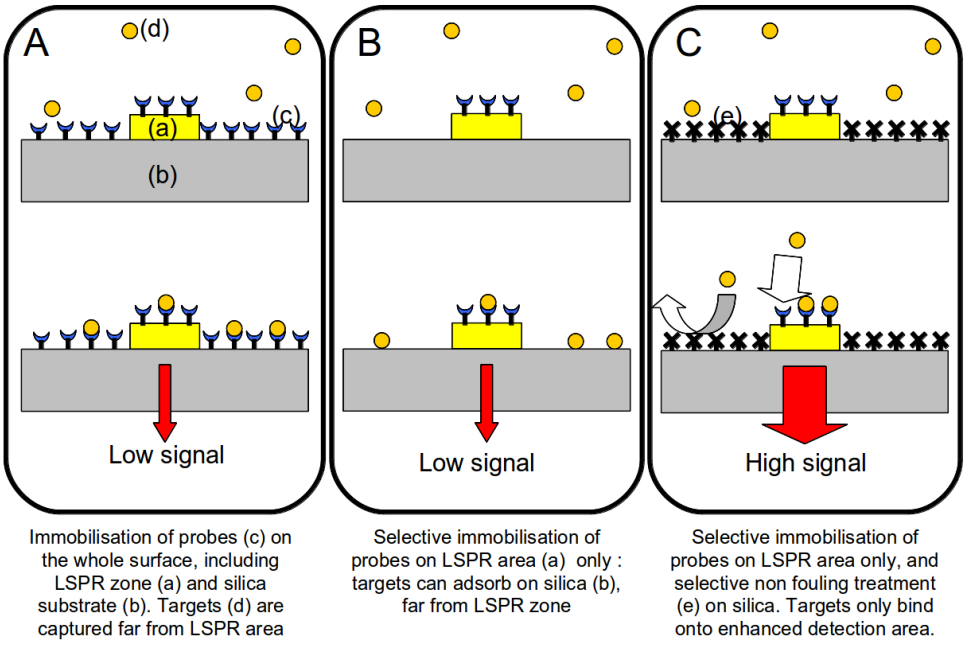

Figure 8 – Schematic representation of the use of orthogonal functionalizations to enhance the sensibility of a plasmonic biosensor (enhanced signal with constant number of molecules).

Given the above mentioned reasons, we have chosen to use the covalent bonding of small molecules (few nanometers) with a functional headgroup for the precise targeting of biomolecules and colloids onto predefined regions of a heterogeneous substrate. Unless otherwise specified, the words "functionalization", "surface functionalization" and/or "surface chemical functionalization" will refer to the modification of a surface by the covalent bonding of small organic molecules. As previously stated, for simplicity's sake we will talk about the formation of a *SAM*, though it is important to keep in mind that the so-formed organic layers may not represent an exact monolayer (sub-monolayer or multi-layer coverage) and may not be perfectly crystalline (orientation of adjacent chains more or less defined).
Orthogonal functionalizations, ie : the building of two complementary SAMs, one ensuring the anchoring of targets onto one material while the other repels them from the surrounding surface, allows a precise targeting on a heterogeneous substrate. This can be used to enhance the sensitivity of a plasmonic biosensor (see Fig. 8) or for the placement of nano-objects onto a microsystem (see Fig. 7).

The present work deals with heterogeneous gold/silica surfaces, namely gold micro and nanostructres on a silica (or glass) substrate. These materials correspond to the wide majority of plasmonic transducers. It is however possible to expand this work to other materials, specially other metal / oxide couples.
The first chapter of this manuscript presents the state of the art on the precise targeting of molecules and colloids through physical and chemical methods, followed by an in-depth presentation of gold and silica chemical functionalizations and applications of orthogonal functionalizations. Characterization methods are also highlighted. The second chapter presents in detail the materials and methods used during this PhD to obtain the results that are presented on the third chapter. These results deal first with rather fundamental studies of functionalization on gold, silica and mixed substrates, followed by different applications to the placement

of colloids and biomolecules detection. Eventually, a general conclusion is given to summarize the obtained results and place them in today's scientifical and technological context to suggest different possible evolutions.

References

[1] M. Piliarik and J. Homola. *Optics express*, 17,16505–16517 **(2009)**.

[2] F. Palazon, P. Rojo Romeo, A. Belarouci, C. Chevalier, H. Chamas, E. Souteyrand, A. Souifi, Y. Chevolot, and J.-P. Cloarec. Site-selective self-assembly of nano-objects on a planar substrate based on surface chemical functionalization. In C. Joachim, editor, *Advances in Atom and Single Molecule Machines*. Springer (in press) **(2014)**.

[3] M. Kolibal, M. Konecny, F. Ligmajer, D. Skoda, T. Vystavel, J. Zlamal, P. Varga, and T. Sikola. *ACS nano*, 6,10098–10106 **(2012)**.

[4] L. Feuz, P. Jönsson, M. P. Jonsson, and F. Höök. *ACS nano*, 4,2167–77 **(2010)**.

[5] K. Kumar, A. B. Dahlin, T. Sannomiya, S. Kaufmann, L. Isa, and E. Reimhult. *Nano letters*, 13,6122–6129 **(2013)**.

[6] L. Feuz, M. P. Jonsson, and F. Höök. *Nano letters*, 12,873–9 **(2012)**.

Liste of Tables

List of Figures

Glossary

Activation SAMs may have a functional headgroup that requires to be modified in order to react with a target. This process is called activation. In this manuscript, unless otherwise specified, activation refers to the derivatization of carboxylic acids into NHS-ester for subsequent covalent coupling with an amine to form an amide bond. 54

Biosensor Device that aims at detecting and possibly quantifying a biological entity (eg : biomolecule) present in an analyte solution. Biosensors can be roughly presented as the coupling of a *bioreceptor* ensuring the biochemical recognition of the target entity and a *transducer* translating this biochemical recognition into a measurable signal (eg : electronic tension). 24, 49, 53, 135

Characterization Determination of a sample's structural and/or physicochemical properties. Unless otherwise specified, refers to the properties of *surfaces* in this manuscript. x, 44–46, 51, 53, 54, 78, 84, 86, 94, 114

Functionalization Also referred to as *surface functionalization* or *surface chemical functionalization*. Functionalization is the process of modifying a surface to give it a specific *function*, such as to capture a given biomolecule. Functionalization may be performed in different ways. However, unless otherwise specified, we shall only refer to the covalent grafting of small linear molecules (ie : 1-2 nm long) on the surface. We will consider that these molecules form a so-called self-assembled monolayer (see corresponding glossary entry for more details). xxxv, 1, 11–13, 16, 22–25, 35–37, 42–44, 49–51, 53, 54, 80, 81, 86, 94, 114, 115, 117, 120, 121, 123, 138

Orthogonal (in *orthogonal functionalizations*). Selective functionalizations of two different materials of a heterogeneous substrate with two different SAMs. In this manuscript, it refers to the thiolation and silanization of patterned gold on silica substrates. Other uses in the literature may include the building of different SAMs on a homogeneous substrate (e.g., through micro-contact printing and back-filling). However, unless otherwise specified, we will refer only to heterogeneous substrates with material-selective functionalizations. xxxiv, xxxv, 114–117, 119, 120

Piranha Solution created by mixing sulfuric acid and oxygen peroxide in ratios around 7/3 (v/v). Widely used to remove organic contamination of surfaces. 81, 83, 94, 142

Self-assembled monolayer Pseudo-crystalline molecular arrangement arising from a self-assembly process of small organic molecules onto a solid surface. This term is often used for any thin (ie : few nm) organic layer covalently grafted onto a surface, disregarding the actual degree of ordering or surface coverage. xxxii, 1, 24, 44, 46, 49, 53

Substrate Solid surface onto which something is deposited. In this manuscript, this term refers to the surface onto which SAMs are formed. Thus, if we consider a silicon wafer with a deposited thin film of gold with a chromium interlayer, we shall speak about a *gold substrate* for the formation of an alkanethiolate SAM. This may depart from the *classical* microfabrication point-of-view which would consider the silicon wafer as the substrate in this case. xxxii, 1, 12, 13, 15, 16, 19, 21–24, 42, 49, 51, 53, 54, 80, 81, 86, 94, 98, 114, 117, 121, 123, 135, 136, 138

Target Colloidal object or single biomolecule that has to be specifically anchored at given regions (traps) of a surface. This may depart from the more restrictive *classical* biosensor point-of-view in which targets are biomolecules (e.g., antigen) which are recognized by other *probe* biomolecules (e.g., antibody). x, 1, 2, 22, 24, 29, 30, 53–55, 78, 86

Trap Specific predefined region of a solid surface where a target is expected to be anchored. These regions may differ from the surrounding surface by their topography and/or chemical composition. xxix, xxxii, xxxv, 2, 13–23, 53, 86, 87, 94, 121, 123, 125

Acronyms

AFM Atomic Force Microscopy. xi, 42, 47, 48, 54, 55, 78, 83, 84, 98, 154, 156

AUF 1H,1H,2H,2H-Perfluorodecanethiol. xxxv, 80, 82, 117, 119, 120

BOE Buffered Oxide Etch. 139

C-AFM Conductive Atomic Force Microscopy. 47

CFA Capillary Force Assembly. xxxii, 13, 14, 22

CFM Chemical Force Microscopy. 47, 156

CNT Carbon Nanotube. 12, 16

CTAB Cationic hexadecylTrimethyl Ammonium Bromide. 139

CV Cyclic Voltametry. 45

DCC N,N'-DiCyclohexylCarbodiimide. 99

DCE DiChloroEthane. 139

DCM DiChloroMethane. 35, 81–83, 115, 139, 143, 144

DEP Dielectrophoresis. 16, 17, 19

DIC Diisopropylcarbodiimide. 81, 83, 99, 103, 107

DLVO Derjaguin, Landau, Verwey, Overbeek. xi, xxxv, 12, 123, 145, 147

DMF DiMethylFormamide. 35

DMSO DiMethyl SulfOxide. 99

DNA DeoxyriboNucleic Acid. 49, 50, 99

DNQ DiazoNaphthoQuinone. 136, 138

EDC 1-Ethyl-3-(3-Dimethylaminopropyl)Carbodiimide hydrochloride. xxix, 33, 81, 83, 99, 103, 105

EG Ethylene Glycol. 37

EG3-COOH HS-$(CH_2)_{11}$-EG_3-COOH. 80

EG3-OME HS-$(CH_2)_{11}$-EG_3-OCH_3. 80

EG6-COOH HS-$(CH_2)_{11}$-EG_6-COOH. 81

EG6-OME HS-$(CH_2)_{11}$-EG_6-OCH_3. 80

EIS Electrochemical Impedance Spectroscopy. 45

ESCA Electron Spectroscopy for Chemical Analysis. 46

FTIR Fourier-Transform Infrared Spectrosocpy. xi, 84, 149, 150

GAE4E Glycolic Acid Ethoxylate 4-tert-butylphenyl Ether. 139

HMDS Hexamethyldisilazane. 140, 141, 143

HSQ Hydrogen SilsesQuioxane. 136, 138

IEF Institut d'Électronique Fondamentale. 142, 143

INL Institut des Nanotechnologies de Lyon. 84, 142, 143

IPA IsoproPAnol. 139, 143

IR Infrared. 45, 46, 48, 149

IRRAS Infrared Reflection Absorption Spectroscopy. 84, 149, 150

ISA Institut des Sciences Analytiques. 84, 117

LSPR Localized Surface Plasmon Resonance. 49–51, 54, 55, 123

LTDS Laboratoire de Tribologie et Dynamique des Surfaces. 84, 117

MFM Magnetic Force Microscopy. 47

MIBK Methyl isobutyl ketone. 136, 138, 143

MIF Metal-Ion Free. 143

MMA Methyl methacrylate. 143

MUA 11-mercapto-1-undecanoic acid. xxxiii–xxxv, 35, 49, 54, 80–82, 94, 98, 100, 103, 115–117, 120

MUAM 11-amino-undecanethiol hydrochloride. xxxiii, 80, 81, 87, 100, 121, 123

MU-BIOT HS-$(CH_2)_{11}$-NH-C(O)-Biotin. xxxiii, 54, 80, 81, 100, 121

MUOH 11-mercapto-1-undecanol. 35, 80, 81

MWCNT Multi-Wall Carbon Nanotube. 16

NHS *N*-hydroxysuccinimide. xxxiii, 1, 54, 81, 83, 94, 98, 99, 102–105, 107

NMP *N*-Methyl Pyrrolidone. 139

OEG Oligo(Ethylene Glycol). xxix, xxxiv, 29, 49, 107, 108, 110–112, 114

PBS Phosphate Buffered Saline. 86, 87, 99, 123, 148

PDMS Poly(dimethyl siloxane). 36

PEG Poly(Ethylene Glycol). xxxiv, 24, 29, 30, 34, 37, 42, 46, 49–51, 54, 81, 82, 94, 108, 111, 116, 117

PEG-SI 2-[methoxy(polyethyleneoxy)propyl]trimethoxysilane (MW=460 g/mol ; i.e., 6 ethyleneglycol units in average). xxxiv, xxxv, 54, 81, 82, 107, 115–117, 119, 120

PEM PhotoElastic Modulator. 84, 85, 150–152

PFM Piezoelectric Force Microscopy. 47

PLL Poly-L-Lysine. 50, 51

PM-IRRAS Polarization-Modulation InfraRed Reflection Absorbtion Spectroscopy. xi, xxxiii, xxxiv, 35, 46, 54, 78, 84, 99, 100, 103, 105, 108, 111, 113–115, 121, 149–151

PMMA Poly(methyl methacrylate). 94, 136, 138, 139, 142, 143

PMT PhotoMultiplier Tube. 88

POE Poly(OxyEthylene). 108

PTFE PolyTetraFluoroEthylene. 108

PVC Poly(Vinyl Chloride). 108

PVDF PolyVinyliDene Fluoride. 108

QCM Quartz Crystal Microbalance. 44, 143, 144

RIE Reactive Ion Etching. 94

RMS Root Mean Square. 98

RNA RiboNucleic Acid. 99

SAM Self-Assembled Monolayer. x, xxix, xxxii, xxxiii, 1, 2, 10, 24, 25, 29, 30, 33–39, 41–47, 49, 50, 54, 78, 81, 83, 84, 86, 94, 98–100, 103, 156

SEM Scanning Electron Microscopy. xi, xxxv, 51, 54, 55, 86, 87, 117, 121, 122, 125, 136, 157

SERS Surface-Enhanced Raman Spectroscopy. 46

SET Single Electron Transistor. 50

SIF Trichloro(1H,1H,2H,2H-perfluorooctyl)silane. xxxv, 54, 81, 82, 117, 120

SPR Surface Plasmon Resonance. 44, 51, 55

STEM Scanning Transmission Electron Microscope or Microscopy. 138

STM Scanning Tunnelling Microscopy. 47, 48

SWCNT Single-Wall Carbon Nanotube. 16

TASA Template-Assisted Self Assembly. 13

TERS Tip-Enhanced Raman Spectroscopy. 46–48

THF TetraHydroFuran. xxxiii, 35, 81, 83, 99, 103–107

TMAH TetraMethylAmmonium Hydroxide. 136, 138, 140, 143

TOF-SIMS Time-of-Flight Secondary Ion Mass Spectroscopy. xi, xxxiii, xxxv, 46, 48, 54, 55, 78, 84, 85, 99, 103, 105, 106, 114, 117, 120, 153

UDT Undecanethiol. 80, 81

UHV Ultrahigh Vacuum. 37, 42

UV Ultraviolet. 54, 94, 108, 117, 135, 136, 138, 143

XPS X-ray Photoelectron Spectroscopy. xi, xxix, xxxiii, xxxiv, 35, 45, 46, 48, 54, 55, 78, 80, 84–86, 94, 95, 97, 99, 107, 108, 110–115, 117, 120, 144, 152, 153

XRD X-Ray Diffraction. xi, 78, 83, 84, 98, 156, 157

YAG Yttrium Aluminium Garnet, $Y_3Al_5O_{12}$. 141

Chapter 1

State of the art

Résumé du Chapitre 1

Pour répondre à la problématique posée dans cette thèse, à savoir : *Comment positionner précisément un ensemble de biomolécules ou de colloïdes provenant d'un milieu complexe sur une pluralité de régions micro et nanométriques prédéfinies sur une surface ?* l'étude de la littérature apporte certaines réponses.

Tout d'abord, il existe des méthodes que nous pouvons qualifier de « méthodes physiques » telles que la diélectrophorèse, les pinces optiques ou magnétiques ou encore l'assemblage par forces capillaires. Ces méthodes peuvent être adaptées pour des particules relativement grandes (en général au dessus de quelques dizaines de nanomètres jusqu'à quelques microns) mais difficilement pour la localisation de molécules individuelles de quelques nanomètres à quelques dizaines de nanomètres (oligonucléotides ou protéines). De plus, les méthodes physiques connaissent certaines limitations même dans le cas de la localisation de colloïdes : d'une part, pour les pinces optiques ou électroniques ((di-)électrophorèse) elles fonctionnent uniquement sous l'application d'un champ externe (tension électrique ou laser) et donc ne permettent pas de piéger un objet de manière définitive (après avoir éteint le champ) ; d'autre part, pour l'assemblage par forces capillaires, les objets à piéger doivent en général être commensurables en taille avec les « pièges » ; finalement, ces méthodes impliquent souvent des contraintes dans les matériaux des objets à localiser comme par exemple le caractère ferro ou paramagnétique pour les pinces magnétiques. La fonctionnalisation chimique de surface, tel qu'expliqué dans l'introduction générale, apparaît alors comme une méthode pouvant palier à ces défauts tout en se combinant éventuellement avec ces méthodes physiques pour plus d'efficacité.

Étant donné les applications visées (biocapteur photonique), nous nous sommes intéressés notamment aux fonctionnalisations des surfaces d'or et de silice. L'abondante littérature cumulée depuis quelques dizaines d'années sur ce sujet (fonctionnalisation des surfaces d'or et de silice prises *séparément*) montre la diversité de molécules et de protocoles pouvant être utilisés à ces fins. Certaines tendances se dégagent cependant. Pour la fonctionnalisation de l'or, de nombreux articles présentent l'utilisation d'alkylthiols d'une longueur d'environ une dizaine de groupements méthylènes, dissouts dans l'éthanol. L'utilisation des SAMs mixtes associant deux thiols différents dans la même couche, l'un permettant de greffer des biomolécules et l'autre limitant l'adsorption non spécifique, est parfois préconisée pour améliorer la réactivité globale de la SAM.[1] De même, l'utilisation de chaînes oligo(ethylene glycol) (OEG) est aussi mise en avant dans certains articles.[2–11] Celles-ci sont aussi bien préconisées pour améliorer la réactivité d'un groupement fonctionnel (ex : COOH)[11] que pour leur effet passivant (réduction de l'adsorption non-spécifique) dans le cas d'un groupement hydroxy ou methyl.[12–26] Sur silice, l'utilisation d'alkoxy et chlorosilanes semble le plus répandu. En revanche, contrairement à l'or, les protocoles semblent diverger davantage dans la littérature. Ceci est probablement dû au fait que les silanes peuvent polymériser en solution (pour les di- et trivalents) ce qui rend le processus plus complexe et qui amène à s'intéroger davantage sur l'influence du taux d'humidité dans la solution ainsi que sur l'importance d'étapes de recuit à haute température. La caractérisation des ces couches organiques apparaît alors comme un sujet primordial, intrinsèquement lié au développement de la fonctionnalisation de surface. Différentes techniques permettent d'évaluer ces couches sous différents aspects tels que leurs propriétés physicochimiques globales (angle de contact, ellipsométrie), leur composition et structuration moyenne (spectroscopies infrarouge, de photoémission ou de masse) ou encore leur composition et structuration à l'échelle nanométriques (microscopies à champ proche telle que la microscopie à force atomique -AFM-, la microscopie tunnel à balayage -STM- ou la spectroscopie Raman exaltée par pointe -TERS-).

Si l'étude de la fonctionnalisation de surfaces d'or et de silice séparément date de plusieurs dizaines d'années (bien que ce soit toujours un sujet de recherche actif, notamment avec le développement de nouveaux outils de caractérisation), la fonctionnalisation orthogonale de surfaces micro ou nanostructurées pour la localisation de colloïdes ou biomolécules est un sujet en plein essor, notamment depuis environ 2010.[27,28] Les publications parues sur ce sujet montrent l'intérêt de cette méthodologie mais révèlent par la même occasion un certain nombre de points à approfondir pour l'amélioration et la généralisation de ce concept. En premier lieu, il existe souvent un manque de caractérisation chimique « directe » prouvant l'orthogonalité des fonctionnalisations, souvent relégué à une mesure « en fin de processus », c'est à dire à la lecture d'un signal SPR ou à l'observation par microscopie du dépôt de colloïdes. De plus, les fonctionnalisations utilisées récemment pour certains biocapteurs plasmoniques[28,29] peuvent être grandement améliorées tant sur la sélectivité des groupements permettant l'ancrage sur l'un ou l'autre matériau que sur l'épaisseur de ces couches, qui doivent être le plus fines possibles dans le cas d'un transducteur à ondes évanescentes. En outre, si la plupart des démonstrations effectuées à ce jour demeurent sur des cas relativement « simples » (interactions streptavidine/biotine ou dépôt de colloïdes d'or sur structures d'or) nous pouvons espérer des applications plus complexes et intéressantes d'un point de vue des biocapteurs (par ex : détection de marqueurs cancéreux ou placement de carboxylatex fluorescents sur nano-antennes plasmoniques).

L'analyse de l'état de l'art ci-dessus nous conduit naturellement aux objectifs précis de cette thèse. Ces objectifs incluent la fonctionnalisation de surfaces d'or et de silice ainsi que de surfaces mixtes or/silice structurées à différentes échelles (macro, micro et nanostructures d'or sur silice) avec une emphase particulière portée à la caractérisation chimique de ces couches organiques. Ces fonctionnalisations seront faites à l'aide de différents thiols (pour la capture de biomolécules ou colloïdes sur or) et silanes (pour la passivation de la silice environnante), basées sur une reconnaissance biotine/avidine mais aussi sur une chimie -COOH et NHS-ester pour la capture de molécules aminées. Cette capture sélective sur or sera appliquée à la localisation de carboxylatex magnétiques ou fluorescents ainsi qu'à la détection de biomolécules (ADN ou protéines) par LSPR.

Contents

Introduction to the state of the art

As explained in the general introduction to this manuscript, the issue that we are about to discuss can be summarized as follows :

Given a heterogeneous solid surface with predefined micro and nanometric sites and given a complex medium with target molecules or colloidal nano-objects, how can we ensure that the targets are deposited onto the predefined sites while avoiding non-specific adsorption on the surrounding surface ?

This question is especially relevant in the increasing field of localized-plasmon based sensors as previously explained. However, it is not limited to this field and can be seen as a major current issue in nanofabrication. Indeed, especially for colloids, answering this question is a major step in bridging the gap between bottom-up built nano-objects and top-down defined substrates. This chapter presents the state of the art concerning this subject.

First, we will review different *physical approaches* to answer the stated issue. We will highlight the theoretical and experimental limitations of these methods to conclude on the need of reliable orthogonal *chemical functionalizations*. Second, we will present in greater detail the chemical functionalizations of gold and silica surfaces with an emphasis on characterization tools. Third, we will present the orthogonal functionalizations of heterogeneous gold/silica (or, more generally, metal/oxide) substrates, [5] with recent demonstrations of this method's capabilities on the precise targeting of molecules and colloids reported in the literature. Eventually we will conclude on the state of the art and present the choices that were taken for the following work.

5. The top-down fabrication of heterogeneous substrates is obviously a necessary condition to the aforementioned studies and a full part of the work developed during this PhD. However, as the processes used are rather standard and have not been the object of active research during this work, the details concerning this work are presented in appendix A along with the matter of residue removal at the end of the top-down processes (lithography) and prior to chemical functionalization.

1.1 Physical approaches and their limitations for the precise placement of targets onto patterned substrates

1.1.1 Introduction

Before discussing surface chemical functionalization, we will review different physical approaches to answer the main issue of this work. The following review is adapted from our previous publication on this subject.[30] This review deals only with colloids (spherical particles, nanorods, nanowires, nanotubes and other objects, see Table 1.1), often bigger than 100nm and not single molecules. This is one of the major drawbacks of these methods, as we will discuss at the end of this section, to introduce the need of surface functionalization. Eventually, the methods presented here require a preliminary condition : *colloid stabilization* in the bulk liquid volume. This issue and the corresponding DLVO theory is presented in appendix B.

	Aspect ratio = 1 (spherical) particles	**Aspect ratio > 1 rods and other structures**	**Aspect ratio >> 1 wires and tubes**
Organic	Latex beads[31,32]	*rare*	*rare*
Silica	SiO_2 beads[33]	*rare*	*rare*
Semi-conductor	Quantum Dots[34,35]	CdSe nanorods[36]	Semi-conductor nanowires[37] Carbon Nanotube (CNT)[38]
Hybrid	Core(Au)-shell(SiO_2)[39]	Janus[40] Core-shell nanorod[41]	Organo-silica nanowires[42]
Metallic	Au beads[43]	Au nanorod[44]	Au nanowire[45] CNT[38]

Table 1.1 – Different types of objects considered in this chapter.

1.1.2 Different trapping forces

A particle in a colloidal dispersion will naturally be subject to two transport phenomena : diffusion and sedimentation (which takes into account gravity, viscous drag and Archimede's force). Depending on the particle size and density, these phenomena might not be strong enough to make the particle reach a given surface in an acceptable timescale. Most importantly, these phenomena will bring the particles everywhere on the surface and not specifically onto certain regions of interest. Therefore, external stimulation is needed to achieve this.

Colloidal particles can be driven onto specific nanosites of a substrate by applying different external fields. The most common ones used in the literature are either hydrodynamic or electromagnetic.

Of course, the choice of one or another method lies on the physico-chemical properties of the particles, which often depends on its material and geometry, as we will see in the different examples.

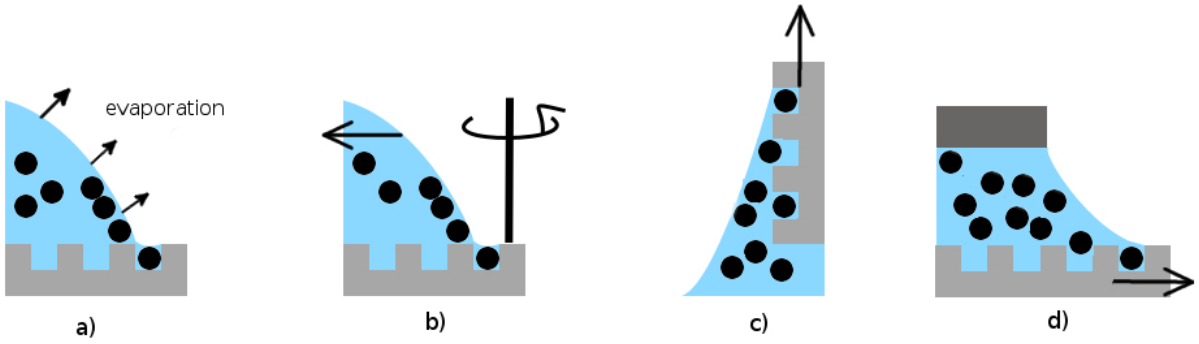

FIGURE 1.1 – Different fluidic approaches for CFA : a) Drop-casting b) Spin-coating c) Dip-coating d) Confined solution with moving substrate.

1.1.2.1 Capillary force assembly

Probably the most straightforward mean to address nano-objects on specific regions of a substrate is to drag them by hydrodynamic forces and have them trapped on topographically defined regions by CFA, sometimes referred to as Template-Assisted Self Assembly (TASA).[46,47] In CFA, a meniscus is created between the colloidal solution and the substrate. As the meniscus (contact line) advances at the surface (substrate dewetting) the particles are deposited by capillary forces in the topographically defined regions. The creation and relative movement of the meniscus can be achieved by various techniques including drop-casting,[32] spin-coating,[48–50] dip-coating[32,51] or confined solution between fixed plate and moving substrate[32,52–56] (See Fig. 1.1).

In some cases, capillary and contact forces (Van der Waals) are strong enough to make the particles adhere exclusively to the topographically defined regions (holes) while in other cases topography patterning is coupled with surface functionalization[57] (see section 1.1.3.2) to avoid non-specific adsorption. It is interesting to note that in some cases CFA is used to deposit particles on a Poly(dimethyl siloxane) (PDMS) substrate that can be later used as a stamp for micro-contact printing.[53–55] Alternatively, some papers present a substrate with a patterned layer of polymer ; after deposition of particles everywhere, the ones on the polymer layer are removed by dissolution of the polymer, as a standard lift-off technique (see Fig. 1.2).[50]

To the best of our knowledge, CFA was first demonstrated in 1997, when Van Blaaderen et al.[58] trapped single 525nm radius silica particles with this technique. Many papers have reported CFA in the last 15 years with isotropic[32,33,46,48–50,52–55,57,59,60] and anisotropic[51,61–63] objects. Good reviews on CFA can be found in the literature.[47,64–68] Spherical particles can be trapped in trenches (eg : V-grooves[33]) or in individual traps (as isolated particles or small aggregates). In the latter case, a summary of different published results can be found in Fig. 1.3.

1.1.2.2 Electronic tweezers

Electric fields can induce movement of colloidal particles via **electrophoresis** (coulombic interaction of a DC field with a charged particle) and/or **dielectrophoresis** (polarization effects of a non-uniform DC or AC field on a polarizable particle -charged or not-). Some reviews on electrophoresis and dielectrophoresis with their uses for micro and nanoparticle trapping can be found in the literature.[67,69–74]

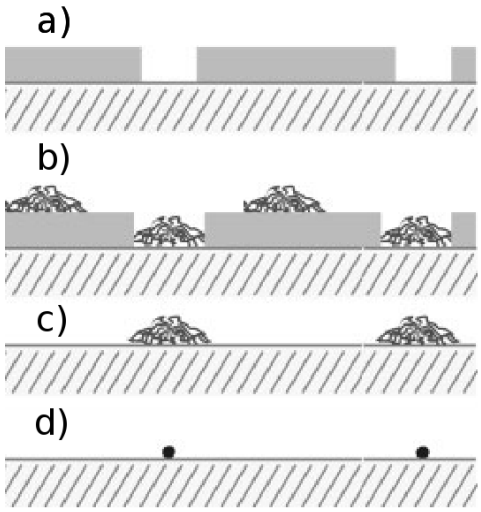

Figure 1.2 – Schematic representation of the localized deposition of nanoparticles through e-beam lithography, CFA and lift-off. (a) E-beam resist is first patterned by lithography. (b) Micelles containing a metallic nanoparticle at their core are then deposited on the surface, some trapped on the holes defined in the e-beam resist by CFA while some remain on top of the resist layer. (c) A standard lift-off method dissolves the e-beam resist, removing the micelles adsorbed on it (outside the lithography-defined holes). (d) Eventually, the micelles remaining on the surface are dissolved to liberate their metallic nanoparticle cores. Adapted from.[50]

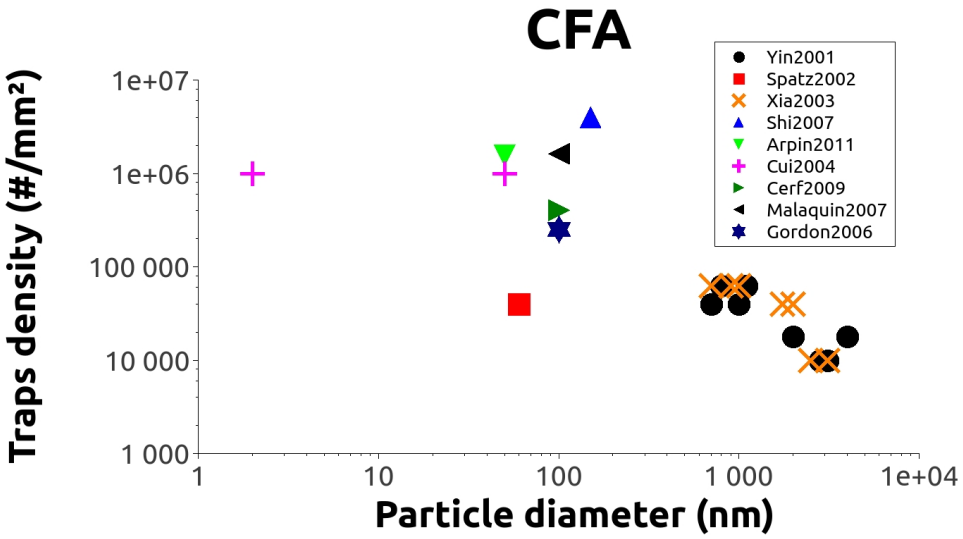

Figure 1.3 – Trap density vs particle size using CFA.

1.1.2.2.1 Electrophoresis

A charged particle placed in a DC field will accelerate until reaching a final velocity at which the electrophoretic force and the viscous drag compensate each other. We can then define the electrophoretic mobility $\mu_{EP} = \frac{v}{E}$, where v is the velocity and E is the electric field magnitude. Different expressions for μ_{EP} can be found depending on the particle size :

$$\mu_{EP} = \frac{2\varepsilon\varepsilon_0\zeta}{3\eta} \quad \text{Hückel equation, for } r \ll \lambda_D$$

$$\mu_{EP} = \frac{\varepsilon\varepsilon_0\zeta}{\eta} \quad \text{Helmholtz-Smoluchowski equation for } \lambda_D \ll r$$

where ε and ε_0 are the dielectric permittivity of the media and vacuum, η is the fluid dynamic viscosity, ζ is the electrostatic potential at Stern's plane (see section B.2) and r and λ_D are the particle radius and Debye's length.

Electrophoresis has been used in the 90's to deposit different micro and nanoparticles such as gold, latex and silica on macroscopic anodes.[75–79] These papers concentrate on the crystal-like 2D arrangement of particles, but the substrate remains macroscopic with no individual trapping.

With the evolution of microfabrication techniques, namely UV and e-beam lithography, it has been possible to create individually addressable microelectrodes on an insulating substrate. Thus, in 2007 and 2009, Dehlinger and co-workers[80,81] used a 400-microelectrodes (55µm diameter) array to globally position polystyrene particles (40nm diameter) functionalized with biotin or neutravidin. The functionalization played two roles : first, making the particle surface become negatively charged so that it responded to electrophoresis and second, allowing biochemical recognition on the streptavidin-functionalized substrate as discussed in section 1.1.3.2. They formed uniform nanoparticle layers on the electrodes while only a few percent surface coverage was observed in between the electrodes in only 15s.

Electrophoresis has also been used with CNT whose precise placement is an important challenge in microelectronics. It has been found that Multi-Wall Carbon Nanotubes (MWCNTs)[82] as well as Single-Wall Carbon Nanotubes (SWCNTs)[83] in isopropyl alcohol accumulate at the anode with applied voltage around 0.7V. Alignment of these CNTs has also been demonstrated using AC voltage,[83,84] suggesting that the implied phenomenon is not only electrophoresis but rather dielectrophoresis, which is specially relevant for anisotropic particles as we will see now.

1.1.2.2.2 Dielectrophoresis

Dielectrophoresis (DEP) results from the polarization of a neutral particle placed in a non uniform electric field. A good explanation of this phenomenon with references to its use in nanotechnology can be found in Burke's review.[74] The electric field polarizes the particle whose induced dipole moment interacts with the external field, so that, for a spherical particle we can determine :[85]

$$\vec{F} = 2\pi r^3 \varepsilon_m^* \alpha_r \vec{\nabla}(\vec{E}_{rms}^2)$$

Where ε_m^* is the complex medium dielectric constant, r is the particle radius and α_r is the real part of Clausius-Mossotti factor :

$$\alpha_r = \mathrm{Re}\left(\frac{\varepsilon_p^* - \varepsilon_m^*}{\varepsilon_p^* + 2\varepsilon_m^*}\right)$$

Where ε_p^* is the particle dielectric constant.
From the expression of α_r we can see that it can be either positive, inducing particles to move toward maximum electric field region (*positive dielectrophoresis*) or negative, inducing particles to move toward minimum electric field region (*negative dielectrophoresis*). Moreover because of dispersion we have $\varepsilon^* = \varepsilon^*(\sigma, \omega) = \varepsilon - j\frac{\sigma}{\omega}$, ($\sigma$ being the conductivity and ω the field frequency) which means that the same particle in the same medium may experience positive or negative dielectrophoresis depending on σ and ω[86] (the frequency for which $\alpha_r(\omega) = 0$ is called the crossover frequency). For a further study on this subject and on the role of the electric double layer, one may read Hughes' article from 2002.[87]

The first description and preliminary results of dielectrophoresis were given by Herbert Ackland Pohl in the 50's[88,89] with a more comprehensive study in 1978.[90] Since then, and specially with improved lithography techniques for microelectrode design, dielectrophoresis has been widely used for particle trapping. Since the late 90's, most reported results in the literature have been obtained with latex beads. The reasons for this relate to the fact that they are commercially available in different sizes and can be fluorescently labeled.[74]

Many experimental results were presented mainly by Fuhr's and Morgan and Hughes' groups. In these papers[31,85,86,91–103] nanoparticles ranking from 14nm[93] to 93nm[96] have been trapped using different electrode geometries and voltages. From the beginning of the years 2000's until today, DEP has been used with organic latexes in a certain number of papers[80,81,104–129] but these contributions mainly focus on the application of DEP to biological samples (cells, viruses, biomolecules...) and on ever more complex systems.

Dielectrophoretic trapping of metallic and semiconductor nanoparticles has also been reported and remains a field of active research. In 1997, Bezryadin and Dekker[130,131] demonstrated the possibility of bridging Pt nanoelectrodes with gaps as small as 4nm with Pd colloids (as small as 17nm) trapped individually. Further work has been conducted with 60nm and 40nm gold nanoparticles (Clausius-Mossotti factor can be assumed to be equal to +1 in most cases)[132] by Krahne et al.[133,134] to fill a 10nm gap. Similar results were found independently by Amlani, Rawlett et al.[135–137] Other groups used 20nm beads to bridge gaps of different sizes ranging from 5 to 150nm.[43,138,139] These papers also demonstrate the gap-size-dependency of the previously noticed[134] threshold voltage.[138] Two interesting approaches were described by Khondaker and Yao[140] who used 50nm gold colloids to bridge a large gap (400nm bridged by a collection of particles and 45nm bridged by a single particle) and subsequently broke that bridge by applying a strong DC voltage, thus resulting in sub-10nm gaps. Zheng et al.[104] used carbon nanotubes as the electrodes for DEP trapping of gold colloids as small as 2nm, albeit not as single particle trapping. Finally, gold colloids have also been trapped as dimers, linked by dithiol.[141,142]

We have seen how spherical particles can be trapped by DEP. Nonetheless it is obvious that particles having a geometrical anisotropy (nanorods, nanowires and nanotubes) are perfect candidates for dielectrophoretic trapping as the polarization can occur preferentially along the long axis. Moreover, DEP trapping is often used for the purpose of bridging two electrodes. Thus, one needs a particle with one dimension larger than the others in combination with metallic or semiconducting properties.

For all these reasons, extensive literature can be found on DEP using nanowires that can be either metallic (such as Au,[44,45,143–145] Ag,[146] NiSi[147] and Rh[148,149]), semiconducting with different energy gaps (Si,[144,149–151] ZnO,[152–158] SnO_2,[146,159] GaN,[146,160–166] InAs,[167] SiC[168] and Ga_2O_3[146] among others) or more complex materials.[169] In the past 5 years, different pa-

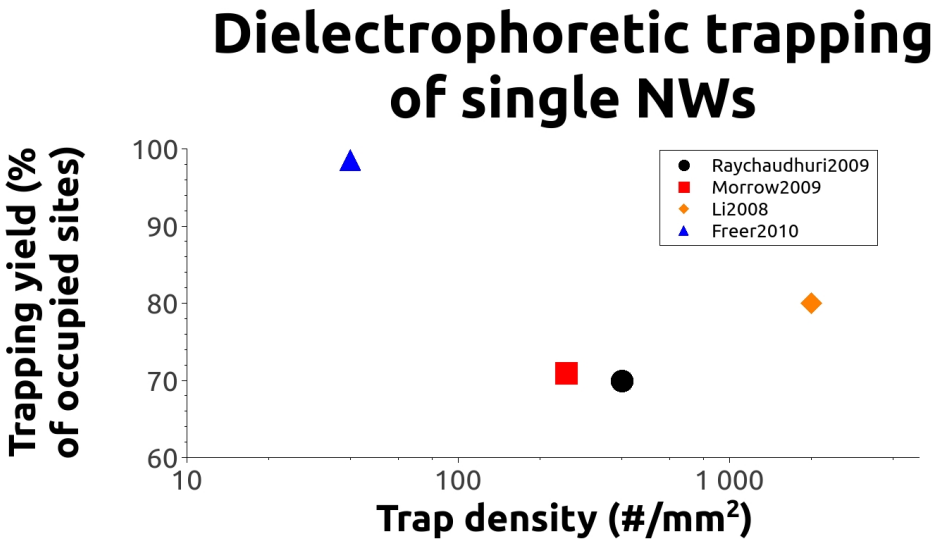

Figure 1.4 – Efficiency of parallel DEP trapping of single nanowires.

pers have demonstrated parallel single nanowire trapping using DEP, with different trapping yields and trap densities, as summarized in Fig. 1.4. DEP has also been thouroughly used to trap carbon nanotubes.[38,84,136,137,156,170–194] A review by Huang et al. can be found on this subject.[195]

Among these papers, some achieved *single* CNT trapping[173–175,178,185,192,194] and **parallel** trapping (single or bundled) on arrays.[172,173,175,178,182,192,194] The main results for parallel CNT trapping are summarized in Fig. 1.5.

1.1.2.3 Photonic and plasmonic tweezers

Much has been written about optical trapping since Ashkin and Dziedzic's seminal work in the 70's and 80's.[196–198] From a physical point of view, an "optical field" is no more than an oscillating electromagnetic field. In that sense, optical tweezers can be viewed as DEP tweezers operating at different frequencies : typical DEP operates in the megahertz range while visible light is in the hundreds of terahertz. Thus, it is not strange to find that the optical force for a spherical particle is such that $F \propto v\alpha\nabla E^2$, where v is the volume of the particle and α is the polarizability, as for DEP.

Optical tweezers resulting from a focused gaussian beam have proven their ability to trap particles in the Rayleigh ($r \ll \lambda$) and Mie ($\lambda \ll r$) regimes -r and λ being the particle radius and the optical wavelength- and extensive references can be found in different reviews.[199–208]

However, in order to have global self-assembly of a colloidal dispersion onto pre-defined regions of a substrate, one should be able to pattern optical traps on the substrate. This has become possible with the advent of plasmonic traps using arrays of structures (eg : gold nanodisks) supporting surface plasmons that can be excited globally with an external beam. Theory of plasmon physics can be found in Homola's book[207] and an excellent review on "plasmon nano-optical tweezers" is available in Juan's review.[208] The first experimental demonstration of particle (1µm polystyrene and 500nm gold) trapping with an evanescent field was presented, to the best of our knowledge, by Kawata et al. in 1996.[209] However, in this paper trapping is not achieved in 3D but 2D with movement along a channel. Later, numerical simulations have shown the possibility of 3D trapping by creating a shallow potential dwell (strong field gra-

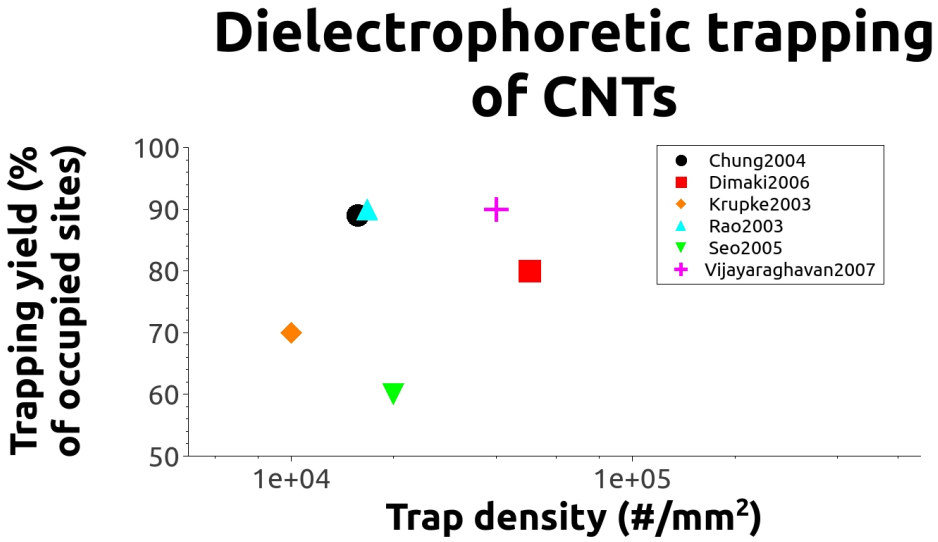

Figure 1.5 – Efficiency of parallel DEP trapping of CNTs.

dient) either between a substrate and a tip[210–212] or around a nanoaperture.[213] An experimental demonstration was made by Kwak in 2004[214] using 200nm polystyrene beads. Eventually, the global excitation of surface plasmons on an array of metallic nanodots on glass (individual nanodots or paired to form nano-antennas), was proposed[215] and demonstrated[216,217] by Quidant et al. It has been the most extensively used configuration for particle trapping.[70,216–223] The main results for global trapping using plasmonic dots are summarized in Fig. 1.6.

Eventually, holography has also been used for parallel trapping[224–227] but this will not be investigated in further detail here.

1.1.2.4 Magnetic tweezers

Magnetic trapping only concerns ferromagnetic and (super-)paramagnetic materials. Unlike dielectrophoresis or photonic/plasmonic trapping, the force exerted by a magnetic field on a particle is not proportional to the field gradient squared but to the product of the field and its gradient, so that for a spherical particle :

$$\vec{F} = \frac{V\Delta\chi}{\mu_0}(\vec{B}.\nabla)\vec{B}$$

Where V is the volume of the particle, $\chi = \chi_{particle} - \chi_{medium}$ is its effective susceptibility and $\mu_0 = 4\pi \times 10^{-7}\ N.A^{-2}$ is the magnetic permeability of free space.[228] Further theoretical developments can be found in the literature.[228–234]
This force has been widely used to drive and separate magnetic particles in fluidic channels[235–260] or aggregate them along long wires.[261–265]

Magnetic manipulation of micro and nanoparticles has been reviewed by Gijs in 2010.[266] The patterned traps are usually nickel, cobalt or permalloy based micropillars. trapping of spherical[267–276] and anisotropic[277–282] particles using such devices has been successfully achieved. In the case of spherical particles, parallel trapping in large arrays has been achieved by different groups as shown in Fig. 1.7.

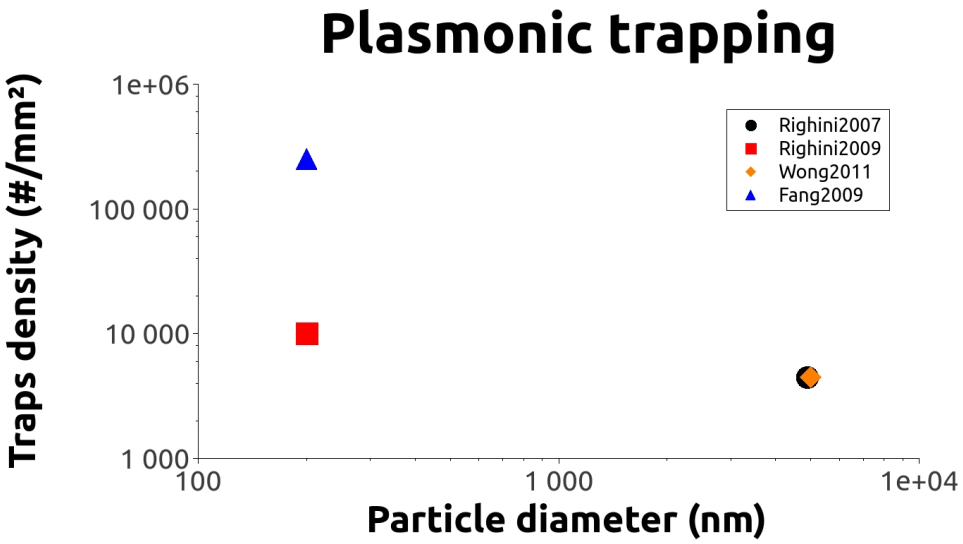

FIGURE 1.6 – Plasmonic array traps for spherical particles.

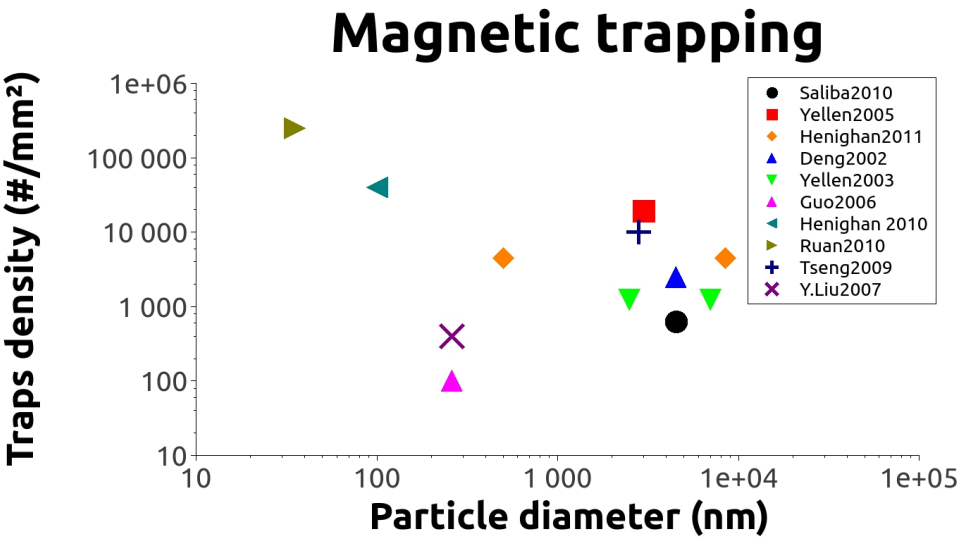

FIGURE 1.7 – Magnetic array traps for spherical particles.

1.1.3 Discussion and conclusion

1.1.3.1 Comparison of the above mentioned methods

A combination of Figs. 1.7, 1.6 and 1.3 can be found in Fig. 1.8, which also shows the performance limit based on close-packing only. Some remarks can be made about this figure which presents the performances of spherical particle trapping using different methods :

1. Capillary assembly seems to yield the best results, according to the references studied in this chapter, without the need of electromagnetic stimulation. However, the differences are not so important that one method can be presented as clearly superior or inferior to the others.

2. Plasmonic trapping over large arrays is not yet as developed in terms of number of publications as capillary force assembly or magnetic trapping.

3. Most importantly, a gap is still left under the close-packing limit on the left side (ie, for particles smaller than 100nm).

Aside from the performances in terms of trap density and particle size, we should highlight that the use of one or the other method can be strongly influenced by the surface and/or the nano-object to be trapped. Indeed each method has its own limitations as summarized in table 1.2 :

We have reviewed the main methods used in the literature to draw colloidal particles onto nanometric scale sites of a substrate. However, few other papers have demonstrated similar results using different approaches. Among them, we can cite the use of thermal gradients[286,287] or acoustic fields.[288–292] To the best of our knowledge these approaches have not yet proven the same performances as the electromagnetic or fluidic methods but they may play an important role in the future.

One of the main concerns about the methods investigated so far is that, in most cases, they only work under external stimulation. This means that once the external field has been switched off, the particle is no longer captured (this is not true for permanently magnetized microtraps or CFA after solvent evaporation). Another problem not mentioned so far is non-specific adsorption (particle adsorbed at the surface outside the traps) resulting from contact forces (Van der Waals, see appendix B.1). Furthermore, these techniques are demonstrated on relatively big objects and it is not straightforward that such approaches can be downscaled to the size of a small molecule (few nanometers). Without entering in too much detail, there are important technological bottelenecks (generating big enough fields and field gradients) as well as scientifical issues (CFA fluidic principle validity with traps of few nm ?) that make these approaches not readily available for single molecule trapping. In order to overcome these problems, surface functionalization can be used.

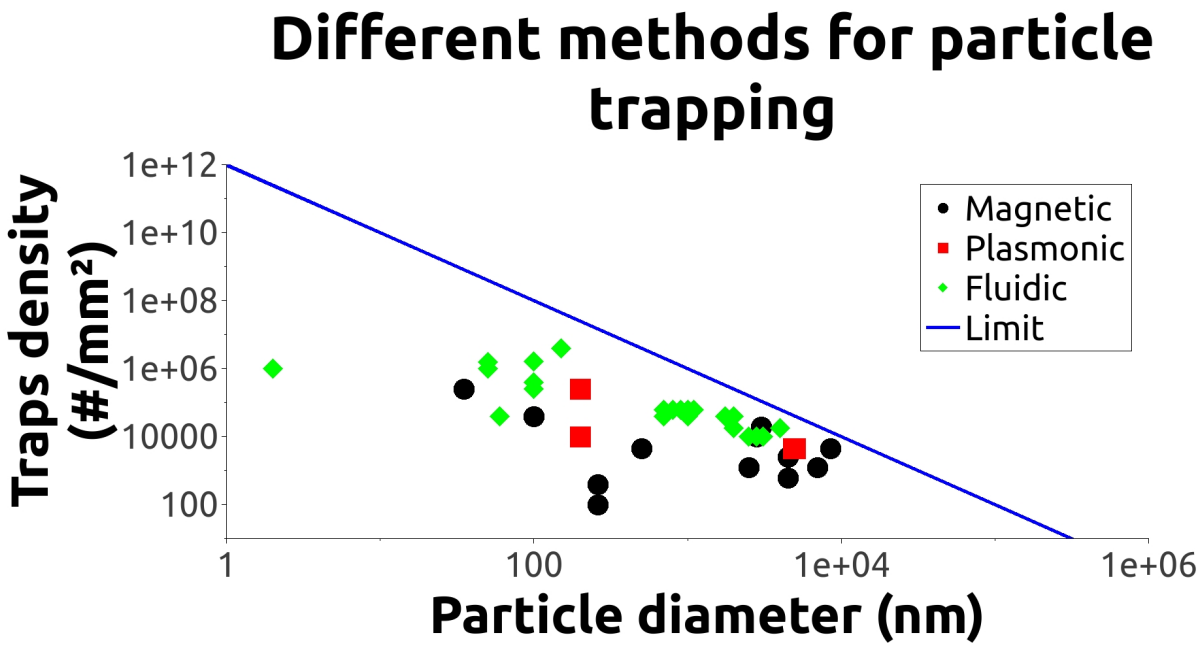

Figure 1.8 – Comparison of different methods for parallel trapping of spherical particles.

Method	Nano-object		Trap surface	
	Material	Geometry	Material	Geometry
CFA	Organic[47] Metallic[54] Silica[47]	Spherical[54] Tube, wire[51]	Any	Topographic holes
Electrophoresis	(Charged) Organic[80] Metallic[138] Silica[283]	Spherical[80] Tube, wire[82]	Metallic	Any
Dielectrophoresis	(Polarizable) Organic[85] Metallic[139] Silica[284]	Spherical[85] Tube, wire[146]	Metallic	Different designs for positive / negative DEP
Plasmonic	Organic[222] Metallic[70]	Spherical[222]	Metallic	Different designs
Magnetic	Magnetic* or with magnetic core	Spherical[267] Janus[285] Tube, wire[279]	Magnetic*	Any

Table 1.2 – Main limitations of the different trapping methods. * Magnetic refers to ferromagnetic or (super-)paramagnetic.

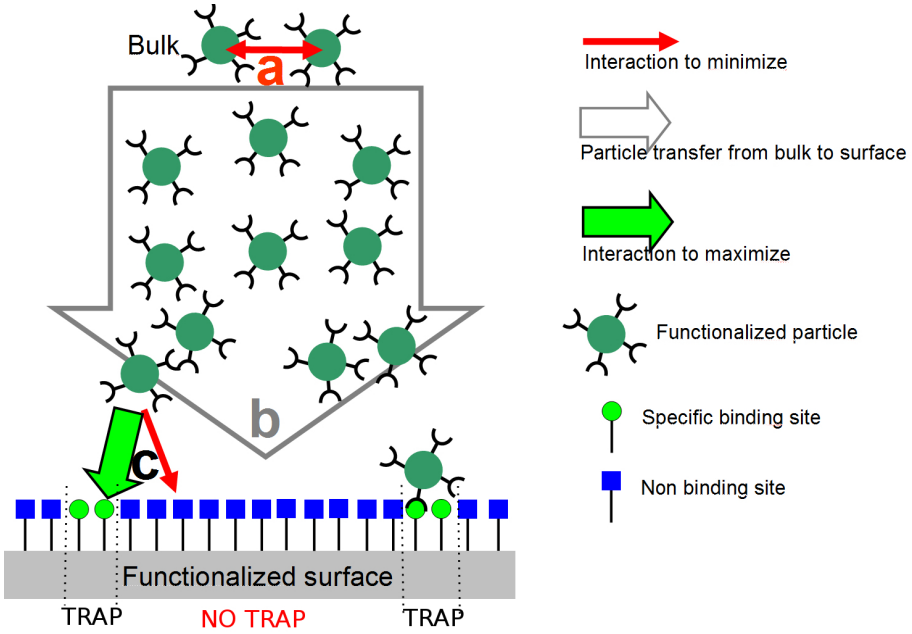

FIGURE 1.9 – Schematic representation of surface functionalization and its use for particle trapping. a) and b) refer to colloid stabilization and transport phenomena, c) refers to selective binding of particle based on surface functionalization. Note that typical binding sites take less than $1nm^2$ while trap' dimensions are often over 100x100 nm (figure is not to scale), meaning that there are many binding sites for one trap.

1.1.3.2 Surface functionalization

Surface functionalization can tune the short-range interaction between the surface and the target, enabling a given region to capture a target while making the rest of the surface repel it. Functionalization refers to grafting *complementary molecules* (or not-complementary for avoiding non-specific adsorption) on the particles' and substrate's surfaces (See Fig. 1.2). The interaction can be electrostatic[293–297] (eg : $-COO^-$ / $-NH_3^+$), covalent binding[298,299] or based on specific biological recognition[27,300,301] (e.g., DNA/DNA, biotin/avidin, and antigene/antibody).

The main advantages of surface functionalization as a mean of colloid trapping are that : (i) it works without the need of an external stimulation (i.e., no need to apply an external field) and (ii) it is only material-selective and therefore highly versatile in terms of substrate patterning. Indeed, the traps can have virtually any shape and size. However, surface functionalization on its own cannot drag the particles from the bulk to the surface (no long range interactions). Nonetheless, functionalization can be used in combination with any of the aforementioned *physical* methods for an enhanced trapping when diffusion and sedimentation are not enough to ensure the particle transfer from the bulk to the surface.

In the following paragraphs, we will consider the case of heterogeneous gold/silica substrates where gold micro and nanostructures are to be used as traps surrounded by silica where non-specific adsorption is to be avoided.

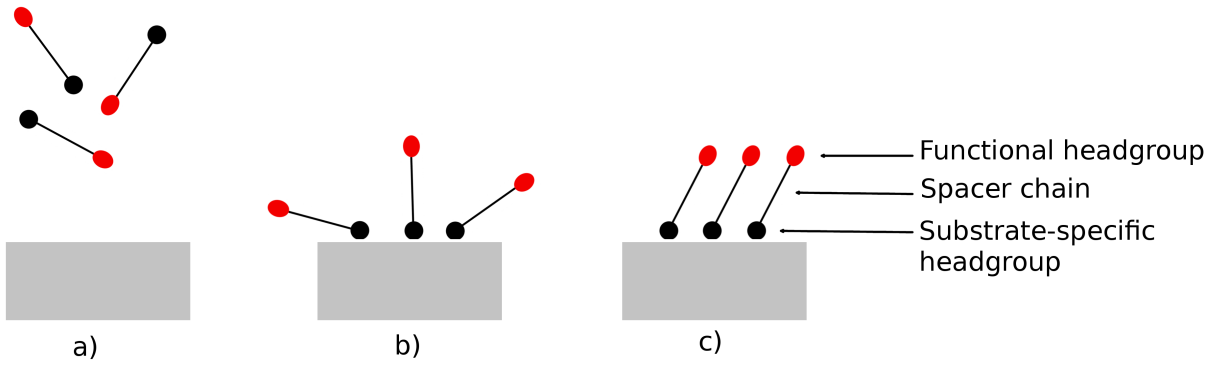

FIGURE 1.10 – Ideal representation of self-assembled monolayers on a solid surface. Molecules from a liquid or gas phase (a) are chemically bonded onto the substrate by their substrate-specific headgroup (b) and self-arrange through Van der Waals interactions to form a pseudo-crystalline monolayer (c). A more realistic representation of SAMs can be found in Fig. 1.16 along with a discussion about the main defects in such organic layers.

1.2 Chemical functionalizations of gold and silica

"Self-assembled monolayers (SAMs) provide a convenient, flexible, and simple system with which to tailor the interfacial properties of metals, metal oxides, and semiconductors."[302]

In many applications such as biosensing, surfaces play a decisive role on the whole system performances. Indeed, biosensors are usually based on the ability to bind a target molecule (e.g : oligonucleotide, peptide, protein) from a complex medium (eg : blood) onto a planar substrate ; this event being then transduced into a measurable physical signal.

Molecular monolayers and SAMs can be built on a wide range of solid surfaces in order to tune their physicochemical properties, specially in regards to target-molecule binding in the development of biosensors. A SAM is a 2D structure composed of organic molecules that are spontaneously bound from a liquid or gas environment onto a solid surface, usually by a covalent bond between one of the molecule's headgroups and the surface (see Fig. 1.10 for an "ideal" representation of a SAM). The remaining available headgroup, separated from the former by a spacer chain (usually alkyl or alkyl-Poly(Ethylene Glycol) (PEG)) can be choosen to fulfill a specific *function* (eg : bind a specific target molecule). This process is therefore referred to as *chemical surface functionalization*. [6]

In the following paragraphs we will quickly review the state of the art of gold and silica surface functionalization with SAMs.

1.2.1 Gold functionalization

Gold is a standard material for many biosensing applications due to its physicochemical properties, e.g., conducting, supporting surface plasmons, stable in biological environment, and non-cytotoxic. etc. Therefore, many groups have investigated the ability to chemically modify gold surfaces with SAMs, specially with the aim of using it for biosensing.

The present literature review is greatly based on different already published reviews on this subject.[302–304]

6. Let us recall that, as stated before in this chapter, it is possible to chemically functionalize surfaces with other approaches than SAMs.

1.2.1.1 Different molecules

As we have seen in Figure 1.10, the molecules that form a SAM have three main elements :

1. A substrate-binding headgroup
2. A spacer chain
3. A functional headgroup

Let us investigate now the reported possibilities for each of the aforementioned elements in the case of gold surface functionalization.

1.2.1.1.1 Gold-binding headgroup

Some of the chemical groups reported in the literature to bind an organic molecule onto a gold surface can be found in Table 1.3. [7]

7. It should be noted that the molecule's name is often used for the defining headgroup. Thus, although a **thiol** is an organic compound with a **sulfhydryl** headgroup (as an alcohol presents an hydroxyl headgroup), the sulfhydryl group itself is often referred to, and will also be in this manuscript, as thiol.

Name	Formula	Mechanism	Comments
Thiol[302]			Good commercial availability. Most widespread and very well documented.
Dithiol[305–307*]			Compared to the single thiol, polythiols may improve the stability of the molecule on gold, though the adjacent sulfhydrils can also form disulfide bonds instead of S-Au bonds.[308,309]
Thioacetyl[310]			Thioacetyls are a protected form of thiols to avoid oxidation. Deprotection (hydrolysis) is better performed under basic conditions with NH_4OH

Name	Formula	Mechanism	Comments
Sulfide[311]	—S–R′	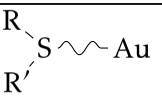	It is believed that dialkyl sulfides bond onto gold through a dative bond, without cleavage of the C-S bonds of the sulfide. This accounts for the weaker robustness compared to SAMs formed from thiols or disulfides. However, assymetric sulfides are interesting to study mixed-SAMs containing different chains or headgroups which are necessarily well-mixed (because covalently bonded).[302]
Disulfide[312]	—S–S–R′	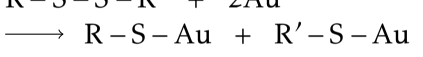	Disulfides can form as thiols get oxidized when stored in air condition, leading thus to a lower solubility than not-oxidized thiols.[302] Assymetric disulfides (different R and R' groups) lead to mixed-SAMs.

Name	Formula	Mechanism	Comments
Cyclic disulfide[313,314]	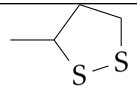	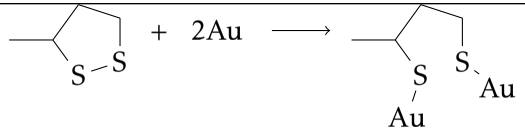	Disulfide bond cleavage leads to an analogue of the dithiol case (see comments on dithiol and polythiols above)
Episulfide[315]	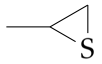	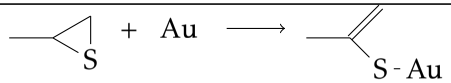	Reported interest as adhesion layer onto precious metals in dentistry.[315]
S-Sodium thiosulfate[307,316**]	$—S—S\text{-}O_3^-Na^{+***}$	$—S—S\text{-}O_3^-Na^+ + Au \longrightarrow —S\text{-}Au + S—O_3^-Na^+$	S-dodecylthiosulfate has been shown to form identical SAMs on gold than dodecanethiol.[307]
Selenol[317,318]	—Se-H	Uncertain, probably analogue to thiol[318]	This analogue of thiol is far less studied, probably due to lesser commercial availability.
Diselenide[318]	—Se-Se-R′	Uncertain, probably analogue to disulfides[318]	This analogue of disulfides is far less studied, probably due to lesser commercial availability.

Table 1.3 – Different gold-binding headgroups. *Dithiol might also refer to a thiol headgroup at each end of the spacer chain in the literature. More generally, polythiols with varying numbers of thiols headgroups can be found. **Reported on nanoparticles[319] and copper substrates.[316]*** Na^+ may be replaced by another monovalent cation.

1.2.1.1.2 Spacer chain

The spacer between the gold-binding headgroup and the functional headgroup is usually an alkyl chain : $(CH_2)_n$, sometimes followed by an OEG or PEG chain : $(CH_2-CH_2-O)_m$.

In the case of an alkyl spacer, different lengths [8] are reported in the literature (some of the following relate to simulation only). The reader can find hereafter references for the use of alkylthiols $HS-(CH_2)_n-X$, with n= :

- **3**[320–330]
- **4**[331,332]
- **6**[324,333–339]
- **7**[324]
- **8**[322,328,331,333,340,341]
- **9**[340,342]
- **10**[321,322,334,336–338,340,342]
- **11**[1,320,323–325,329,330,334–336,339,341–352]
- **12**[322,331,340,342,345–347,353,354]
- **13**[342]
- **14**[327,342]
- **15**[342]
- **16**[1,322–326,331,342,349,351,352,354–359]
- **17**[342]
- **18**[331,332,342,355–357]
- **19**[342]
- **20**[342]
- **22**[348,350]

Two main facts are reported in the literature concerning the alkyl length of thiols forming SAMs on gold :

1. Longer alkyl spacers ($n \gtrsim 10$) form better arranged SAMs than shorter ones ($n \lesssim 10$) due to Van der Waals interactions between chains.[302]
2. For CH_3-terminated thiols in an all-trans configuration, those with an odd number of methylenes form SAMs with higher free energy than those with an even number of methylenes. This is known as the "odd-even" effect and is a consequence of the different projection of the terminal methyl group on the surface (see Fig. 1.11).[302,360–362]

As mentioned above, the spacer chain may include an oligo- or polyethyleneglycol chain in addition to an alkyl chain. Reported chain lengths, in ethylene glycol units ($(CH_2-CH_2-O)_m$) include m= :

- **1**[21]
- **2**[17,19,21]
- **3**[2,15,16,26,363]
- **4**[16,19,21,26]
- **5**[2,16,17,26,364]
- **6**[11,12,16,19,21,25,26]
- **7**[11,17,26]
- **8**[21]
- **10**[21]
- **12**[21]
- **17**[365]
- **45**[366]

PEG chains are often used to passivate the surface (ie : avoid non-specific adsorption of biomolecules or colloids).[12–26] In this case the functional headgroup is a passivating one (OH or CH_3 ; see Table 1.4). In conjunction with the passivating properties of these headgroups, the PEG chain is believed to contribute to the non-specific adsorption reduction by means of steric repulsion. The widespread explanation is that PEG chains have numerous degrees of freedom and therefore repel any object that would constrain them. This phenomenon is also used in colloids' stabilization.

8. In the following list, n refers to the total number of carbon atoms in the chain, which may include an atom from the functional headgroup. This means that $SH-(CH_2)_{10}-COOH$ is counted as n=11, whereas $SH-(CH_2)_{10}-OH$ is counted as n=10

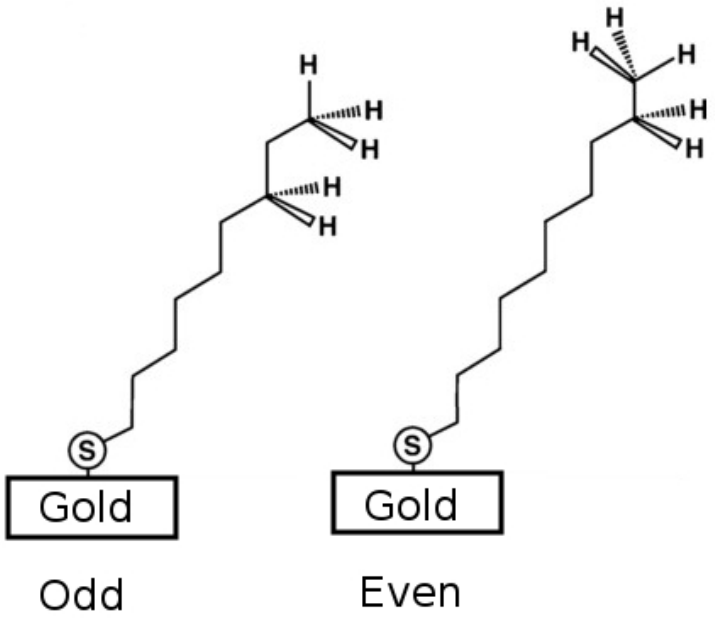

Figure 1.11 – Odd-Even effect. Alkanethiols with odd and even number of methylene units have different projection of the methyl endgroup on the Au(111) surface, leading to differences in hydrophilicity of the so-formed SAMs. Figure adapted from.[302]

However, OEG-thiols can also be used with a target-binding headgroup (mainly COOH ; see Table 1.4).[2–10] In some cases, these SAMs have been found to be more reactive than those from the equivalent carboxy-terminated alkyl-thiols. This greater reactivity for the OEG-thiols has been attributed to the looser packing of the SAM, which would lead to a higher availability of the functional endgroup.[11] Eventually, PEG-thiols can be used in combination with alkylthiols to form mixed-SAMs as we will discuss later.

1.2.1.1.3 Functional headgroup

Table 1.4 shows some reported functional headgroups found on SAMs on gold. These functional headgroups can be separated into three categories :

1. Those whose function is to bind a target molecule from the environment. Carboxylic acids and amines are the most widespread although other functional groups can be used.
2. Those whose function is to avoid non-specific adsorption of molecules from the environment (passivation or anti-fouling). Alcohols[1–3,12–22,26,320,324,327,334–336,341,344–352,359,367] and methyls[13,21,23–26,322–326,331,332,336–340,342,345–348,350,352,354–357,359,367] are widely used. These can also serve as diluting molecules in mixed-SAMs.
3. Those having a different function, such as modifying the electrical properties of the surface.[368]

Chemical group	Intermediate ("activation")	Target	Result
Target-binding headgroups			
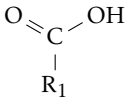 **Carboxyl**	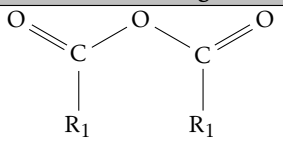 **Anhydride**[369]	 **Amine**	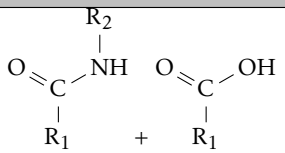 **Amide** **Carboxyl**
	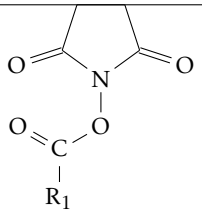 **NHS-ester**[2,3]		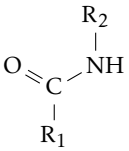 **Amide**
	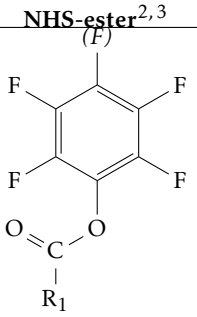 **Fluorophenyl ester**[4,370]		
	None		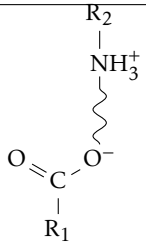 **Electrostatic bond**
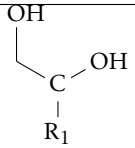 **Diol**	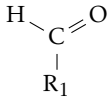 **Aldehyde**[371]		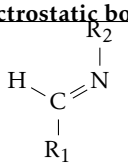 **Imine**
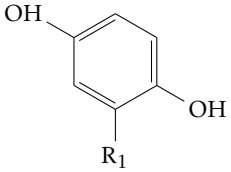 **Hydroquinone**	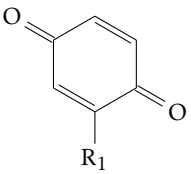 **Quinone**[372]	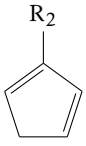 **Cyclopentadiene**	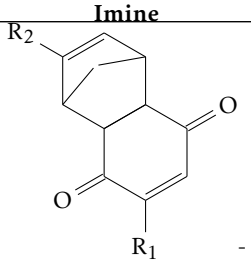 **"Diels-Alder adduct"**

Chemical group	Intermediate ("activation")	Target	Result
 **Amine**	None	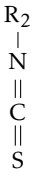 **Isothiocyanate**[373,374]	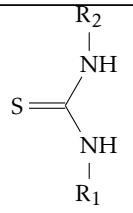 **Thiourea**
		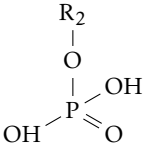 **Phosphate**[375*]	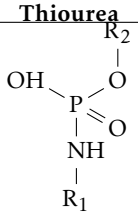 **Phosphoramidate**
		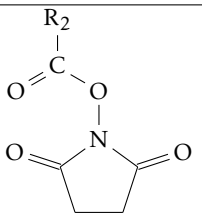 **NHS-Ester**[376]	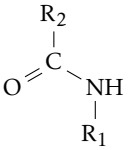 **Amide**
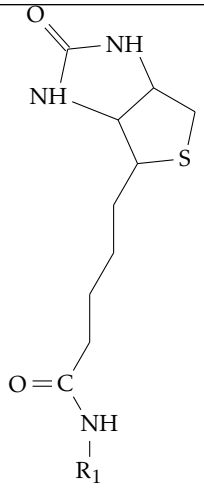 **Biotin**[377]	None	**Avidin**	**Biotin/Avidin complex**
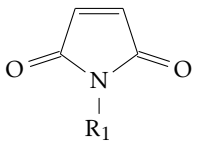 **Maleimide**[18]	None	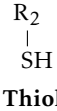 **Thiol**	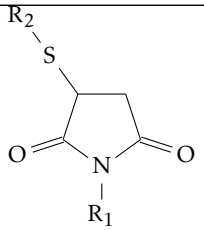
 **Disulfide**[378–380]	None	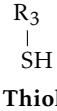 **Thiol**	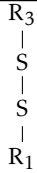 **Disulfide**

Chemical group	Intermediate ("activation")	Target	Result
 **Vinyl**[381]	None	 **Vinyl**	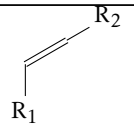 **Vinylic bond**
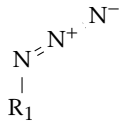 **Azide**[382,383]	None	**Alkyne**	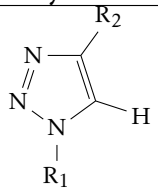 **Triazole ("click" chemistry)**
 **Alkyne**[384]	None	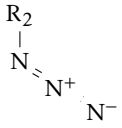 **Azide**	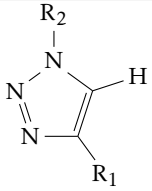 **Triazole ("click" chemistry)**
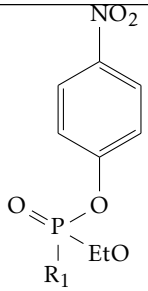 **Phosphonate**[302,385,386]	None	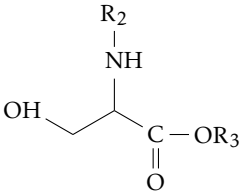 **Cutinase**	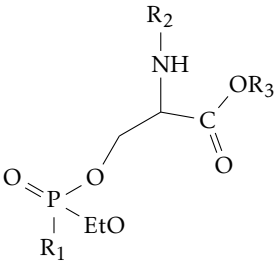 **Phosphonate**
Passivating or diluting headgroups			
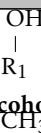 **Alcohol****  **Methyl****	None	None	None
Other functional headgroups			
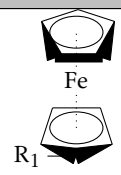 **Ferrocene**[368]	None	Modify work function of the surface.	None

Table 1.4 – Reported functional headgroups of SAMs on gold substrates. * Activated with EDC in the given reference.[375] ** For alcohol and methyls see references in the text.

1.2.1.1.4 Mixed-SAMs

1.2.1.1.4.1 Definition

As we have seen in the previous sections, different molecules can be used to form SAMs on gold surfaces. Thiols are, by far, the most widespread and we shall limit the following study to them. This leaves two elements to differentiate the molecules : the spacer chain and the functional headgroup. It is a common procedure to form self-assembled monolayers from two (rarely more)[387] different thiols. The SAM is therefore referred to as a mixed-SAM. A mixed-SAM may be formed by thiols with different headgroups (HG) or chain length (n) as summarized in Table 1.5.

Spacers	Difference
Alkyl + Alkyl	**n**[11,323,325,329,330,334,336,342,388]
	HG[1,11,12,320,334,336,344,345,347,389,390]
Alkyl + Alkyl-PEG	**n**[11,12,26,364,391,392]
	HG[11,12,26,364,391,392]
Alkyl-PEG + Alkyl-PEG	**n**[2,16,26,364]
	HG[2,16,364]

Table 1.5 – Different combinations of thiolate mixed-SAMs reported in the literature.

1.2.1.1.4.2 Purpose

There are at least two purposes for building mixed-SAMs instead of single-component SAMs :

First, mixed-SAMs allow the fine-tuning of the surface's physicochemical properties by adapting the ratio between the two thiols. Thus, for instance, the mixing of different hydrophobic and hydrophilic thiols has been used to control the overall hydrophilicity of a gold surface.[333]

Second, a mixed-SAM may lead to an increase in reactivity by spacing target-binding functional headgroups with non-reacting (diluting) headgroups. Though this may seem counter-intuitive at first, many papers have shown that having more reactive functional headgroups at the surface did not necessarily lead to a greater overall reactivity. This is often attributed to steric hindrance or interactions (hydrogen bonding) between close-packed reactive headgroups. Thus, diluting the reactive thiols with a non-reactive one can result in an enhanced overall reactivity, due to a greater availability of the reactive sites.[1] This is also an argument in favour of introducing longer PEG chains (less rigid and close-packed than alkyl chains, therefore having headgroups more available) in shorter alkylthiol SAMs.[11]

1.2.1.1.4.3 Properties

Mixed-SAMs are complex systems that present interesting properties. Among them, it should be noted that the surface ratio between the two thiols in the SAM (after self-assembly) may be very different from the ratio of the thiols in solution (before self-assembly).[393] Furthermore, phase segregation can occur leading to the existence of domains enriched with one or the other thiol at the surface.[393] Studies of different alkylthiolate mixed-SAMs report that :

- For methyl-terminated thiols, phase segregation occurs in ethanol when the difference in chain lengths exceeds a certain value N_{min} which depends on the temperature. At room temperature $N_{min} \approx 4$ while at 50°C $N_{min} \approx 8$.[331,342] Furthermore, phase segregation may occur as a function of the solvent if both molecules are not solvated equally.[393]
- Concerning thiols with same length but different headgroups, reports of MUA/C9-CH3 and MUA/11-mercapto-1-undecanol (MUOH) mixed-SAMs in ethanol show that the surface ratio of both thiols is generally in good agreement with the solution ratio, as evidenced by XPS[320,336,344,390] and PM-IRRAS.[336,344,389]
- Phase segregation does not seem to occur between co-adsorbed MUA/MUOH,[344] MUA/C11-CH3[345] or MUOH/C11-CH3 in ethanol.[345] However in the last two examples, when mixed-SAMs were prepared by a gradient immersion followed by back-filling, different domains appeared.[345]
- Moreover, relationship between the binding efficiency of mixed-SAMs and their composition is a matter of debate. Haussling et al.[394] used biotinylated-thiol/MUOH mixed-SAMs at different ratios and found a much greater streptavidin binding on the least biotinylated SAMs. They attributed this to the greater spacing between biotin headgroups that should minimize steric hindrance for biorecognition. As we will see in the results of this thesis, our results do not suggest the same as we achieved high streptavidin binding with a pure biotinylated SAM. The binding efficiency in our case was not improved by SAM dilution. In another report on mixed-SAMs reactivity[334] it is suggested that some mixed-SAMs may lead to a greater binding of a given protein albeit with a lower amount of subsequent biorecognition by a further antibody.

Given the above-mentioned comments on reported works on mixed-SAMs it seems reasonable to say that a general consensus on mixed-SAMs composition, structuration and specially reactivity has not been reached. Moreover, concerning reactivity towards proteins, given the complexity of the latter, it is possible that optimum conditions of the mixed-SAMs might not apply from one study to another (from one protein to another). We can rather imply that such optimization should be made for each precise case, that is for each precise biological test.

1.2.1.2 Different protocols

So far we have seen that a great diversity of thiols can be used to build SAMs on gold but we have not mentioned *how* this functionalization can be achieved. In the following paragraphs we will briefly summarize different protocols reported in the literature to build these SAMs from a liquid or gas phase.

1.2.1.2.1 From solution

An easy way to form thiolate SAMs on a gold surface is to immerse the sample (gold substrate) into a liquid solvent containing the desired thiols at room temperature. The most common solvent to form SAMs from alkylthiols as well as PEG-thiols is pure ethanol, although other solvents are also reported such as water/ethanol mixture,[19,314] THF,[390,395] chloroform,[356] DiMethylFormamide (DMF),[314,395] hexadecane,[395] carbon tetrachloride (CCl_4),[314,395] DiChloroMethane (DCM),[356] diethyl ether,[356] cyclooctane,[395] toluene,[395] acetonitrile,[314,356,395] ethyl acetate,[356] bicyclohexyl[396] and even a pure thiol liquid.[395] Reports on the use of different solvents[314,395] show that SAMs can be formed from all of the above. Whether one is preferable to another seems to depend on which molecule is used for the SAM as well as which

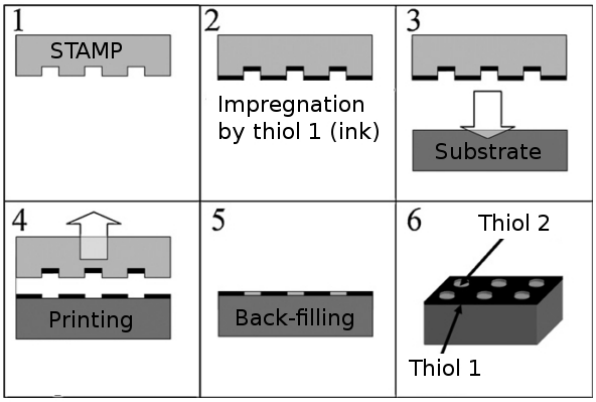

Figure 1.12 – Micro-contact printing. Adapted from.[411]

characteristic is desired so that general rules on this matter do not seem to be established. It is reasonable to believe that ethanol, for its commercial availability, its low dangerosity and extensive reports with this solvent will continue to be the most common solvent for building alkanethiolate SAMs on gold. In the following paragraphs we will focus on ethanolic thiol solutions.

Studies of thiolate SAM formation kinetics in ethanol as a function of thiol concentration[367,395,397–399] infer the following characteristics :

- Thiols adsorb on gold very fast even at very low concentrations (less than a minute in less than 1 mM).[367]
- Ordering and close-packing of the SAM takes more time than the initial adsorption. Some reports suggest that it remains nevertheless a relatively fast process, as the final physicochemical properties of the surface are quickly reached ($\approx 30min$ in $\leq 1mM$).[367] Indeed, in order to have distinct SAM islands on the surface (low coverage) from a thiol solution, the concentration and immersion time have to be very small (eg : 2µM and 10s).[399] However, others suggest that it can take several hours or days for the SAM to adopt its final crystalline configuration.[302,304]
- Thiols go through a lying-down phase before self-assembly in the standing-up phase.[397]
- Thiols can also undergo lateral diffusion on the surface.[399]

A survey of recent publications shows that most protocols use concentrations of 1-10mM with functionalization times of 3-24h.[389,398,400–406] This may be "more than needed"[367] but no evidence of a negative impact of high concentration or functionalization time is found in the literature.

Microcontact printing (μCP)[407] represents an alternative to the simple immersion method to form SAMs from a liquid solvent. μCP consists in a two step process : first, the surface of a topographically patterned elastomer (usually PDMS) stamp is brought in contact with a thiol solution (*ink*) and second, the PDMS surface, with its ink layer is *stamped* on the gold substrate (see Fig. 1.12). The result of this process is the formation of SAMs at different regions of the substrate. This can be used to form mixed-SAMs, if the non-functionalized regions are *backfilled* by immersion into a solution of a different thiol.[298,408–410]

1.2.1.2.2 From gas phase

Thiolate SAMs can also be formed by adsorption from a gas phase in ultrahigh vacuum.[303,412] This method is not as widely used as the adsorption from a liquid phase though, as it is more difficult to implement and often yields less densely packed SAMs.[302] However, adsorption from a gas phase has been used to obtain fundamental information about the SAM formation mechanisms and kinetics, specially at the early stages. Some of the fundamental characteristics that will be detailed in section 1.2.1.3.2 could only be evidenced by formation from an Ultrahigh Vacuum (UHV) gas phase. Furthermore, from an UHV phase, there is no competing solvent-substrate or solvent-thiols interactions which can hinder the formation of the SAM.[302]

1.2.1.3 Summary and main characteristics of SAMs on gold

As we have seen in the previous paragraphs, gold surfaces can be functionalized with many different SAMs (see section 1.2.1.1) formed in different conditions (see section 1.2.1.2). However, since the introduction of these systems, some choices have been much more widely spread and become a sort of "standard". In the following paragraphs we will summarize these common choices and give some fundamental characteristics about the so-formed SAMs.

1.2.1.3.1 Towards a standard protocol for gold functionalization

From the comments and number of cited papers in sections 1.2.1.1 and 1.2.1.2 we can conclude that for most applications requiring gold functionalization (specially in biosensing technology) SAMs are formed from adsorption of **thiols** in **ethanol** at a concentration of around **1-10 mM** during **3-10 h**. These thiols usually have an alkyl or alkyl-PEG (specially for anti-fouling) spacer with common lengths of around **6-16** methylene units (**10**, **11** and **16** being specially common) and **3-6** Ethylene Glycol (EG) units in the case of alkyl-PEGs. The most common headgroups for biosensing applications are **COOH** (often activated by **NHS-ester**) and $\mathbf{NH_2}$ for biomolecule binding and **OH** and $\mathbf{CH_3}$ for anti-fouling. Eventually, mixed-SAMs are also widely used, often combining a target-binding thiol and a **diluting** one to separate the reactive sites at the surface. These are commonly formed by two alkylthiols or an alkylthiol and a PEG-thiol.

Obviously, this short summary does not mean that all the other alternatives cited in the previous sections do not deserve our attention but for reasons that probably include simplicity, previous knowledge and experience as well as economic cost, these are the most common choices made for gold functionalization.

1.2.1.3.2 Characteristics of thiolate SAMs on Au(111)

So far we have adopted a rather "practical" point of view and not discussed in much detail the most fundamental aspects of SAM formation. However, questions such as *what is the nature of the Gold-SAM bond? what is the nature and kinetics of the intermolecular forces that drive the formation of a close-packed SAM?* or *what are the SAMs' most common defects and how do they relate to the substrate's characteristics?* have been and still are a matter of active research[302,413–423] that we shall briefly summarize in the following paragraphs. We shall limit this study to SAMs formed by alkylthiols on Au(111) substrates, which is the most commonly obtained orientation by methods such as e-beam evaporation.

1.2.1.3.2.1 Mechanisms, energetics and kinetics of SAM formation

The formation of SAMs of alkanethiols on gold involves three kinds of interactions : [9]
- Van der Waals forces between the alkyl chain and the gold substrate (physisorption), on the order of 40-100kJ/mol.[413]
- Chemisorption of the sulfur atom on gold (iono-covalent bond), on the order of 80-200kJ/mol.[302,413,424,425]
- Van der Waals forces between adjacent alkyl chains, on the order of 4-8kJ/mol per methylene unit.[426]

The mechanism of alkanethiols SAM formation on gold has been described as a two-step process involving :

1. A **"striped" phase** where thiols are lying down on gold with a low surface coverage. This stage can actually be divided into two sub-stages :

   (a) First, thiols (retaining their SH group) are physisorbed through Van der Waals interactions between the alkyl chains and the substrate in a metastable state.

   (b) Eventually the sulfhydryl group is "activated" (dissociated) by the gold surface and the so-formed thiolate is covalently (and fully reversibly) bound onto gold (the activation energy is on the order of 30kJ/mol whereas the reverse cleavage of the Au-S bond is on the order of 120kJ/mol).[302] Thus, for chemisorption to occur, the thiol must first be sufficiently strongly physisorbed onto the surface. This explains that short alkanethiols are harder to graft on gold as their weak physisorption may kinetically prevent their subsequent dissociation into a thiolate form that could be chemisorbed (ie : they do not stick long enough).[302] It is also interesting to note that for chains longer than ca. 6 methylene units, the energy barrier to go from a physisorbed thiol to a thiolate is lower than the energy needed to desorb the thiol.[302] This discussion is best summarized in Fig. 1.13.

2. A **crystalline phase** where thiols are standing upright (with a given angle to the surface that will be discussed later) and the chains are close-packed (high surface coverage) by Van der Waals interactions between them. This upright phase occurs only after the completion of the lying down phase[304] and it can take hours or days depending on chain length.[304]

1.2.1.3.2.2 Surface arrangement and density on Au(111)

The pseudo-crystalline arrangement of thiols on Au(111) surfaces has been well documented. It is widely accepted that thiolate SAMs on Au(111) arrange on a $\sqrt{3} \times \sqrt{3}$ R30° lattice (positions of the sulfur atoms on the gold lattice) yielding thus a surface coverage of $\Gamma_s = 1/3$ (one sulfur atom for every three gold atoms) as shown in Fig. 1.14. The orientation of the alkanethiols can be defined by three angles : the tilt angle, α, being the angle between the alkyl backbone and the surface normal ; the twist angle, β, being the angle between the plane of the CCC bond and the plane defined by the surface normal and the alkyl backbone and finally the

9. For thiols having a polar head group hydrogen bonding should also be considered, though the basics of SAM formation should remain the same. The importance of head group's polarity will rather be addressed when discussing phase segregation in mixed-SAMs.

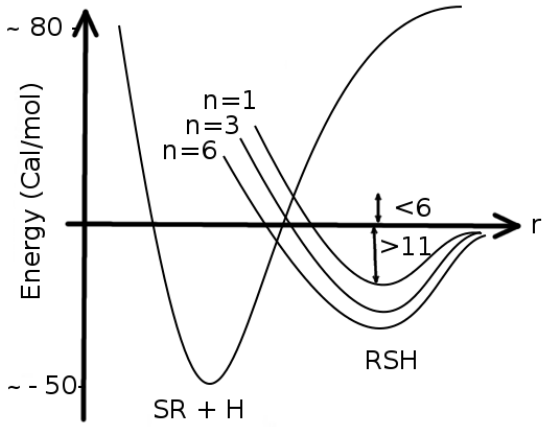

FIGURE 1.13 – Schematic representation of binding energies of thiols and thiolates on gold. Adapted from.[427]

precession angle, χ_t, being the angle between the projection of the alkyl backbone on the surface and the axis between adjacent sulfur atoms in the susbstrate's cristallographic axis[303] (see Figs. 1.15a and 1.15b). Alkanethiols are found to adopt rather well-defined values for these angles : $\alpha \approx 30°$ $\beta \approx 55°$ and $\chi_t \approx 14°$. As can be seen in Fig. 1.14, the alternating orientation of the alkyl chains defines a c(4×2) superlattice structure. This arrangement seems to be independent of the functional head group, as it has been observed not only with methyl-terminated thiols but also with COOH[428] and NH_2[429] terminated ones.

1.2.1.3.2.3 SAMs' defects

It is common to represent a SAM as a homogeneous and perfectly crystalline organic layer (see Fig. 1.10 at the beginning of this chapter). However, a more realistic representation of the self-assembly result of thiols on gold can be found in Fig. 1.16.

Some of these defects are directly linked to the substrate : cleanliness (thiols may not be able to displace an adsorbate on the surface), grain boundaries and atomic steps being some of them. Other are in fact due to the dynamic nature of the SAM itself. Indeed thiols in SAMs may experiment different phenomena such as desorption, lateral diffusion or multi-layer adsorption. For more information about defects in SAMs the reader is referred to the corresponding paragraphs of published reviews.[302,304]

1.2.1.3.2.4 Current issues

Although many fundamental studies have been carried since 1983, there is still a number of issues under current debate, which include :

– ***The exact mechanisms involved in the cleavage of the sulfhydryl group and bonding on gold :***
The transition between the physisorbed thiol on the gold surface and its subsequent chemisorption can be written as such :
$RSH_{phys}Au \longrightarrow RS-Au + 1/2\, H_2$

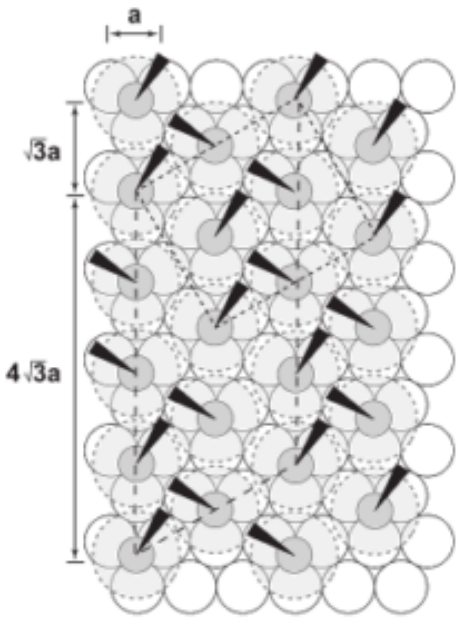

FIGURE 1.14 – Structural model of the commensurate adlayer formed by thiols on the gold lattice. The arrangement shown is a $\sqrt{3} \times \sqrt{3}$ R30° structure where the sulfur atoms (dark gray circles) are positioned in the 3-fold hollows of the gold lattice (white circles, a = 0.288nm). The light gray circles with the dashed lines indicate the approximate projected surface area occupied by each alkane chain ; the dark wedges indicate the projection of the CCC plane onf the alkane chain onto the surface. Note the alternating orientation of the alkane chains defines a c(4×2) superlattice structure. The formal c(4 × 2) unit cell is marked (long dashes), an equivalent $2\sqrt{3} \times \sqrt{3}$ unit cell is marked by lines with short dashes. The alkane chains tilt in the direction of their next-nearest neighbors. Figure and legend originally published in.[302]

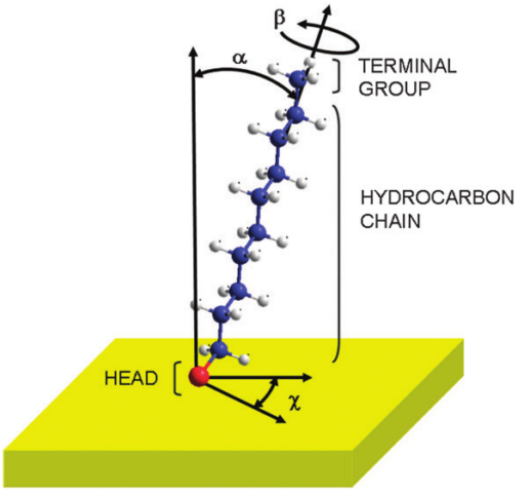

(a) Figure originally published in.[304]

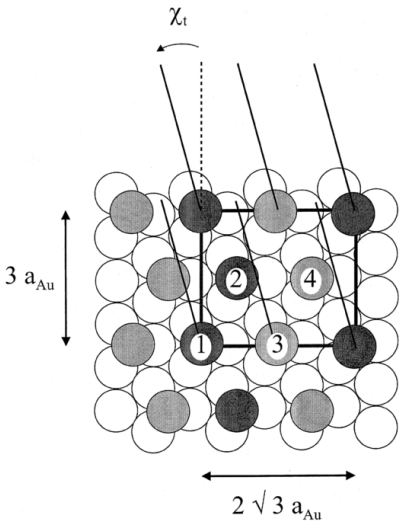

(b) Figure originally published in.[303]

FIGURE 1.15 – Tilt, twist and precession angles of alkanethiolates on gold.

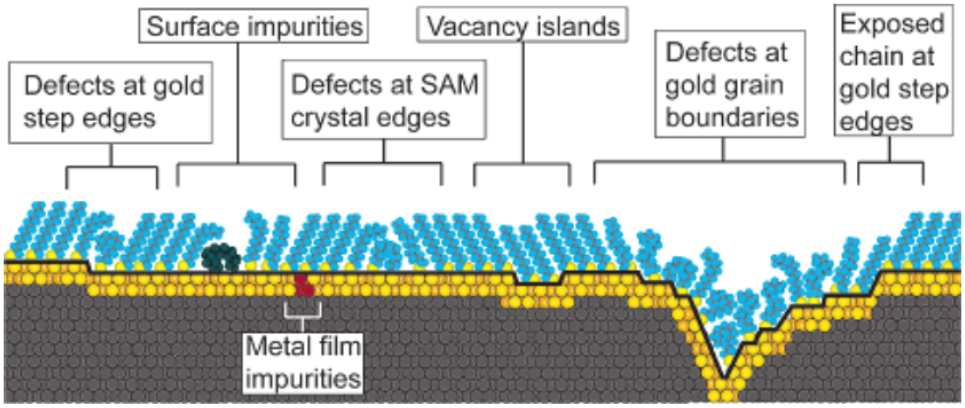

FIGURE 1.16 – Schematic illustration of some of the intrinsic and extrinsic defects found in SAMs formed on polycrystalline substrates. The dark line at the metal-sulfur interface is a visual guide for the reader and indicates the changing topography of the substrate itself. Figure and legend originally published in.[302]

However, the exact mechanism involved in this reaction has not been clearly identified. The most common explanation is that the process relies on an oxidative adsorption of the S-H bond by the gold substrate[430] followed by a reductive desorption of the hydrogen :
$RSH + Au^0 \longrightarrow RS^-Au^+ + 1/2\, H_2$
It is not explained though, what species are involved in this oxidative process (ion, radical... etc[304]). Moreover whether the SH group is dissociated at all is still under debate for short thiols.[431]

– ***The fate of the hydrogen atom from the cleaved sulfhydryl group :***
The previous discussion on chemisorption implies a desorption of hydrogen in the form of H_2. This has been hypothesized for a long time without clear evidence.[432]

– ***The existence of a striped phase in solution :***
Striped phases have been observed in UHV. The existence of such phases in solution has been a matter of active discussion.[302,303] In-situ Atomic Force Microscopy (AFM) studies[397] have shown that thiols go through a low-coverage lying-down phase in solution too, although it is not clear if they adopt a long-range ordered structure as in UHV.

– ***The reconstruction of the gold surface upon SAM formation :***
The exact position of the sulfur atoms in regard to the Au lattice are a matter of current debate, specially since it was suggested that the gold surface itself undergoes reconstruction presenting vacancies and adatoms upon thiolate bonding.[304]

– ***Stability of mono and polythiols :***
From a more pragmatical point of view, because of the reversibility of the Au-S bond, it has been suggested that polythiols can be used to enhance the stability of the so-formed SAMs.[308] However, the stability has not been found to monotonically increase with the number of thiol head groups as competing disulfide bonds can hinder the anchoring on gold.

1.2.2 Silica functionalization

Silica surfaces can also be chemically functionalized by covalently grafting organic molecules. As presented for gold, these molecules typically have a surface-binding headgroup, a spacer chain and a functional headgroup. Typical spacer chains include alkyl and PEG chains, and common functional headgroups are also similar to those found on thiols and presented in section 1.2.1.1. For this reason, and also because the study of silica functionalization represents a much lesser part of the work developped during this PhD, we will not go in such a great detail of literature reports as we have done concerning gold functionalization. Nonetheless, let us briefly present those aspects of silica functionalization that depart from the gold case, namely the choice of the binding headgroup and differences in standard protocols.

1.2.2.1 Silanes

The main difference between silica and gold functionalization is obviously the choice of the headgroup used to covalently bind the molecule onto the substrate. The grafting of a molecule on silica (and other oxides) involves hydroxyl groups at the surface (silanols, Si – OH, in the case of silica).

These hydroxyl groups at the surface of the oxide can form siloxane bonds (Si – O – Si) with a silane as presented in Fig. 1.1 :

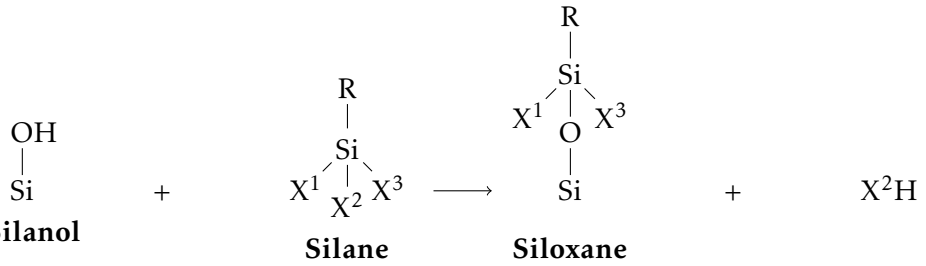

Scheme 1.1 – Simplified reaction scheme for silanization of silica surfaces. This reaction may result from direct condensation (as shown) or with an intermediate silanol group on the silane, resulting from hydrolysis of the X^2 group (not shown).

This reaction, often referred to as silanization or silanation (of the surface), requires that at least one of the X^i groups (X^2 in scheme 1.1) may be dissociated (hydrolysed). To this end, the most common X^i groups are alkoxy ($CH_3 - (CH_2)_n - O$)[433–436] and chlorosilanes (X=Cl).[434,436–438] Furthermore, it has been suggested that nitrogen-containing head groups such as dimethylsilazane or dimethyl(dimethylamino)silane can yield better bonding.[439]

Eventually, because silicon is tetravalent there are, as presented in scheme 1.1, three different X^i groups in alkylsilanes. This leaves the possibility of having one, two or three groups which can form siloxane bonds (the corresponding silane is often called monofunctional, bifunctional or trifunctional respectively). Multifunctional silanes can in principle bind to a greater extent on oxide surfaces while monofunctional silanes may yield sub-monolayer coverages. However, by the same hydrolysis/condensation reaction multifunctional silanes may also polymerize (siloxane bonding between silanes) in solution. Monovalent silanes may also form siloxane bonds between them but only form dimers with no X^i groups susceptible to hydrolysis, so that these dimers cannot covalently bind onto the surface anymore and are therefore washed away.

1.2.2.2 Protocols

As in gold functionalization, silanization is usually carried out by immersing the sample surface into a dilute solution of silanes in an organic solvent. However the choice of the solvent and experimental conditions is somehow more delicate than for thiols on gold because of the competing hydrolysis/condensation of silanes in solution (polymerization) as already mentioned. Organic solvents used for silanization include : toluene,[435,437,438,440,441] ethanol,[433] xylene,[439] pentane,[441] bicyclohexyl,[396] acetone,[442,443] CCl_4,[439,441] benzene,[441] cyclooctane,[441] hexadecane,[441] octane,[441] cyclohexane,[441] hexane,[441] dioxane[441] and dichloromethane.[441]

These solvents are either dried,[440] used in normal conditions (neither dried nor mixed with added water) or mixed with ultrapure water.[442,443] Additional curing steps are sometimes undertaken, heating the sample above 100°C for cross-linking of the layer.[439,440]

In order to partly circumvent some of these issues, silanization from a gas phase has also been investigated.[444,445]

1.2.2.3 Summary and main characteristics of SAMs on silica

Given the large differences in reported protocols of silanization, it is reasonable to conclude that this process is somehow more complex than gold functionalization with thiols due to the possible siloxane bonding of silanes in solution leading to polymerization (multifunctional silanes) or dimerization (monofunctional silanes). Indeed, it seems that the amount of water, the temperature, the hydroxylation of the surface and the nature of the silane (specially monofunctional vs polyfunctional) can affect the formation and stability of the organic layer. However, *how* exactly each of these parameters affect the final result is still a matter of debate.[439]

1.2.3 Chemical characterization

There are several tools to probe the chemistry of self-assembled monolayers at a solid surface. These can roughly be separated by the kind of information that they provide : [10]

1. Average information on the physicochemical properties of the surface (e.g., surface charge or hydrophilicity).
2. Average chemical and structural composition of the organic layer (e.g., ratio of different molecules in mixed-SAMs or general degree of hydrogen bonding between headgroups).
3. Local information about the layer composition and organization (e.g., phase segregation in mixed-SAMs or pinhole defects).

It is not the purpose of this section to give extensive details about these techniques but rather to understand what kind of information can be obtained by them. Of all the following tools, only those that were used to obtain the results presented in this manuscript will be explained in more detail in the next chapter and corresponding appendixes.

10. Depending on the use that is made of each of these tools, different informations can be obtained which, of course, make this separation somehow questionable. However it is obvious that some tools are better suited for obtaining some information than others and it is in this "general" case of "standard" use of the tools that this classification is made.

1.2.3.1 General physicochemical properties ("macroscopic methods")

This section quickly describes *macroscopic* methods for the characterization of SAMs on homogeneous planar surfaces. These methods do not give direct chemical information about the surface but rather physical properties such as wettability, thickness or electrical behaviour of the SAM, which have to be linked to the chemical composition under some assumptions. The SAMs considered here are typically formed from *small* organic molecules (chain length of around 10 methylene units). For bigger molecules, other methods commonly employed in biosensing technology such as Surface Plasmon Resonance (SPR)[446] or Quartz Crystal Microbalance (QCM)[335] may be used.

1.2.3.1.1 Contact angle

The contact angle of a liquid drop with a surface directly translates the surface wettability (hydrophilicity in the case of water), which can be related to the presence and composition of a SAM. Thus, contact angle measurements (goniometry) are usually undertaken as a rapid mean to prove the success of the functionalization, followed by more in-depth characterizations such as different spectroscopies.[447–449]

However, despite its apparent simplicity, careful examination of contact angle measurements have been used to determine important characteristics of SAMs, such as :

- The odd/even effect[302,360–362] that was previously discussed within the considerations of the spacer chain lenghts in paragraph 1.2.1.1.2 and that suggests that alkanethiols of different lengths form SAMs with a well-defined tilt angle.
- The relative amount and mixing of different molecules in mixed-SAMs.[450–453]
- The effect of pH on the functional head group.[405]
- The effect of different parameters (time, solvent, concentration, substrate cleanliness) on SAM formation.[395]

1.2.3.1.2 Ellipsometry

Ellipsometry provides information about a thin film's thickness (given its refractive index) which can be used as a method for SAM characterization. The most straightforward used of this method is to link the so-measured thickness to the chain length of the molecules. It can therefore be used as a routine characterization to prove the formation of a SAM and check the absence of adsorbed multi-layers.[448] It can however also be used for more in-depth parametric investigations on SAM formation (as a function of time, concentration, solvent or substrate "cleanliness").[395]

As contact angle goniometry, ellipsometry is however rarely used as the sole characterization method of a SAM but rather followed by some spectroscopy (XPS, Infrared (IR)) to probe the chemical composition of the surface in more detail.[448,449,454,455]

Eventually, it should be noted that conducting ellipsometry measurements on typical SAMs having a thickness of less than 2nm can be cumbersome as the potential errors on the measurements become close to the total measured thickness. As the values given by this technique rely on the input model given for the layer that has to be characterized, they may be more questionable than the values given by other *direct* techniques.

1.2.3.1.3 Electrochemistry

Electrochemistry -Cyclic Voltametry (CV) or Electrochemical Impedance Spectroscopy (EIS)- has been used to characterize alkanethiolate SAMs on gold. It is for instance possible to link the electronic (blocking) properties of the SAM to its thickness (thicker SAMs are obviously less conducting), its packing density or the presence and nature of defects.[456]

1.2.3.2 Average chemical and structural composition (spectroscopies)

Spectroscopy's main advantage over the previously cited methods is that it provides *relatively* unambiguous information about the chemical composition of the surface. Different spectroscopies are therefore widely used in the characterization of SAMs on planar substrates, that we shall briefly describe hereafter. From a spatial resolution point of view, these techniques can be either macroscopic (the irradiated region -beam spot on the surface- being over $1mm^2$) or offer micrometric resolution if the beam can be focused on that scale.

1.2.3.2.1 Infrared spectroscopy

Infrared spectroscopy is based on the absorbtion of infrared photons by chemical bonds (excitation of different vibration modes). It is therefore very useful in determining the structure of molecules grafted on a surface. Examples of typical bonds evidenced in SAMs through IR spectroscopy include CH_3, CH_2, O = C – NH (amide), COOH, COO^-, and C – OH. Furthermore the exact position (excitation wavenumber) and shape of the peaks can yield valuable information about the environment of the molecule. For instance C = O vibration modes of terminal carboxylic acids have different positions depending on the hydrogen-bonding with an adjacent group.[457–459] Similarly, CH_2 vibration modes of alkyl chains shift with the presence of an adjacent chain, so that the position of the peak can translate the degree of order and close-packing in the SAM.[335,344,460]

PM-IRRAS is an important development of IR spectroscopy for probing metallic surfaces, which will be discussed in the next chapter and corresponding appendix.

1.2.3.2.2 Raman spectroscopy

Raman spectroscopy is similar to IR spectroscopy in the sense that it uses infrared radiation to excite vibration modes of chemical bonds. However, in Raman spectroscopy, the infrared photons are scattered in an inelastic way (Stokes or anti-stokes scattering). Therefore some chemical groups may give a weaker or stronger signal in one or the other method. Surface-Enhanced Raman Spectroscopy (SERS) is an important development of Raman spectroscopy that can be very useful in the characterization of SAMs.[461]

Moreover, Tip-Enhanced Raman Spectroscopy (TERS) is a very promising technique also based on Raman spectroscopy, but we shall discuss its potential separately in section 1.2.3.3.

1.2.3.2.3 XPS

XPS is another widely used method for the characterization of SAMs. XPS probes the binding energy of core-level electrons in atoms. Thus, it is in principle an *elemental* characterization tool as opposed to IR or Raman spectroscopies. However the exact values of these binding energies also depend on the surrounding electronic environment (chemical bonds in which the given atom takes part) ; i.e., the binding energy of 1s orbital of a carbon atom in an alkyl chain

(C1s level of C-*C*-C) is different than that of 1s orbital of a carbon atom in a PEG chain (C1s level of C-*C*-O).[19] Therefore, XPS is also used to determine the chemical composition of molecules on a surface. This explains that XPS is also known as Electron Spectroscopy for Chemical Analysis (ESCA).

1.2.3.2.4 ToF-SIMS

ToF-SIMS, whose principle will be detailed in the next chapter, is a very sensitive surface analysis method that can be used to characterize SAMs and monitor its formation kinetics.[462]

1.2.3.3 Localized nanometric information (scanning probe microscopies)

Scanning probes microscopies, which could in fact be referred to as *nanoscopies*, are very important in the investigation of self-assembled monolayers. With their nanometric spatial resolution, they are specially suited to investigate such questions as the mixing or phase segregation of molecules in mixed-SAMs or the existing of a lying-down low-coverage phase in self-assembly.

1.2.3.3.1 STM

Scanning Tunnelling Microscopy (STM) has been widely used to study alkanethiolate SAMs on gold.[321,322,325–327,331,340,354,378,463,464] The use of STM has specially been crucial in early fundamental studies of SAM formation showing evidence of different low-coverage and high-coverage phases and crystalline arrangements as well as defects both in one-component and binary (mixed) SAMs. A review entirely devoted to such investigations by STM was published in 1997 by Gregory E. Poirier.[412] STM remains a reference tool nowadays for investigation of more complex SAMs.[465]

1.2.3.3.2 AFM

AFM might be the most widespread scanning probe microscopy. A reason for this is that it can work on very different materials, unlike STM which requires a conducting substrate for instance, and under different conditions (vacuum, air or liquid). AFM has been used in the past and is still widely used to characterize different SAMs.[331,332,335,466,467] The in-situ evidence of low-coverage phases during thiolate SAM formation from solution is an example of an important contribution by AFM measurements to the knowledge of SAM formation.[397]

As a consequence of AFM versatility, there have been numerous variations of the *standard* AFM, that correspond to different functionalities of the tip such as Piezoelectric Force Microscopy (PFM) or Magnetic Force Microscopy (MFM). Among them, Chemical Force Microscopy (CFM) -not to be mistaken with Conductive Atomic Force Microscopy (C-AFM)- is specially interesting for probing surface functionalization.[468]

1.2.3.3.3 TERS

In a nutshell, TERS is the combination of Raman Spectroscopy and AFM. Indeed, in a TERS experiment, a far-field beam is coupled to a local probe (modified AFM tip) to irradiate only a small region (down to ca. 10nm x 10nm) of the surface that will provide a Raman signal. This technique is very promising as it combines the best of both worlds : unique spatial resolution with unique spectral signatures for identification of different molecules. A remarkable example by Stadler et al.[410] shows how TERS can clearly distinguish domains of different thiolate isomers deposited on a surface through microcontact-printing and back-filling. TERS is a rather recent method which requires very careful considerations in the tip and setup design.[469]

1.2.3.4 Summary of characterization methods

The aforementioned techniques are summarized with some of their characteristics in Table 1.6. The values given in this table are obviously only indicative and do not reflect all the complexity of each method, whose performances may vary depending on different parameters such as the precise device technical characteristics or the exact material being probed.

Technique	Principle	Information	Depth of analysis	Spatial resolution	Sensitivity
Contact angle	Angle measurements of liquids wetting a surface	Surface energy	0.3-2nm	1mm	Depends on chemical composition
Ellipsometry	Refractive index	film thickness, dielectric constant, phases changes	10nm	10-100µm	sub-monolayer
Electrochemistry (EIS, CV)	C-V, I-V curves	Electric properties (impedance, capacitance)	0.1nm	-	sub-monolayer
IR spectroscopy	Molecular vibration	Chemical	1-5µm	10µm	0.1 monolayer
Raman spectroscopy	Inelastic scattering (molecular vibration)	Chemical	depends on material, typically ≥ 100nm	1µm	sub-monolayer
XPS	Photoelectronic effect	Chemical, elemental	2-5nm	10-50µm	0.1 - 1% of a monolayer
ToF-SIMS	Ion sputtering	Chemical	1nm	sub-micrometer	10^{-5} of a monolayer
STM	Electron tunnelling	Elemental	0.1nm	0.1nm	-
AFM	Local non-covalent bonds interactions	Surface topography map, elasticity, friction, other forces depending on the tip functionalities	0.2-0.3nm	0.1nm	-
TERS	Raman spectroscopy coupled with local probe	Chemical	0.2-0.3nm	10nm	-

Table 1.6 – Summary of different surface chemistry characterization tools.

1.3 Orthogonal functionalizations of heterogenous substrates and its applications

1.3.1 Introduction to orthogonal functionalizations

Building SAMs on plain gold and silica surfaces is now a rather common procedure known for a few decades (though some fundamental questions are still open to debate and optimal conditions or "standard protocols" -specially for silanization- have not been clearly shown). However, in many nanotechnology fields such as biosensing, the current trend leads to complex devices with heterogeneous (patterned) surfaces. Periodic gold nanostructres on a silica surface, for instance, can serve as an Localized Surface Plasmon Resonance (LSPR)-based biosensor.[470] The main challenge from a functionalization point of view is thus to achieve the building of different SAMs selectively onto the different materials at the surface. This process has been designated as *orthogonal functionalizations*[302] or *site-selective patterning*[471] in the literature. [11]

1.3.2 Reported examples of orthogonal functionalizations

Gold structures on silica (or other metallic structures on oxide) is quite a common case as it may have different applications in optics and electronics. Different uses of orthogonal functionalization on these patterned substrates can be found in the literature. We will briefly present some of them hereafter :

- Laibinis et al.[472] were the first, to the best of our knowledge, to present orthogonal functionalizations of micropatterned gold/oxyde surfaces.

- Our group reported the use of MUA and PEG-silane on patterned gold on glass (millimetric patterning) for the selective binding of magnetic bead filaments onto the gold regions.[299]

- Pradier and co-workers[442] worked on 100µm diameter SiO_2 areas surrounded by gold. The silica regions were biotinylated while the surrounding gold was rendered inert with OEG. This allowed specific binding of streptavidin onto the silica regions, followed by biotinylated anti-rIgG. Eventually, the specificity of bio-recognition onto the silica regions was monitored by fluorescence (targets were fluorescently labeled). Though discarded in the article, it is however reasonable to question the lack of fluorescence quenching on possibly adsorbed targets on gold.

- Udo Bach and co-workers[27,300,473,474] used orthogonal functionalizations for the nanometric precise placement of gold colloids. Using thiolated DeoxyriboNucleic Acid (DNA) and PEG-silanes, they achieved almost single-particle capture with 40nm beads and less than 1% of non-specific adsorption (beads adsorbed on silica surrounding gold nanostructures) on millimetric overall surfaces.[27] This methodology, combined with elec-

11. From the given references, orthogonal functionalization designates a broader concept including the building of different self-assembled monolayers on a homogeneous substrate (eg : through micro-contact printing and backfilling). However, unless otherwise specified we will refer only to heterogeneous substrates with material-selective functionalizations.

trostatic interactions between DNA-modified beads and aminofunctionalized gold, was used to develop a complex "Gutenberg-style printing of Self-Assembled Nanoparticle Arrays".[300]

– Yutaka Majima and co-workers[475–477] used dithiols to bind gold nanoparticles on the gap between two gold electrodes. This methodology is surprising, since it relies on the fact that the dithiols will bind onto the colloid particle and onto the electrode, instead of binding by both endgroups onto the same surface. In fact, the dithiols were inserted into previously thiol SAMs on the electrodes, which may explain that one of the thiol extremities remained free to bind the colloidal particle instead of having the dithiol bind twice onto the electrode. Anyhow, they achieved single particle capture on the gap of the electrodes, which resulted in the realization of a Single Electron Transistor (SET) ; where the colloidal gold particle behaves as a Coulomb island. This work, however did not use functionalizations on the surrounding surface to limit non-specific adsorption.

– Höök and co-workers[28,478,479] used orthogonal functionalizations of Au/SiO_2 and Au/TiO_2 patterns to enhance the sensitivity of LSPR biosensors. They modified gold and oxide surfaces with an SH-PEG and Poly-L-Lysine (PLL)-g-PEG respectively, each of which could be biotinylated or not. Depending on which PEG beared a biotin moiety, they could control the binding of NeutrAvidin onto one or the other material, demonstrating the enhanced sensitivity of the sensor when gold was rendered "bioactive" (biotinylated).

– With the same functionalization (SH-PEG(-biotin) and PLL-g-PEG) and nitrodopamin-PEG-biotin (to bind onto TiO_2 via the catechol group), Zhang et al.[480] achieved streptavidin localization at the hotspots of plasmonic nano-antennas.

– In a similar, though simpler (and somehow more questionable) approach, Kumar et al.[29] adsorbed PLL-g-PEG on a patterned silicon nitride / gold surface, followed by streptavidin immobilization which according to the authors is meant to replace the PLL-g-PEG on the gold regions while having no effect on the silicon nitride regions. Though this assumption is questionable, the authors report it as a mean to localize biotinylated vesicles into LSPR supporting gold regions.

1.3.3 Conclusions and perspectives of orthogonal functionalizations

As we can see from this literature survey, the orthogonal functionalizations of patterned gold on silica (or other oxides) has already been undertaken by a few groups throughout the world. It seems that this methodology is gaining importance since 2010. Indeed, the articles of Lalander et al.[27] and Feuz et al.[28] in ACS Nano are very good examples of the issue presented in this thesis. Both show how orthogonal functionalizations can be used either for the precise placement of colloids[27] or the enhancement of LSPR-based biosensor with selective capture of target proteins on sensitive areas.[28] Despite further improvements since 2010,[300,473,474,479] a number of points can still be raised, which, to the best of our knowledge are not yet fully answered in the literature :

1. **Direct chemical characterization :** Most of the examples presented above lack direct chemical characterization of the functionalization step. This means that the measurements are taken at the end of the process, involving colloid deposition (assessed by SEM for instance) or SPR signal reading. The problem with such "end of process measurements" is that it is difficult to explain some of the results and point out which step may have failed and to what extent. For instance, in the work of Feuz et al.,[28] the authors observe an SPR signal even when only the non-sensitive oxide regions are meant to be bio-functionalized. In this case, in the absence of chemical characterization at the functionalization step, it is impossible to know if this signal is due to an imperfect orthogonal functionalization or to non-specific adsorption of target biomolecules (on a perfectly functionalized substrate). It is reasonable to think that in that precise case[28] (and even more so on the paper by Kumar et al.[29] as previously explained) the chemical functionalization may have not been perfectly orthogonal, as the PLL-g-PEG used may have adsorbed on bare or functionalized gold as well as on TiO_2, which brings us to the second point.

2. **Selective attachment layers :** It is obviously important to achieve functionalizations that are truly orthogonal. This means that the two molecules used should be highly selective towards one or the other material. It also means that washing steps may play a crucial role in removing non-specifically adsorbed molecules.

3. **Single-step functionalizations :** To the best of our knowledge, all the so-far reported orthogonal functionalizations involve two steps : functionalization of one material (+ washing) followed by functionalization of the second material. However, if functionalizations are truly orthogonal (material-selective), there is no reason why both functionalizations could not be operated simultaneously. This would greatly simplify the process, which in general is already complex if one takes into account all the steps from top-down fabrication to the final biological test.

4. **Thin attachment layers :** Moreover, for sensors based on evanescent waves (SPR), it is important that the final target be as close to the surface as possible. As such, it is important to develop chemical functionalizations with small molecules (few nm ; few hundreds g/mol) instead of -big- polymers or other macromolecules (2-3 kg/mol).[28]

5. **Diversity :** Obviously, even if we restrict ourselves to the orthogonal functionalizations of one kind of substrate (patterned gold on silica) there are infinite possibilities that are yet to be explored, regarding the functionalization itself as well as the applications. Udo Bach and co-workers[27] nicely presented the localization of gold colloids based on orthogonal functionalizations, but the use of latex beads, possibly with added functionalities such as magnetic or fluorescent properties can be an interesting branching of this methodology, specially if these beads are placed on *active* regions of a surface (eg : electrodes, plasmonic antennas or microcantilevers). Similarly, the group of Höök and co-workers[28] used orthogonal functionalizations on LSPR biosensors to detect NeutrAvidin on biotinylated surfaces. Yet, with slightly different chemistry, many other proteins can be investigated, such as cancer marker proteins. In summary, we are in front of a novel methodology,

where the proofs of concept have been clearly exposed in the last few years. Other than the previous points, which concern *improving* the method, we can expect a diversification of this method with a multitude of applications, not necessarily better than the already presented, but different.

1.4 Conclusions on the state of the art and presentation of following work

As explained in the introduction, the aim of the work that is about to be presented is to investigate the orthogonal functionalizations of patterned gold on silica substrates with different self-assembled monolayers. We have seen from the literature survey above, that many choices are available for the different tasks involved in this work. It should be recalled that this general framework is developped with the intention to serve primarily in the field of plasmonic biosensors. This application implies that gold is to be functionalized primarily for biomolecule target binding whereas silica is to be functionalized primarily for anti-fouling (passivation). The main challenges of the following work can thus be presented as follows :

1. Develop chemical protocols to achieve selective and orthogonal functionalizations on patterned gold/silica substrates.
2. Demonstrate these functionalizations with appropriate characterization methods.
3. Prove the interest of such methodology for different targets' (colloids and/or biomolecules) trapping.

The following paragraphs present the choices that were made to address these challenges.

1.4.1 Substrates and patternings

Different substrates were used during this work (see Fig. 1.17), which we can separated into the following categories :

- **Plain silica** substrates
- **Plain gold** substrates
- Patterned gold on silica (or glass) substrates with different sizes for the gold structures :
  - **"Macro-patterned"**, corresponding to a ca. 1cm^2 silica or glass substrate with half of the surface covered by gold.
  - **Micro-patterned**, with structures ranging from 5µm x 5µm to 100µm x 100µm
  - **Nano-patterned**, with structures of ca. 100nm x 100nm

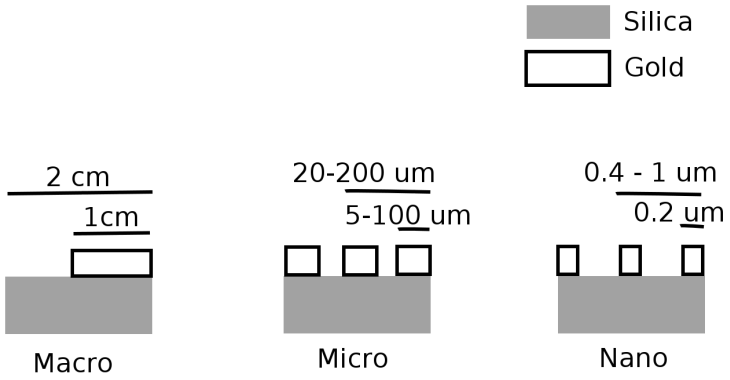

Figure 1.17 – Schematic representation of samples' dimensions (not to scale).

The reasons for working with all these different substrates can be summarized as follows : Plain substrates are the easiest to obtain and allow an easy monitoring of different functionalizations by methods such as PM-IRRAS, XPS or contact angle goniometry. They were therefore used for investigating and optimizing different protocols independent of orthogonal functionalizations (eg : NHS activation of COOH-terminated SAMs). Nano-patterned substrates are the most promising in terms of applications, namely in the field of biophotonic transducers. However given the difficulty of characterizing surface chemistry at that scale and the fact that their fabrication remains rather time-consuming, it was decided to test orthogonal functionalizations on macro and micro-patterned substrates as well.

Plain substrates were either commercial (silica on silicon wafer and glass slides) or made by deposition (e-beam evaporation for gold or sputtering for silica) of a thin film on a silicon wafer (macro-patterned substrates were made by masking half of the substrate during gold evaporation). Micro-patterned substrates were made by Ultraviolet (UV)-lithography and nano-patterned ones by e-beam lithography. These substrates were prepared either by myself or by co-workers, as explained in appendix A.

1.4.2 Functionalizations and applications

Two main molecules were used for gold functionalization : **MUA** with subsequent **NHS** activation and **MU-Biot**. These choices were made for their ability to bind amine-containing molecules (such as proteins) and avidins (neutravidin, streptavidin) respectively. Also, these thiols are long enough to ensure, in principle, well-ordered SAMs and are readily available commercially. Both thiols were used in pure SAM as well as in combination with **11-mercapto-1-undecanol** to form mixed-SAMs, though no significant improvement was noticed in such binary SAMs. Other thiols investigated in collaboration with the work of Alice Goudot and Anaïs Garnier include COOH and CH_3 terminated PEG-thiols (**HS-$(CH_2)_{10}$-$EG_{3,6}$-COOH** and **HS-$(CH_2)_{10}$-$EG_{3,6}$-CH_3**). Eventually perfluorinated thiols (**1H,1H,2H,2H-Perfluorodecanethiol**) were also used, mainly for ToF-SIMS and XPS imaging.

On silica **PEG-Si** was used for passivation, as well as SiF mainly for ToF-SIMS and XPS element imaging.

Details on the functionalization and activation protocols are given in the next chapter.

These functionalizations were tested in regards of two different applications :

1. The localized positioning of colloidal carboxylatex from solution onto previously defined regions of a heterogenous substrate.
2. The selective binding of target biomolecules onto LSPR-supporting nanostructures.

1.4.3 Characterizations

In the course of this PhD, the following characterization methods were used :

- For substrate characterization (prior to functionalization) :
  - **SEM**, to ensure the presence and conformity of the patterns.
  - **PM-IRRAS** and **XPS** to check the cleanliness and oxidation of the surface.
  - **AFM** and **XRD** for information on roughness and crystallinity.

- For chemical characterization of SAMs
  - **PM-IRRAS** on bare gold and “macro-patterned” surfaces.

  - **XPS** on bare gold, silica and "macro-patterned" surfaces, as well as micropatterned (element imaging).
  - **Contact angle goniometry** on bare gold, silica and "macro-patterned" surfaces.
  - **AFM** on bare gold surfaces.
  - **ToF-SIMS** on bare gold and micropatterned surfaces (element imaging).

- For evaluation of the target-binding applications
  - **SEM** to visualize the position of deposited nano-objects.
  - **SPR or LSPR** for monitoring target biomolecule binding.

References

[1] D.-J. Kim and K.-K. Koo. *J. Ind. Eng. Chem.*, 10,920–926 **(2004)**.

[2] J. Lahiri, L. Isaacs, J. Tien, and G. M. Whitesides. *Analytical chemistry*, 71,777–90 **(1999)**.

[3] J. Lahiri, L. Isaacs, B. Grzybowski, J. D. Carbeck, and G. M. Whitesides. *Langmuir*, 15,7186–7198 **(1999)**.

[4] J. Lahiri, E. Ostuni, and G. M. Whitesides. *Langmuir*, 15,2055–2060 **(1999)**.

[5] A. Myrskog, H. Anderson, T. Aastrup, B. Ingemarsson, and B. Liedberg. *Langmuir*, 26,821–9 **(2010)**.

[6] A. R. Lokanathan, S. Zhang, V. R. Regina, M. a. Cole, R. Ogaki, M. Dong, F. Besenbacher, R. L. Meyer, and P. Kingshott. *Biointerphases*, 6,180–8 **(2011)**.

[7] S. R. Coyer, E. Delamarche, and A. J. García. *Advanced materials*, 23,1550–1553 **(2011)**.

[8] C. a. Simpson, A. C. Agrawal, A. Balinski, K. M. Harkness, and D. E. Cliffel. *ACS nano*, 5,3577–84 **(2011)**.

[9] M. Bruns, C. Barth, P. Brüner, S. Engin, T. Grehl, C. Howell, P. Koelsch, P. Mack, P. Nagel, V. Trouillet, D. Wedlich, and R. G. White. *Surface and Interface Analysis*, 44,909–913 **(2012)**.

[10] V. Sanz, J. a. Conde, Y. Hernández, P. V. Baptista, M. R. Ibarra, and J. M. Fuente. *Journal of Nanoparticle Research*, 14,917 **(2012)**.

[11] M. J. Shuster, A. Vaish, M. L. Gilbert, M. Martinez-Rivera, R. M. Nezarati, P. S. Weiss, and A. M. Andrews. *The Journal of Physical Chemistry C*, 115,24778–24787 **(2011)**.

[12] K. L. Prime and G. M. Whitesides. *Science*, 245,1164–1167 **(1991)**.

[13] K. L. Prime and G. M. Whitesides. *Journal of the American Chemical Society*, 115,10714–10721 **(1993)**.

[14] M. Mrksich and G. M. Withesides. *Annu. Rev. Biophys. Biomol. Struct.*, 25,55–78 **(1996)**.

[15] G. B. Sigal, C. Bamdad, A. Barberis, J. Strominger, and G. M. Whitesides. *Anal. Chem.*, 68,490–497 **(1996)**.

[16] B. T. Houseman and M. Mrksich. *Biomaterials*, 22,943–55 **(2001)**.

[17] B. T. Houseman, J. H. Huh, S. J. Kron, and M. Mrksich. *Nature biotechnology*, 20,270–274 **(2002)**.

[18] B. T. Houseman, E. S. Gawalt, and M. Mrksich. *Langmuir*, 19,1522–1531 **(2003)**.

[19] L. Li, S. Chen, J. Zheng, B. D. Ratner, and S. Jiang. *The Journal of Physical Chemistry B*, 109,2934–41 **(2005)**.

[20] Q. Yu, S. Chen, A. D. Taylor, J. Homola, B. Hock, and S. Jiang. *Sensors and Actuators B*, 107,193–201 **(2005)**.

[21] R. Valiokas, L. Malysheva, A. Onipko, H.-H. Lee, v. Ruželė, S. Svedhem, S. C. T. Svensson, U. Gelius, and B. Liedberg. *Journal of Electron Spectroscopy and Related Phenomena*, 172,9–20 **(2009)**.

[22] J. Maciel, M. I. Oliveira, R. M. Gonçalves, and M. a. Barbosa. *Acta biomaterialia*, 8,3669–77 **(2012)**.

[23] R. J. Chen, H. C. Choi, S. Bangsaruntip, E. Yenilmez, X. Tang, Q. Wang, Y.-L. Chang, and H. Dai. *Journal of the American Chemical Society*, 126,1563–1568 **(2004)**.

[24] M. L. Walker, D. J. Vanderah, and K. a. Rubinson. *Colloids and surfaces. B, Biointerfaces*, 82,450–455 **(2011)**.

[25] S. Zorn, U. Dettinger, M. W. Skoda, R. M. Jacobs, H. Peisert, A. Gerlach, T. Chassé, and F. Schreiber. *Applied Surface Science*, 258,7882–7888 **(2012)**.

[26] C. Pale-Grosdemange, E. S. Simon, K. L. Prime, and G. M. Whitesides. *Journal of the American Chemical Society*, 113,12–20 **(1991)**.

[27] C. H. Lalander, Y. Zheng, S. Dhuey, and S. Cabrini. *ACS nano*, 4,6153–6161 **(2010)**.

[28] L. Feuz, P. Jönsson, M. P. Jonsson, and F. Höök. *ACS nano*, 4,2167–77 **(2010)**.

[29] K. Kumar, A. B. Dahlin, T. Sannomiya, S. Kaufmann, L. Isa, and E. Reimhult. *Nano letters*, 13,6122–6129 **(2013)**.

[30] F. Palazon, V. Monnier, Y. Chevolot, J.-P. Cloarec, and E. Souteyrand. *Journal of Colloid Science and Biotechnology*, 2,1–14 **(2013)**.

[31] T. Muller, A. Gerardino, T. Schnelle, S. G. Shirley, F. Bordoni, G. D. Gasperis, R. Leoni, and G. Fuhr. *Journal of Physics D : Applied Physics*, 29,340–349 **(1996)**.

[32] J. Shi, S. S. Guo, M. H. Sun, D. Baigl, and Y. Chen. *Microelectronic Engineering*, 84,1471–1475 **(2007)**.

[33] Y. Yin, Y. Lu, B. Gates, and Y. Xia. *Journal of the American Chemical Society*, 123,8718–29 **(2001)**.

[34] X. D. Hoa, M. Martin, a. Jimenez, J. Beauvais, P. Charette, a. Kirk, and M. Tabrizian. *Biosensors & bioelectronics*, 24,976–81 **(2008)**.

[35] Q. Zhang, T. Xu, D. Butterfield, M. J. Misner, D. Y. Ryu, T. Emrick, and T. P. Russell. *Nano letters*, 5,357–61 **(2005)**.

[36] D. Baranov, A. Fiore, M. van Huis, C. Giannini, A. Falqui, U. Lafont, H. Zandbergen, M. Zanella, R. Cingolani, and L. Manna. *Nano letters*, 10,743–749 **(2010)**.

[37] P. J. Pauzauskie, A. Radenovic, E. Trepagnier, H. Shroff, P. Yang, and J. Liphardt. *Nature materials*, 5,97–101 **(2006)**.

[38] R. Krupke, F. Hennrich, H. V. Löhneysen, and M. M. Kappes. *Science (New York, N.Y.)*, 301,344–7 **(2003)**.

[39] N. Sui, V. Monnier, Y. Zakharko, Y. Chevolot, S. Alekseev, J.-M. Bluet, V. Lysenko, and E. Souteyrand. *Journal of Nanoparticle Research*, 14 **(2012)**.

[40] R. M. Erb, H. S. Son, B. Samanta, V. M. Rotello, and B. B. Yellen. *Nature*, 457,999–1002 **(2009)**.

[41] J. Choma, D. Jamioła, J. Ludwinowicz, and M. Jaroniec. *Colloids and Surfaces A : Physicochemical and Engineering Aspects*, 411,74–79 **(2012)**.

[42] J. Yuan, Y. Xu, A. Walther, S. Bolisetty, M. Schumacher, H. Schmalz, M. Ballauff, and A. H. E. Müller. *Nature materials*, 7,718–722 **(2008)**.

[43] D. Cheon, S. Kumar, and G.-H. Kim. *Applied Physics Letters*, 96,013101 **(2010)**.

[44] W. Ahmed, E. S. Kooij, A. van Silfhout, and B. Poelsema. *Nano letters*, 9,3786–94 **(2009)**.

[45] P. a. Smith, C. D. Nordquist, T. N. Jackson, T. S. Mayer, B. R. Martin, J. Mbindyo, and T. E. Mallouk. *Applied Physics Letters*, 77,1399 **(2000)**.

[46] Y. Xia, Y. Yin, Y. Lu, and J. McLellan. *Advanced Functional Materials*, 13,907–918 **(2003)**.

[47] M. Rycenga, P. H. C. Camargo, and Y. Xia. *Soft Matter*, 5,1129 **(2009)**.

[48] D. Xia, a. Biswas, D. Li, and S. R. J. Brueck. *Advanced Materials*, 16,1427–1432 **(2004)**.

[49] D. Xia and S. R. J. Brueck. *Journal of Vacuum Science & Technology B : Microelectronics and Nanometer Structures*, 22,3415 **(2004)**.

[50] B. J. P. Spatz, F.-m. Kamm, A. Plettl, and P. Ziemann. *Advanced Materials*, 14,1827–1832 **(2002)**.

[51] J. Huang, R. Fan, S. Connor, and P. Yang. *Angewandte Chemie (International ed. in English)*, 46,2414–7 **(2007)**.

[52] L. Malaquin, T. Kraus, H. Schmid, E. Delamarche, and H. Wolf. *Langmuir*, 23,11513–21 **(2007)**.

[53] A. Cerf, C. Thibault, M. Geneviève, and C. Vieu. *Microelectronic Engineering*, 86,1419–1423 **(2009)**.

[54] A. Cerf, G. Molnár, and C. Vieu. *ACS applied materials & interfaces*, 1,2544–50 **(2009)**.

[55] A. Cerf and C. Vieu. *Colloids and Surfaces A : Physicochemical and Engineering Aspects*, 342,136–140 **(2009)**.

[56] C. Hamon, M. Postic, E. Mazari, T. Bizien, C. Dupuis, P. Even-Hernandez, A. Jimenez, L. Courbin, C. Gosse, F. Artzner, and V. Marchi-Artzner. *ACS nano*, 6,4137–46 **(2012)**.

[57] K. a. Arpin, J. H. Pikul, W. P. King, H. Fan, and P. V. Braun. *Soft Matter*, 7,10252 **(2011)**.

[58] A. V. Blaaderen, R. Ruel, and P. Wiltzius. *Nature*, 385,321–323 **(1997)**.

[59] M. J. Gordon and D. Peyrade. *Applied Physics Letters*, 89,053112 **(2006)**.

[60] Y. Cui, M. T. Bjork, J. A. Liddle, C. Sonnichsen, B. Boussert, and A. P. Alivisatos. *Nano Letters*, 4,1093–1098 **(2004)**.

[61] Y. Huang, X. Duan, Q. Wei, and C. M. Lieber. *Science (New York, N.Y.)*, 291,630–3 **(2001)**.

[62] Y. Huang, X. Duan, Y. Cui, L. J. Lauhon, K. H. Kim, and C. M. Lieber. *Science*, 294,1313–7 **(2001)**.

[63] D. Whang, S. Jin, and Y. Wu. *Nano Letters*, 3,1255–1259 **(2003)**.

[64] J. Y. Cheng, C. a. Ross, H. I. Smith, and E. L. Thomas. *Advanced Materials*, 18,2505–2521 **(2006)**.

[65] T. P. Rivera. *Assemblage convectif de colloides par forces de capillarité en milieu confiné : applications en plasmonique*. PhD thesis **(2009)**.

[66] A. Cerf. *Assemblage dirigé de nano-objets*. PhD thesis **(2010)**.

[67] O. D. Velev and S. Gupta. *Advanced Materials*, 21,1897–1905 **(2009)**.

[68] X. Ye and L. Qi. *Nano Today*, 6,608–631 **(2011)**.

[69] O. D. Velev and K. H. Bhatt. *Soft Matter*, 2,738 **(2006)**.

[70] W. Zhang, L. Huang, C. Santschi, and O. J. F. Martin. *Nano letters*, 10,1006–1011 **(2010)**.

[71] R. Pethig and G. H. Markx. *Trends in biotechnology*, 15,426–32 **(1997)**.

[72] A. Kuzyk. *Electrophoresis*, 32,2307–2313 **(2011)**.

[73] B. Cetin and D. Li. *Electrophoresis*, 32,2410–27 **(2011)**.

[74] P. J. Burke. *Encyclopedia of Nanoscience and Nanotechnology*, X,1–19 **(2003)**.

[75] M. Giersig and P. Mulvaney. *Langmuir*, 9,3408–3413 **(1993)**.

[76] M. Giersig and P. Mulvaney. *The Journal of Physical Chemistry*, 97,6334–6336 **(1993)**.

[77] M. Bohmer. *Langmuir*, 12,5747–5750 **(1996)**.

[78] M. Trau, D. A. Saville, and I. A. Aksay. *Science*, 272,706–709 **(1996)**.

[79] M. Trau, D. A. Saville, and I. A. Aksay. *Langmuir*, 13,6375–6381 **(1997)**.

[80] D. a. Dehlinger, B. D. Sullivan, S. Esener, and M. J. Heller. *Small (Weinheim an der Bergstrasse, Germany)*, 3,1237–44 **(2007)**.

[81] J. Ryu, D. Dehlinger, M. Heller, and T. Hahn. *Particle & Particle Systems Characterization*, 26,275–282 **(2009)**.

[82] F. Wakaya, T. Nagai, and K. Gamo. *Microelectronic Engineering*, 63,27–31 **(2002)**.

[83] X. Q. Chen, T. Saito, H. Yamada, and K. Matsushige. *Applied Physics Letters*, 78,3714 **(2001)**.

[84] K. Yamamoto, S. Akita, and Y. Nakayama. *Journal of Physics D : Applied Physics*, 31,34–36 **(1998)**.

[85] N. G. Green and H. Morgan. *Journal of Physics D : Applied Physics*, 30,2626–2633 **(1997)**.

[86] N. Green and H. Morgan. *Journal of Physics D : Applied Physics*, 30,41–44 **(1997)**.

[87] M. P. Hughes. *Journal of colloid and interface science*, 250,291–4 **(2002)**.

[88] H. a. Pohl. *Journal of Applied Physics*, 22,869 **(1951)**.

[89] H. A. Pohl. *Journal of Applied Physics*, 29,1182 **(1958)**.

[90] H. A. Pohl, K. Pollock, and J. S. Crane. *J. Biol. Phys.*, 6,133–160 **(1978)**.

[91] T. Schnelle, R. Hagedorn, G. Fuhr, S. Fiedler, and T. Müller. *Biochimica et biophysica acta*, 1157,127–40 **(1993)**.

[92] T. Müller, a. M. Gerardino, T. Schnelle, S. G. Shirley, G. Fuhr, G. Gasperis, R. Leoni, and F. Bordoni. *Il Nuovo Cimento D*, 17,425–432 **(1995)**.

[93] N. G. Green, H. Morgan, and J. J. Milner. *Journal of biochemical and biophysical methods*, 35,89–102 **(1997)**.

[94] M. P. Hughes and H. Morgan. *Analytical Chemistry*, 71,3441–3445 **(1999)**.

[95] M. Hughes, H. Morgan, and M. Flynn. *Journal of colloid and interface science*, 220,454–457 **(1999)**.

[96] M. P. Hughes and H. Morgan. *Journal of Physics D : Applied Physics*, 31,2205–2210 **(1998)**.

[97] A. Ramos, H. Morgan, and N. G. Green. *Journal of Physics D : Applied Physics*, 31,2338–2353 **(1998)**.

[98] N. Green and H. Morgan. *Journal of Physics D : Applied Physics*, 31,25–30 **(1998)**.

[99] A. Ramos, H. Morgan, N. G. Green, and A. Castellanos. *Journal of colloid and interface science*, 217,420–422 **(1999)**.

[100] A. Ramos, H. Morgan, N. G. Green, and A. Castellanos. *Journal of electrostatics*, 47,71–81 **(1999)**.

[101] S. Fiedler, S. G. Shirley, T. Schnelle, and G. Fuhr. *Analytical chemistry*, 70,1909–15 **(1998)**.

[102] T. Muller, G. Gradl, S. Howitz, S. Shirley, and G. Fuhr. *Biosensors & Bioelectronics*, 14,247–256 **(1999)**.

[103] T. Schnelle, T. Müller, R. Hagedorn, a. Voigt, and G. Fuhr. *Biochimica et biophysica acta*, 1428,99–105 **(1999)**.

[104] L. Zheng, J. P. Brody, and P. J. Burke. *Biosensors & bioelectronics*, 20,606–19 **(2004)**.

[105] N. Gadish and J. Voldman. *Analytical chemistry*, 78,7870–6 **(2006)**.

[106] M. Wiklund, P. Spégel, S. Nilsson, and H. M. Hertz. *Ultrasonics*, 41,329–333 **(2003)**.

[107] J. L. Baylon-Cardiel, N. M. Jesús-Pérez, A. V. Chávez-Santoscoy, and B. H. Lapizco-Encinas. *Lab on a chip*, 10,3235–42 **(2010)**.

[108] E. B. Cummings and A. K. Singh. *Analytical chemistry*, 75,4724–31 **(2003)**.

[109] K. Khoshmanesh, C. Zhang, F. J. Tovar-Lopez, S. Nahavandi, S. Baratchi, K. Kalantar-zadeh, and A. Mitchell. *Electrophoresis*, 30,3707–17 **(2009)**.

[110] D. J. Bakewell and H. Morgan. *Measurement Science and Technology*, 15,254–266 **(2004)**.

[111] D. J. Bennett, B. Khusid, C. D. James, P. C. Galambos, M. Okandan, D. Jacqmin, and A. Acrivos. *Applied Physics Letters*, 83,4866 **(2003)**.

[112] A. P. Hsiao and M. J. Heller. *Journal of Biomedicine and Biotechnology*, 2012,1–9 **(2012)**.

[113] R. Krishnan, D. a. Dehlinger, G. J. Gemmen, R. L. Mifflin, S. C. Esener, and M. J. Heller. *Electrochemistry communications*, 11,1661–1666 **(2009)**.

[114] W. J. Tian, J. P. Huang, and K. W. Yu. *Journal of Applied Physics*, 105,102044 **(2009)**.

[115] A. Rosenthal and J. Voldman. *Biophysical journal*, 88,2193–205 **(2005)**.

[116] H. Zhou, L. R. White, and R. D. Tilton. *Journal of colloid and interface science*, 285,179–91 **(2005)**.

[117] Z. Gagnon and H.-C. Chang. *Electrophoresis*, 26,3725–37 **(2005)**.

[118] J. Wu, Y. Ben, D. Battigelli, and H.-C. Chang. *Industrial & Engineering Chemistry Research*, 44,2815–2822 **(2005)**.

[119] D. R. Albrecht, R. L. Sah, and S. N. Bhatia. *Biophysical journal*, 87,2131–2147 **(2004)**.

[120] S. O. Lumsdon, E. W. Kaler, and O. D. Velev. *Langmuir*, 20,2108–2116 **(2004)**.

[121] L. Zheng, S. Li, J. P. Brody, and P. J. Burke. *Langmuir*, 20,8612–9 **(2004)**.

[122] P. K. Wong, C.-Y. Chen, T.-H. Wang, and C.-M. Ho. *Analytical chemistry*, 76,6908–14 **(2004)**.

[123] J. Voldman, M. Toner, M. Gray, and M. Schmidt. *Journal of Electrostatics*, 57,69–90 **(2003)**.

[124] G. Medoro, N. Manaresi, a. Leonardi, L. Altomare, M. Tartagni, and R. Guerrieri. *IEEE Sensors Journal*, 3,317–325 **(2003)**.

[125] M. Frénéa, S. P. Faure, B. Le Pioufle, P. Coquet, and H. Fujita. *Materials Science and Engineering : C*, 23,597–603 **(2003)**.

[126] K. F. Hoettges, M. B. McDonnell, and M. P. Hughes. *Journal of Physics D : Applied Physics*, 36,101–104 **(2003)**.

[127] J. Auerswald and H. F. Knapp. *Microelectronic Engineering*, 68,879–886 **(2003)**.

[128] A. Castellanos, A. Ramos, A. Gonzalez, N. G. Green, and H. Morgan. *Journal of Physics D : Applied Physics*, 36,2584–2597 **(2003)**.

[129] M. Dürr, J. Kentsch, T. Müller, T. Schnelle, and M. Stelzle. *Electrophoresis*, 24,722–31 **(2003)**.

[130] A. Bezryadin, C. Dekker, and G. Schmid. *Applied Physics Letters*, 71,1273 **(1997)**.

[131] A. Bezryadin. *Journal of Vacuum Science & Technology B : Microelectronics and Nanometer Structures*, 15,793 **(1997)**.

[132] B. C. Gierhart, D. G. Howitt, S. J. Chen, R. L. Smith, and S. D. Collins. *Langmuir*, 23,12450–12456 **(2007)**.

[133] R. Krahne, A. Yacoby, H. Shtrikman, I. Bar-Joseph, T. Dadosh, and J. Sperling. *Applied Physics Letters*, 81,730 **(2002)**.

[134] R. Krahne, T. Dadosh, Y. Gordin, A. Yacoby, H. Shtrikman, D. Mahalu, J. Sperling, and I. Bar-Joseph. *Physica E : Low-dimensional Systems and Nanostructures*, 17,498–502 **(2003)**.

[135] I. Amlani, A. M. Rawlett, L. a. Nagahara, and R. K. Tsui. *Applied Physics Letters*, 80,2761 **(2002)**.

[136] I. Amlani, A. M. Rawlett, L. a. Nagahara, and R. K. Tsui. *Journal of Vacuum Science & Technology B : Microelectronics and Nanometer Structures*, 20,2802 **(2002)**.

[137] A. M. Rawlett, T. J. Hopson, I. Amlani, R. Zhang, J. Tresek, L. A. Nagahara, R. K. Tsui, and H. Goronkin. *Nanotechnology*, 14,377–384 **(2003)**.

[138] R. J. Barsotti, M. D. Vahey, R. Wartena, Y.-M. Chiang, J. Voldman, and F. Stellacci. *Small (Weinheim an der Bergstrasse, Germany)*, 3,488–499 **(2007)**.

[139] S. Kumar, S.-H. Yoon, and G.-H. Kim. *Current Applied Physics*, 9,101–103 **(2009)**.

[140] S. I. Khondaker and Z. Yao. *Applied Physics Letters*, 81,4613 **(2002)**.

[141] T. Dadosh, Y. Gordin, R. Krahne, I. Khivrich, D. Mahalu, V. Frydman, J. Sperling, A. Yacoby, and I. Bar-Joseph. *Nature*, 436,677–80 **(2005)**.

[142] J.-S. Na, J. Ayres, K. L. Chandra, C. Chu, C. B. Gorman, and G. N. Parsons. *Nanotechnology*, 18,035203 **(2007)**.

[143] D. L. Fan, R. C. Cammarata, and C. L. Chien. *Applied Physics Letters*, 92,93115 **(2008)**.

[144] R. J. Hamers, J. D. Beck, M. a. Eriksson, B. Li, M. S. Marcus, L. Shang, J. Simmons, and J. a. Streifer. *Nanotechnology*, 17,S280–S286 **(2006)**.

[145] J. J. Boote and S. D. Evans. *Nanotechnology*, 16,1500–1505 **(2005)**.

[146] H. W. Seo, C.-S. Han, S. O. Hwang, and J. Park. *Nanotechnology*, 17,3388–93 **(2006)**.

[147] L. Dong, J. Bush, V. Chirayos, R. Solanki, J. Jiao, Y. Ono, J. F. Conley, and B. D. Ulrich. *Nano letters*, 5,2112–2115 **(2005)**.

[148] S. Evoy, N. DiLello, V. Deshpande, a. Narayanan, H. Liu, M. Riegelman, B. R. Martin, B. Hailer, J.-C. Bradley, W. Weiss, T. S. Mayer, Y. Gogotsi, H. H. Bau, T. E. Mallouk, and S. Raman. *Microelectronic Engineering*, 75,31–42 **(2004)**.

[149] M. Li, R. B. Bhiladvala, T. J. Morrow, J. a. Sioss, K.-K. Lew, J. M. Redwing, C. D. Keating, and T. S. Mayer. *Nature nanotechnology*, 3,88–92 **(2008)**.

[150] A. D. Wissner-Gross. *Nanotechnology*, 17,4986–4990 **(2006)**.

[151] E. M. Freer, O. Grachev, X. Duan, S. Martin, and D. P. Stumbo. *Nature nanotechnology*, 5,525–30 **(2010)**.

[152] C. S. Lao, J. Liu, P. Gao, L. Zhang, D. Davidovic, R. Tummala, and Z. L. Wang. *Nano letters*, 6,263–266 **(2006)**.

[153] S.-Y. Lee, A. Umar, D.-I. Suh, J.-E. Park, Y.-B. Hahn, J.-Y. Ahn, and S.-K. Lee. *Physica E : Low-dimensional Systems and Nanostructures*, 40,866–872 **(2008)**.

[154] W. J. Liu, J. Zhang, L. J. Wan, K. W. Jiang, B. R. Tao, H. L. Li, W. L. Gong, and X. D. Tang. *Sensors and Actuators B : Chemical*, 133,664–670 **(2008)**.

[155] J. Suehiro, N. Nakagawa, S.-I. Hidaka, M. Ueda, K. Imasaka, M. Higashihata, T. Okada, and M. Hara. *Nanotechnology*, 17,2567–73 **(2006)**.

[156] J. Suehiro. *Biomicrofluidics*, 4,1–10 **(2010)**.

[157] S. Kumar, Y.-K. Seo, and G.-H. Kim. *Applied Physics Letters*, 94,153104 **(2009)**.

[158] D. Wang, R. Zhu, Z. Zhou, and X. Ye. *Applied Physics Letters*, 90,103110 **(2007)**.

[159] S. Kumar, S. Rajaraman, R. a. Gerhardt, Z. L. Wang, and P. J. Hesketh. *Electrochimica Acta*, 51,943–951 **(2005)**.

[160] S.-Y. S.-K. Lee, T.-H. Kim, D.-I. Suh, E.-K. Suh, N.-K. Cho, and W.-K. Seong. *Applied Physics A*, 87,739–742 **(2007)**.

[161] S.-K. Lee, T.-H. Kim, S.-Y. Lee, K.-C. Choi, and P. Yang. *Philosophical Magazine*, 87,2105–2115 **(2007)**.

[162] A. I. Baca, J. J. Brown, K. a. Bertness, and V. M. Bright. *Nanotechnology*, 23,245301 **(2012)**.

[163] A. Motayed, M. He, A. V. Davydov, J. Melngailis, and S. N. Mohammad. *Journal of Applied Physics*, 100,114310 **(2006)**.

[164] S.-Y. Lee, T.-H. Kim, D.-I. Suh, N.-K. Cho, H.-K. Seong, S.-W. Jung, H.-J. Choi, and S.-K. Lee. *Chemical Physics Letters*, 427,107–112 **(2006)**.

[165] T. H. Kim, S. Y. K. Lee, N. K. Cho, H. K. Seong, H. J. Choi, and S. W. Jung. *Nanotechnology*, 17,3394–3399 **(2006)**.

[166] J.-W. Lee, K.-J. Moon, M.-H. Ham, and J.-M. Myoung. *Solid State Communications*, 148,194–198 **(2008)**.

[167] S. Raychaudhuri, S. a. Dayeh, D. Wang, and E. T. Yu. *Nano letters*, 9,2260–6 **(2009)**.

[168] K. Oh, J.-H. Chung, J. J. Riley, Y. Liu, and W. K. Liu. *Langmuir*, 23,11932–40 **(2007)**.

[169] T. J. Morrow, M. Li, J. Kim, T. S. Mayer, and C. D. Keating. *Science*, 323,2009 **(2009)**.

[170] A. Bezryadin, R. M. Westervelt, and M. Tinkham. *Applied Physics Letters*, 74,2699 **(1999)**.

[171] L. a. Nagahara, I. Amlani, J. Lewenstein, and R. K. Tsui. *Applied Physics Letters*, 80,3826 **(2002)**.

[172] J. Suehiro, G. Zhou, and M. Hara. *Journal of Physics D : Applied Physics*, 36 **(2003)**.

[173] R. Krupke, F. Hennrich, H. B. Weber, M. M. Kappes, and H. v. Löhneysen. *Nano Letters*, 3,1019–1023 **(2003)**.

[174] J. Chung and J. Lee. *Sensors and Actuators A : Physical*, 104,229–235 **(2003)**.

[175] J. Chung, K.-H. Lee, J. Lee, and R. S. Ruoff. *Langmuir*, 20,3011–7 **(2004)**.

[176] C. K. M. Fung, V. T. S. Wong, R. H. M. Chan, and W. J. Li. *IEEE Transactions On Nanotechnology*, 3,395–403 **(2004)**.

[177] J. Suehiro, G. Zhou, H. Imakiire, W. Ding, and M. Hara. *Sensors and Actuators B : Chemical*, 108,398–403 **(2005)**.

[178] H.-W. Seo, C.-S. Han, D.-G. Choi, K.-S. Kim, and Y.-H. Lee. *Microelectronic Engineering*, 81,83–89 **(2005)**.

[179] M. Lucci, P. Regoliosi, a. Reale, a. Di Carlo, S. Orlanducci, E. Tamburri, M. L. Terranova, P. Lugli, C. Di Natale, a. D'Amico, and R. Paolesse. *Sensors and Actuators B : Chemical*, 111-112,181–186 **(2005)**.

[180] R. Krupke, S. Linden, M. Rapp, and F. Hennrich. *Advanced Materials*, 18,1468–1470 **(2006)**.

[181] M. Lucci, a. Reale, a. Di Carlo, S. Orlanducci, E. Tamburri, M. L. Terranova, I. Davoli, C. Di Natale, a. D'Amico, and R. Paolesse. *Sensors and Actuators B : Chemical*, 118,226–231 **(2006)**.

[182] M. Dimaki and P. Bø ggild. *Physica Status Solidi (a)*, 203,1088–1093 **(2006)**.

[183] J.-E. Kim, J.-K. Park, and C.-S. Han. *Nanotechnology*, 17,2937–2941 **(2006)**.

[184] D. Sickert, S. Taeger, I. Kühne, M. Mertig, W. Pompe, and G. Eckstein. *Physica Status Solidi (B)*, 243,3542–3545 **(2006)**.

[185] M. Riegelman, H. Liu, and H. H. Bau. *Journal of Fluids Engineering*, 128,6 **(2006)**.

[186] R. Zhou, P. Wang, and H.-C. Chang. *Electrophoresis*, 27,1376–85 **(2006)**.

[187] K. Wai, C. Lai, C. Kar, M. Fung, V. Tak, S. Wong, M. Lai, Y. Sin, W. J. Li, and C.-p. Kwong. *IEEE Transactions on automation science and engineering*, 3,218–227 **(2006)**.

[188] Z.-B. Zhang, S.-L. Zhang, and E. E. B. Campbell. *Chemical Physics Letters*, 421,11–15 **(2006)**.

[189] S. Taeger, D. Sickert, P. Atanasov, G. Eckstein, and M. Mertig. *Physica Status Solidi (B)*, 243,3355–3358 **(2006)**.

[190] N. Mureau, E. Mendoza, and S. R. P. Silva. *Electrophoresis*, 28,1495–8 **(2007)**.

[191] T. Schwamb, T.-Y. Choi, N. Schirmer, N. R. Bieri, B. Burg, J. Tharian, U. Sennhauser, and D. Poulikakos. *Nano Letters*, 7,3633–3638 **(2007)**.

[192] A. Vijayaraghavan, S. Blatt, D. Weissenberger, M. Oron-Carl, F. Hennrich, D. Gerthsen, H. Hahn, and R. Krupke. *Nano letters*, 7,1556–1560 **(2007)**.

[193] J. Suehiro, N. Ikeda, A. Ohtsubo, and K. Imasaka. *Microfluidics and Nanofluidics*, 5,741–747 **(2008)**.

[194] S. Rao, L. Huang, and W. Setyawan. *Nature*, 425,36–37 **(2003)**.

[195] L. Huang, Z. Jia, and S. O'Brien. *Journal of Materials Chemistry*, 17,3863 **(2007)**.

[196] A. Ashkin and J. M. Dziedzic. *Applied Physics Letters*, 19,283 **(1971)**.

[197] A. Ashkin and J. M. Dziedzic. *Applied Physics Letters*, 30,202 **(1977)**.

[198] A. Ashkin, J. M. Dziedzic, J. E. Bjorkholm, and S. Chu. *Optics letters*, 11,816–818 **(1986)**.

[199] A. Ashkin. *Selected Topics in Quantum Electronics, IEEE*, 6,841–856 **(2000)**.

[200] D. G. Grier. *Nature*, 424,810–6 **(2003)**.

[201] K. C. Neuman and S. M. Block. *The Review of scientific instruments*, 75,2787–2809 **(2004)**.

[202] K. Dholakia and P. Reece. *Nano Today*, 1,18–27 **(2006)**.

[203] K. Dholakia, P. Reece, and M. Gu. *Chemical Society reviews*, 37,42–55 **(2008)**.

[204] K. C. Neuman and A. Nagy. *Nature methods*, 5,491–505 **(2008)**.

[205] J. R. Moffitt, Y. R. Chemla, S. B. Smith, and C. Bustamante. *Annual review of biochemistry*, 77,205–228 **(2008)**.

[206] S. Kinge, M. Crego-Calama, and D. N. Reinhoudt. *Chemphyschem : a European journal of chemical physics and physical chemistry*, 9,20–42 **(2008)**.

[207] J. Homola and J. Dostálek. *Surface plasmon resonance based sensors* **(2006)**.

[208] M. L. Juan, M. Righini, and R. Quidant. *Nature Photonics*, 5,349–356 **(2011)**.

[209] S. Kawata and T. Tani. *Optics letters*, 21,1768–70 **(1996)**.

[210] L. Novotny, R. Bian, and X. Xie. *Physical Review Letters*, 79,645–648 **(1997)**.

[211] P. Chaumet, A. Rahmani, and M. N. Vesperinas. *Physical Review Letters*, 88,10–13 **(2002)**.

[212] M. N. Vesperinas, P. C. Chaumet, and A. Rahmani. *Philosophical transactions. Series A, Mathematical, physical, and engineering sciences*, 362,719–37 **(2004)**.

[213] K. Okamoto and S. Kawata. *Physical review letters*, 83,4534–4537 **(1999)**.

[214] E. Kwak, T. Onuta, and D. Amarie. *J. Phys. Chem. B*, 108,13607–13612 **(2004)**.

[215] R. Quidant, D. Petrov, and G. Badenes. *Optics letters*, 30,1009–11 **(2005)**.

[216] M. Righini, A. S. Zelenina, C. Girard, and R. Quidant. *Nature Physics*, 3,477–480 **(2007)**.

[217] M. Righini, P. Ghenuche, S. Cherukulappurath, V. Myroshnychenko, F. García de Abajo, and R. Quidant. *Nano letters*, 9,3387–3391 **(2009)**.

[218] Z. Fang, F. Lin, S. Huang, W. Song, and X. Zhu. *Applied Physics Letters*, 94,63306 **(2009)**.

[219] a. N. Grigorenko, N. W. Roberts, M. R. Dickinson, and Y. Zhang. *Nature Photonics*, 2,365–370 **(2008)**.

[220] A. Baev, E. P. Furlani, P. N. Prasad, A. N. Grigorenko, and N. W. Roberts. *Journal of Applied Physics*, 103,084316 **(2008)**.

[221] M. Righini, G. Volpe, C. Girard, D. Petrov, and R. Quidant. *Physical Review Letters*, 100,8–11 **(2008)**.

[222] H. M. K. Wong, M. Righini, J. C. Gates, P. G. R. Smith, V. Pruneri, and R. Quidant. *Applied Physics Letters*, 99,061107 **(2011)**.

[223] B. J. Roxworthy, K. D. Ko, A. Kumar, K. H. Fung, E. K. C. Chow, G. L. Liu, N. X. Fang, and K. C. Toussaint. *Nano letters*, 12,796–801 **(2012)**.

[224] J. E. Curtis, B. A. Koss, and D. G. Grier. *Optics Communications*, 207,169–175 **(2002)**.

[225] R. Agarwal, K. Ladavac, Y. Roichman, G. Yu, C. Lieber, and D. Grier. *Optics express*, 13,8906–8912 **(2005)**.

[226] W. Hossack, E. Theofanidou, J. Crain, K. Heggarty, and M. Birch. *Optics express*, 11,2053–2059 **(2003)**.

[227] E. Schonbrun, R. Piestun, P. Jordan, J. Cooper, K. Wulff, J. Courtial, and M. Padgett. *Optics express*, 13,3777–3786 **(2005)**.

[228] S. S. Guo, Y. L. Deng, L. B. Zhao, H. L. W. Chan, and X.-Z. Zhao. *Journal of Physics D : Applied Physics*, 41,105008 **(2008)**.

[229] C. Mikkelsen, M. Fougt Hansen, and H. Bruus. *Journal of Magnetism and Magnetic Materials*, 293,578–583 **(2005)**.

[230] C. Mikkelsen and H. Bruus. *Lab on a chip*, 5,1293–7 **(2005)**.

[231] E. P. Furlani. *Journal of Applied Physics*, 99,24912 **(2006)**.

[232] E. Furlani and K. Ng. *Physical Review E*, 73,1–10 **(2006)**.

[233] K. Smistrup, M. Bu, A. Wolff, H. Bruus, and M. F. Hansen. *Microfluidics and Nanofluidics*, 4,565–573 **(2008)**.

[234] B. Hallmark, N. J. Darton, T. James, P. Agrawal, and N. K. H. Slater. *Journal of Nanoparticle Research*, 12,2951–2965 **(2010)**.

[235] M. Berger, J. Castelino, R. Huang, M. Shah, and R. H. Austin. *Electrophoresis*, 22,3883–92 **(2001)**.

[236] I. F. Lyuksyutov, D. G. Naugle, and K. D. D. Rathnayaka. *Applied Physics Letters*, 85,1817 **(2004)**.

[237] Z. G. Forbes, B. B. Yellen, K. A. Barbee, and G. Friedman. *IEEE Transactions on Magnetics*, 39,3372–3377 **(2003)**.

[238] Y. A. Lin, T.-S. Wong, U. Bhardwaj, J.-M. Chen, E. McCabe, and C.-M. Ho. *Journal of Micromechanics and Microengineering*, 17,1299–1306 **(2007)**.

[239] T. Lund-Olesen, H. Bruus, and M. F. Hansen. *Biomedical microdevices*, 9,195–205 **(2007)**.

[240] H. Chen, M. D. Kaminski, and A. J. Rosengart. *Medical engineering & physics*, 30,1–8 **(2008)**.

[241] D. W. Inglis, R. Riehn, R. H. Austin, and J. C. Sturm. *Applied Physics Letters*, 85,5093 **(2004)**.

[242] K.-H. Han and a. B. Frazier. *Journal of Micromechanical Systems*, 14,67–73 **(2005)**.

[243] K.-H. Han and a. B. Frazier. *Lab on a chip*, 6,265–73 **(2006)**.

[244] J.-W. Choi, C. H. Ahn, S. Bhansali, and H. Henderson. *Sensors and Actuators B : Chemical*, 68,34–39 **(2000)**.

[245] J. W. Choi, T. M. Liakopoulos, and C. H. Ahn. *Biosensors & bioelectronics*, 16,409–416 **(2001)**.

[246] C. H. Ahn, M. G. Allen, W. Trimmer, Y.-N. Jun, and S. Erramilli. *Journal of Microelectromechanical Systems*, 5,151–158 **(1996)**.

[247] J. Do, J.-w. Choi, and C. H. Ahn. *IEEE Transactions on Magnetics*, 40,3009–3011 **(2004)**.

[248] Q. Ramadan, V. Samper, D. Poenar, and C. Yu. *Journal of Magnetism and Magnetic Materials*, 281,150–172 **(2004)**.

[249] Q. Ramadan, V. Samper, D. Poenar, and C. Yu. *International Journal of Nanoscience*, 4,489–499 **(2005)**.

[250] Q. Ramadan, V. Samper, D. P. Poenar, and C. Yu. *Biosensors & bioelectronics*, 21,1693–702 **(2006)**.

[251] Q. Ramadan, C. Yu, V. Samper, and D. P. Poenar. *Applied Physics Letters*, 88,32501 **(2006)**.

[252] Q. Ramadan, V. Samper, D. Poenar, Z. Liang, C. Yu, and T. M. Lim. *Sensors and Actuators B : Chemical*, 113,944–955 **(2006)**.

[253] Q. Ramadan, D. P. Poenar, and C. Yu. *Microfluidics and Nanofluidics*, 6,53–62 **(2008)**.

[254] M. Barbic, J. J. Mock, A. P. Gray, and S. Schultz. *Applied Physics Letters*, 79,1897 **(2001)**.

[255] S.-H. Song, B.-S. Kwak, J.-S. Park, W. Kim, and H.-I. Jung. *Sensors and Actuators A : Physical*, 151,64–70 **(2009)**.

[256] S.-H. Song, H.-L. Lee, Y. H. Min, and H.-I. Jung. *Sensors and Actuators B : Chemical*, 141,210–216 **(2009)**.

[257] M. Tondra, M. Granger, R. Fuerst, M. Porter, C. Nordman, J. Taylor, and S. Akou. *IEEE Transactions on Magnetics*, 37,2621–2623 **(2001)**.

[258] N. Pekas, M. Granger, M. Tondra, A. Popple, and M. D. Porter. *Journal of Magnetism and Magnetic Materials*, 293,584–588 **(2005)**.

[259] T. Deng, G. M. Whitesides, M. Radhakrishnan, G. Zabow, and M. Prentiss. *Applied Physics Letters*, 78,1775 **(2001)**.

[260] C. Liu, L. Lagae, R. Wirix-Speetjens, and G. Borghs. *Journal of Applied Physics*, 101,024913 **(2007)**.

[261] K. Smistrup, B. G. Kjeldsen, J. L. Reimers, M. Dufva, J. Petersen, and M. F. Hansen. *Lab on a chip*, 5,1315–9 **(2005)**.

[262] K. Smistrup, O. Hansen, H. Bruus, and M. F. Hansen. *Journal of Magnetism and Magnetic Materials*, 293,597–604 **(2005)**.

[263] K. Smistrup, T. Lund-Olesen, M. F. Hansen, and P. T. Tang. *Journal of Applied Physics*, 99,08P102 **(2006)**.

[264] K. Smistrup, P. T. Tang, O. Hansen, and M. F. Hansen. *Journal of Magnetism and Magnetic Materials*, 300,418–426 **(2006)**.

[265] N. Haddour, Y. Chevolot, M. Trévisan, E. Souteyrand, and J.-P. Cloarec. *Journal of Materials Chemistry*, 20,8266 **(2010)**.

[266] M. a. M. Gijs, F. Lacharme, and U. Lehmann. *Chemical reviews*, 110,1518–1563 **(2010)**.

[267] A.-E. Saliba, L. Saias, E. Psychari, N. Minc, D. Simon, F.-C. Bidard, C. Mathiot, J.-Y. Pierga, V. Fraisier, J. Salamero, V. Saada, F. Farace, P. Vielh, L. Malaquin, and J.-L. Viovy. *Proceedings of the National Academy of Sciences of the United States of America*, 107,14524–14529 **(2010)**.

[268] B. B. Yellen, O. Hovorka, and G. Friedman. *Proceedings of the National Academy of Sciences of the United States of America*, 102,8860–8864 **(2005)**.

[269] T. Henighan, D. Giglio, a. Chen, G. Vieira, and R. Sooryakumar. *Applied Physics Letters*, 98,103505 **(2011)**.

[270] T. Deng, M. Prentiss, and G. M. Whitesides. *Applied Physics Letters*, 80,461 **(2002)**.

[271] B. Yellen, G. Friedman, and a. Feinerman. *Journal of Applied Physics*, 93,7331 **(2003)**.

[272] S. Guo, C. Zuo, W. Huang, C. Peroz, and Y. Chen. *Microelectronic Engineering*, 83,1655–1659 **(2006)**.

[273] T. Henighan, a. Chen, G. Vieira, a. J. Hauser, F. Y. Yang, J. J. Chalmers, and R. Sooryakumar. *Biophysical journal*, 98,412–7 **(2010)**.

[274] G. Ruan, G. Vieira, T. Henighan, A. Chen, D. Thakur, R. Sooryakumar, and J. O. Winter. *Nano letters*, 10,2220–4 **(2010)**.

[275] P. Tseng, D. Di Carlo, and J. W. Judy. *Nano letters*, 9,3053–9 **(2009)**.

[276] Y.-J. Liu, S.-S. Guo, Z.-L. Zhang, W.-H. Huang, D. Baigl, M. Xie, Y. Chen, and D.-W. Pang. *Electrophoresis*, 28,4713–22 **(2007)**.

[277] M. Liu, J. Lagdani, H. Imrane, C. Pettiford, J. Lou, S. Yoon, V. G. Harris, C. Vittoria, and N. X. Sun. *Applied Physics Letters*, 90,103105 **(2007)**.

[278] Y. Rheem, C. M. Hangarter, and N. V. Myung. *IEEE Transactions on Nanotechnology*, 7,251–255 **(2008)**.

[279] C. M. Hangarter, Y. Rheem, B. Yoo, E.-H. Yang, and N. V. Myung. *Nanotechnology*, 18,205305 **(2007)**.

[280] M. Tanase, D. M. Silevitch, a. Hultgren, L. a. Bauer, P. C. Searson, G. J. Meyer, and D. H. Reich. *Journal of Applied Physics*, 91,8549 **(2002)**.

[281] D. P. Long, J. L. Lazorcik, and R. Shashidhar. *Advanced Materials*, 16,814–819 **(2004)**.

[282] M. Liu, X. Li, H. Imrane, Y. Chen, T. Goodrich, Z. Cai, K. S. Ziemer, J. Y. Huang, and N. X. Sun. *Applied Physics Letters*, 90,152501 **(2007)**.

[283] R. J. Kershner, J. W. Bullard, and M. J. Cima. *Journal of colloid and interface science*, 278,146–54 **(2004)**.

[284] H. Fudouzi, M. Kobayashi, and N. Shinya. *Journal of Nanoparticle Research*, 3,193–200 **(2001)**.

[285] R. M. Erb, N. J. Jenness, R. L. Clark, and B. B. Yellen. *Advanced materials (Deerfield Beach, Fla.)*, 21,4825–9 **(2009)**.

[286] D. Braun and A. Libchaber. *Physical Review Letters*, 89,2–5 **(2002)**.

[287] R. T. Schermer, C. C. Olson, J. P. Coleman, and F. Bucholtz. *Optics express*, 19,10571–86 **(2011)**.

[288] T. Lilliehorn, U. Simu, M. Nilsson, M. Almqvist, T. Stepinski, T. Laurell, J. Nilsson, and S. Johansson. *Ultrasonics*, 43,293–303 **(2005)**.

[289] H. M. Hertz. *Journal of Applied Physics*, 78,4845 **(1995)**.

[290] P. Glynne-Jones, C. E. M. Démoré, C. Ye, Y. Qiu, S. Cochran, and M. Hill. *IEEE transactions on ultrasonics, ferroelectrics, and frequency control*, 59,1258–66 **(2012)**.

[291] J. Lee, C. Lee, and K. K. Shung. *IEEE transactions on ultrasonics, ferroelectrics, and frequency control*, 57,2305–10 **(2010)**.

[292] F. Zheng, Y. Li, H.-S. Hsu, C. Liu, C. Tat Chiu, C. Lee, H. Ham Kim, and K. K. Shung. *Applied Physics Letters*, 101,214104 **(2012)**.

[293] M. Kolibal, M. Konecny, F. Ligmajer, D. Skoda, T. Vystavel, J. Zlamal, P. Varga, and T. Sikola. *ACS nano*, 6,10098–10106 **(2012)**.

[294] R. Nidetz and J. Kim. *Nanotechnology*, 23,45602 **(2012)**.

[295] S. Gilles, C. Kaulen, M. Pabst, U. Simon, a. Offenhäusser, and D. Mayer. *Nanotechnology*, 22,295301 **(2011)**.

[296] P. Maury, M. Escalante, D. N. Reinhoudt, and J. Huskens. *Advanced Materials*, 17,2718–2723 **(2005)**.

[297] J. Yang, K. Im, and S. Lim. *Applied Surface Science*, 257,5476–5479 **(2011)**.

[298] Y. Jie, J. R. Niskala, A. C. Johnston-Peck, P. J. Krommenhoek, J. B. Tracy, H. Fan, and W. You. *Journal of Materials Chemistry*, 22,1962 **(2012)**.

[299] M. Trevisan, Y. Chevolot, V. Monnier, J.-P. Cloarec, E. Souteyrand, A. Duval, J. Moreau, and M. Canva. *International Journal of Nanoscience*, 11,1240012 **(2012)**.

[300] Y. Zheng, C. H. Lalander, T. Thai, S. Dhuey, S. Cabrini, and U. Bach. *Angewandte Chemie (International ed. in English)*, 50,4398–4402 **(2011)**.

[301] M. Trévisan, M. Schawaller, G. Quapil, E. Souteyrand, Y. Mérieux, and J.-P. Cloarec. *Biosensors & bioelectronics*, 26,1631–1637 **(2010)**.

[302] J. C. Love, L. a. Estroff, J. K. Kriebel, R. G. Nuzzo, and G. M. Whitesides. *Chemical reviews*, 105,1103–1169 **(2005)**.

[303] F. Schreiber. *Progress in Surface Science*, 65,151–256 **(2000)**.

[304] C. Vericat, M. E. Vela, G. Benitez, P. Carro, and R. C. Salvarezza. *Chemical Society reviews*, 39,1805–1834 **(2010)**.

[305] R. Colorado, R. J. Villazana, and T. R. Lee. *Langmuir*, 14,6337–6340 **(1998)**.

[306] Y.-s. Shon and T. R. Lee. *The Journal of Physical Chemistry B*, 104,8192–8200 **(2000)**.

[307] Y.-s. Shon, S. M. Gross, B. Dawson, M. Porter, and R. W. Murray. *Langmuir*, 16,6555–6561 **(2000)**.

[308] M. Lereau, C. Fournier-Wirth, J. Mayen, C. Farre, A. Meyer, V. Dugas, J.-F. Cantaloube, C. Chaix, J.-J. Vasseur, and F. Morvan. *Analytical chemistry*, 85,9204–12 **(2013)**.

[309] T. R. Lee, P. Chinwangso, and A. C. Jamison. *Accounts of chemical research*, 44,511–519 **(2011)**.

[310] J. M. Tour, L. Jones, D. L. Pearson, J. J. S. Lamba, T. P. Burgin, G. M. Whitesides, D. L. Allara, A. N. Parikh, and S. Atre. *Journal of the American Chemical Society*, 117,9529–9534 **(1995)**.

[311] E. B. Troughton, C. D. Bain, G. M. Whitesides, R. G. Nuzzo, D. L. Allara, and M. D. Porter. *Langmuir*, 4,365–385 **(1988)**.

[312] R. G. Nuzzo and D. L. Allara. *Journal of the American Chemical Society*, 105,4481–4483 **(1983)**.

[313] T. M. Willey, A. L. Vance, C. Bostedt, T. van Buuren, R. W. Meulenberg, L. J. Terminello, and C. S. Fadley. *Langmuir*, 20,4939–44 **(2004)**.

[314] Z. Li, T. Niu, Z. Zhang, G. Feng, and S. Bi. *Thin Solid Films*, 519,4225–4233 **(2011)**.

[315] M. Suzuki, T. Miyazaki, H. Hisamitsu, Y. Kadoma, and Y. Morioka. *Langmuir*, 15,7409–7410 **(1999)**.

[316] A. T. Lusk and G. K. Jennings. *Langmuir*, 17,7830–7836 **(2001)**.

[317] L. V. Protsailo, W. R. Fawcett, D. Russell, and R. L. Meyer. *Langmuir*, 18,9342–9349 **(2002)**.

[318] S. W. Han and K. Kim. *Journal of colloid and interface science*, 240,492–497 **(2001)**.

[319] Y.-s. Shon, S. Lee, R. Colorado, S. S. Perry, and T. R. Lee. *Langmuir*, 122,7556–7563 **(2000)**.

[320] F. Tielens, V. Humblot, C.-M. Pradier, M. Calatayud, and F. Illas. *Langmuir*, 25,9980–9985 **(2009)**.

[321] T. Sawaguchi, Y. Sato, and F. Mizutani. *Journal of Electroanalytical Chemistry*, 496,50–60 **(2001)**.

[322] H. Munakata, S. Kuwabata, Y. Ohko, and H. Yoneyama. *Journal of Electroanalytical Chemistry*, 496,29–36 **(2001)**.

[323] S.-i. Imabayashi, N. Gon, T. Sasaki, D. Hobara, and T. Kakiuchi. *Langmuir*, 14,2348–2351 **(1998)**.

[324] S.-i. Imabayashi, D. Hobara, T. Kakiuchi, and W. Knoll. *Langmuir*, 13,4502–4504 **(1997)**.

[325] D. Hobara, T. Sasaki, S.-i. Imabayashi, and T. Kakiuchi. *Langmuir*, 15,5073–5078 **(1999)**.

[326] D. Hobara, M. Ota, S.-i. Imabayashi, K. Niki, and T. Kakiuchi. *Journal of Electroanalytical Chemistry*, 444,113–119 **(1998)**.

[327] D. Hobara and T. Kakiuchi. *Electrochemistry communications*, 3,154–157 **(2001)**.

[328] C. Singh, A. M. Jackson, F. Stellacci, and S. C. Glotzer. *Journal of the American Chemical Society*, 131,16377–16379 **(2009)**.

[329] M. L. Carot, V. Macagno, P. Paredes-Olivera, and E. M. Patrito. *Journal of Physical Chemistry C*, 111,4294–4304 **(2007)**.

[330] J. W. Lee, S. J. Sim, S. M. Cho, and J. Lee. *Biosensors & bioelectronics*, 20,1422–7 **(2005)**.

[331] S. Chen, L. Li, C. L. Boozer, and S. Jiang. *Langmuir*, 16,9287–9293 **(2000)**.

[332] K. Tamada, M. Hara, H. Sasabe, and W. Knoll. *Langmuir*, 7463,1558–1566 **(1997)**.

[333] R. L. Grimm, N. M. Barrentine, C. J. H. Knox, and J. C. Hemminger. *Journal of Physical Chemistry C*, 112,890–894 **(2008)**.

[334] E. Briand, M. Salmain, J.-m. Herry, H. Perrot, C. Compère, and C.-m. Pradier. *Biosensors and Bioelectronics*, 22,440–448 **(2006)**.

[335] E. Briand, M. Salmain, C. Compère, and C.-M. Pradier. *Biosensors & bioelectronics*, 22,2884–90 **(2007)**.

[336] E. Briand, M. Salmain, C. Compère, and C.-M. Pradier. *Colloids and surfaces. B, Biointerfaces*, 53,215–24 **(2006)**.

[337] J.-M. Chang, F.-G. Tseng, and C.-C. Chieng. *IEEE transactions on nanobioscience*, 9,289–296 **(2010)**.

[338] S.-W. Hung, J.-K. Hwang, F. Tseng, J.-M. Chang, C.-C. Chen, and C.-C. Chieng. *Nanotechnology*, 17,S8–S13 **(2006)**.

[339] Z.-H. Wang, A. S. Viana, G. Jin, and L. M. Abrantes. *Bioelectrochemistry (Amsterdam, Netherlands)*, 69,180–186 **(2006)**.

[340] G. Xu, D. P. Woodruff, N. Bennett, M. Elliott, and J. E. Macdonald. *Langmuir*, 26,8174–9 **(2010)**.

[341] S. Tombelli, M. Mascini, and a. P. F. Turner. *Biosensors & bioelectronics*, 17,929–36 **(2002)**.

[342] A. V. Shevade, J. Zhou, M. T. Zin, and S. Jiang. *Langmuir*, 17,7566–7572 **(2001)**.

[343] T. Kakiuchi, M. Iida, N. Gon, D. Hobara, S.-i. Imabayashi, and K. Niki. *Langmuir*, 17,1599–1603 **(2001)**.

[344] F. Tielens, D. Costa, V. Humblot, and C.-m. Pradier. pages 182–190 **(2008)**.

[345] S. M. Morgenthaler, S. Lee, and N. D. Spencer. *Langmuir : the ACS journal of surfaces and colloids*, 22,2706–2711 **(2006)**.

[346] Y. Arima and H. Iwata. *Journal of Materials Chemistry*, 17,4079–4087 **(2007)**.

[347] Y. Arima and H. Iwata. *Biomaterials*, 28,3074–3082 **(2007)**.

[348] J. P. Folkers, P. E. P. E. Laibinis, and G. M. G. M. Whitesides. *Langmuir*, 8,1330–1341 **(1992)**.

[349] L. Li, S. Chen, S. Oh, and S. Jiang. *Analytical chemistry*, 74,6017–22 **(2002)**.

[350] J. P. Folkers, P. E. Laibinis, and Whitesides. *J. Phys. Chem.*, 98,563–571 **(1994)**.

[351] F. Frederix, K. Bonroy, W. Laureyn, G. Reekmans, A. Campitelli, W. Dehaen, and G. Maes. *Langmuir*, 19,4351–4357 **(2003)**.

[352] S. N. Rodrigues, I. C. Gonçalves, M. C. L. Martins, M. a. Barbosa, and B. D. Ratner. *Biomaterials*, 27,5357–5367 **(2006)**.

[353] T. J. Mullen, A. a. Dameron, and P. S. Weiss. *The Journal of Physical Chemistry B*, 110,14410–7 **(2006)**.

[354] T. Kakiuchi, K. Sato, M. Iida, D. Hobara, S.-i. Imabayashi, and K. Niki. *Langmuir*, 16,7238–7244 **(2000)**.

[355] K. Salaita, A. Amarnath, D. Maspoch, T. B. Higgins, and C. a. Mirkin. *Journal of the American Chemical Society*, 127,11283–11287 **(2005)**.

[356] H. Bayat, D. Tranchida, B. Song, W. Walczyk, E. Sperotto, and H. Schönherr. *Langmuir*, 27,1353–8 **(2011)**.

[357] Q. Tang, C.-H. Xu, S.-Q. Shi, and L.-M. Zhou. *Synthetic Metals*, 147,247–252 **(2004)**.

[358] S. Helali, H. Fredj, K. Cherif, A. Abdelghani, C. Martelet, and N. Jaffrezicrenault. *Materials Science and Engineering C*, 28,588–593 **(2008)**.

[359] S. J. Stranick, S. V. Atre, and A. N. Parikh. *Nanotechnology*, 7,438–442 **(1996)**.

[360] I. Wenzl, C. M. Yam, D. Barriet, and T. R. Lee. *Langmuir*, 19,10217–10224 **(2003)**.

[361] S. Lee, A. Puck, M. Graupe, R. Colorado, Y.-s. Shon, T. R. Lee, and S. S. Perry. *Langmuir*, 17,7364–7370 **(2001)**.

[362] B. Park, M. Chandross, M. J. Stevens, and G. S. Grest. *Langmuir*, 19,9239–9245 **(2003)**.

[363] Y. Kwon, Z. Han, E. Karatan, M. Mrksich, and B. K. Kay. *Anal. Chem.*, 76,5713–5720 **(2004)**.

[364] J. Vidic, M. Pla-Roca, J. Grosclaude, M.-A. Persuy, R. Monnerie, D. Caballero, A. Errachid, Y. Hou, N. Jaffrezic-Renault, R. Salesse, E. Pajot-Augy, and J. Samitier. *Analytical chemistry*, 79,3280–3290 **(2007)**.

[365] J. Rundqvist, J. H. Hoh, and D. B. Haviland. *Langmuir*, 22,5100–5107 **(2006)**.

[366] J. Fick, R. Steitz, V. Leiner, S. Tokumitsu, M. Himmelhaus, and M. Grunze. *Langmuir*, 20,3848–53 **(2004)**.

[367] S. Morgenthaler, S. Lee, S. Zürcher, and N. D. Spencer. *Langmuir*, 19,10459–10462 **(2003)**.

[368] S. Watcharinyanon, E. Moons, and L. S. O. Johansson. *The Journal of Physical Chemistry C*, 113,1972–1979 **(2009)**.

[369] L. Yan, C. Marzolin, A. Terfort, and G. M. Whitesides. *Langmuir*, 13,6704–6712 **(1997)**.

[370] M. R. Lockett, M. F. Phillips, J. L. Jarecki, D. Peelen, and L. M. Smith. *Langmuir*, 24,69–75 **(2008)**.

[371] C.-h. Jang, B. D. Stevens, R. Phillips, M. A. Calter, and W. A. Ducker. *Nano Letters*, 3,5–8 **(2003)**.

[372] M. N. Yousaf and M. Mrksich. *J. Am. Chem. Soc.*, 121,12009–12010 **(1999)**.

[373] E. Delamarche, G. Sundarababu, H. Biebuyck, B. Michel, C. Gerber, H. Sigrist, H. Wolf, H. Ringsdorf, N. Xanthopoulos, and H. J. Mathieu. *Langmuir*, 12,1997–2006 **(1996)**.

[374] J. Spadavecchia, J. Moreau, J. Hottin, and M. Canva. *Sensors and Actuators B*, 143,139–143 **(2009)**.

[375] X. Sun, P. He, S. Liu, J. Ye, and Y. Fang. *Talanta*, 47,487–95 **(1998)**.

[376] C.-M. Yam, C.-M. Pradier, M. Salmain, P. Marcus, and G. Jaouen. *Journal of colloid and interface science*, 235,183–189 **(2001)**.

[377] R. Maalouf, C. Fournier-Wirth, J. Coste, H. Chebib, Y. Saïkali, O. Vittori, A. Errachid, J.-P. Cloarec, C. Martelet, and N. Jaffrezic-Renault. *Analytical chemistry*, 79,4879–86 **(2007)**.

[378] R. K. Smith, S. M. Reed, P. a. Lewis, J. D. Monnell, R. S. Clegg, K. F. Kelly, L. a. Bumm, J. E. Hutchison, and P. S. Weiss. *The Journal of Physical Chemistry B*, 105,1119–1122 **(2001)**.

[379] E. a. Smith, W. D. Thomas, L. L. Kiessling, and R. M. Corn. *Journal of the American Chemical Society*, 125,6140–6148 **(2003)**.

[380] G. J. Wegner, H. J. Lee, and R. M. Corn. *Analytical chemistry*, 74,5161–8 **(2002)**.

[381] J. Lee, K. Lee, D. Kim, and I. Choi. *Langmuir*, 19,8141–8143 **(2003)**.

[382] J. P. Collman, N. K. Devaraj, and C. E. D. Chidsey. *Langmuir*, 20,1051–1053 **(2004)**.

[383] J. P. Collman, N. K. Devaraj, T. P. a. Eberspacher, and C. E. D. Chidsey. *Langmuir*, 22,2457–2464 **(2006)**.

[384] J. K. Lee, Y. S. Chi, and I. S. Choi. *Langmuir*, 20,3844–3847 **(2004)**.

[385] C. D. Hodneland, Y.-S. Lee, D.-H. Min, and M. Mrksich. *Proceedings of the National Academy of Sciences of the United States of America*, 99,5048–52 **(2002)**.

[386] W. L. Murphy, K. O. Mercurius, S. Koide, and M. Mrksich. *Langmuir*, 20,1026–30 **(2004)**.

[387] V. Dharuman, B.-Y. Chang, S.-M. Park, and J. H. Hahn. *Biosensors & bioelectronics*, 25,2129–34 **(2010)**.

[388] L. Li, S. Chen, and S. Jiang. *Langmuir*, 19,2974–2982 **(2003)**.

[389] N. Afara, S. Omanovic, and M. Asghari-Khiavi. *Thin Solid Films*, 522,381–389 **(2012)**.

[390] R. Schweiss, D. Pleul, F. Simon, A. Janke, P. B. Welzel, B. Voit, W. Knoll, and C. Werner. *The Journal of Physical Chemistry B*, 108,2910–2917 **(2004)**.

[391] J. T. Liu, C. J. Chen, T. Ikoma, T. Yoshioka, J. S. Cross, S.-J. Chang, J.-Z. Tsai, and J. Tanaka. *Analytica chimica acta*, 703,80–6 **(2011)**.

[392] R. G. Chapman, E. Ostuni, L. Yan, and G. M. Whitesides. *Langmuir*, 16,6927–6936 **(2000)**.

[393] R. K. Smith, P. a. Lewis, and P. S. Weiss. *Progress in Surface Science*, 75,1–68 **(2004)**.

[394] L. Haussling, H. Ringsdorf, F.-J. Schmitt, and W. Knoll. *Langmuir*, 7,1837–1840 **(1991)**.

[395] D. Colin, E. B. T. Y.-t. Tao, G. M. Whitesides, and C. D. Bain. *Journal of the American Chemical Society*, 111,321–335 **(1989)**.

[396] K. Shabtai, S. R. Cohen, H. Cohen, and I. Rubinstein. *The Journal of Physical Chemistry B*, 107,5540–5546 **(2003)**.

[397] S. Xu, S. J. N. Cruchon-Dupeyrat, J. C. Garno, G.-Y. Liu, G. Kane Jennings, T.-H. Yong, and P. E. Laibinis. *The Journal of Chemical Physics*, 108,5002 **(1998)**.

[398] N. Battaglini, Z. Qin, P. Campiglio, V. Repain, C. Chacon, S. Rousset, and P. Lang. *Langmuir*, 28,15095–15105 **(2012)**.

[399] E. Barrena, C. Ocal, and M. Salmeron. *The Journal of Chemical Physics*, 111,9797 **(1999)**.

[400] J. Houplin, L. Amiaud, V. Humblot, I. Martin, E. Matar, R. Azria, C.-M. Pradier, and a. Lafosse. *Physical Chemistry Chemical Physics*, 15,7220–7227 **(2013)**.

[401] L. Liu, D. Deng, Y. Xing, S. Li, B. Yuan, J. Chen, and N. Xia. *Electrochimica Acta*, 89,616–622 **(2013)**.

[402] V. Lebec, J. Landoulsi, S. Boujday, C. Poleunis, C.-M. Pradier, and a. Delcorte. *The Journal of Physical Chemistry C*, 117,11569–11577 **(2013)**.

[403] A. Scholten, B. Menges, M. Juebner, M. a. Rothschild, and K. Bender. *The Analyst*, 138,1705–12 **(2013)**.

[404] J. N. Ngunjiri, D. J. Stark, T. Tian, K. a. Briggman, and J. C. Garno. *Analytical and bioanalytical chemistry*, 405,1985–93 **(2013)**.

[405] A. Vallée, V. Humblot, R. Al Housseiny, S. Boujday, and C.-M. Pradier. *Colloids and surfaces. B, Biointerfaces*, 109C,136–142 **(2013)**.

[406] D. Mercier, C. Mercader, S. Quere, L. Hairault, C. Méthivier, and C. Pradier. *Applied Surface Science*, 258,9518–9525 **(2012)**.

[407] A. Kumar and G. M. Whitesides. *Applied Physics Letters*, 63,2002 **(1993)**.

[408] H. X. He, H. Zhang, Q. G. Li, T. Zhu, S. F. Y. Li, and Z. F. Liu. *Langmuir*, 16,3846–3851 **(2000)**.

[409] R. J. Barsotti, Jr. and F. Stellacci. *Journal of Materials Chemistry*, 16,962 **(2006)**.

[410] J. Stadler, T. Schmid, L. Opilik, P. Kuhn, P. S. Dittrich, and R. Zenobi. *Beilstein journal of nanotechnology*, 2,509–515 **(2011)**.

[411] J.-P. Cloarec, Y. Chevolot, E. Laurenceau, M. Phaner-Goutorbe, and E. Souteyrand. *ITBM-RBM*, 29,105–127 **(2008)**.

[412] G. E. Poirier. *Chemical reviews*, 97,1117–1128 **(1997)**.

[413] D. J. Lavrich, S. M. Wetterer, and S. L. Bernasek. *J. Phys. Chem. B*, 102,3456–3465 **(1998)**.

[414] O. Alévêque, C. Gautier, M. Dias, T. Breton, and E. Levillain. *Physical Chemistry Chemical Physics*, 12,12584–90 **(2010)**.

[415] K. Aoki. *Journal of Electroanalytical Chemistry*, 513,1–7 **(2001)**.

[416] T. Doneux and Y. De Decker. *Langmuir*, 25,2199–2203 **(2009)**.

[417] D. Fischer and A. Curioni. *Langmuir*, 19,3567–3571 **(2003)**.

[418] P. Mehring, a. Beimborn, and C. Westphal. *Applied Surface Science*, 256,7265–7269 **(2010)**.

[419] E. Pensa, E. Cortés, G. Corthey, P. Carro, C. Vericat, M. H. Fonticelli, G. Benítez, A. a. Rubert, and R. C. Salvarezza. *Accounts of chemical research*, 45,1183–1192 **(2012)**.

[420] J. K. Saha, Y. Ahn, H. Kim, G. C. Schatz, and J. Jang. *The Journal of Physical Chemistry C*, 115,13193–13199 **(2011)**.

[421] E. Torres. *DFT Study of Alkanethiol Self-assembled Monolayers on Gold(111) Surfaces*. PhD thesis **(2009)**.

[422] J.-g. Wang. *The Journal of Physical Chemistry C*, 111,12149–12151 **(2007)**.

[423] Y. Yourdshahyan, H. Zhang, and a. Rappe. *Physical Review B*, 63,81405 **(2001)**.

[424] R. G. Nuzzo, B. R. Zegarski, and L. H. Dubois. *Journal of the American Chemical Society*, 109,733–740 **(1987)**.

[425] J. B. Schlenoff, M. Li, and H. Ly. *Journal of the American Chemical Society*, 117,12528–12536 **(1995)**.

[426] L. Salem. *The Journal of Chemical Physics*, 37,2100 **(1962)**.

[427] L. H. Dubois, B. R. Zegarski, and R. G. Nuzzo. *The Journal of Chemical Physics*, 98,678 **(1993)**.

[428] O. Azzaroni, M. E. Vela, H. Martin, A. Herna, G. Andreasen, and R. C. Salvarezza. *Langmuir*, 17,6647–6654 **(2001)**.

[429] E. J. Calvo, M. S. Rothacher, C. Bonazzola, I. R. Wheeldon, R. C. Salvarezza, M. E. Vela, and G. Benitez. *Langmuir : the ACS journal of surfaces and colloids*, 21,7907–7911 **(2005)**.

[430] A. Ulman. *Chem Rev*, 96,1533–1554 **(1996)**.

[431] I. I. Rzeźnicka, J. Lee, P. Maksymovych, and J. T. Yates. *The journal of physical chemistry. B*, 109,15992–15996 **(2005)**.

[432] L. Kankate, A. Turchanin, and A. Gölzhäuser. *Langmuir : the ACS journal of surfaces and colloids*, 25,10435–8 **(2009)**.

[433] Y. Zheng, T. Thai, P. Reineck, L. Qiu, Y. Guo, and U. Bach. *Advanced Functional Materials*, 23,1519–1526 **(2013)**.

[434] K. L. Lusker, J.-R. Li, and J. C. Garno. *Langmuir*, 27,13269–75 **(2011)**.

[435] P. J. Rodríguez-Cantó, M. Martínez-Marco, F. J. Rodríguez-Fortuño, B. Tomás-Navarro, R. Ortuño, S. Peransí-Llopis, and a. Martínez. *Optics express*, 19,7664–7672 **(2011)**.

[436] N. Herzer, S. Hoeppener, and U. S. Schubert. *Chemical communications (Cambridge, England)*, 46,5634–52 **(2010)**.

[437] G.-S. Chen, S.-T. Chen, Y. W. Chen, and Y.-C. Hsu. *Langmuir*, 29,511–8 **(2013)**.

[438] J. Duchet, B. Chabert, J. P. Chapel, J. F. Ge, and J. M. Chovelon. *Langmuir*, 104,2271–2278 **(1997)**.

[439] V. Dugas, C. Demesma, Y. Chevolot, and E. Souteyrand. *Use of organosilanes in biosensors* **(2010)**.

[440] J. Kim, G. J. Holinga, and G. A. Somorjai. *Langmuir*, 27,5171–5175 **(2011)**.

[441] M. E. McGovern, K. M. R. Kallury, and M. Thompson. *Langmuir*, 10,3607–3614 **(1994)**.

[442] E. Briand, V. Humblot, J. Landoulsi, S. Petronis, C.-M. Pradier, B. Kasemo, and S. Svedhem. *Langmuir*, 27,678–685 **(2011)**.

[443] Z. Guo, R. A. Guilfoyle, A. J. Thiel, R. Wang, and L. M. Smith. *Nucleic acids research*, 22,5456–5465 **(1994)**.

[444] C. a.E. Hamlett, K. Critchley, M. Gorzny, S. D. Evans, P. D. Prewett, and J. a. Preece. *Surface Science*, 602,2724–2733 **(2008)**.

[445] U. Jonsson, G. Olofsson, M. Malmqvist, and I. Ronnberg. *Thin Solid Films*, 124,117–123 **(1985)**.

[446] E. Maillart, K. Brengel-Pesce, D. Capela, A. Roget, T. Livache, M. Canva, Y. Levy, and T. Soussi. *Oncogene*, 23,5543–50 **(2004)**.

[447] M. Lestelius, B. Liedberg, and P. Tengvall. *Langmuir*, 13,5900–5908 **(1997)**.

[448] H.-F. Chieh, F.-C. Su, J.-D. Liao, S.-C. Lin, C.-W. Chang, and M.-R. Shen. *Soft Matter*, 7,3808 **(2011)**.

[449] S. V. Atre, B. Liedberg, and D. L. Allara. *Langmuir*, 11,3882–3893 **(1995)**.

[450] P. E. Laibinis, R. G. Nuzzo, and G. M. Whitesides. *J. Phys. Chem.*, 96,5097–5105 **(1992)**.

[451] A. V. Zhuk, A. G. Evans, J. W. Hutchinson, and G. M. Whitesides. *Journal of Materials Research*, 13,3555–3564 **(1998)**.

[452] B. D. Beake and G. J. Leggett. *Physical Chemistry Chemical Physics*, 1,3345–3350 **(1999)**.

[453] C.-H. Shen and J.-C. Lin. *Colloids and surfaces. B, Biointerfaces*, 79,156–63 **(2010)**.

[454] M. D. Porter, T. B. Bright, D. L. Allara, and C. E. D. Chidsey. *Journal of the American Chemical Society*, 109,3559–3568 **(1987)**.

[455] E. L. Smith, C. A. Alves, J. W. Anderegg, and M. D. Porter. *Langmuir*, 8,2707–2714 **(1992)**.

[456] S. M. Mendoza, I. Arfaoui, S. Zanarini, F. Paolucci, and P. Rudolf. *Langmuir*, 23,582–588 **(2007)**.

[457] C. Methivier, B. Beccard, and C. M. Pradier. *Langmuir*, 19,8807–8812 **(2003)**.

[458] H. C. Yang, D. L. Dermody, C. Xu, A. J. Ricco, and R. M. Crooks. *Langmuir*, 12,726–735 **(1996)**.

[459] C. E. Jordan, B. L. Frey, S. Kornguth, and R. M. Corn. *Langmuir*, 10,3642–3648 **(1994)**.

[460] B. L. Frey, R. M. Corn, and S. C. Weibel. *Handbook of Vibrational Spectroscopy*, 2,1042–1056 **(2001)**.

[461] L. Opilik, T. Schmid, and R. Zenobi. *Annual review of analytical chemistry (Palo Alto, Calif.)*, 6,379–98 **(2013)**.

[462] L. Houssiau and P. Bertrand. *Applied Surface Science*, 175-176,399–406 **(2001)**.

[463] P. a. Lewis, R. K. Smith, K. F. Kelly, L. a. Bumm, S. M. Reed, R. S. Clegg, J. D. Gunderson, J. E. Hutchison, and P. S. Weiss. *The Journal of Physical Chemistry B*, 105,10630–10636 **(2001)**.

[464] S. J. Stranick, a. N. Parikh, Y.-T. Tao, D. L. Allara, and P. S. Weiss. *The Journal of Physical Chemistry*, 98,7636–7646 **(1994)**.

[465] V. Humblot, F. Tielens, N. B. Luque, H. Hampartsoumian, and C.-m. Pradier. *Langmuir*, 30,203–212 **(2014)**.

[466] C. Munuera and C. Ocal. *The Journal of chemical physics*, 124,206102 **(2006)**.

[467] F. Tantakitti, J. Burk-Rafel, F. Cheng, R. Egnatchik, T. Owen, M. Hoffman, D. N. Weiss, and D. M. Ratner. *Langmuir*, 28,6950–9 **(2012)**.

[468] N. J. Brewer and G. J. Leggett. *Langmuir*, 20,4109–4115 **(2004)**.

[469] K. F. Domke and B. Pettinger. *Chemphyschem : a European journal of chemical physics and physical chemistry*, 11,1365–73 **(2010)**.

[470] K. Ma, D. J. Kim, K. Kim, S. Moon, and D. Kim. *IEEE Journal of Selected Topics in Quantum Electronics*, 16,1004–1014 **(2010)**.

[471] M. Bergkvist, N. Niamsiri, A. D. Strickland, and C. a. Batt. *Surface Science*, 602,2121–2127 **(2008)**.

[472] P. E. P. E. Laibinis, J. J. J. J. Hickman, M. S. M. M. S. Wrighton, and G. M. Whitesides. *Science*, 245,845–847 **(1989)**.

[473] P. Anstaett, Y. Zheng, T. Thai, A. M. Funston, U. Bach, and G. Gasser. *Angewandte Chemie (International ed. in English)*, 52,4217–4220 **(2013)**.

[474] T. Thai, Y. Zheng, S. H. Ng, S. Mudie, M. Altissimo, and U. Bach. *Angewandte Chemie International Edition*, 51,8732–8735 **(2012)**.

[475] Y. Azuma, S. Suzuki, K. Maeda, N. Okabayashi, D. Tanaka, M. Sakamoto, T. Teranishi, M. R. Buitelaar, C. G. Smith, and Y. Majima. *Applied Physics Letters*, 99,073109 **(2011)**.

[476] N. Okabayashi, K. Maeda, T. Muraki, D. Tanaka, M. Sakamoto, T. Teranishi, and Y. Majima. *Applied Physics Letters*, 100,033101 **(2012)**.

[477] K. Maeda, N. Okabayashi, S. Kano, S. Takeshita, D. Tanaka, M. Sakamoto, T. Teranishi, and Y. Majima. *ACS nano*, 6,2798–803 **(2012)**.

[478] R. Marie, A. B. Dahlin, J. O. Tegenfeldt, and F. Höök. *Biointerphases*, 2,49–55 **(2007)**.

[479] L. Feuz, M. P. Jonsson, and F. Höök. *Nano letters*, 12,873–9 **(2012)**.

[480] N. Zhang, Y. J. Liu, J. Yang, X. Su, J. Deng, C. C. Chum, M. Hong, and J. Teng. *Nanoscale*, 6,1416–22 **(2014)**.

Chapter 2

Materials and methods

Contents

Résumé du Chapitre 2

Ce chapitre présente l'ensemble des matériels et méthodes utilisés pour l'obtention des résultats qui seront présentés par la suite. Le lecteur trouvera en annexes A et C quelques aspects théoriques liés aux techniques de caractérisation et de fabrication des échantillons (lithographie). Plusieurs thiols et silanes ont été utilisés pour la fonctionnalisation de l'or et de la silice. Les différentes thiolations ont été conduites dans l'éthanol à des concentrations d'environ 1 à 10 mM pour des temps d'environ 4h. Les silanisations et double-fonctionnalisations (en une seule étape) ont été conduites dans le dichlorométhane a différentes concentrations et sur des temps plus longs, d'environ 48-72h. Une activation NHS-ester des groupements COOH a été conduite aussi bien dans l'eau que dans le THF avec différents protocoles optimisés pour un certain nombre de paramètres.[1] L'immobilisation de colloïdes et/ou de biomolécules sur ces surfaces fonctionnalisées a été menée dans des tampons aqueux, notamment du PBS-1X ou tout simplement de l'eau ultrapure. Différents outils de caractérisation structurale (SEM, AFM, XRD -sigles anglais-) et physicochimique (Angle de contact, PM-IRRAS, XPS, ToF-SIMS, -sigles anglais-) ont été utilisés avec des paramètres détaillés dans ce chapitre. De la même manière, différents outils ont été employés pour déterminer l'interaction (ancrage) de colloïdes et biomolécules sur surfaces fonctionnalisées (scanner de fluorescence et microscopie électronique).

Introduction to Chapter 2

This chapter presents the different materials and methods used to obtain the results presented in this manuscript. In order for the reader to find this information as simply as possible, it is given in this chapter separately from more general information about the techniques themselves. This more general information can be found in appendixes A and C.

2.1 Surface chemical functionalization

2.1.1 Substrates

Functionalization was carried on on different patterned gold and silica substrates with pattern dimensions going from 1cm to 100nm as already schematically presented in Fig. 1.17. The fabrication of these substrates (mostly through lithography processes) cannot be considered as part of the specific scientific research developped during this PhD and was mostly done by others as specified in appendix A.2. We shall however specify that, after some optimization of the cleaning protocols (see next chapter), it was decided to clean all substrates 24h prior to functionalization, by oxygen plasma with the following parameters :

- Applied (forward) power = 350W (typical reflected power was 10W)
- Oxygen flow = 400 sccm
- Pressure = 90Pa
- Time = 5min

This was conducted in an Anatech© chamber where only oxygen and nitrogen are introduced. When this process was conducted in an etching chamber with input lines of different fluorinated gases (SF_6, CHF_3) fluor contamination was detected afterwards by XPS analysis (see next chapter for more details).

2.1.2 Chemicals

The following chemicals were used for surface functionalization (a short name is given between brackets, which may be a standard short name in the literature or unique to this manuscript) :

- Gold functionalization :
  - 11-mercapto-1-undecanoic acid (MUA) 97 %, from Sigma-Aldrich
  - 11-mercapto-1-undecanol (MUOH) 99 %, from Sigma-Aldrich
  - Undecanethiol (UDT) 98 %, from Sigma-Aldrich
  - 11-amino-undecanethiol hydrochloride (MUAM) 99 %, from Sigma-Aldrich
  - HS-$(CH_2)_{11}$-NH-C(O)-Biotin (MU-Biot) 95 %, from Prochimia
  - 1H,1H,2H,2H-Perfluorodecanethiol (AuF) 97 %, from Sigma-Aldrich
  - HS-$(CH_2)_{11}$-EG_3-OCH_3 (EG3-OMe) , from Prochimia (used in collaboration with Anaïs Garnier)
  - HS-$(CH_2)_{11}$-EG_3-COOH (EG3-COOH), from Prochimia (used in collaboration with Anaïs Garnier)
  - HS-$(CH_2)_{11}$-EG_6-OCH_3 (EG6-OMe), from Prochimia (used in collaboration with Anaïs Garnier)

  - HS-$(CH_2)_{11}$-EG_6-COOH (EG6-COOH), from Prochimia (used in collaboration with Anaïs Garnier)

- Silica functionalization :
  - 2-[methoxy(polyethyleneoxy)propyl]trimethoxysilane (MW=460 g/mol; i.e., 6 ethyleneglycol units in average) (PEG-Si), from abcr.
  - Trichloro(1H,1H,2H,2H-perfluorooctyl)silane (SiF) 97 %, from abcr.

- Activation of COOH terminated SAMs :
  - 1-Ethyl-3-(3-Dimethylaminopropyl)Carbodiimide hydrochloride (EDC) 98 %, from Sigma-Aldrich
  - Diisopropylcarbodiimide (DIC) 99 %, from Sigma-Aldrich
  - *N*-hydroxysuccinimide (NHS) 98 %, from Sigma-Aldrich

- Solvents :
  - Ethanol 99.8 % (EtOH), from Sigma-Aldrich
  - TetraHydroFuran (THF) 99.9 %, from Sigma-Aldrich
  - DiChloroMethane (DCM) 99.5 %, from Sigma-Aldrich

2.1.3 Protocols

2.1.3.1 General considerations

Independently of the substrate or the organic compound used for functionalization, some general considerations were always taken into account :

1. All solvents were degassed (removal of dissolved oxygen) by bubbling nitrogen. DCM and THF were also dried over freshly prepared molecular sieves.
2. All glassware was cleaned by piranha solution, rinsed with abundant water until no acid residue could be found (pH paper evaluation), dried in furnace and then rinsed once with the corresponding solvent prior to functionalization.
3. At the end of the functionalization process, samples were washed for 2x5 minutes in corresponding pure solvent under sonication, rinsed with water and dried under a stream of nitrogen.

2.1.3.2 Gold functionalization

The following protocol [12] was used for the functionalization of gold surfaces [13] with different thiols :

1. Prepare solution by dissolving thiols into ethanol at a concentration of either 10 mM (MUA, MUOH) or 1 mM (UDT, MU-Biot, MUAM, PEG-thiols).
   - For biotinylated thiols previously stored at -20°C, let it heat up to room temperature before opening.

12. Some slight variations of this protocol were used in the different experiments, such as slightly different concentrations or reaction times.

13. Note that this protocol was used either on plain gold substrates or on patterned gold on silica when silica was not functionalized. When silica was also functionalized, the protocol used for orthogonal functionalizations was a single-step protocol (thiols + silanes in DCM) and is presented afterwards.

- A short sonication (30 sec) can help dissolving the thiols

2. Gold functionalization
   (a) Introduce the gold sample previously cleaned by O_2 plasma (at least 24h before to avoid gold oxide) in a glass reactor.
   (b) Introduce the ethanolic thiol solution into the reactor so that the gold sample is completely immersed (for MUA and PEG-thiols, add ultrapure water ; 95/5 v/v ethanol/water).
   (c) Close reactor and let react for 4h, no agitation needed.
3. Wash and dry the sample

2.1.3.3 Silica functionalization

Silanization of silica surfaces with PEG-Si was conducted according to the following protocol :

1. Pure silane (liquid) is stored in a glovebox under nitrogen and only used at the moment of functionalization (no silane solution in DCM prepared beforehand).
2. Silica functionalization
   (a) Introduce the dried DCM into a reactor.
   (b) Add PEG-Si (10µL for 25mL of DCM).
   (c) Introduce the silica sample previously cleaned by O_2 plasma in the reactor.
   (d) Close reactor and let react for 48h - 72h, no agitation needed.
3. Wash and dry the sample

2.1.3.4 Single-step orthogonal functionalizations

For the orthogonal functionalizations of mixed surface, a one-step protocol was used (ie : thiolation and silanization conducted at the same time -in DCM-) :

1. No solution is prepared beforehand, thiols and silanes are introduced directly into the reactor at the moment of functionalization.
2. Functionalization
   (a) Introduce the dried DCM into a clean reactor.
   (b) Add the silanes and thiols in different amounts (given for 25mL of DCM) :
      - MUA / SiF : 50mg / 10µL
      - MUA / PEG-Si : 50mg / 10µL
      - AuF / PEG-Si : 100µL / 10µL
   (c) Introduce the sample previously cleaned by O_2 plasma (at least 24h prior to functionalization) in the reactor.
   (d) Close reactor and let react for 48h - 72h, no agitation needed.
3. Wash and dry the sample

2.1.3.5 Activation of COOH terminated SAMs

After testing different conditions to find optimum parameters,[1] it was decided to carry out NHS-ester formation from -COOH terminated SAMs (activation) either in water or in THF with the following protocols :

1. In water, with EDC :
   - Take EDC out of the freezer (-20°C) and let it come to room temperature.
   - In a previously cleaned (piranha) reactor, add ultrapure water and NHS + EDC at 100mM each. Note that as EDC is very hygroscopic it may be difficult to weight it correctly. Therefore, if possible, use a full unopened flask of EDC (exact weight given by provider) and dilute further if needed.
   - If needed, a short sonication (15 sec) can help dissolve NHS.
   - Introduce solid sample in the reactor and let it react for 30min (longer times are unwanted because of NHS-ester hydrolysis)
   - Rinse with ultrapure water in clean beaker 2x5 min with ultrasounds.
   - Dry with nitrogen

2. In THF, with DIC :
   - In a previously cleaned (piranha) reactor, add dry THF and NHS + DIC at 100mM each.
   - If needed, a short sonication (15 sec) can help dissolve NHS.
   - Introduce solid sample in the reactor and let it react for 24h (activation in THF takes longer times than in water, but has some advantages such as no hydrolysis of NHS-ester or byproduct formation)
   - Rinse with fresh THF in clean beaker 5 min with ultrasounds + another 5 min with ultrasounds in DCM. Soak (5 sec) in ultrapure water.
   - Dry with nitrogen

2.2 Characterization

2.2.1 Substrate properties

AFM and XRD were used mainly to determine the gold surface's roughness and crystallinity before functionalization. AFM characterization was also conducted on functionalized samples, though no clear information could be extracted in our conditions (non-functionalized tip and not atomically flat gold surface). AFM characterization was carried on with the help of Francesca Zuttion and Magali Phaner Goutorbe, and XRD characterization was conducted with the help of José Peñuelas.

2.2.1.1 Atomic Force Microscopy (AFM)

The principle of Atomic Force Microscopy, with an emphasis on its uses for SAM characterization can be found in appendix C.5.

Topography and phase images were taken in air, at room temperature, using a SMENA B (NT-MDT) AFM microscope in the Amplitude Modulation (AM) AFM mode with Mikromash XSC11 with Al backside tips (resonance frequency = 80 kHz). The data analysis was performed with Gwyddion Software.

2.2.1.2 X-Ray Diffraction (XRD)

XRD allows the characterization of a material's cristallinity (grain sizes and crystalline orientations) as explained in appendix C.6.

For the characterization of gold substrates we used a Rigaku Smartlab diffractometer with a rotating anode (power = 9kW). The source emits CuKα radiation and is monochromatised by a double Ge (220) crystal to select the CuKα 1 ray (λ = 0.15406nm). The detector is a point scintillation counter.

2.2.2 SAM *direct* chemical characterization

Functionalized surfaces were characterized by contact angle measurements, PM-IRRAS, XPS, and ToF-SIMS to determine the presence of the different thiols and silanes as well as their chemical composition, environment (e.g., hydrogen-bonding between adjacent chemical groups) and relative proportions. ToF-SIMS analysis were carried on with the help of Didier Léonard at Institut des Sciences Analytiques (ISA). XPS analysis were carried on with the help of Djawhar Ferrah, Claude Botella, and Geneviève Grenet at Institut des Nanotechnologies de Lyon (INL) as well as Thierry Le Mogne at Laboratoire de Tribologie et Dynamique des Surfaces (LTDS) for XPS imaging.

2.2.2.1 Polarization-Modulation InfraRed Reflection Absorbtion Spectroscopy (PM-IRRAS)

The principle of PM-IRRAS has been described by others[2–4] and a summary can be found in appendix C.1.

In short, in a PM-IRRAS setup, as opposed to conventional Infrared Reflection Absorption Spectroscopy (IRRAS), the incident beam polarization is switched from p to s by a PhotoElastic Modulator (PEM) at a given high frequency. This makes it possible to acquire two different signals, corresponding to the difference and sum reflectivities : $|R_p - R_s|$ and $R_p + R_s$. The ratio $\frac{\Delta R}{R_0} = \frac{|R_p - R_s|}{R_p + R_s}$ constitutes a spectrum of the surface, without the need to acquire a background spectrum as in conventional IRRAS. However, the PEM is not efficient at all wavenumbers simultaneously which results in a low-frequency superimposition on the spectrum corresponding to a second order Bessel function.[3]

Thus, the baseline was corrected each time by dividing the experimental spectrum by a spline line fitted to the regions where no peak was expected.[4,5] This method is often used as it gives the correct relative peak intensities albeit yielding arbitrary units for the Y-axis.[5,6]

We used a Nicolet 6700© Fourier-Transform Infrared Spectrosocpy (FTIR) spectrometer coupled to a Hinds Instrument© PEM-100 photoelastic modulator. The optical head model is II-ZS50©. This is a ZnSe crystal, with a nominal frequency of **50 kHz** (polarization switch from p to s at 100 kHz), a useful aperture of 14mm and can work as half-wave plate for different wavelengths in the range of 1µm to 10µm (10000cm^{-1} to 1000cm^{-1}). Unless otherwise specified, the wavenumber of optimum detection (wavenumber at which the PEM works as an oscillating half-wave plate) was set at 2000cm^{-1} for a "full scan" (4000cm^{-1}-1000cm^{-1}). All spectra were acquired at 8cm^{-1} resolution and an angle of incidence of 85° for optimum sensitivity on gold. Further analysis on the spectra were performed with TQ Analyst© and Origin 8.0© software.

2.2.2.2 X-ray Photoelectron Spectroscopy (XPS)

The principle of XPS can be found in detail in appendix C.2.

The XPS results presented here were obtained in a Vacuum Science Workshop (VSW©) chamber equipped with a focused monochromatized X-ray source (AlK_α= 1486.6eV). The acceptance angle of the hemispherical energy analyser is around 3°. On insulating substrates, a "flood gun" was used to add low energy electrons to compensate for charging. Take-off angle was set at 90 degrees. Unless otherwise specified, spectra were acquired with a 0.025eV resolution. When possible, several scans (usually 3 to 10) were co-added to obtain a better signal-to-noise ratio. The spectra on silica were referenced by the Si2p peak at 103.6eV, while the spectra on gold were referenced by the $Au4f_{7/2}$ peak at 84.0eV.

Spectra analysis was carried out with CasaXPS©, Origin8© and Matlab© software.

2.2.2.3 Time-of-Flight Secondary Ion Mass Spectroscopy (ToF-SIMS)

The principle of ToF-SIMS can be found in appendix C.3.

ToF-SIMS measurements were performed with a Physical Electronics TRIFT III instrument (Physical Electronics©, Chanhassen, USA) operated with a pulsed 22keV Au^+ ion gun (ion current of 2nA) rastered over a 300µm × 300µm area. Ion dose was kept below the static conditions limits. Data were analyzed using the WinCadence™ software. Mass calibration was performed on hydrocarbon secondary ions. The maximum deviation between the measured m/z for ToF-SIMS peaks and the exact m/z for the corresponding assigned ions was 20 milli atomic mass unit. Data were normalized to the total intensity minus $H^{+/-}$ intensity because of its low reproducibility and expressed as percentage : $I_{norm} = \frac{I}{I_{total} - I_{H^{+/-}}} \times 100$.

2.2.2.4 Contact angle

The measure of the angle between a drop of liquid and a solid surface (contact angle goniometry) can give important information about the surface's chemistry as explained in appendix C.4.

Static water contact angles were measured on the gold surface at room temperature. A 0.8µL drop of ultrapure water was deposited on three different points throughout the surface. The contact angles were measured right after deposition with WinDrop software from GBX©.

2.2.3 Characterization of SAMs' target-binding and anti-fouling properties

Eventually, it was important to test the SAMs' reactivity towards different targets and assess wheter we could use surface functionalization for the selective trapping of those targets onto precise regions (traps) on the surface. To this purpose, we used mainly functionalized colloids. After depositing the colloids onto the patterned functionalized substrates with different protocols described hereafter, it was easy to assess their localization (efficiency of the selective trapping) by SEM observations.

Additionally, the antifouling properties of PEGylated silica surfaces towards streptavidin could also be assessed by fluorescence scans (streptavidin was previously fluorescently labeled). These antifouling properties were found to vary upon exposure to X-rays used during XPS characterization.

2.2.3.1 Colloid trapping

2.2.3.1.1 Streptavidin-functionalized latex selective immobilization

Streptavidin-functionalized magnetic beads were purchased from Ademtech ("Bioadembeads Streptavidin Plus", 200nm diameter, magnetic core, polymer shell) and deposited onto a patterned biotinylated surface with the following protocol :

1. Wash the beads
   (a) Pour 200µL bead solution into 2mL ultrapure water in an eppendorf tube (the solution is dark brown).
   (b) Perform a magnetic separation of the beads with a neodym magnet placed beside the eppendorf tube until all beads are separated (the solution is transparent again and a dark brown spot is seen close to the magnet ; ca. 5 min)
   (c) Remove supernatant and reintroduce fresh ultrapure water, remove the magnet for dissolving the beads (no need for vortexing and specially no need for ultrasounds that could damage the proteins).
   (d) Repeat magnetic separation and removal of supernatant.
   (e) Resuspend in Ademtech's immobilization buffer 1X (composition of the buffer unknown) [14]
2. Immobilization
   (a) Introduce biotinylated solid sample in the beads solution, in the eppendorf tube. Note : all samples used were small enough (ca. 2x5 mm pieces of silicon wafer) to fit in the 2mL eppendorf tubes. Samples should be kept in a vertical position in order for the beads not to sediment onto the surface (possibly leading to high non-specific adsorption on the whole surface).
   (b) Leave the sample in the bead solution overnight (shorter times may be sufficient but were not tested).
3. Wash the sample
   (a) Let the sample soak in fresh ultrapure water for 2x5 minutes.
   (b) Dry under nitrogen flow.

2.2.3.1.2 Fluorescent carboxylatex selective immobilization

Fluorescent carboxylatex (polystyrene) beads were purchased from Life Technologies (Infrared (715/755) Fluospheres, 109nm diameter, product code : F8799). Micro and nanopatterned gold on silica surfaces were functionalized with MUAM leading to aminated gold patterns. This allowed the specific binding of the fluorescent carboxylatex beads on gold through electrostatic forces. It should be noted that given the small size and density ($1.05 g/cm^3$) it is difficult to wash the beads either by centrifugation or filtration, which explains why the following protocol does not include such a step.

1. Dissolve 100µL of bead solution into 1mL PBS-1X (pH=7.4) in a clean flask.
2. Introduce aminated surface (in these conditions the aminated surface is charged positive NH_3^+ and the beads' surface is negative COO^-.
3. Let react overnight
4. Wash the samples 2x5 min in ultrapure water
5. Let the sample dry by evaporation or gently blowing nitrogen.

14. It may be possible to use Phosphate Buffered Saline (PBS)-1X instead of Ademtech's "immobilization buffer 1X" but we did not test this possibility as the commercial buffer was readily available and not expensive.

2.2.3.1.3 Scanning Electron Microscopy (SEM) assessment of colloid trapping

The principle of SEM can be found in appendix C.7.

The SEM used for observation (different than the one used for nanolithography) was a Mira3 Tescan. It was operated with an acceleration tension of 5kV, a current beam of ca. 250µA with a detection of secondary electrons. These observations allowed us, in the first place, to check the geometry and dimensions of the gold patterns on silica and furthermore to assess the selectivity of the colloid trapping. SEM image analysis with ImageJ software allowed us to compute quantitative data (i.e., percentages of total silica and gold surface covered by colloids).

2.2.3.2 Anti-fouling properties

2.2.3.2.1 Fluorescently labeled streptavidin adsorption

Antifouling properties of PEGylated silica before and after X-ray irradiation (during XPS analysis) were assessed by studying the adsorption of fluorescently labeled streptavidin. Alexa-Fluor-labeled streptavidin (Strepta-F555) was purchased from Life Technologies. PEGylated silica samples were immersed into a 1µg/mL (ca. 0.01 µM) PBS-1X (pH = 7.4) solution of Strepta-F555 for 30min under mild agitation. Then, they were rinsed with PBS-Tween20 0.1% for 2x5min, soaked in ultrapure water and dried under nitrogen.

2.2.3.2.2 Fluorescence scanning

In order to assess the adsorption of fluorescently-labeled streptavidin on different silica surfaces (irradiated or not by X-rays) we used the following protocol : After protein adsorption on two different samples (irradiated and non-irradiated), both samples were scanned simultaneously with the same parameters on a fluorescence scanner (InnoScan 710, from Innopsys). The resolution was set at 3µm and the samples were scanned with a 532nm laser. The focus was manually adjusted, laser power set to "high" (a "low" and "high" value are possible, though the exact power is not given) and PhotoMultiplier Tube (PMT) linear gain set to 80 %. For assessing the fluorescence level on both samples, a 12mm^2 region was evaluated (over 1 megapixel). Fluorescence values were converted to 8 bits and binned by 2 (128 bins) to compute the fluorescence histogram.

References

[1] F. Palazon, C. Montenegro Benavides, D. Léonard, E. Souteyrand, Y. Chevolot, and J.-P. Cloarec. *Langmuir : the ACS journal of surfaces and colloids*, 30,4545–50 **(2014)**.

[2] M. a. Ramin, G. Le Bourdon, N. Daugey, B. Bennetau, L. Vellutini, and T. Buffeteau. *Langmuir : the ACS journal of surfaces and colloids*, 27,6076–84 **(2011)**.

[3] T. Buffeteau, B. Desbat, J. M. Turlet, and C. D. P. Moleculaire. *Applied Spectroscopy*, 45,380–389 **(1991)**.

[4] B. L. Frey, R. M. Corn, and S. C. Weibel. *Handbook of Vibrational Spectroscopy*, 2,1042–1056 **(2001)**.

[5] C. Methivier, B. Beccard, and C. M. Pradier. *Langmuir*, 19,8807–8812 **(2003)**.

[6] E. Briand, M. Salmain, C. Compère, and C.-M. Pradier. *Colloids and surfaces. B, Biointerfaces*, 53,215–24 **(2006)**.

Chapter 3

Results and discussion

Contents

Résumé du Chapitre 3

Les protocoles détaillés au chapitre précédent ont été mis en oeuvre sur diverses surfaces d'or et de silice. Aussi, nous avons pu obtenir des résultats innovants par rapport à l'état de l'art, tant sur la fonctionnalisation chimique et la caractérisation que sur des applications comme l'ancrage sélectif de diverses nanoparticules.

Pour ce faire, nous nous sommes d'une part penchés sur la question de la compatibilité entre les processus de lithographie et de fonctionnalisation chimique de surface. Un de nos objectifs primordiaux était de nous assurer que les opérations unitaires de nanofabrication employées pour la fabrication de nanostructures diverses à l'INL pouvaient être réellement compatibles avec les protocoles de fonctionnalisation chimique de surface développés dans l'équipe Chimie et Nanobiotechnologies. Ceci impliquait d'étudier en détail l'état de surface de nos échantillons après soulèvement (« lift-off »), et de développer des méthodes de traitement de surface spécifiques. Nous avons notamment optimisé notre processus de nettoyage en fin de lithographie pour assurer le bon état de surface des échantillons avant la fonctionnalisation. En effet, il apparaît que les procédés couramment utilisés pour le lift-off des couches minces déposés sur résine laissent des traces carbonées (résidus de résine polymérique) importantes. Ces procédés basés sur la dissolution en solvant organique (acétone, alcool) ne semblent donc pas suffisants pour assurer la compatibilité des méthodes de lithographie et de fonctionnalisation de surface. De ce fait, nous avons décidé de nettoyer les échantillons au plasma d'oxygène. Si celui-ci se révèle très efficace pour enlever les résidus carbonés, deux problèmes peuvent surgir : d'une part, si ce plasma est réalisé dans un bâti de gravure avec entrées de gaz fluorés (tels que SF_6 ou CHF_3), des traces de fluor peuvent contaminer la surface des échantillons ; d'autre part, le plasma d'oxygène sur surface d'or crée une couche d'oxyde Au_2O_3 qui néanmoins est instable. De ce fait, nous avons choisi de réaliser le nettoyage de tout échantillon par plasma d'oxygène dans un bâti dédié, 24h avant la fonctionnalisation.

D'autre part, nous nous sommes intéressés à la fonctionnalisation de surfaces homogènes d'or et de silice et à la caractérisation de ces couches, notamment par XPS et PM-IRRAS. Ces études nous ont permis non seulement de vérifier le bon déroulement de la fonctionnalisation avec nos protocoles, mais surtout de mettre en évidence deux faits marquants :

1. Le rendement et la cinétique d'activation des groupements COOH présents à la surface des SAMs formés par du MUA (dérivation de COOH en NHS-ester) dépend de plusieurs facteurs tels que le solvant et carbodiimide utilisé ou le temps de réaction.[1]

2. Les rayons X utilisés lors des caractérisations XPS induisent une dégradation des surfaces PEGylées qui peut engendrer une perte des propriétés passivantes vis-à-vis de l'adsorption de protéines.

Par ailleurs, nous avons développé des méthodes de fonctionnalisation chimique de substrats *hétérogènes*, plus précisément comportant deux matériaux différents en surface : l'or et la silice. Notre objectif était de simplifier autant que possible les procédures de fonctionnalisation de surface. Nous avons démontré la possibilité d'opérer une double fonctionnalisation (thiolation+silanisation) orthogonale en une seule étape avec le protocole décrit au chapitre 2. La bonne orthogonalité de ces fonctionnalisations a été prouvée à l'échelle macro et microscopique, notamment par cartographie XPS et ToF-SIMS.

Enfin, nous avons mis à profit la fonctionnalisation sélective de micro et nanostructures d'or sur silice, afin de capturer des nanoparticules de latex sur les micro et/ou nanostructures d'or. Ces captures sélectives ont été menées en nous appuyant uniquement sur les interactions entre particules et surfaces fonctionalisées, sans emploi de pince optique ou autre champ de force externe. Nous avons prouvé que cette méthode permet le piégeage sélectif sur des matrices de nanostructures uniques qui sont conçues pour avoir des effets de nano-antennes plasmoniques.[2]

Introduction to Chapter 3

This chapter presents the main results of this thesis. First we will deal with the study of the surface prior to functionalization, specially focussing on the removal of lithography resist residues. Then we will present different results obtained with single functionalizations on plain gold or silica substrates. These results include the optimization of the NHS activation of MUA SAMs[1] and the study of PEG degradation under X-rays used during XPS characterization. Furthermore, we will present chemical characterizations to prove the orthogonal functionalizations of macro and micropatterned gold/silica substrates. Eventually, we will demonstrate how the selective functionalization of gold micro and nanopatterns on silica allows the precise trapping of different latex nanoparticles.

3.1 Surface preconditioning

Before performing surface chemical functionalizations it is important to know the state of the surface. Specially for substrates that have undergone some top-down fabrication steps, it is important to ensure that the surfaces are clean (eg : no photo or e-beam polymeric resists residues). We have therefore tested different cleaning procedures whose performances will be discussed hereafter, along with possible side-effects. Eventually gold surfaces were characterized in regards to their roughness and crystallinity.

3.1.1 Cleaning and (de)oxidation

Before performing surface chemical functionalizations, we must ensure that the surface is appropriately clean. However, surfaces that have undergone lithography processes involving the spin-coating and baking of different polymeric resists may yield residual carbon pollutions.[3] Different approaches can be used to remove such residues, some of which are summarized in appendix A.1.2. For simplicity and availability, we decided to investigate approaches based on organic solvents and on oxygen plasma. [15]

In order to test the efficiency and side-effects of different cleaning procedures, we spin-coated and baked PMMA e-beam resist on silica surfaces. We then removed the resist with the different procedures (dissolution in organic solvents or plasma ashing) and assessed the state of the surface by XPS. Figure 3.1 shows the results of such procedures which can be summarized as follows :

- Organic solvents (acetone + alcohol) could not efficiently remove the polymeric resist. Indeed, high amounts of carbon can be seen on the surface, as evidenced by the C1s peak at 285eV (see Fig. 3.1, top spectrum).
- Plasma ashing conducted in a Reactive Ion Etching (RIE) machine efficiently removed PMMA (low C1s intensity) but left fluorine residues as evidenced by the F1s and FKLL peaks (see Fig. 3.1, middle spectrum). These residues probably come from the use of fluorinated gases such as SF_6 or CHF_3 in the RIE chamber, though these gases were not used here.

15. Piranha solution is often used, specially for uniform surfaces such as plain glass slides. However, previous experiences in the lab have lead to delamination of gold thin films and nanostructures, so that piranha cleaning was dismissed for the present work. UV/ozone was also tested in conjunction with the work of Alice Goudot, PhD student at that time. However, as it did not prove to give better results than oxygen plasma, it was not used further.

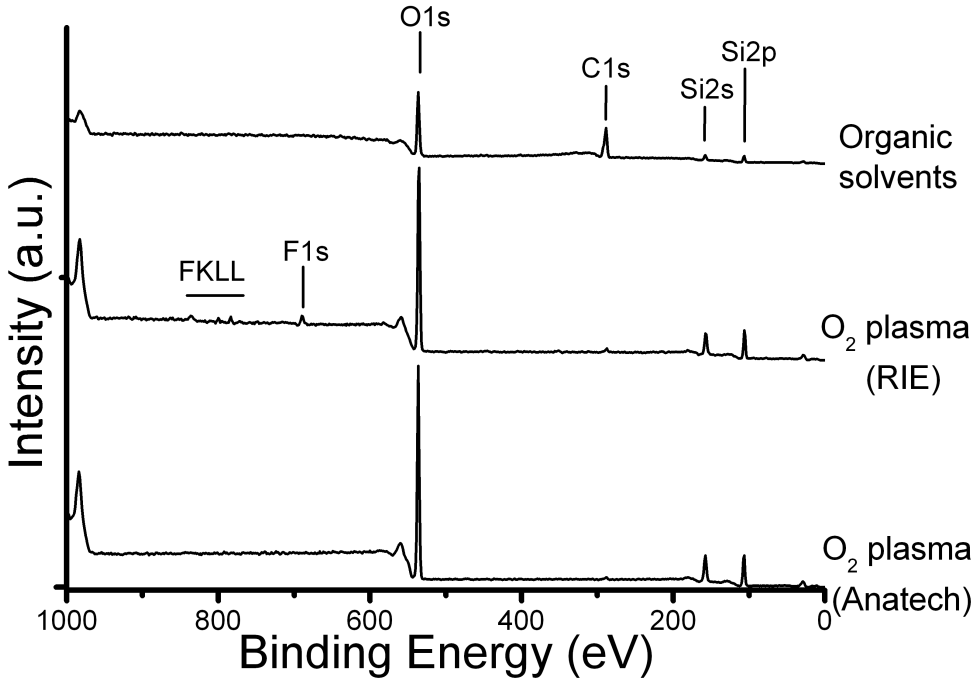

Figure 3.1 – XPS spectra of silica surfaces exposed to PMMA and cleaned with different procedures. (Top) Cleaning with organic solvents leaves polymer residues (high intensity of C1s peak at 285eV). (Middle) Plasma ashing in an RIE machine efficiently removes PMMA but leads to fluorine contamination (F1s and FKLL peaks). (Bottom) Oxygen plasma ashing in a dedicated machine (Anatech) without other gas lines than oxygen and nitrogen, leads to efficient cleaning without introducing other contaminations.

– Plasma ashing conducted in a dedicated machine (Anatech) without lines for other gases than oxygen and nitrogen efficiently removed PMMA without leaving any other contamination (see Fig. 3.1, bottom spectrum).

Thus, oxygen plasma ashing in the Anatech machine seems the best method to clean samples after lithography. However, when the same process (400 sccm oxygen flow with a plasma power of 350 W for 5 min) was used on a *gold* surface, this lead to the formation of gold oxide. Such oxide formation has already been reported by others under similar[4] and different[5,6] conditions. Nonetheless, this oxide layer is known to be unstable and we could follow the surface spontaneous deoxidation by XPS (see Fig. 3.2).

On the basis of these observations, we decided to clean all samples with oxygen plasma 24h prior to surface functionalization. Clean samples are stored in a closed fluoroware box during this time.

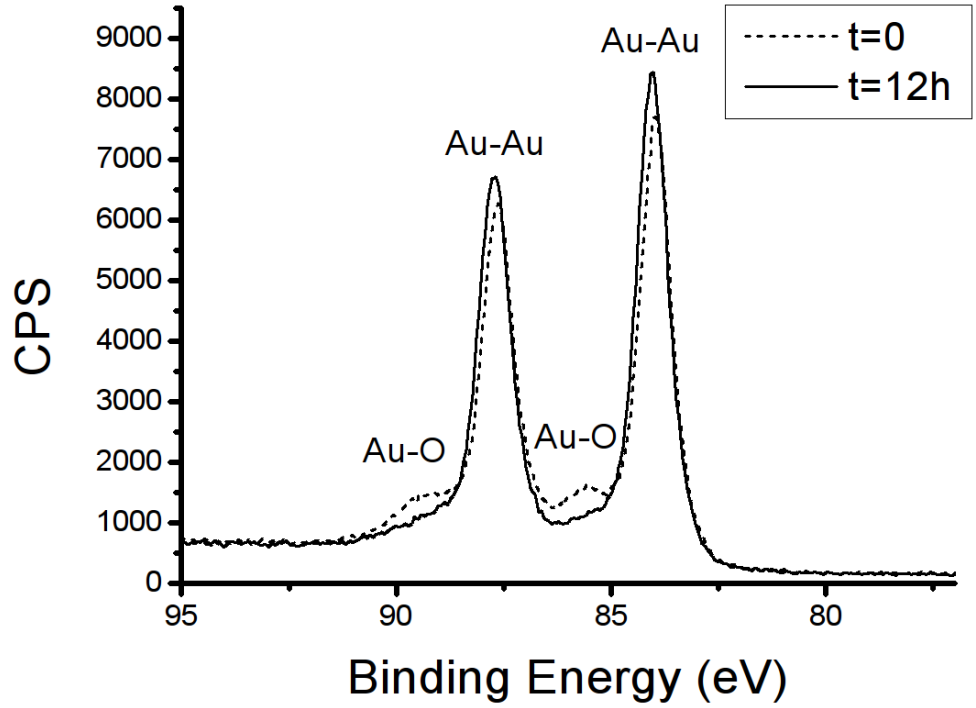

FIGURE 3.2 – Au4f XPS spectra of a gold sample right after undergoing oxygen plasma cleaning and 12h later. Two main peaks can be seen at 87.5eV and 84.0eV corresponding to $Au4f_{5/2}$ and $Au4f_{7/2}$ of plain gold. Two more contributions are detected which are assigned to gold oxide and whose intensity decays over time. This shows that though gold oxide is formed upon exposure to oxygen plasma, the oxygen is desorbed and the surface recovers its metallic nature in ca. 1 day.

3.1.2 Roughness and crystallinity of deposited gold

We investigated the roughness and crystallinity of the deposited gold thin films (ca. 50nm by e-beam evaporation on silica, with an adhesion interlayer of chromium or titanium of ca. 1-3nm). AFM characterization (see Fig. 3.3a) shows that the surface topography of such deposited gold layers is formed by islands having a width of ca. 50-100nm and heights of ca. 4-8nm. The Root Mean Square (RMS) rugosity was found to be around 0.7-1nm. This rugosity was confirmed by X-ray reflectivity measurements (data not shown) and does not seem to be significantly altered by the cleaning method (e.g., oxygen plasma). This surface topography suggests that it would be difficult to obtain information on SAMs built on such surfaces through topography as the SAMs are expected to be on the order of 1nm thick. Indeed, if topography is used to obtain information on such SAMs in the literature, the gold layer is usually made to be atomically flat,[7] which greatly departs from our case. Moreover XRD characterization showed a unique (111) crystalline orientation (see Fig. 3.3b) with grain size in the order of few tens of nanometers, obtained through Scherrer's formula applied to the XRD (111) peak. The (111) gold crystalline orientation is the most widely studied for the formation of thiolate SAMs and most fundamental characteristics of these SAMs described in section 1.2.1.3.2 (e.g., chain orientation and packing density) imply such orientation, though some studies also deal with thiolate SAMs on other crystalline orientations such as (100).[8,9]

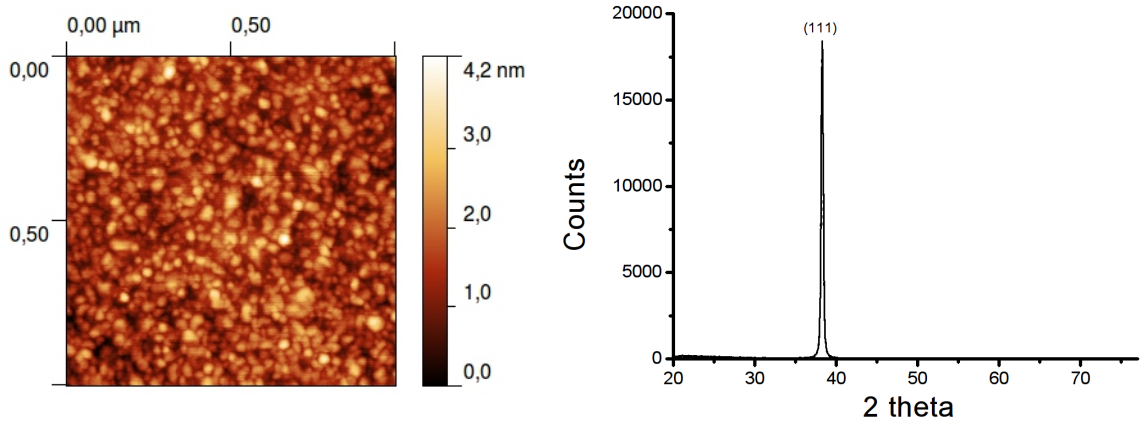

(a) AFM topography image on a gold surface deposited by evaporation (50 nm) onto silica with a chromium adhesion interlayer (2 nm).

(b) XRD characterization of gold surface showing a unique (111) orientation revealed by the peak at $2\theta = 38°$

Figure 3.3 – Gold surface roughness (a) and crystallinity (b)

3.2 Plain substrate functionalizations

Before working on patterned gold/silica substrates, we investigated the functionalization of plain gold and silica. This allowed us in the first place to evidence the formation of different SAMs on these surfaces (see sections 3.2.1.1 and 3.2.2). Most importantly, it allowed us to optimize the NHS activation protocol on MUA SAMs (section 3.2.1.2) and study the degradation of different PEGylated surfaces upon exposure to X-rays during XPS analysis (section 3.2.3).

3.2.1 Plain gold functionalization with different alkylthiols

3.2.1.1 SAMs characterization

Gold was functionalized with different thiols. Though other techniques such as ToF-SIMS, XPS and contact angle measurements have been used to characterize alkylthiolate SAMs on gold, as will be shown in the next sections, PM-IRRAS was most extensively used for this purpose. Indeed, this technique gives a more accurate chemical information than contact angle measurements yet operating in milder conditions (ambient environment) than XPS or ToF-SIMS. Therefore, we could demonstrate the success of our functionalization protocols to form SAMs on gold with alkylthiolates having different headgroups such as biotin, amine or carboxylic acid (see Fig. 3.4). In all cases, the main vibration modes for the undecyl chain can be seen in the spectra : $\nu_{CH_2}^{assym}$ at ca. 2922cm^{-1}, $\nu_{CH_2}^{sym}$ at ca. 2850cm^{-1} and δ_{CH_2} at ca. 1460cm^{-1}. Furthermore, the position of the $\nu_{CH_2}^{assym}$ indicates the close-packing of the alkyl chains in the SAM.[10–14]

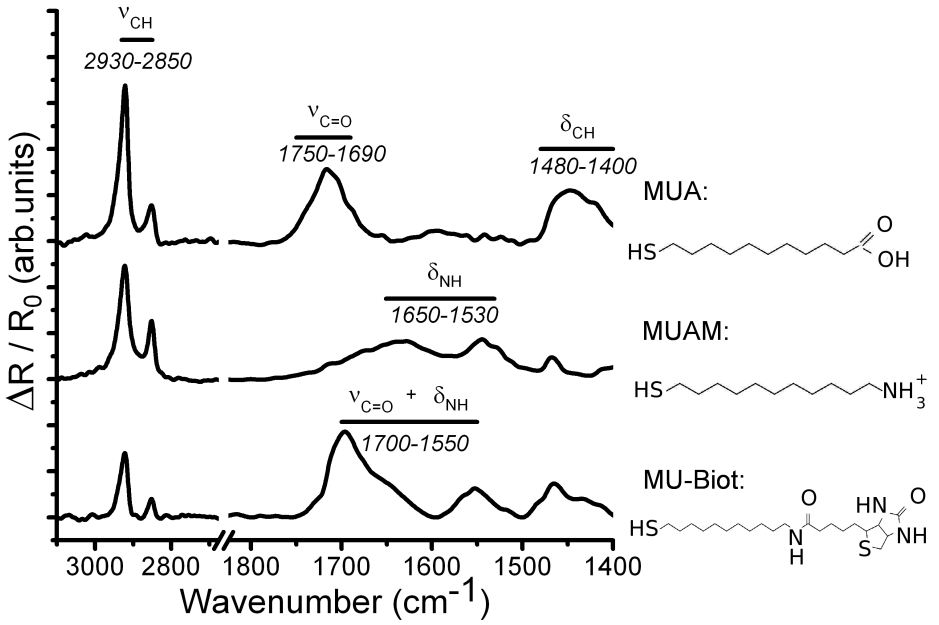

Figure 3.4 – PM-IRRAS spectra of MU-Biot, MUAM and MUA SAMs on gold. The most relevant infrared peaks of each molecules can be clearly identified on the corresponding spectrum, showing the success of the chemical functionalizations.

MUA (Fig. 3.4, top spectrum) exhibits a main peak around 1710cm^{-1} corresponding to $\nu_{C=O}$. The broadness of this band probably indicates different contributions emerging from various degrees of hydrogen bonding between adjacent headgroups.[10,12,15–20] The absence of a contribution around 1590cm^{-1} ($\nu_{O=C-O^-}^{assym}$) indicates the absence of carboxylates[16,17,19,20] though it is known that deprotonation occurs when functionalization is carried on in ethanol.[10] Indeed, the final soaking in ultrapure water of the MUA-functionalized samples allows for the re-protonation of carboxylates into carboxylic acids.[17] We also found that carrying the functionalization in an ethanol/water mixture (95/5 v/v) slowed the rate of MUA deprotonation (data not shown) though it did not prevent it and no clear evidence on its influence on the final SAM structure could be shown.

MUAM (Fig. 3.4, middle spectrum) shows typical vibration modes associated with δ_{NH} at ca. 1650cm^{-1} and 1530cm^{-1}. These bands are associated with the protonated form of the primary amine headgroup (NH_3^+).[21]

MU-Biot (Fig. 3.4, bottom spectrum) exhibits two dominant peaks at ca. 1690cm^{-1} and 1550cm^{-1} which correspond to amide I and amide II vibrations.[12,22,23]

3.2.1.2 NHS-ester activation of MUA-functionalized gold

NB : The following paragraphs are adapted from our previous publication.[1]

Among the different head groups available for immobilizing biomolecules, carboxylic acids (COOH) are commonly chosen for their ability to bind amine groups (NH_2) that are present in proteins, peptides or amino-functionalized oligonucleotides (eg : DNA, RiboNucleic Acid (RNA) or aptamers). COOH and NH_2, being oppositely charged in most biological buffers such as PBS 1X (pH=7.4), can interact electrostatically without further derivatization. However, if covalent binding is desired, it is necessary to *activate* the COOH groups. Activation commonly consists of forming a reactive NHS-ester by a two-step reaction between the acid and a carbodiimide to form *O*-acylurea followed by a reaction between *O*-acylurea and NHS to yield the activated NHS-ester[24] (see Scheme 3.1).

Given the widespread use of this methodology,[12,25–31] it could be thought that a well-established protocol leading to efficient activation exists. However, as noted by others,[24] an important number of parameters vary greatly between studies. Indeed, activation may be performed in water with EDC[12,25–28] but also in organic solvents such as DiMethyl SulfOxide (DMSO)[29] or THF[30] with other carbodiimides such as N,N'-DiCyclohexylCarbodiimide (DCC)[29,31] or DIC.[30] Carbodiimide and NHS concentrations as well as activation time are also found to vary greatly.[23,25,29] Furthermore, there is often no chemical characterization at this stage to prove the efficiency of the activation process. It should be noted that achieving the immobilization of a protein does not constitute a proof of an efficient activation, as proteins can be easily physisorbed and may actually bind to a greater extent on non-activated COOH rather than on NHS-ester.[32]

Recent publications[24,33,34] have highlighted the fact that activation of carboxylic acids on SAMs is a complex reaction (see Scheme 3.2) which can lead not only to the desired NHS-ester formation (reaction (3)) but also to different byproducts such as *N*-acylurea (reaction (1)) or anhydrides (reaction (2)) :

In addition to the different possible reactions reported in Scheme 3.2, it should be noted that hydrolysis of different species can furthermore complexify the overall reaction scheme. Most importantly, carboxylic acids can be regenerated at the surface through the hydrolysis of *O*-acylurea[35] or NHS-ester.[36] Additionally the hydrolysis of carbodiimides and *O*-acylurea can also produce other byproducts such as urea derivatives.[35,37]

Sam et al.[24] showed the impact of EDC and NHS concentration on the efficiency of the activation process and the appearance of the aforementioned byproducts, with a systematic infrared characterization of the different terminal groups at the surface, albeit not providing information about the kinetics of the different reactions.

ToF-SIMS and PM-IRRAS are surface-sensitive methods specially suited for this study. Indeed, as shown by Frey et al.[23] the activation process can be monitored by the presence of an infrared absorption peak at ca. 1820cm^{-1}. It should be noted that during the activation, other bands appear at ca. 1785cm^{-1} and 1745cm^{-1}, the latter being the most prominent one. However, these two are linked to NHS (be it covalently bonded or just adsorbed) and are therefore not representative of the activated ester (NHS covalently bonded to the acid head group).

Step 1 :

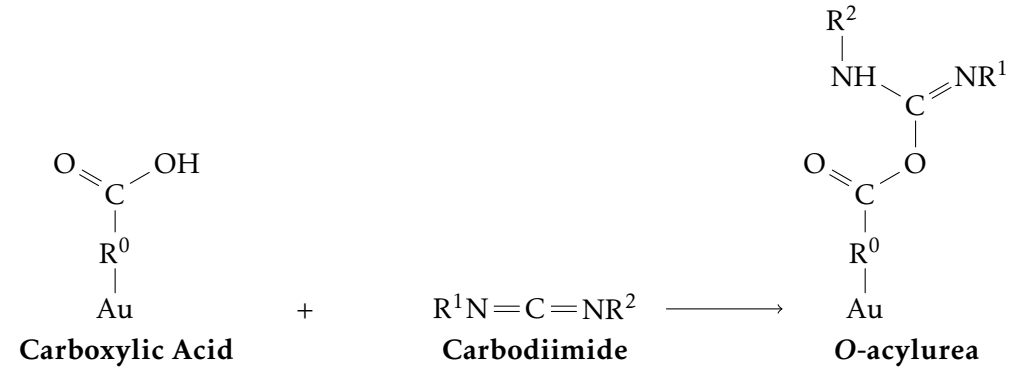

Step 2 :

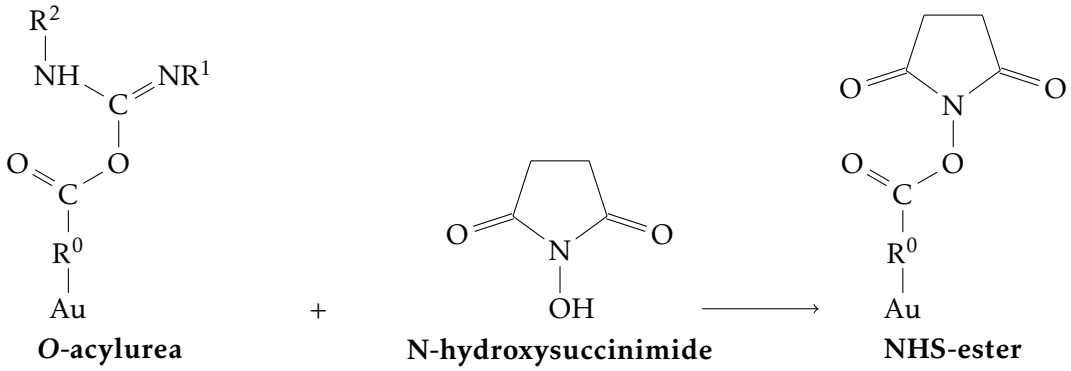

Scheme 3.1 – Activation of carboxylic acids by carbodiimide and NHS without byproducts.[24]

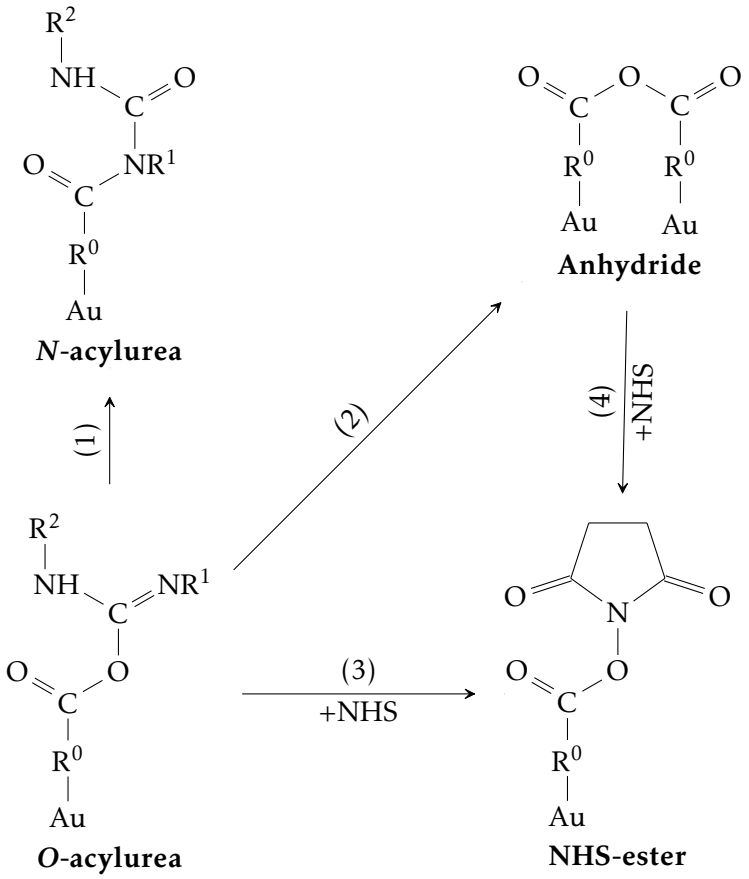

Scheme 3.2 – Possible derivatizations of *O*-acylurea in the presence of NHS, including the expected NHS-ester and main byproducts : *N*-acylurea and anhydride.[24]

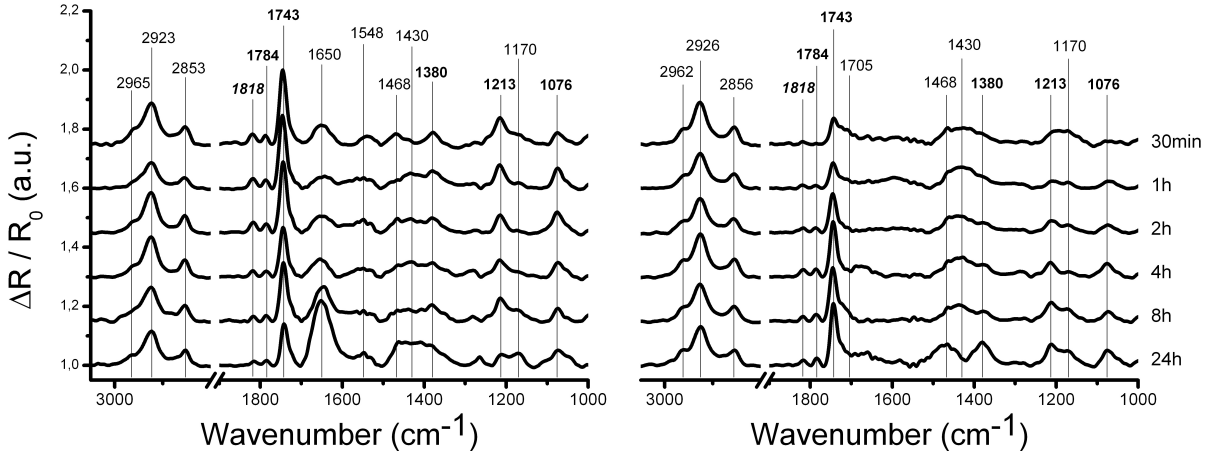

(a) Water (b) THF

Figure 3.5 – Samples activated in (a) water and (b) THF with 100 mM concentrations of corresponding carbodiimide and NHS. Characteristic NHS absorption wavenumbers are written in bold and 1818cm^{-1} peak, characteristic of NHS-ester is written in bold and italics.

Hereafter we present a methodological study on the activation process of 1-mercapto-11-undecanoic acid (MUA) SAMs on gold under different conditions, characterized by PM-IRRAS and ToF-SIMS. The following results highlight the different esterification and byproduct formation kinetics depending on the nature of the carbodiimide and corresponding solvent (EDC in water vs DIC in THF) as well as the reactants' concentrations.

Fig. 3.5 show the evolution of the surface upon activation in water and THF with concentrations of 100mM in carbodiimide and NHS.

Many features can be distinguished in these spectra, some of which relate to the presence of NHS : $\nu_{C=O}$ triplet at 1818cm^{-1}, 1784cm^{-1} and 1743cm^{-1}, ν_{NCO}^{sym} at 1076cm^{-1}, ν_{CNC}^{assym} at 1213cm^{-1} and ν_{CNC}^{sym} at 1380cm^{-1} (with a possible contribution from $\delta_{CH_3}^{rock}$ that will be discussed later).

To quantify the activation of carboxylic acids, it is tempting to consider the ca. 1743cm^{-1} band, as it is the most prominent one in succinimidyl esters. However, this band is not characteristic of the activated ester as it is also present in potentially physisorbed succinimide. Furthermore, it can be overlapped by the $\nu_{C=O}$ of free carboxylic acids. Therefore we have quantified the area under the 1818cm^{-1} band, characteristic of the NHS-ester. It should be noted that this attribution implies the lack of anhydride at the surface, which is consistent with the lack of a peak at 1750cm^{-1} and the similar evolution and widths of the 1818cm^{-1} and 1784cm^{-1} peaks which suggest a unique contribution for both.[24] Moreover, this is consistent with the literature[24] that suggests that the direct NHS-ester formation is dominant in comparison to the anhydride intermediate at such high concentrations of NHS, although an anhydride intermediate may have been formed at the very early stages (first few minutes) of the reaction[34] and therefore not detected here. Very different behaviours were shown depending on the solvent (and corresponding carbodiimide), the concentration and time. These are summarized in Figure 3.6. One can see that activation in water occurs very fast (<30 min) at both concentrations and then decays (immediately at 20 mM ; after 2 h at 100 mM) to yield almost no activated esters at 24 h. This can be explained by the competing hydrolysis of the ester in water.[36]

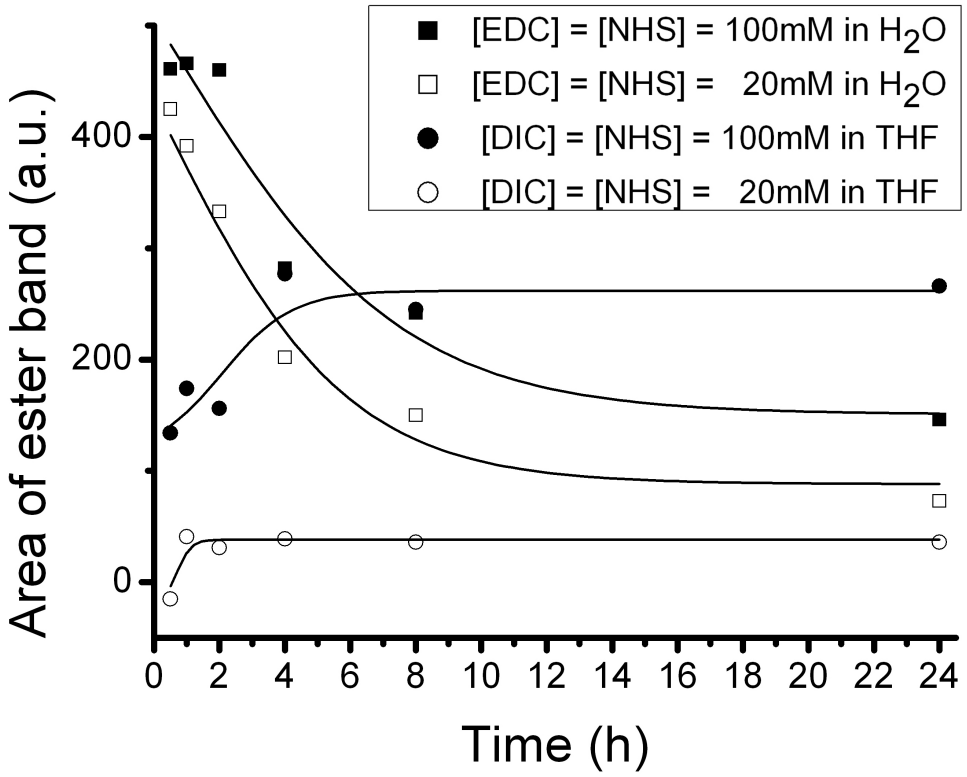

Figure 3.6 – Area of the 1818cm^{-1} peak for different solvents/carbodiimides, concentrations and times. Below a value of 150 a.u. the peak is barely noticeable.

In THF, however, activation is only evidenced for the higher concentration (100 mM) and after ca. 1 h. After 4 h a more or less constant level is maintained until 24 h (no measurements were performed at times greater than 24 h).

It should be noted from Fig. 3.5 that the peaks corresponding to the NHS (cycle) (1784cm^{-1}, 1743cm^{-1}, 1076cm^{-1}, 1213cm^{-1} and 1380cm^{-1}) evolve in the same way as the NHS-ester peak 1818cm^{-1} which suggests that there is no adsorbed NHS at the surface.

Concerning the other peaks present in Fig. 3.5 (activation in water and in THF), the bands at 2926cm^{-1}-2923cm^{-1}, 2856cm^{-1}-2853cm^{-1} and 1468cm^{-1} can be attributed to vibration modes of the alkyl chain ($\nu_{CH_2}^{assym}$, $\nu_{CH_2}^{sym}$ and δ_{CH_2} respectively) which are independent of the activation process and therefore more or less constant in both cases.

The region between 1743cm^{-1} and 1468cm^{-1} is more interesting as it presents clear differences between water and THF as well as different evolutions in each sample. First we can see that two bands are present at 1650cm^{-1} and 1548cm^{-1} in the sample activated in water and not in THF. These bands are strongly evocative of amide I and II vibrations which suggest the presence of *N*-acylurea byproduct. A contribution from δ_{H_2O} of adsorbed water may also be possible, as noted by others in similar studies[17,34]. Such increase in hydrophilicity would be consistent with the hydrolysis of NHS-ester into carboxylic acids.[34] However, the principal assignment of this peak to *N*-acylurea seems more likely, considering the following characterization by ToF-SIMS as well as the fact that, in order for physisorbed water to have a significant signal by PM-IRRAS, most water molecules should have a precise orientation in regards to

the surface (PM-IRRAS is insensitive to isotropic dipoles). In THF, no water or amide bands could be detected. In contrast, the carbonyl region was found to be much broader (1743cm^{-1}-1705cm^{-1}) which suggests unreacted carboxylic acids at the surface. This is consistent with the slower kinetics of esterification in this solvent.

ToF-SIMS measurements were carried out on these surfaces for further analysis of the final products (see Fig. 3.7) and normalized intensities ($I_{norm} = \frac{I}{I_{total} - I_{H^{+/-}}} \times 100$) of various characteristic ions were calculated. Figs 3.7a and 3.7b indicate the detection on both surfaces of CN^- at m/z=26 (3.87% in THF and 6.85% in water) and of CNO^- at m/z=42 (11.72% in THF and 5.82% in water). However, other signatures indicate a different nitrogen-based surface chemistry. Indeed, in THF we can observe an intense peak at m/z=98 (9.48%) which can be assigned to $C_4H_4NO_2^-$ of NHS.[38] This represents only 0.35% on the sample activated in water. The m/z=114 peak in Fig. 3.7b can also be assigned to an NHS moiety ($C_4H_4NO_3^-$)[38] and is absent in Fig. 3.7a. Conversely, in positive mode (Figs. 3.7c and 3.7d) we can see a main difference at m/z=30 which can be assigned to CH_3NH^+. This represents 5.54% in water versus 0.75% in THF. This, as well as the m/z=84 peak ($C_4H_6NO^+$) are consistent with the structure of EDC-derivated *N*-acylurea. These peaks could also originate from other EDC-derivatives including *O*-acylurea, physisorbed EDU (EDC urea derivative from hydrolysis[37]) or plain unreacted EDC. However, the assignment to *N*-acylurea seems more reasonable given the high reactivity of *O*-acylurea and the thorough washing under sonication as well as the previously mentioned amide bands on the PM-IRRAS spectra. In summary, ToF-SIMS analysis confirm the higher amount of NHS on the sample activated in THF after 24h compared to the one activated in water and the predominance of an EDC-derivated byproduct assigned to *N*-acylurea on the latter.

Furthermore, a shoulder to the $\nu_{CH_2}^{assym}$ peak in Fig. 3.5 could be detected in both samples at 2965cm^{-1}-2962cm^{-1}. This peak may be attributed to $\nu_{CH_3}^{assym}$ (the corresponding $\nu_{CH_3}^{sym}$ around 2870cm^{-1} is likely too weak and overlapped by the $\nu_{CH_2}^{assym}$ and $\nu_{CH_2}^{sym}$ peaks to be clearly identified). The presence of CH_3 groups at the surface may be assigned to alkyl moieties of *N*-acylurea byproduct in water and unreacted *O*-acylurea in THF.

The 1430cm^{-1} peak may be assigned to δ_{OH}^{COOH}. Another contribution to this peak could come from $\nu_{O=C-O^-}^{sym}$ of carboxylates (the corresponding $\nu_{O=C-O^-}^{assym}$ at ca. 1580cm^{-1} is hardly detected due to the dipole's orientation to the surface). Deprotonation of carboxylic acids occur as they interact with the carbodiimide. This peak's important decrease in THF from 8h to 24h is not translated into an increase of NHS-ester but rather an increase in $\nu_{CH_3}^{sym}$ and $\nu_{CH_3}^{assym}$ which would suggest a higher conversion of COOH into unreacted *O*-acylurea.

Eventually, a peak at 1170cm^{-1} is present in Fig. 3.5 whose interpretation is uncertain.

NHS activation with different solvents and carbodiimides at different concentrations has been investigated by PM-IRRAS and ToF-SIMS. Our results show that, though the common procedure of activation in water with EDC/NHS does indeed lead to rapid esterification of the carboxylic acids even at 20mM concentration, these activated esters are very unstable and rapidly hydrolized. Their presence could barely be detected after 24h by the 1818cm^{-1} and the m/z=98 peaks (PM-IRRAS and ToF-SIMS respectively). Furthermore, especially at high concentrations of EDC and NHS, significant amounts of *N*-acylurea byproduct may be formed, as suggested by the infrared amide I and II bands as well as CH_3NH^+ and $C_4H_6NO^+$ ToF-SIMS peaks. Moreover, an important increase in the 1650cm^{-1} band between 8h and 24h suggests the contribution of adsorbed water (increase in hydrophilicity of the surface).

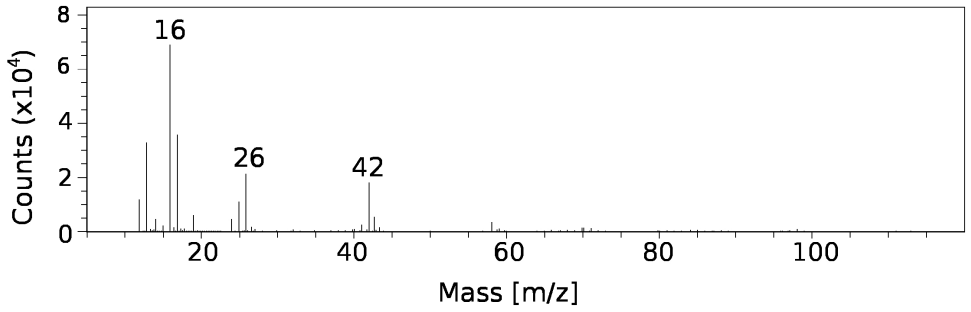

(a) Water - negative

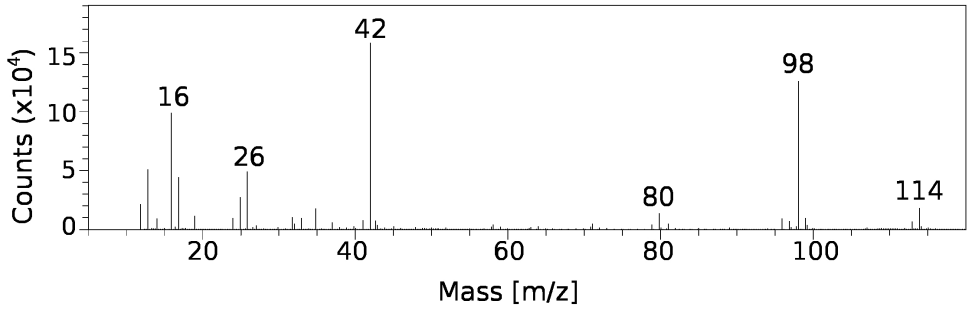

(b) THF - negative

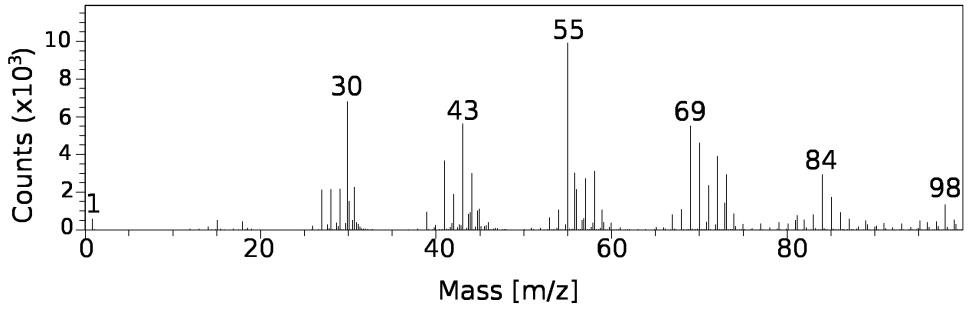

(c) Water - positive

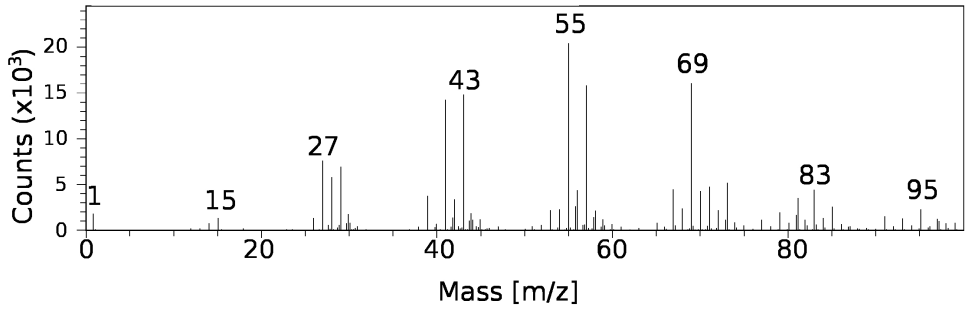

(d) THF - positive

Figure 3.7 – Negative ((a) and (b)) mode and positive ((c) and (d)) mode ToF-SIMS spectra of samples activated in water ((a) and (c)) and THF ((b) and (d)) after 24h, in the range of m/z=5-120 (negative mode) and m/z=0-100 (positive mode).

In contrast, activation conducted in THF with DIC requires higher concentrations of carbodiimide and NHS and longer times ; but is more stable, and does not form *N*-acylurea. However, it seems that unreacted *O*-acylurea remained after 24h, evidenced by the methyl band at 2965cm^{-1}-2962cm^{-1}.

3.2.2 Plain silica functionalization with PEG-silanes

We also investigated the silanization of silica surfaces with PEG-Si to make these surfaces resistant to protein adsorption. Figure 3.8 shows an XPS spectrum of the C1s core-level of a PEGylated silica surface.

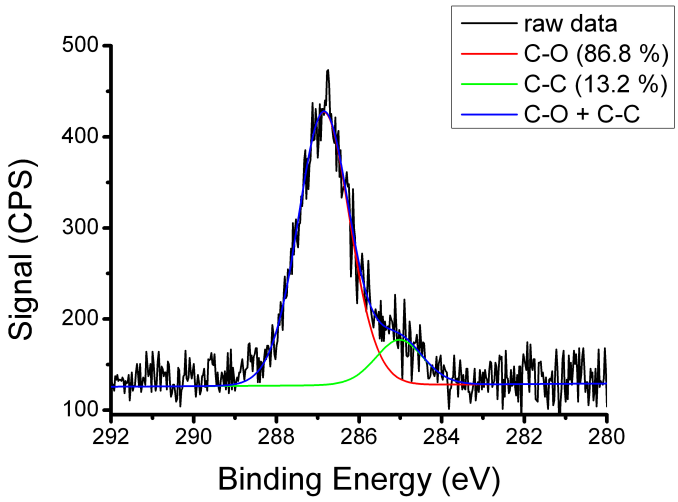

Figure 3.8 – C1s XPS spectrum of PEGylated silica surface. Because of the degradation of such molecule under irradiation a single scan is presented instead of the usual co-addition of several scans which, in the absence of degradation, would yield a better signal-to-noise ratio.

The spectrum is dominated by a peak at ca. 287eV which can be assigned to the ether carbons in the OEG chain C-*C*-O (86.8 % of C1s peak). A second contribution can be detected at ca. 285eV corresponding to the propyl chain of the silane, though this contribution is obviously far less intense (13.2 % of C1s peak). The O1s peak is largely dominated by the contribution of the silica substrate and therefore not shown here since we could not extract the contribution of the OEG chain. Similarly, no chemical shift could clearly be identified on the Si2s and Si2p peaks linked to the silanes. The characterization of PEGylated surfaces by XPS led us to an unplanned study of the effects of X-ray irradiation on such organic layers. This study, is presented in the next section.

3.2.3 Effect of X-rays on PEGylated surfaces

Surfaces modified with OEG and PEG are well known for their antifouling abilities. PEGylated gold[39,40] and silica[41–45] surfaces are thus widely used in biosensor and microarray technologies, lowering non specific adsorption of interfering species.[46,47] In some circumstances, ethylene glycol moieties can be degraded. Modifications of PEGylated surfaces upon UV or electronic irradiation have already been described.[48–50] PEG can be degraded in ambient atmosphere by photo-oxydation under UV irradiation, for instance via UV photolithography, or near-field optical microscopy.[48] This causes a cleavage of ether bonds, and yields drastic modifications of the PEG film properties, such as antifouling loss. Oxidative degradation of monolayers of OEG-functionalized alkenes on silicon were performed using an AFM probe with a bias potential.[49] PEG and Poly(OxyEthylene) (POE) films can also be crosslinked with submicrometer resolution under e-beam exposure.[51] During XPS analysis, X-rays provide another type of irradiation, proven to modify polymers. This is the case with halogenated polymers -

PolyVinyliDene Fluoride (PVDF),[52] Poly(Vinyl Chloride) (PVC),[53,54] PolyTetraFluoroEthylene (PTFE),[54]- or sulfonated polyethers.[55] However, to our knowledge, the effect of X-rays irradiation on OEG and PEG surfaces in ultra high vaccum during XPS measurements was never reported. Yet XPS[44,56,57] is a common method to characterize surfaces, and is commonly used for characterizing surface functionalized bioanalytical systems or biomaterials. Therefore, exploring the impact of X-rays on PEG layers may be useful for better interpreting XPS characterization of such layers, and understanding their limits.

In the present work, we explored how X-ray Photoelectron Spectroscopy measurements can directly affect the properties of PEGylated surfaces. In situ XPS was used for both characterizing and modifying PEGylated silica and gold surfaces. Other surface-sensitive techniques such as PM-IRRAS,[1,58,59] static water contact angle and fluorescence measurements provided additional characterizations of PEGylated surfaces. We demonstrated that X-rays generated during XPS measurements can damage and partially remove the ethylene glycol moieties of thiols and silanes bound on gold and silica surfaces. Eventually, we showed how this degradation directly impacts the antifouling properties of PEGylated surfaces.

The C1s XPS spectrum of molecules containing alkyl and OEG chains shows two characteristic peaks at 286.5eV (assigned to *C*-O of OEG chain) and 285.0eV (assigned to *C*-C of alkyl chain). Both of these contributions are clearly evidenced on the PEGylated silica (Fig. 3.9) and gold (Fig. 3.10) surfaces.

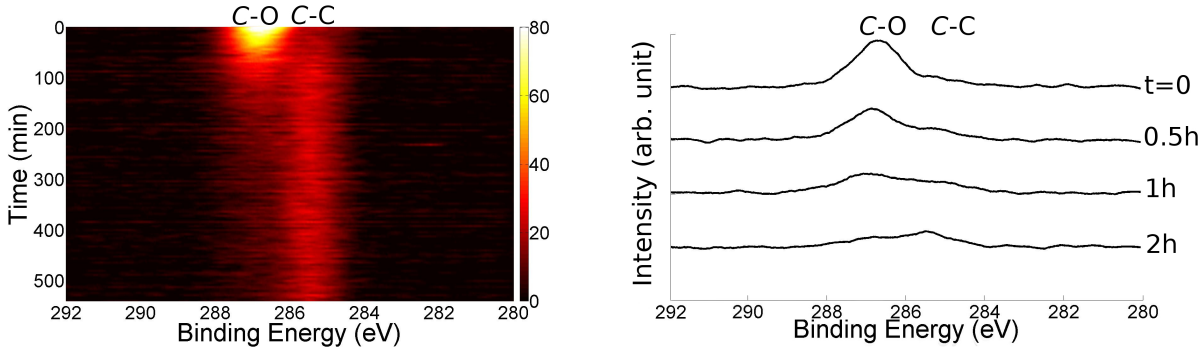

(a) (b)

Figure 3.9 – Evolution of the C1s spectra of PEGylated silica. Left image shows a map of the spectrum over time. The time between two scans is ca. 3.6 minutes. Right image shows 4 spectra in detail at selected times.

In both cases, it can be seen that upon X-ray irradiation, the intensity of the *C*-O peak decreases while the intensity of the *C*-C is maintained. On gold, the observed decrease of the contribution at 286.5eV is accompanied by the decrease of the O1s core level intensity and an increase of the Au4f contribution to the surface, suggesting a shrinking of the organic layer (see Fig. 3.11 and Table 3.1).

As can be seen in Fig. 3.12 the relative intensities of both carbon contributions ($\frac{CO}{CO+CC}$; $\frac{CC}{CO+CC}$) vary over the course of the measurement. The different kinetics found on gold and silica will be discussed along with possible reaction mechanisms in a further section.

These results suggest that characterization by XPS itself can be impacted. Indeed, it is common to characterize such SAMs by evaluating the relative intensities of both contributions. However, specially for silica, the degradation seems fast enough to make it difficult to achieve an authentic account of the surface.

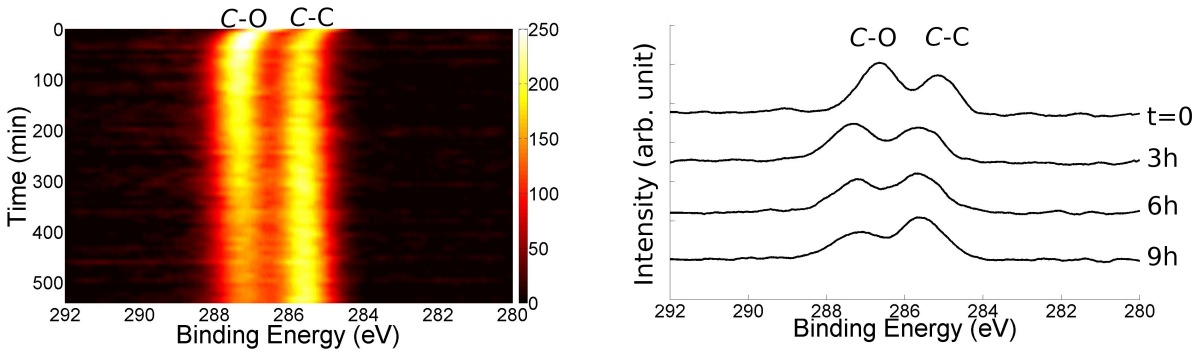

(a) (b)

Figure 3.10 – Evolution of the C1s spectra of PEGylated gold. Left image shows a map of the spectrum over time. The time between two scans is ca. 9 minutes. Right image shows 4 spectra in detail at selected times.

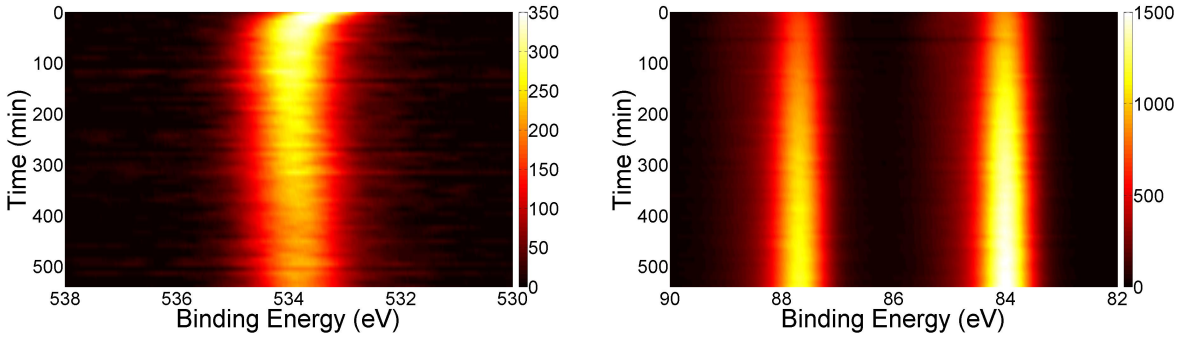

(a) O1s (b) Au4f

Figure 3.11 – Evolution (map) of the O1s (a) and Au4f (b) spectra of PEGylated gold over time of continuous irradiation. The time between two scans is ca. 9 minutes.

Element	Atomic % at t=0	Atomic % at t=9h
Oxygen	28.14	20.58
Carbon	60.20	61.67
Gold	11.66	17.75

Table 3.1 – Atomic percentages of oxygen, carbon and gold on PEGylated gold surfaces before and after 9h irradiation, determined by XPS. This evolution confirms the shaving of OEG moiety with the decrease of O1s and increase of gold substrate contribution. The carbon amount, though decreasing in absolute value, has roughly the same contribution to the surface composition (few nanometers) which is consistent with the stability of the alkyl chains on the surface.

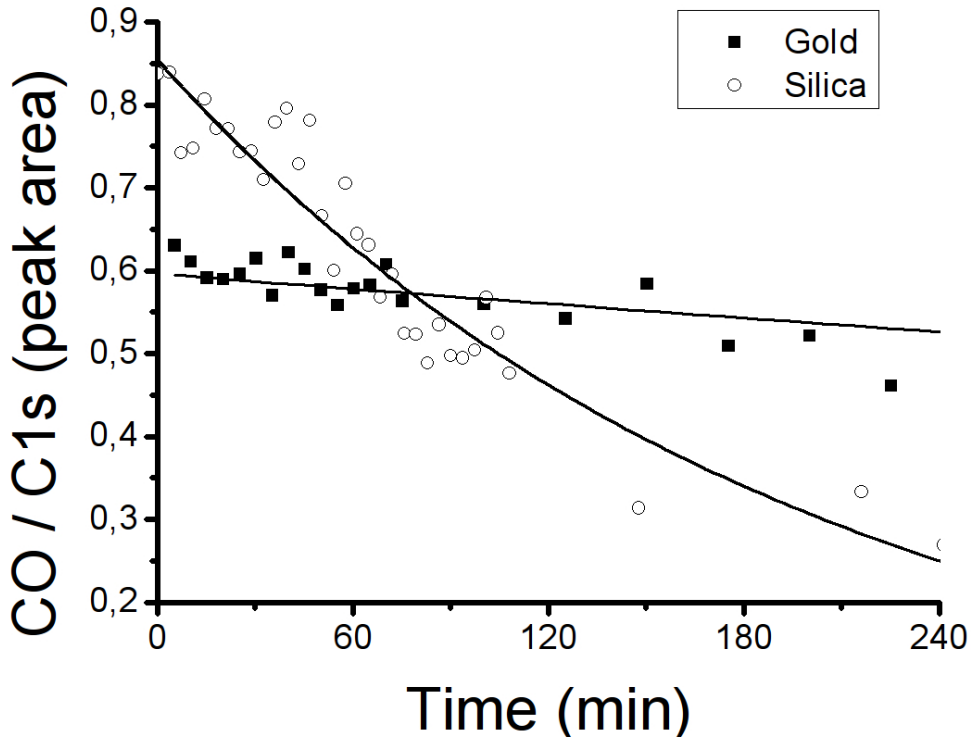

FIGURE 3.12 – Relative contributions of OEG (CO peak) to the total C1s amount. On silica, the low intensity of peaks after 4h makes it difficult to fit both contributions. On gold, the normalized CO intensity continues to decay linearly reaching a value of under 0.3 after 9h (not shown here).

This decay of the *C*-O peak in XPS is consistent with PM-IRRAS characterization of the PEGylated gold surface before and after X-ray irradiation (see Fig. 3.13).

Indeed, PM-IRRAS spectra before and after X-ray irradiation show the decrease of OEG-related vibration modes. Because of the baseline correction in PM-IRRAS, it is not straightforward to compare absolute values between both spectra. However, it is safe to compare the relative contributions of OEG and alkyl related modes. Before irradiation, the spectrum is dominated by the stretching mode of ether bonds in OEG, ν_{C-O-C}. After irradiation this peak has severely decayed and become secondary to the stretching modes of methylenes in the alkyl chain, ν_{CH_2}. Other peaks also show an evolution that is consistent with the decay of OEG tails and COOH headgroups and the relative stability of alkyl chains, as can be seen in Fig. 3.13.

Furthermore, static water contact angle measurements before and after irradiation of a PEGylated gold surface showed a decrease in hydrophilicity of the surface from $\cos\theta = 0.778 \pm 0.010$ to $\cos\theta = 0.614 \pm 0.017$. This is also consistent to the loss of the COOH head-group and shortening (or complete loss) of the PEG moiety.

Finally, we introduced a reference PEGylated silica sample along with the irradiated one in the XPS chamber (exposed to flood gun low energy electrons, but not irradiated by X-rays). Characterization of the surface before and after 18 hours in the chamber can be seen in Fig. 3.14. These spectra show an almost identical surface composition, dominated by carbons in OEG tails.

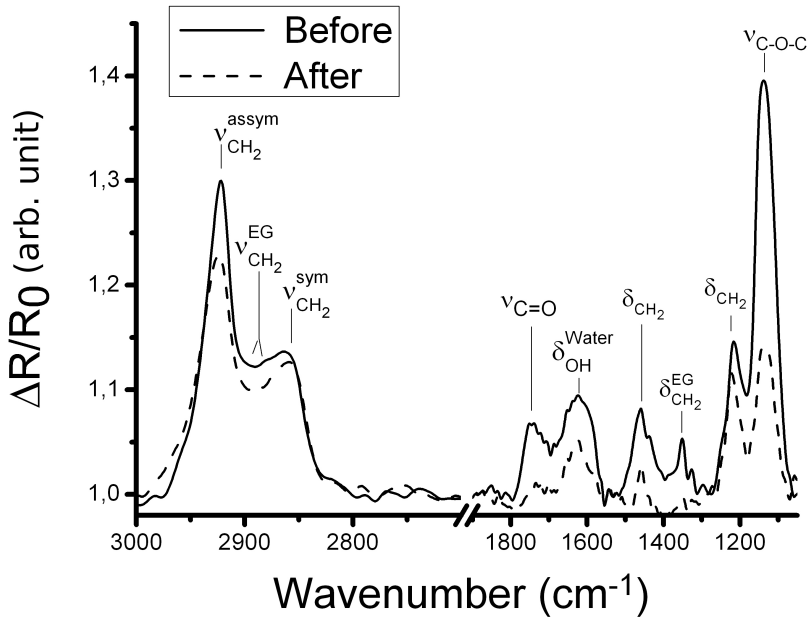

Figure 3.13 – PM-IRRAS spectra of a PEGylated gold sample before and after 18 hours X-Ray irradiation by continuous XPS measurements.

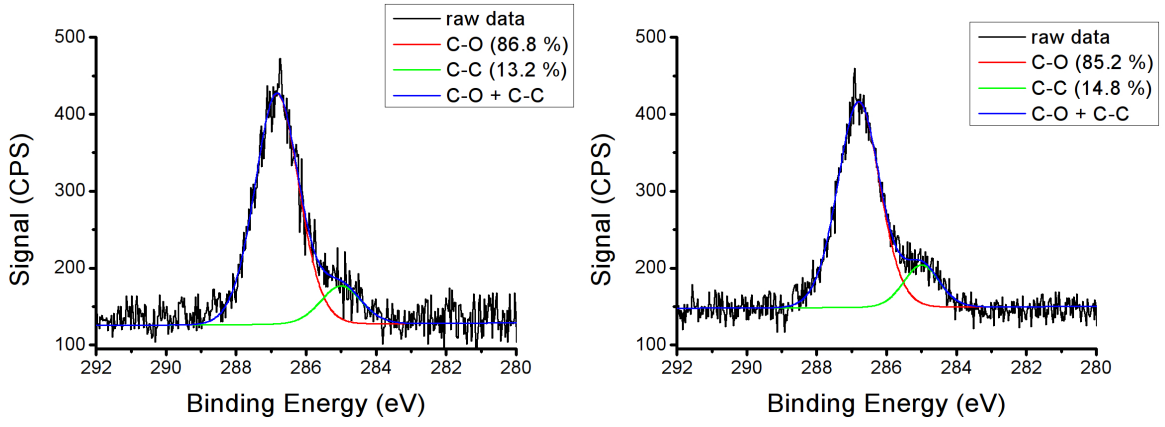

(a) 0 hour

(b) 18 hours

Figure 3.14 – Spectra of PEGylated silica surface at times a) 0 hour and b) 18 hours, without irradiation between the two measurements. The surface is conserved in the XPS chamber away from the X-ray spot and under the flood gun.

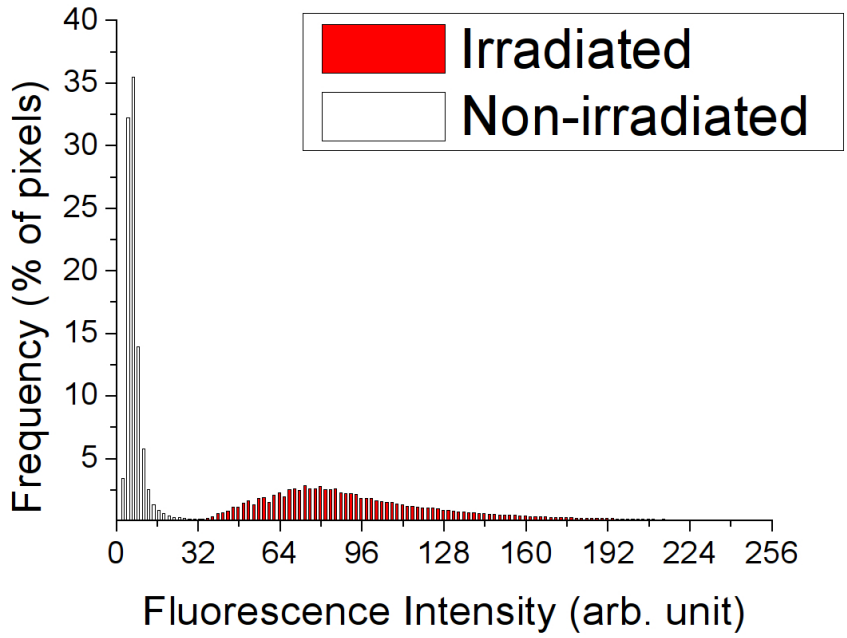

FIGURE 3.15 – Fluorescence intensities after adsorption of fluorescently-labeled streptavidin on an irradiated and non-irradiated sample. A 12mm^2 area was scanned at 3µm resolution with fluorescence intensities converted to 8 bits and values binned by 2 (128 bins). Non-irradiated sample shows a very low fluorescence (average intensity around 7) compared to the irradiated sample (average around 100) which translates a much higher amount of protein adsorption on the irradiated sample.

As stated in the introduction, the widespread use of OEG chains in biosensing applications is due to the antifouling properties of such molecules. Cai and co-workers[49] used the localized OEG degradation under short electron pulses as a basis for a novel lithography process, showing that the degraded regions became prone to protein adsorption, whereas the non-degraded regions remained anti-fouling. Thus, it is interesting to evaluate whether the damage induced by X-rays has an impact on such properties. In order to assess this, we immersed non-irradiated and irradiated (3 hours) PEGylated silica samples into a fluorescently-labeled protein solution as explained in the experimental section. As shown in Fig. 3.15 the irradiated sample showed much higher fluorescence intensities translating a higher amount of adsorbed proteins. Indeed, in an 8-bit scale for fluorescence intensity, 90 % of the surface showed a fluorescence above a value of 52 out of 256 while for the non-irradiated sample, 90% of the surface showed a fluorescence intensity below 12 out of 256. This confirms that X-ray irradiation, through the shortening or total removal of the OEG moiety takes away the anti-fouling properties of PEGylated silica.

We have seen that under the course of XPS measurements, different PEGylated organic layers on solid surfaces were degraded, with their OEG tail partially or totally removed while seemingly keeping their alkyl moiety intact. Let us now discuss different possible reasons for this degradation as well as different behaviours observed on gold and silica :

First of all, it is important to note that the degradation is indeed due to exposure to X-ray irradiation and not other factors such as ultrahigh vacuum or low-energy electrons. Indeed, as shown by the spectra on the reference sample (Fig. 3.14), the surface is not changed when submitted to the same conditions (vacuum, flood gun) except for X-ray irradiation.

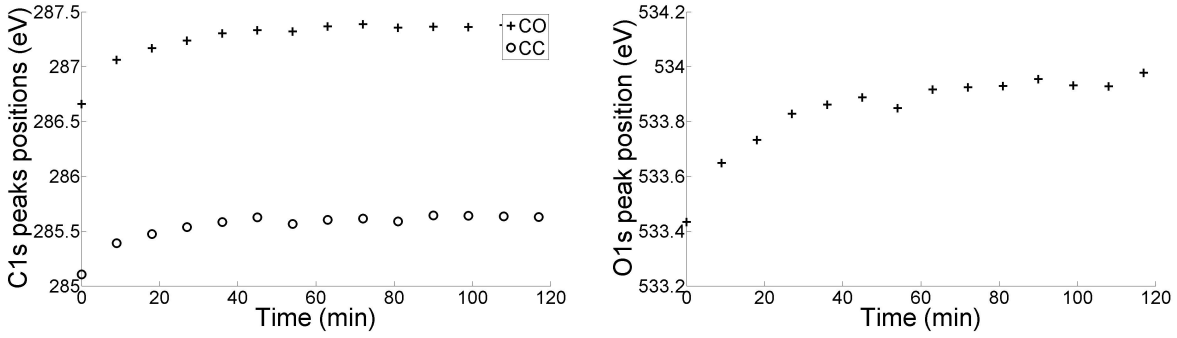

(a) C1s (b) O1s

Figure 3.16 – Evolution of the C1s (a) and O1s (b) peaks positions of PEGylated gold over time of continuous irradiation.

Second, it is interesting to see that despite major differences of both surfaces (gold vs silica) : polycrystalline metallic substrate vs amorphous oxide substrate ; propyl vs undecyl chains of the molecules ; O-CH3 vs COOH headgroup and expected differences on the organic layer composition and density (with possible polymerization of the trimethoxysilane), both show a similar evolution of their XPS spectrum, with decay of the *C*-O peak and the stability of the *C*-C one. This suggests that the main phenomenon involved is the progressive shaving of the OEG moiety through ether bond cleavage under X-rays leading to volatile compounds. Such a cleavage of the ether bonds leading to progressive shortening of the OEG tail has been evidenced under electron beams[49] or UV irradiation[48], where the comparatively stronger C-C bonds remained intact.

Third, major differences in degradation kinetics were observed on both surfaces (see Fig. 3.12). On silica, the decay of the CO peak can be fitted with an exponential function $A = A_0 e^{-t/\tau}$ having a characteristic time $\tau \approx 2h$. On gold, the decay seems rather linear. As we have previously stated, there are numerous differences between the two cases (different substrates and organic molecules) which makes such differences in kinetics not surprising. In both cases, the degradation seems to be total (for gold the linear decay is maintained at longer times, not shown in Fig 3.12 and the value of the relative CO contribution at t=9h has dropped below 30 % of the total carbon amount).

Eventually, a shift of the XPS peaks on gold was observed at the early stages (ca. 30 minutes ; see Fig. 3.16). The reason for these shifts remains uncertain. Charging phenomena could hardly be associated to these shifts considering the conducting substrate. In order to further investigate this, we conducted experiments on gold under a flood-gun, and found that the shifts were consistent. Second, PM-IRRAS characterization showed no new peaks after irradiation (see Fig. 3.13) so that it is unlikely that new chemical bonds were formed, as could happen from oxidative processes[48,50]. This is not surprising since those processes are expected to be very slow in ultrahigh vacuum.

Gold and silica surfaces were respectively modified with an alkythiol and a silane, both bearing an alkyl chain, and an oligo(ethylene glycol) moiety. We showed that on both surfaces the ethylene glycol moieties were degraded under XPS measurements while the alkyl chains remained unreacted. This led to varying ratios of CO/CC peak intensities. The reaction kinetics were found to be different for the two surfaces, as can be expected since both cases show numerous differences concerning the substrate properties as well as the organic layer. Static contact angle measurements showed a loss of hydrophilicity after X-ray irradiation. No new chemical

functions were evidenced by PM-IRRAS. This suggests the partial shaving of the OEG moieties resulting in the loss of hydrophilicity. Furthermore, we have shown that the degradation of the OEG moieties directly impacts the surfaces' anti-fouling properties. Indeed, protein adsorption was found to increase as a function of exposure time to X-rays under XPS measurements. It seems crucial to investigate the effect of XPS measurements on PEGylated surfaces with a better sensitivity because it is not suitable that surface chararacterization be conducted for hours and better temporal resolution because the degradation (specially on silica) is very fast. We plan to carry this investigation focusing on the early stages of degradation with the use of a fast detector as the TEMPO beamline in synchrotron soleil. Nevertheless, our findings suggest that the characterization of such surfaces may be impacted by the degradation of the PEGylated moiety.

3.3 Orthogonal functionalizations of patterned gold/silica surfaces

As presented in the introduction to this manuscript, the main goal of the present work is to investigate the orthogonal functionalizations of patterned gold and silica substrates. In the following paragraphs we will demonstrate by direct chemical characterizations our ability to carry on these orthogonal functionalizations with different molecules and substrates. First, we will prove this orthogonality on macropatterned substrates (i.e., gold and silica regions of ca. 1cm^2) as these allow an easier characterization with tools having low spatial (lateral) resolution. Then, we will demonstrate orthogonal functionalizations on the microscale by XPS and ToF-SIMS imaging.

3.3.1 At the macroscale

Because most of the surface chemical characterization tools readily available in the lab (PM-IRRAS, XPS, contact angle) probe millimetric surfaces (spot or drop size on the surface) we decided to test the orthogonality of chemical functionalizations on "macro-patterned" surfaces. Such surfaces usually consisted of a ca. 2cm^2 silica (on silicon) substrate onto which half of the surface was covered by a gold thin film or viceversa : a 2cm^2 gold film (on glass) half-covered by a silica thin film.

Figure 3.17 shows the XPS C1s spectra of the gold and silica regions of a heterogeneous sample functionalized with MUA and PEG-Si (both functionalizations made simultaneously by mixing both molecules in DCM, as explained in Chapter 2). On gold the carbon peaks correspond to MUA (C-*C*-C peak at 285eV, 93.2% of total C1s area and *C*OOH contribution at 289eV, 6.8% of total C1s area) while on silica, the spectrum is dominated by ether carbons C-*C*-O at 287eV (88.5 % of total C1s area) with a small contribution of the propyl chain at 285eV (11.5 % of total C1s area). The reader can see that the spectrum on the silica region of this sample -Fig 3.17b- is very similar to the spectrum of a plain silica sample functionalized uniquely with PEG-Si -Fig. 3.8-. Because of the degradation of PEG under X-rays, the percentages of ether and alkyl carbons on silica are less certain than the deconvolution of *C*-OOH and C-*C*-C on gold.

Water contact angle measurements and PM-IRRAS also tend to corroborate the good orthogonality of the double functionalization.

The contact angles of water on gold and silica were found to change from ca. 75° to ca. 54° (on gold) and from ca. 22° to ca. 38° (on silica). This seems coherent with the orthogonal functionalizations and values given in the literature[60,61] though it should be noted that big uncertainties remain due to the fact that : 1) the reference samples' hydrophilicity changes

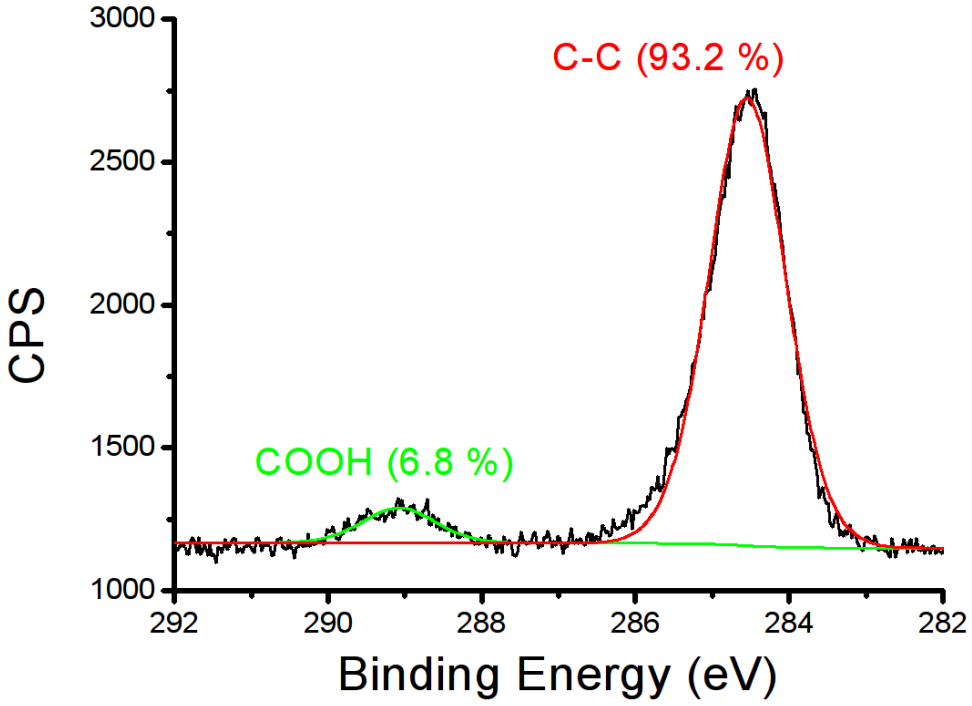

(a) Gold

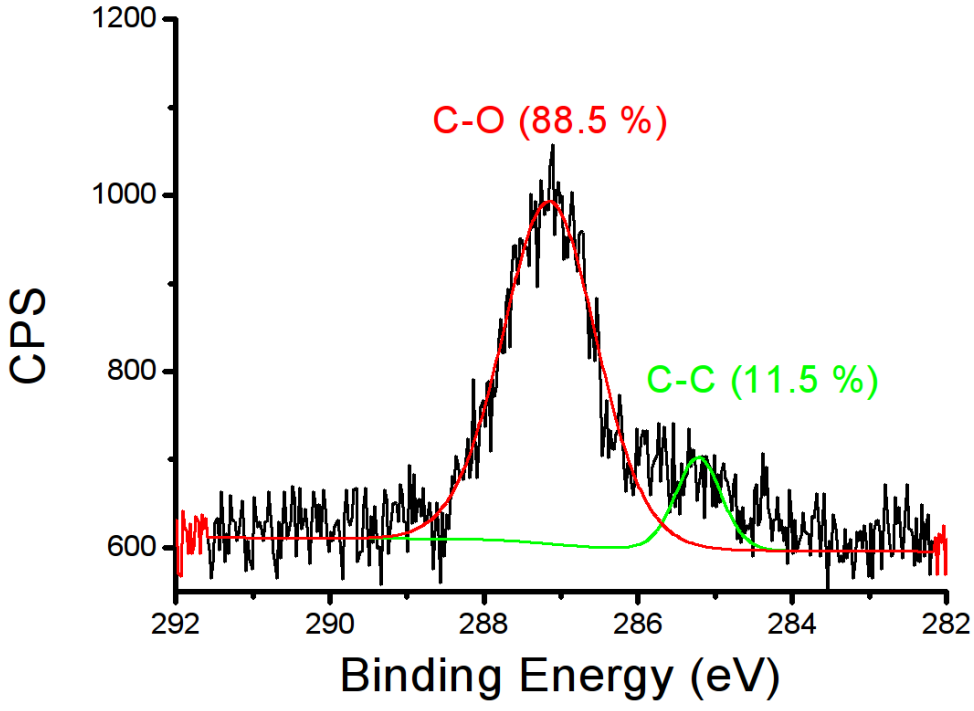

(b) Silica

Figure 3.17 – XPS C1s spectra on the gold (a) and silica (b) regions of an heterogeneous sample orthogonally functionalized with MUA and PEG-Si. The different carbon contributions show that MUA is selectively bound onto gold while PEG-Si is selectively bound onto silica without any detectable cross-contamination (thiols on silica or silanes on gold). On silica, a single scan was performed to limit PEG degradation. On gold, no PEG was detected after a single scan. Thus, the spectrum presented here is the result of 8 co-added scans to improve the signal-to-noise ratio.

upon ageing (both, gold and silica, are found to be very hydrophilic just after oxygen plasma cleaning but become more hydrophobic in few hours of remaining in a closed box in the lab) and 2) measurements are taken in an uncontrolled environment in regards to humidity and not finely controlled in regards to temperature.

Regarding PM-IRRAS, we could identify MUA on the gold region (spectrum not shown) but we were unable to clearly identify the organic layer on silica. It is in principle not impossible to conduct PM-IRRAS characterization of an organic layer on silica if the silica layer is only a thin film on top of a metallic substrate.[58] However, one still has to appropriately substract the silica -dominant- contribution to the spectrum in order to obtain the spectrum of the organic adlayer only. Moreover, the molecular structure of PEG-Si is largely dominated by C – O – C bonds whose main vibration mode is very close to the main vibration mode of silica Si – O – Si bonds around 1100cm^{-1}. This makes the detection of PEG-Si by PM-IRRAS more difficult than other silanes[58] as the main peak of the organic molecule is *drowned* inside the signal of the underlying silica.

Single-step double functionalizations seem to be appropriately orthogonal *on average* over macroscopic surfaces. We therefore decided to test the orthogonality of such functionalizations on a smaller scale, which implies the use of different characterization tools as we will see in the next chapter.

3.3.2 At the microscale

In order to test the orthogonality of single-step double functionalizations on micropatterned surfaces, we performed XPS and ToF-SIMS analysis with lateral resolution of few to ten microns, with the help of Thierry Le Mogne at LTDS and Didier Léonard at ISA respectively.

Different micropatterned samples were prepared by UV-lithography. The surface of these samples yielded gold microsquares of ca. 90µm surrounded by silica lines of equivalent width. We then performed single-step thiolation+silanization of these patterned substrates and checked the orthogonality of the functionalizations (presence of the thiol only on the gold microsquares and presence of the silane only on the silica lines). For an easier analysis we decided to perform the double functionalizations including a perfluorinated molecule (fluorine being a strong emitter for XPS and ToF-SIMS). Two orthogonal functionalizations were conducted on different micropatterned samples :

1. AuF + PEG-Si
2. SiF + MUA

If the functionalizations are truly orthogonal, we expect to find fluorine only on the gold microsquares in the first case (AuF + PEG-Si) and vice-versa in the second (SiF + MUA). This was indeed shown by XPS and ToF-SIMS.

3.3.2.1 XPS analysis

Micropatterned gold on silica substrates functionalized with either (1) AuF and PEG-Si or (2) SiF and MUA were analyzed by XPS. On both surfaces, a first image was acquired by scanning and collecting all secondary electrons (same principle as an SEM). This allows to visualize the gold microsquares (brighter) and surrounding silica lines (darker) as can be seen in Figs. 3.18 and 3.19. Then, two different regions (ca. 10µm) corresponding to gold and silica surfaces were selected to perform a "full" spectrum (1000eV-0eV). These spectra show the following :

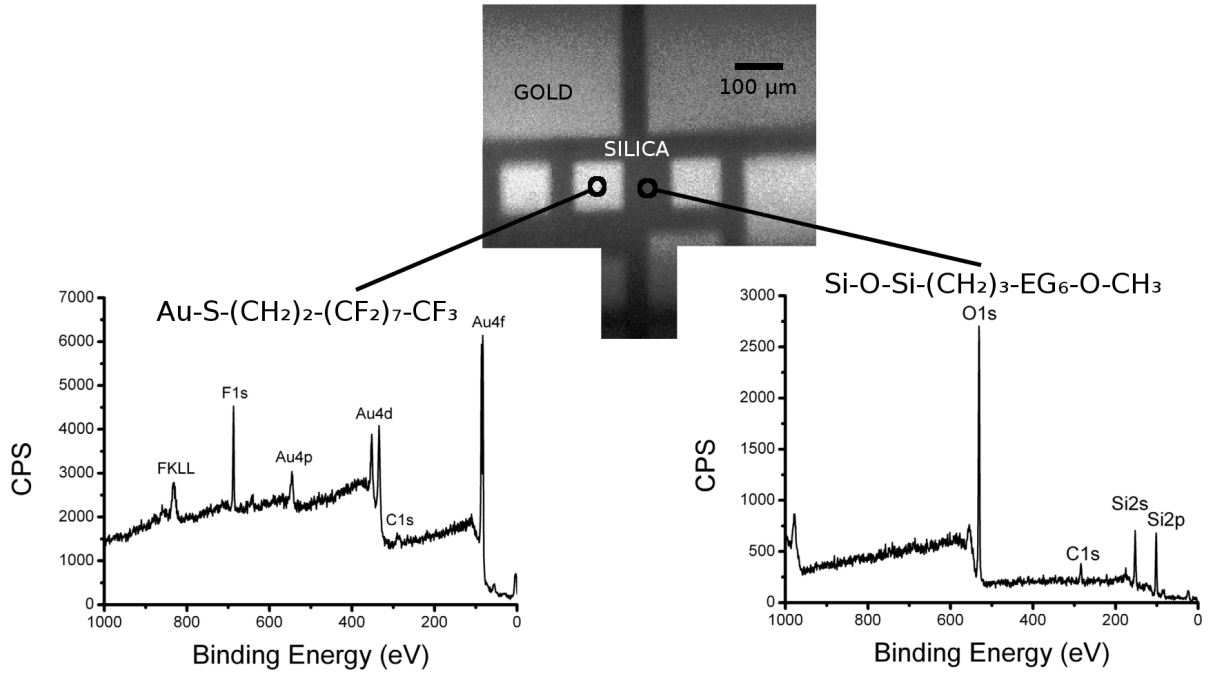

Figure 3.18 – XPS image of a micropatterned gold on silica substrate orthogonally functionalized with AuF and PEG-Si and corresponding spectra on gold and silica. The analyzed regions for the spectra are roughly 10 microns and their approximate localization is represented on the image. Scale bar on the image is 100 microns. For further interpretation of the figure, read main text.

- In the case where the sample is functionalized with a perfluorinated thiol and a PEG-silane (Fig. 3.18)
  - On gold (left spectrum), fluorine is clearly present as evidenced by the F1s and FKLL peaks, showing the **presence of the perfluorinated thiol** (molecular structure given on top of spectrum). Furthermore, no Si2s or O1s peaks can be detected, showing the **absence of the PEG-silane**.
  - On silica (right spectrum), fluorine is clearly absent as evidenced by the lack of F1s or FKLL peaks, showing the **absence of the perfluorinated thiol**. Furthermore, an important carbon contribution is detected through the presence of the C1s peak whose intensity cannot be only adscribed to organic contamination and therefore reflects the **presence of the PEG-silane** (molecular structure given on top of spectrum).
- In the case where the sample is functionalized with a perfluorinated silane and an alkyl-thiol (Fig. 3.19), the orthogonality of the functionalization is proven by the same arguments as above, the main one being the presence of fluorine on silica and not on gold.

High resolution spectra of the C1s region (ca. 300-280eV) on both regions of both samples could bring further proof of the orthogonality of such functionalizations, as different contributions could be assigned to C-F_3 (293eV), C-F_2 (290eV), C-C (285eV) and C-O (287eV) bonds. Unfortunately, we could not conduct this analysis for technical reasons (machine availability).

However, we did conduct a mapping of the surfaces in regard to gold (Au4f) and fluorine (F1s) as presented in figures 3.20 and 3.21. On the sample functionalized with AuF and PEG-Si (Fig. 3.20), fluorine is homogeneously present in the same regions as gold, demonstrating the good orthogonality and homogeneity of the surface functionalization. On the other sample (Fig. 3.21) it is less obvious that fluorine is preferentially present on the silica regions (around the

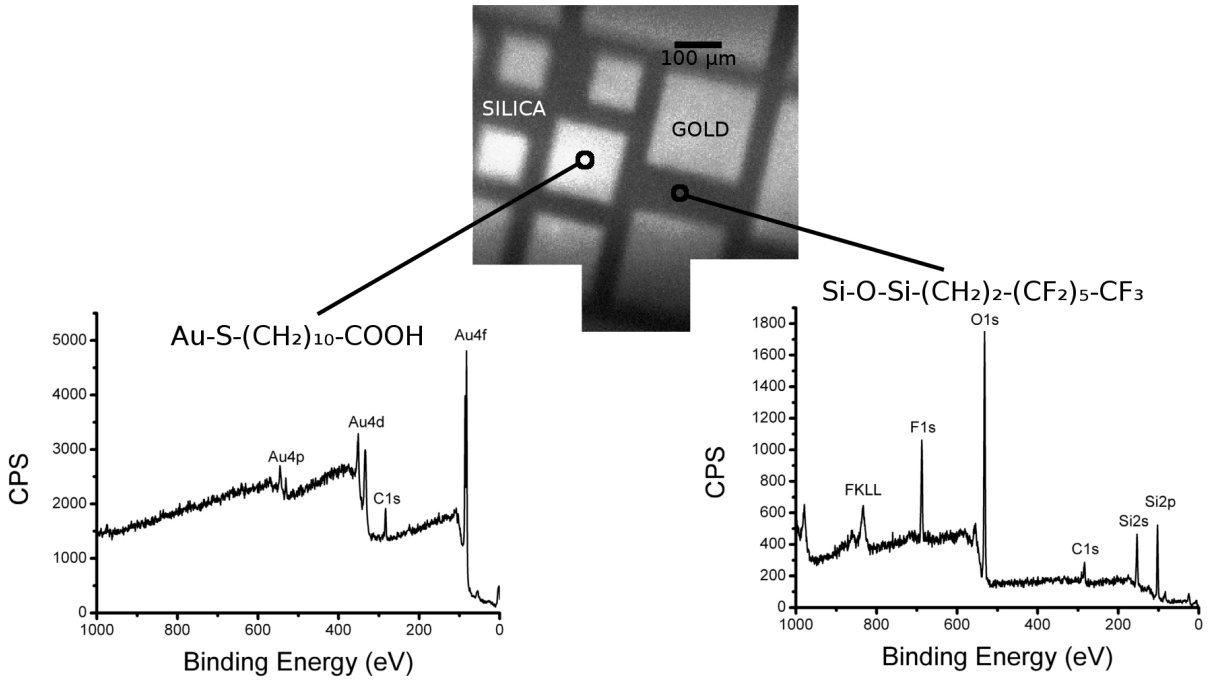

Figure 3.19 – XPS image of a micropatterned gold on silica substrate orthogonally functionalized with MUA and SiF and corresponding spectra on gold and silica. The analyzed regions for the spectra are roughly 10 microns and their approximate localization is represented on the image. Scale bar on the image is 100 microns. For further interpretation of the figure, read main text.

squares). This is due to the overall low level in image 3.21. This low level can be partly assigned to some degradation induced by X-rays over the course of the mapping (several hours) and may also be linked to the lack of a curing step in the functionalization protocol (curing above 100°C is often recommended for silanization[62,63] though it is not recommended in this case, since thiols could desorb at high temperature). Indeed we found (data not shown) that the level of C1s and F1s had dropped on this sample between the beginning and the end of the mapping. Thus, the poor contrast in image 3.21 reveals an issue that is not in contradiction with the good orthogonality of the functionalizations unambiguously proven by the scans showed at Fig. 3.19, performed prior to the element mapping (thus prior to a probable degradation).

3.3.2.2 ToF-SIMS analysis

Similar analysis were conducted by ToF-SIMS. Unfortunately, because of a technical issue, we could not acquire reliable full spectra on different regions such as the ones acquired with XPS (Figs. 3.18 and 3.19). However, we conducted a mapping of fluorine (m/z = 19.045 - 19.05) on micropatterned substrates functionalized with AuF + PEG-Si (Fig. 3.22a) and SiF + MUA (Fig. 3.22b). In each case fluorine is only (or very predominantly) present on the gold microsquares (Fig. 3.22a) or the surrounding silica (Fig. 3.22b) but not on both, which demonstrates the good orthogonality of the single-step double functionalizations.

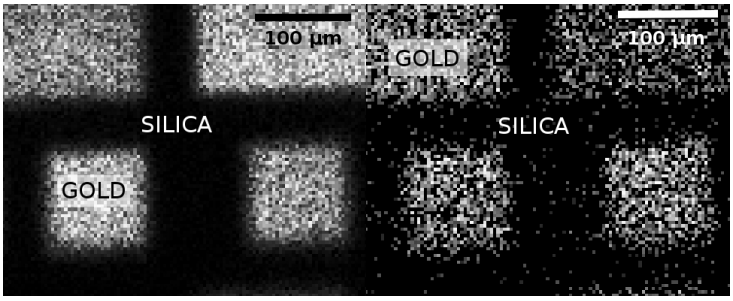

(a) Au4f (b) F1s

Figure 3.20 – [XPS Au4f and F1s mapping of micropatterned gold on silica surface orthogonally functionalized with AuF and PEG-Si.]XPS Au4f (a) and F1s (b) mapping of micropatterned gold on silica surface orthogonally functionalized with AuF and PEG-Si. Fluorine is only and homogeneously found in the same regions as gold, demonstrating the good orthogonality of the functionalizations.

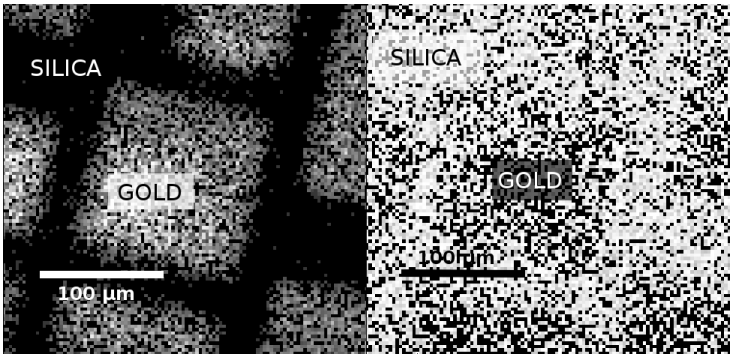

(a) Au4f (b) F1s

Figure 3.21 – XPS Au4f (a) and F1s (b) mapping of micropatterned gold on silica surface orthogonally functionalized with SiF and MUA. Fluorine is expected to be found only on silica (i.e., where no gold is found). This is not obvious in the image, which presents an overall low intensity (read main text for more details).

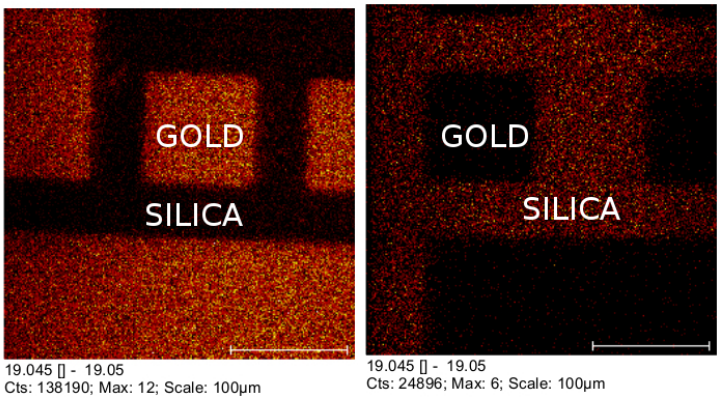

(a) Fluorine on gold (b) Fluorine on silica

Figure 3.22 – ToF-SIMS fluorine mapping of patterned gold on silica surfaces orthogonally functionalized with AuF + PEG-Si (a) and SiF + MUA (b). In each case fluorine is predominant either on the gold microsquares (a) or the surrounding silica lines (b), which demonstrates the good orthogonality of the functionalizations.

(a) Bio-affinity

(b) Electrostatic

FIGURE 3.23 – Schematic representation of the *bio-affinity* and *electrostatic* approaches to the selective anchoring of different nanoparticles. Gold micropatterns are functionalized with biotinylated- or amino-thiols to bind streptavidin-functionalized or carboxy-latex.

3.4 Applications to colloid trapping

NB : The following paragraphs are adapted from a paper currently submitted for publication.[2]

Selective functionalizations of gold micro and nanopatterns on silica with different alkylthiols were used for colloid trapping. Based on the thiols' headgroup two approaches were developped (see Fig. 3.23) :

1. A *bio-affinity* approach based on affinity of biotinylated thiols (MU-Biot) with streptavidin-functionalized latexes.
2. An *electrostatic* approach based on attractive interaction between positively charged aminothiols (MUAM) and negatively charged carboxylatex nanoparticles.

NB : The molecular structures of MU-Biot and MUAM have already been given together with their PM-IRRAS spectra in Fig. 3.4.

In both cases, non-specific adsorption was limited by electrostatic repulsive interactions between the negatively charged silica and latex particles and efficient washing steps. Indeed the isoelectric point of streptavidin, the pKa of carboxylic acids and the point of zero charge of silica are roughly equal to 5, 4 and 2 respectively, which is below the pH that was used during colloid trapping (pH=7.4). SEM observations allowed us to determine the position of the colloids on the patterned substrates and therefore estimate the efficiency of the trapping by the functionalized gold structures.

3.4.1 Colloid trapping on micropatterns

Figure 3.24 shows typical SEM images of micropatterned functionalized gold on silica after colloid deposition and rinsing. These images (and other similar ones not shown) were analyzed with ImageJ software to compute the trapping on gold and silica (i.e., the percentage of the gold and silica surface that was covered by colloids). This quantitative analysis is presented in Fig. 3.25.

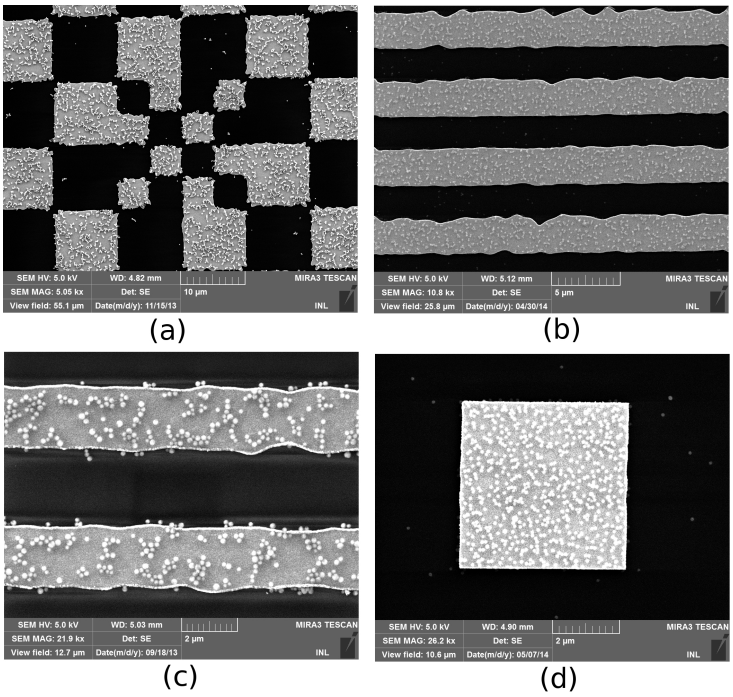

Figure 3.24 – SEM images of patterned functionalized samples after colloid deposition. The gold structures (lines, squares) appear brighter than the surrounding silica. Colloidal particles can be seen on the surface, with a preferential deposition on the gold regions. Images (a) and (c) are taken on bio-affinity based samples while (b) and (d) are taken on electrostatic based samples.

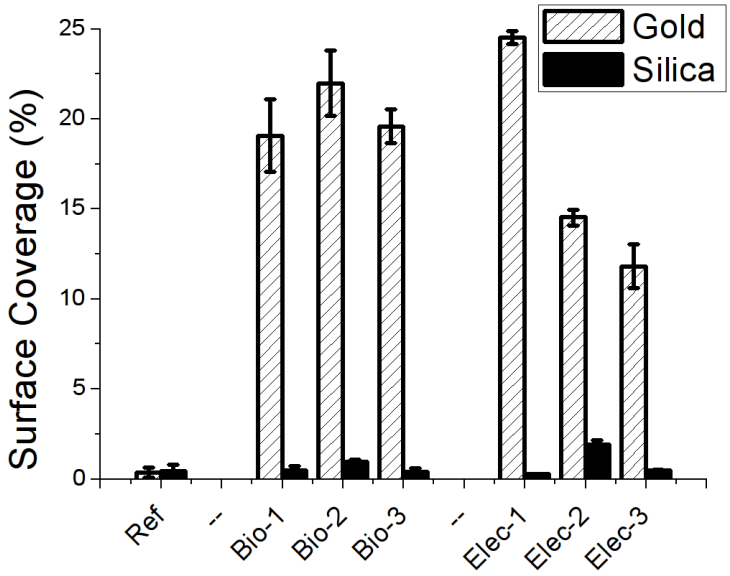

Figure 3.25 – Histogram presenting the surface coverage by latex nanoparticles on gold and silica regions of differently functionalized samples : "Ref" refers to a non-functionalized surface ; "Bio" refers to a biotinylated surface (streptavidin-functionalized beads) and "Elec" to an amino-functionalized surface (carboxylatex beads). Different columns correspond to different samples and error bars represent the measured standard deviation between three regions of the same sample.

Fig. 3.25 clearly shows the efficiency of the selective surface functionalization for colloid trapping : When no functionalization is made ("Ref" sample) then colloids are not significantly adsorbed on gold or silica (surface coverage of ca. 1%). However, when substrates are appropriately functionalized, surface coverage on gold increases to ca. 10-25 % while non-specific adsorption on silica remains below 2%. The results appear to be homogeneous throughout the samples (error bars represent the measured standard deviation) and reproducible (specially for the *bio* approach) though the number of tested samples as well as distinct measurements throughout them (3 in each case) is probably too small to have an accurate assessment of reproducibility and homogeneity.

Another approach was tested in which the carboxylatex beads were activated for a covalent amide coupling to MUAM. However, this led to particle aggregation. It must be noted that the negative charge on the carboxylatexes are responsible for their colloidal stability (see appendix B on DLVO theory). Therefore, it seems that additional precautions have to be taken into consideration when modifying the surface chemistry of colloidal nanoparticles.

3.4.2 Colloid trapping on large arrays of individual nanostructures

We have shown in the previous paragraphs how colloids could efficiently be trapped on micrometric gold regions by surface (bio)chemical interactions, tuned by appropriate functionalization. However, many potential applications of colloid trapping imply the anchoring of individual nanoparticles onto arrays of individual nanotraps. LSPR-based devices, for instance, imply the presence of metallic nanostructures which are commensurable to the colloids presented here (few hundreds nm).

The beads used in the *electrostatic* method (see Fig. 3.23b) are fluorescent infrared beads. It can be expected that the precise anchoring of such beads on an array of plasmonic nano-antennas would yield unprecedented photonic properties resulting from the coupling of the beads' fluorescence and the nano-antenna localized plasmons modes and preferential direction of emission. [16] Therefore, we decided to apply the same methodology with aminothiols to bind the fluorescent carboxylatex particles on individual nano-antennas. The nano-antennas are dimers of triangles (bow-tie), ovals and rectangles with typical dimensions of 100nm separated by a 10, 20 or 50nm gap. This geometry is based on photonic simulations that are not presented here, performed by Ali Belarouci. The samples were prepared by e-beam lithography by Pedro Rojo Romeo and Céline Chevalier.

Figure 3.26 shows a 3x4 array of dimer nano-antennas (bright ovals) surrounded by silica surface. Fluorescent nanobeads can be seen in light gray. As highlighted in green in the image, 11 out of 12 nano-antennas have at least one bead attached. Furthermore, non-specific adsorption on the surrounding silica surface is low (only three beads can be seen on the ca. 10x15µm silica surface, highlighted in yellow in the image). Indeed, in the conditions of beads' deposition (in PBS 1X at pH=7.4), only the functionalized gold structures have an attractive electrostatic interaction with the beads through the protonated amine headgroup while the silica surface is mainly negatively charged and therefore repels the beads (see Fig. 3.23b).

We took several images as the one shown in Fig. 3.26 to make a more meaningfull statistics over the millimetric sample. 75 out of 109 randomly chosen nano-antennas were found to be occupied by nano-beads (i.e., 68.8 %).

16. The coupling of a fluorescent nanobead to a localized plasmon is not straightforward. Indeed a few aspects have to be taken into consideration, especially regarding quenching of the fluorescence by the metal and distribution of the localized enhanced field. These photonic considerations will not be discussed in further detail here.

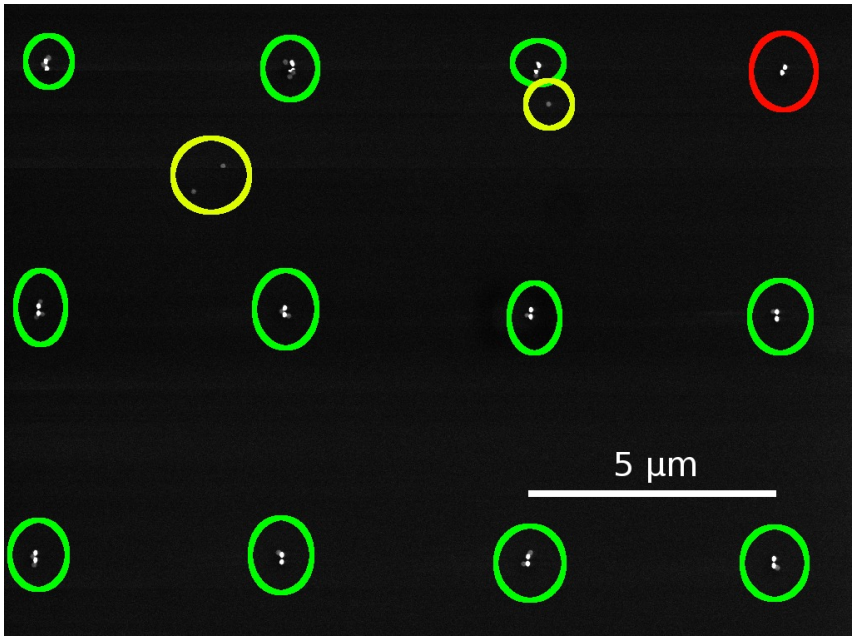

Figure 3.26 – 3x4 array of dimer nano-antennas with fluorescent nanobeads attached through surface chemical functionalization. 11 out of 12 nano-antennas (green circles) are occupied by one, two or three nanobeads, preferentially anchored at the edges and corners. Only one nano-antenna is found unoccupied (red circle) while low non-specific adsorption (yellow circles) is found on the surrounding silica.

There are however a certain number of additional issues that become apparent when looking more closely at the nanostructures (Fig. 3.27) :

1. At this stage, the metallic dimers do not have the desired geometry. Indeed, it appears that some dimers are bridged (Fig. 3.27b) and others have a gap bigger than 50nm (Fig. 3.27a).

2. Though it is possible to find a single bead localized on the gap of the dimer (Fig. 3.27a), we generally found 1, 2 (Fig. 3.27b) or 3 (Fig. 3.27c), not necessarily on the gap of the dimer. It does not seem reasonable to think that surface functionalization alone can finely tune the position of the beads on the nanostructures. However, a combination of surface functionalization and photonic approaches[64] may overcome this issue.

Furthermore, it must be noted that non-specific adsorption was generally higher that what can be seen in Fig. 3.26 although it remained low (few tens of beads on a 10x15µm surface). Mixing and washing procedures will have to be improved in the future, for enabling an homogeneous behaviour on large areas.

Nonetheless, these results prove that selective surface chemical functionalizations can be used to arrange different colloids onto large arrays of individual *nanotraps* which may serve as a general framework for the development of novel systems combining the physical properties of nano-objects and the high degree of complexity (miniaturization and diversification) allowed by lithography nanopatterning of a substrate.

(a) Single particle on a bigger than expected gap

(b) Two particles captured on a bridged "dimer"

(c) Three particles on a dimer and two non-specifically adsorbed on surrounding silica

Figure 3.27 – SEM images of single dimer nano-antennas with trapped nanobeads

3.5 Conclusions on the experimental results

We have presented in this chapter experimental evidence of the coupling between top-down processes (lithography, thin film deposition) and bottom-up molecular self-assembled structures in 2D (SAMs) and 3D (colloids).

First of all, an efficient and non-destructive method for substrate cleaning after lithography and prior to chemical functionalization was found by oxygen plasma ashing. Indeed we found that oxygen plasma ashing was more efficient than organic solvents and UV/ozone for removing polymeric residues. Furthermore, it does not cause delamination of thin films and nanostructures as piranha solution. However, two main issues were raised in relation to the use of oxygen plasma : (1) When performed in an RIE device with lines for fluorinated gases such as CHF_3 or SF_6, fluorine contamination was found on the surface and (2) the use of oxygen plasma on gold surfaces led to the formation of an oxide layer (Au_2O_3). Therefore, it was decided to perform oxygen plasma ashing in a dedicated device (Anatech) without other gases than oxygen and nitrogen and wait 24h before functionalization in order to let the surface recover its metallic nature (the oxide layer is thermodynamically unstable in normal pressure and temperature conditions).

Second, we could prove the efficient building of different SAMs on plain gold and silica substrates by PM-IRRAS and XPS. On gold, we optimized the activation protocol of MUA-terminated SAMs in water and THF.[1] We showed that activation could be conducted very quickly in water (less than 30min) albeit yielding important amounts of urea byproduct that increases as NHS-ester are hydrolized. Conversely, in THF, activation takes higher amounts of NHS and DIC but yields a more stable NHS-ester surface. Another study conducted on plain functionalized substrates showed the shaving of OEG-terminated SAMs induced by X-rays during XPS characterization. This shaving leads to a loss of anti-fouling properties of PEGylated surfaces.

Third, we showed *direct* chemical characterization by XPS and ToF-SIMS imaging proving the orthogonality of double functionalizations (thiolation + silanization) conducted simultaneously on micropatterned gold/silica substrates.

Eventually, we demonstrated the use of selective thiolation of micro and nanopatterned substrates to trap different latex nanoparticles. This was especially used to demonstrate the possibility of trapping individual nanobeads onto large arrays of nanostructures envisioned to work as plasmonic nano-antennas. We achieved 68.8 % trapping yield with low non-specific adsorption on the surrounding silica surface (less than one nanobead -100nm diameter- per $5\mu m^2$).

Further work is under way focussing on : (1) the characterization of orthogonal functionalizations at the nanoscale through local probes, (2) the coupling of fluorescent nanobeads and plasmonic nanoantennas and (3) the use of orthogonal functionalizations for enhancing the sensitivity of LSPR-based biosensors.

References

[1] F. Palazon, C. Montenegro Benavides, D. Léonard, E. Souteyrand, Y. Chevolot, and J.-P. Cloarec. *Langmuir : the ACS journal of surfaces and colloids*, 30,4545–50 **(2014)**.

[2] F. Palazon, C. Chevalier, P. R. Romeo, T. Géhin, E. Souteyrand, Y. Chevolot, and J.-P. Cloarec. *Journal of colloid and interface science*, submitted **(2014)**.

[3] D. S. Macintyre, O. Ignatova, S. Thoms, and I. G. Thayne. *Journal of Vacuum Science & Technology B : Microelectronics and Nanometer Structures*, 27,2597 **(2009)**.

[4] H. Tsai. *Surface Science*, 537,L447–L450 **(2003)**.

[5] H. Ron, S. Matlis, and I. Rubinstein. *Langmuir*, 14,1116–1121 **(1998)**.

[6] K. M. Cook and G. S. Ferguson. *Chemical communications (Cambridge, England)*, 47,12550–2 **(2011)**.

[7] J. te Riet, T. Smit, M. J. J. Coenen, J. W. Gerritsen, A. Cambi, J. a. a. W. Elemans, S. Speller, and C. G. Figdor. *Soft Matter*, 6,3450 **(2010)**.

[8] J. C. Love, L. a. Estroff, J. K. Kriebel, R. G. Nuzzo, and G. M. Whitesides. *Chemical reviews*, 105,1103–1169 **(2005)**.

[9] L. H. Dubois, B. R. Zegarski, and R. G. Nuzzo. *The Journal of Chemical Physics*, 98,678 **(1993)**.

[10] F. Tielens, D. Costa, V. Humblot, and C.-m. Pradier. pages 182–190 **(2008)**.

[11] B. L. Frey, R. M. Corn, and S. C. Weibel. *Handbook of Vibrational Spectroscopy*, 2,1042–1056 **(2001)**.

[12] E. Briand, M. Salmain, C. Compère, and C.-M. Pradier. *Biosensors & bioelectronics*, 22,2884–90 **(2007)**.

[13] F. Bensebaa, R. Voicu, L. Huron, T. H. Ellis, and E. Kruus. *Langmuir*, 13,5335–5340 **(1997)**.

[14] M. Himmelhaus, F. Eisert, M. Buck, and M. Grunze. *The Journal of Physical Chemistry B*, 104,576–584 **(2000)**.

[15] D. Mercier, C. Mercader, S. Quere, L. Hairault, C. Méthivier, and C. Pradier. *Applied Surface Science*, 258,9518–9525 **(2012)**.

[16] D. Mercier, S. Boujday, C. Annabi, R. Villanneau, C.-M. Pradier, and A. Proust. *The Journal of Physical Chemistry C*, 116,13217–13224 **(2012)**.

[17] C. Methivier, B. Beccard, and C. M. Pradier. *Langmuir*, 19,8807–8812 **(2003)**.

[18] E. Briand, M. Salmain, C. Compère, and C.-M. Pradier. *Colloids and surfaces. B, Biointerfaces*, 53,215–24 **(2006)**.

[19] H. C. Yang, D. L. Dermody, C. Xu, A. J. Ricco, and R. M. Crooks. *Langmuir*, 12,726–735 **(1996)**.

[20] C. E. Jordan, B. L. Frey, S. Kornguth, and R. M. Corn. *Langmuir*, 10,3642–3648 **(1994)**.

[21] E. E. Bedford, S. Boujday, V. Humblot, F. X. Gu, and C.-M. Pradier. *Colloids and surfaces. B, Biointerfaces*, 116C,489–496 **(2014)**.

[22] H. Kim, J. H. Park, I.-H. Cho, S.-K. Kim, S.-H. Paek, and H. Lee. *Journal of colloid and interface science*, 334,161–166 **(2009)**.

[23] B. L. Frey and R. M. Corn. *Anal. Chem.*, 68,3187–3193 **(1996)**.

[24] S. Sam, L. Touahir, J. Salvador Andresa, P. Allongue, J.-N. Chazalviel, a. C. Gouget-Laemmel, C. Henry de Villeneuve, a. Moraillon, F. Ozanam, N. Gabouze, and S. Djebbar. *Langmuir*, 26,809–814 **(2010)**.

[25] N. Afara, S. Omanovic, and M. Asghari-Khiavi. *Thin Solid Films*, 522,381–389 **(2012)**.

[26] S. Choi and J. Chae. *Journal of Micromechanics and Microengineering*, 20,075015 **(2010)**.

[27] A.-L. Morel, R.-M. Volmant, C. Méthivier, J.-M. Krafft, S. Boujday, and C.-M. Pradier. *Colloids and surfaces. B, Biointerfaces*, 81,304–12 **(2010)**.

[28] I. Kim, I.-u.-R. Junejo, M. Lee, S. Lee, E. K. Lee, S.-I. Chang, and J. Choo. *Journal of Molecular Structure*, 1023,197–203 **(2012)**.

[29] S. Bellon, W. Buchmann, F. Gonnet, N. Jarroux, M. Anger-Leroy, F. Guillonneau, and R. Daniel. *Analytical chemistry*, 81,7695–7702 **(2009)**.

[30] G. El Khoury, E. Laurenceau, Y. Chevolot, E. Souteyrand, and J.-P. Cloarec. *Biosensors & bioelectronics*, 26,1320–5 **(2010)**.

[31] M. a. C. Campos, A. K. Trilling, M. Yang, M. Giesbers, J. Beekwilder, J. M. J. Paulusse, and H. Zuilhof. *Langmuir*, 27,8126–33 **(2011)**.

[32] Z. Yang, Y. Chevolot, T. Géhin, J. Solassol, A. Mange, E. Souteyrand, and E. Laurenceau. *Biosensors & bioelectronics*, 40,385–92 **(2013)**.

[33] C. Wang, Q. Yan, H.-B. Liu, X.-H. Zhou, and S.-J. Xiao. *Langmuir*, 27,12058–12068 **(2011)**.

[34] L. Touahir, J.-N. Chazalviel, S. Sam, A. Moraillon, C. Henry de Villeneuve, P. Allongue, F. Ozanam, and A. C. Gouget-Laemmel. *The Journal of Physical Chemistry C*, 115,6782–6787 **(2011)**.

[35] M. I. Papisov, a.V. Maksimenko, and V. P. Torchilin. *Enzyme and Microbial Technology*, 7,11–16 **(1985)**.

[36] M. R. Lockett, M. F. Phillips, J. L. Jarecki, D. Peelen, and L. M. Smith. *Langmuir*, 24,69–75 **(2008)**.

[37] Q. P. Lei, D. H. Lamb, A. G. Shannon, X. Cai, R. K. Heller, M. Huang, E. Zablackis, R. Ryall, and P. Cash. *Journal of chromatography. B, Analytical technologies in the biomedical and life sciences*, 813,103–12 **(2004)**.

[38] F. Cheng, L. J. Gamble, D. W. Grainger, and D. G. Castner. *Analytical Chemistry*, 79,8781–8788 **(2007)**.

[39] J. T. Liu, C. J. Chen, T. Ikoma, T. Yoshioka, J. S. Cross, S.-J. Chang, J.-Z. Tsai, and J. Tanaka. *Analytica chimica acta*, 703,80–6 **(2011)**.

[40] L. Li, S. Chen, J. Zheng, B. D. Ratner, and S. Jiang. *The Journal of Physical Chemistry B*, 109,2934–41 **(2005)**.

[41] J.-P. Cloarec, Y. Chevolot, E. Laurenceau, M. Phaner-Goutorbe, and E. Souteyrand. *ITBM-RBM*, 29,105–127 **(2008)**.

[42] Z. Yang, Y. Chevolot, T. Géhin, V. Dugas, N. Xanthopoulos, V. Laporte, T. Delair, Y. Ataman-Önal, G. Choquet-Kastylevsky, E. Souteyrand, and E. Laurenceau. *Langmuir : the ACS journal of surfaces and colloids*, 29,1498–1509 **(2013)**.

[43] Y. Zheng, C. H. Lalander, T. Thai, S. Dhuey, S. Cabrini, and U. Bach. *Angewandte Chemie (International ed. in English)*, 50,4398–4402 **(2011)**.

[44] M. M. Silván, a. Valsesia, D. Gilliland, G. Ceccone, and F. Rossi. *Applied Surface Science*, 235,119–125 **(2004)**.

[45] F. Zhang, S. Liu, Y. Zhang, Z. Chi, J. Xu, and Y. Wei. *Journal of Materials Chemistry*, 22,17159 **(2012)**.

[46] K. L. Prime and G. M. Whitesides. *Journal of the American Chemical Society*, 115,10714–10721 **(1993)**.

[47] D. Beyer, T. M. Bohanon, W. Knoll, H. Ringsdorf, G. Elender, and E. Sackmann. *Langmuir*, 60,2514–2518 **(1996)**.

[48] M. Montague, R. E. Ducker, K. S. L. Chong, R. J. Manning, F. J. M. Rutten, M. C. Davies, and G. J. Leggett. *Langmuir*, 23,7328–37 **(2007)**.

[49] J. Gu, C. M. Yam, S. Li, and C. Cai. *Journal of the American Chemical Society*, 126,8098–9 **(2004)**.

[50] S. Sun, D. G. Thompson, D. Graham, and G. J. Leggett. *Journal of Materials Chemistry*, 21,14173 **(2011)**.

[51] P. Krsko, S. Sukhishvili, M. Mansfield, R. Clancy, and M. Libera. *Langmuir*, 19,5618–5625 **(2003)**.

[52] I. V. Voinkova, N. N. Ginchitskii, I. V. Gribov, I. I. Klebanov, V. L. Kuznetsov, N. A. Moskvina, L. A. Pesin, and S. E. Evsyukov. *Polymer degradation and stability*, 89,471–477 **(2005)**.

[53] K. Artyushkova and J. E. Fulghum. *Surface and Interface Analysis*, 31,352–361 **(2001)**.

[54] G. Coullerez, Y. Chevolot, D. Léonard, N. Xanthopoulos, and H. J. Mathieu. *Journal of Surface Analysis*, 5,235–239 **(1999)**.

[55] S. Pignataro, I. Bertbti, T. Szbkely, B. Keszler, and G. Marletta. *Macromolecules*, 24,99–105 **(1991)**.

[56] S. Sharma, R. W. Johnson, and T. a. Desai. *Biosensors & bioelectronics*, 20,227–39 **(2004)**.

[57] B. Brena, G. V. Zhuang, a. Augustsson, G. Liu, J. Nordgren, J.-H. Guo, P. N. Ross, and Y. Luo. *The journal of physical chemistry. B*, 109,7907–14 **(2005)**.

[58] M. a. Ramin, G. Le Bourdon, N. Daugey, B. Bennetau, L. Vellutini, and T. Buffeteau. *Langmuir : the ACS journal of surfaces and colloids*, 27,6076–84 **(2011)**.

[59] V. Lebec, J. Landoulsi, S. Boujday, C. Poleunis, C.-M. Pradier, and a. Delcorte. *The Journal of Physical Chemistry C*, 117,11569–11577 **(2013)**.

[60] A. Vallée, V. Humblot, R. Al Housseiny, S. Boujday, and C.-M. Pradier. *Colloids and surfaces. B, Biointerfaces*, 109C,136–142 **(2013)**.

[61] N. Faucheux, R. Schweiss, K. Lützow, C. Werner, and T. Groth. *Biomaterials*, 25,2721–2730 **(2004)**.

[62] V. Dugas, C. Demesma, Y. Chevolot, and E. Souteyrand. *Use of organosilanes in biosensors* **(2010)**.

[63] J. Kim, G. J. Holinga, and G. A. Somorjai. *Langmuir*, 27,5171–5175 **(2011)**.

[64] C. M. Galloway, M. P. Kreuzer, S. S. Aćimović, G. Volpe, M. Correia, S. B. Petersen, M. T. Neves-Petersen, and R. Quidant. *Nano letters*, 13,4299–304 **(2013)**.

Conclusion Générale

Pour conclure sur le travail développé jusqu'ici il convient tout d'abord de le resituer dans le contexte scientifique et technologique dans lequel il s'inscrit. Tel qu'expliqué dans l'introduction générale de ce manuscrit, ce contexte est celui du développement de surfaces nanostructurées 2D et 3D sur lesquelles un adressage sélectif de différentes cibles (par ex : biomolécules ou nano-objets) est souhaité. Bien que la méthodologie développée ici puisse s'appliquer dans nombreux domaines, nous nous sommes surtout intéressés au domaine des biocapteurs plasmoniques. Dans ce domaine, un des principaux verrous technologiques actuels réside dans le fait de pouvoir sélectivement ancrer les biomolécules (ou particules) cibles sur des matrices de nanostructures métalliques qui possèdent des modes plasmoniques localisés sans que ces cibles ne s'adsorbent sur la surface diélectrique environnante où la transduction ne peut pas avoir lieu.
La fonctionnalisation chimique de surface est une méthode privilégiée pour permettre un tel ancrage sélectif. Il s'agit alors de modifier chimiquement la surface du métal et du diélectrique (fonctionnalisations orthogonales) pour permettre l'ancrage de la cible sur le premier tout en évitant l'adsorption non-spécifique sur le deuxième. L'étude de l'état de l'art sur ce sujet montre que malgré quelques publications notamment depuis 2010, un certain nombre de lacunes existent auquelles nous avons essayé d'apporter des réponses :

1. **Caractérisation chimique directe :** La caractérisation chimique directe de la fonctionnalisation est souvent négligée et reléguée à des mesures « en fin de processus », c'est à dire souvent à la lecture d'une réponse du capteur après fonctionnalisation chimique, immobilisation de biomolécule sonde et reconnaissance de biomolécule cible. Nous avons voulu présenter ici une caractérisation de surface à chaque étape démontrant le bon déroulement de la fonctionnalisation ainsi que l'activation pour les SAMs terminées NHS-ester (ce qui a notamment conduit à une optimisation des processus d'activation). Cette caractérisation s'est faite par différents outils, notamment PM-IRRAS, XPS et ToF-SIMS. Il est important de noter que nous avons pu démontrer la bonne orthogonalité de diverses fonctionnalisations à l'aide de thiols et silanes à l'échelle micrométrique par cartographie XPS et ToF-SIMS.

2. **Sélectivité des fonctionnalisations :** Nous avons utilisé des molécules (thiols et silanes) hautement spécifiques des deux matériaux étudiés (or et silice) ce qui assure la bonne sélectivité des fonctionnalisations. Ceci est un avantage certain vis-à-vis des fonctionnalisations faites par adsorption non spécifique de divers polymères ou macromolécules, souvent rencontrées dans des publications récentes concernant les biocapteurs LSPR.

3. **Fonctionnalisations en une seule étape :** Grâce à cette grande séléctivité des thiols et silanes pour l'or et la silice respectivement, nous avons pu réaliser les fonctionnalisations orthogonales simultanément dans le dichlorométhane. De telles fonctionnalisations orthogonales en une seule étape n'ont jamais, à notre connaissance, été présentées dans la littérature.
4. **Épaisseur de la couche d'accroche :** Un autre avantage des molécules utilisées dans ce travail est leur petite taille, qui assure l'ancrage des biomolécules à détecter au plus près de la surface métallique. Ceci est évidemment très important pour augmenter la sensibilité dans le cadre d'un capteur à ondes évanescentes.
5. **Diversité :** Nous avons testé diverses molécules comportant des espaceurs alkyls, PEG ou perfluorés et des groupements fonctionnels tels que COOH, NH_2, CH_3 ou biotine. Ceci montre la grande versatilité de cette approche, qui peut être appliquée pour capturer différentes cibles.

Nous avons eu l'occasion de démontrer l'intérêt de ces fonctionnalisations séléctives pour immobiliser divers nanolatex sur des micro et nanostructures d'or sur silice de manière très spécifique, tel que révélé par microscopie électronique à balayage.
Nous pouvons imaginer de nombreuses débouchées et perspectives pour ce travail. À court terme, ces résultats devraient être exploités d'un point de vue photonique. En effet, nous avons d'une part réussi à localiser des nanoparticules fluorescentes sur des matrices de nano-antennes plasmoniques. Un couplage photonique de ces deux nano-objets (nanobille/nano-antenne) est escompté et en cours de caractérisation au moment où l'on écrit cette conclusion. D'autre part, la fonctionnalisation orthogonale devrait permettre un accroissement de la sensibilité d'un capteur LSPR, ce qui est également en cours de test. À plus long terme, ce travail pourra évoluer dans différentes directions. Une diversification est possible tant sur les molécules utilisées pour la fonctionnalisation que sur les matériaux à fonctionnaliser (par ex : nitrure de silicium) ou sur les applications visées (ex : biocapteurs à transduction électronique). En outre, il est important de continuer à étudier de manière plus fondamentale et méthodologique la fonctionnalisation chimique de surfaces hétérogènes. Nous n'avons malheureusement pas pu mettre en évidence par des caractérisations « directes » l'orthogonalité des fonctionnalisations à une échelle inférieure à la dizaine de microns. Cependant, l'utilisation de microscopies à champ proches dérivées de l'AFM (CFM, TERS) ou, peut-être, l'utilisation de sources synchrotron pourraient permettre d'aller plus loin dans la caractérisation, notamment en terme de résolution spatiale.

General Conclusion

The conclusions of the work presented hereby need to be drawn in regards to the scientific and technological context in which this work was developped. As explained in the general introduction to this manuscript, our aim has been to answer the following question : *how can we selectively trap different targets (eg : biomolecules or nano-objects) onto previously defined regions of a patterned surface ?* Though this is quite a broad issue in nanotechnology, we have mainly focused on its applications and implications in the field of plasmonic biosensors. In this field, one of the major current technological bottlenecks comes from the need to selectively anchor biomolecules (or particles) onto large arrays of metallic nanostructures which support localized plasmons while avoiding the non-specific adsorption of these targets onto the surrounding dielectric surface where no detection can happen.
Surface chemical functionalization is specially well suited to answer this issue. The aim is thus to chemically modify the metal and dielectric surfaces so that the target can be bound onto the former while being repelled from the latter. The state of the art on this topic shows that despite some publications specially since 2010, a given number of issues can still be raised to which we tried to bring appropriate responses :

1. **Direct chemical characterization :** At the functionalization step, chemical characterization is often ommited. Instead, only the final sensor signal (after chemical functionalization, biomolecule probe immobilization and target biomolecule recognition) is taken into account. We have tried to provide surface characterizations at each step to prove the success of the functionalization and activation in the case of NHS-ester based SAMs (which has lead us to an optimization of such activation processes). This characterization has been carried out by different tools such as PM-IRRAS, XPS and ToF-SIMS. It is important to note that we were able to prove the efficiency of orthogonal functionalizations with thiols and silanes at the microscale through XPS and ToF-SIMS mapping.
2. **Selectivity :** We have used molecules (thiols and silanes) which are highly specific to the two materials investigated (gold and silica) which ensures the good selectivity of the functionalizations. This is a clear advantage to some recently reported functionalizations in the field of LSPR biosensors, made by non-specific adsorption of different polymers and macromolecules.
3. **Single-step functionalizations :** This above-mentioned selectivity has allowed us to carry out both functionalizations simultaneously in dichloromethane. Such single-step orthogonal functionalizations have, to the best of our knowledge, never been reported in the literature.
4. **Chemical layer thickness :** Another advantage of the molecules used in this work is their small size. This means that the target biomolecules can be anchored very close to the metal surface, which is extremely important for transduction based on evanescent waves.

5. **Diversity :** We have tested a broad range of molecules with different spacer chains including alkyl, PEG and perfluorinated, as well as different headgroups such as COOH, NH_2, CH_3 and biotin. This shows the great versatility of this approach which can be applied to capture different targets.

Furthermore, we have shown how these material-selective functionalizations can be used to anchor different nanolatexes onto micro and nanostructures of gold on silica with very high specificity, as revealed by SEM.
A lot of potential derivations of this work can be expected. In the short term, these results should be exploited from a photonic point of view. Indeed, we have been able to anchor fluorescent nanobeads onto large arrays of plasmonic nanoantennas. A photonic coupling of these two nano-objects (nanobead / nanoantenna) is expected. The appropriate photonic characterizations are under way. Furthermore, orthogonal functionalizations should be able to increase the sensitivity of an LSPR biosensor which is also being tested at the moment. In the long term, this work may know different evolutions. We can expect a diversification of the molecules used for the functionalizations as well as the substrate materials (e.g : silicon nitride) or the final application (e.g : electronic biosensors). Eventually, it is important to continue the deeper characterization of the orthogonal functionalizations on heterogeneous substrates. We could only show direct chemical evidence of this orthogonality at a rather "big" scale (> ten microns). However, the use of scanning probe microscopies derived from AFM (CFM, TERS) or, maybe, the use of synchrotron radiation could allow to go further in the chemical characterization, specially in terms of spatial resolution.

Appendix A

Top-down fabrication and residue removal

A.1 State of the art

> *"The complexity for minimum component costs has increased at a rate of roughly a factor of two per year* [...] *this rate can be expected to continue, if not to increase."*[1]

The development of micro and nanotechnology has been greatly based on the ability of creating large arrays of micro and nanometric structures on a substrate with well-defined geometries and spacings. The most emblematic example is probably the integration of higher amounts of smaller transistors on an electronic chip (Moore's law).[1] However, integrating a large number of micro and nanostructures on a substrate has many applications beyond electronics, such as the development of new photonic components (eg : photonic crystals)[2] or miniaturized and multiplexed biosensors (eg : biochips).[3,4]

Lithography is probably the most widespread technique in micro and nanofabrication to allow the patterning of a solid substrate with different micro and nanostructures. In fact, lithography can be seen as an umbrella term for several different methods that are found under this denomination. In the following paragraphs we will briefly present UV and e-beam lithography and cite a number of *unconventional* alternatives.

Furthermore, as lithographies are based on polymer resists which can leave traces on the surface at the end of the process, we will discuss different cleaning procedures to remove these contaminations.

A.1.1 Lithographies

A.1.1.1 General principle

An overview of lithography is given in Figure A.1 (this simplified description intentionally ignores some possible steps, such as thermal annealing, multiple exposures on inversion resists or deposition of resist bi-layers or primers). At the first step (1-2), a chemical resist (polymer) is deposited by spin-coating on the substrate. Then (3-4), some regions of the resist are chemically modified by an incident beam (UV or electronic). The resist is later *developed* (5) meaning that either the regions that were modified or the ones that were not (depending on the resist being

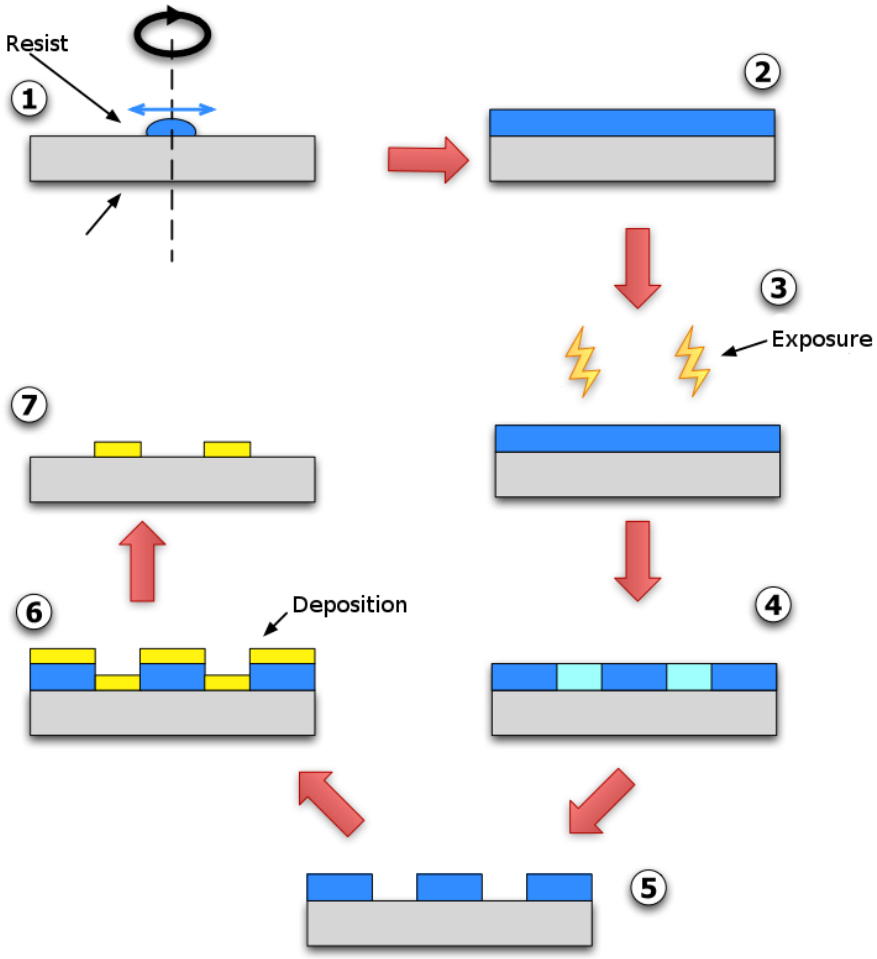

Figure A.1 – Simplified lithography principle. (1-2) Coating of the surface by a polymeric resist layer. (3-4) Exposure of given regions of the layer inducing reticulation changes in the resist. (5) Developing (dissolution) of exposed (vice-versa for negative resists, not shown) areas. (6) Material deposition (or etching, not shown). (7) Dissolution of the resist (lif-off). Figure adapted from.[5]

positive or *negative* ; only the *positive* case is shown in the figure) are dissolved in a solvent. The openings created in the resist are then used, either to deposit a new material (6) or to etch the substrate (not shown). Finally, all the remaining resist is dissolved, thus leaving the desired structures on the surface (in the case of a deposited material, this step is called *lift-off*).

Different resists and exposure beams can be used depending mainly on the expected resolution. Thus, two main techniques exist : UV-lithography and e-beam lithography. Specific information on both techniques will be described in the following sections and summarized in Table A.1.

A.1.1.2 UV lithography

UV-lithography (photolithography) is mainly used for large-scale, high-throughput and low-resolution patterns.

In this technique, the resist is exposed to a UV-light ($\lambda \approx$ 300nm-400nm). In order to expose only given regions of the resist it is necessary to use a mask that is opaque to UV light except in the regions that are to be exposed. This allows the motif on the mask to be transferred to the photoresist. The steps following exposure have been described in the previous section (see Figure A.1).

Photoresists are resin polymers whose solubility in a developer (basic solvent) change when exposed to light. Photoresist chemistry is still an active research field but most common positive photoresists are based on DiazoNaphthoQuinone (DNQ)/Novolac [17] (eg : AZ-5206©) whereas negative photoresists may be epoxy-based (eg : SU-8©). These are usually developed in TetraMethylAmmonium Hydroxide (TMAH) (eg : AZ XXX MIF©).

The main advantage of photolithography is that many microstructures over a large area (several cm^2) can be exposed simultaneously. However, resolution is limited by diffraction, so that photolithography is mainly employed for typical sizes over 1µm. Nonetheless, recent advances in photolithography allow for better resolution (smaller size, smaller spacings and better edge control). These advances and current issues, which shall not be discussed in detail here, include the use of deep and extreme-UV,[6] interferometric lithography[7] and use of superlenses.[8,9]

A.1.1.3 E-beam lithography

Electron-beam lithography is mainly used for small-scale, low-throughput but high-resolution patterns.

In this case, the electron beam of a SEM ($\approx$ 10keV-100keV) is used to directly expose, i.e., *write*, the wanted shapes on the resist. Thus, unlike photolithography, no mask is needed. Similarly to photoresists, electronic resists are resin polymers whose solubility in a developer is changed when exposed to electric charges, namely electrons. Among them, PMMA and, more recently, Hydrogen SilsesQuioxane (HSQ) are widely used. TMAH and Methyl isobutyl ketone (MIBK) are common developers in e-beam lithography.

Using an electron beam to expose the resist is an efficient way to beat the resolution of photolithography, limited by light diffraction. Thus, e-beam lithography can be used for nanometric patterns. However, the exposure process is sequential and can take several hours for small areas ($\leq$ 1cm^2). Recent advances and current issues on e-beam lithography include the use of ultrahigh contrast[10] and Scanning Transmission Electron Microscope or Microscopy (STEM) lithography.[11,12]

A.1.1.4 Summary on UV and e-beam lithographies

In the previous paragraphs we have seen the basic concepts of top-down substrate patterning using conventional lithography. It is not the purpose of this brief introduction to discuss lithography in detail with its many variants. For this matter, the reader can find the appropriate references in the literature.[11]

Table A.1 summarizes the basics of UV and e-beam lithography.

	Photolithography	**Electron-beam lithography**
Exposition source	UV light ($\approx$ 300nm-400nm)	Electron beam (2keV[13]-350keV[13])
Resist	DNQ-Novolac, Epoxy	PMMA, HSQ
Developer	TMAH	TMAH, MIBK
Mask	Yes	No

17. Novolac is a photoresist based on phenol-formaldehyde, enriched in phenol.

	Photolithography	**Electron-beam lithography**
Throughput	High	Low
Resolution [18]	2μm[14]	≤ 5nm[14]
Recent advances	Deep and Extreme-UV (≤ 250nm),[6] interferometry,[7] superlenses[8,9]	ultrahigh contrast,[10] STEM[11,12]

Table A.1 – UV and e-beam lithographies

A.1.1.5 Unconventional lithographies

Though conventional UV and e-beam lithographies are still widely used today, it should be noted that other unconventional lithographies exist, such as : focused ion beam lithography,[14] indentation lithography,[15] dip-pen lithography,[14] soft lithography,[14] colloidal-crystal lithography,[16] beam-pen lithography[17] and nanoimprint lithography.[14] As none of these have been used for the work presented in this manuscript, we shall not go into deeper detail.

A.1.2 Residue removal

As we have seen in the previous paragraphs, the lithography techniques presented here all require a polymeric layer deposited on top of the surface. The total removal of this polymer at the end of the lithography process is not always investigated thoroughly. Nonetheless, it deserves a special attention here since the surface is to be further modified by chemical functionalization.

We will review in the following paragraphs different methods for surface cleaning reported in the literature in wet and dry environments (see Tables A.2 and A.3). These methods will be screened obviously in terms of residue removal but also in terms of side-effects on the surface such as delamination, oxidation and roughness.

18. Smallest possible feature size

A.1.2.1 Wet processes

Main compound	Additives	Principle	Advantages	Drawbacks	Comments
Organic solvents : Acetone[18] Ethanol, IsoproPAnol (IPA)[18] DCM[18] DiChloroEthane (DCE)[18] *N*-Methyl Pyrrolidone (NMP)[18]	None	Organic dissolution	Ease of use, often included in the lithography process (eg : lift-off)	Not enough for total PMMA removal[18]	May be used with ultrasounds and/or heating.
$H_2SO_4 + H_2O_2$ (Piranha)	None	Oxidation	Standard procedure	Possible delamination of thin films. Dangerous.	
H_2O_3[19] (ozonated water)	Surfactant : Glycolic Acid Ethoxylate 4-tert-butylphenyl Ether (GAE4E)[19] Cationic hexadecylTrimethyl Ammonium Bromide (CTAB)[19] Triton[19]	Oxidation + surfactant	Proven efficiency of GAE4E on SiO_2[19]	Efficiency proven on model polystyrene particles, not on actual lithography residues	Possibility to use same surfactant with another solvent.
HF	NH_4F for Buffered Oxide Etch (BOE)	Dissolves SiO_2 : $SiO_2 + 4HF \longrightarrow SiF_4(g) + 2H_2O$ $SiO2 + 6HF \longrightarrow H_2SiF_6 + 2H_2O$	Very efficient on oxides. Commonly used in microfabrication.	Removal of oxide layer may be unwanted. Dangerous.	

Main compound	Additives	Principle	Advantages	Drawbacks	Comments
Basic H_2O[20]	NH_4OH[21] Alkanolamine KOH TMAH	Basic attack	Proven efficiency of KOH and NH_4OH No need for organic solvent Easy rinsing	Not better than organic solvents	Possible to add inhibitors to avoid metal corrosion
Basic aqueous IPA[22]	$NH_4OH + H_2O$ $TMAH + H_2O$	Basic attack + organic dissolution H_2O leads to dissociation of NH_4OH OH^- attacks Si-O-Si bonds between silica surface and Hexamethyldisilazane (HMDS)	Proven efficiency on HMDS removal from SiO_2 Leads to low rugosity	TMAH efficiency not proven	

Table A.2 – Wet processes for surface cleaning (removal of organic residues after lithography).

A.1.2.2 Dry processes

Main compound	Additives	Principle	Advantages	Drawbacks	Comments
O_2 plasma[21]	None	Ashing		Leads to oxidation of metal surfaces	
NH_3 plasma[23]	None	Organic + $NH_3 \longrightarrow HCN + H_2O$			
UV nanosecond laser[21] : ArF (193nm) XeCl (308nm)	None	Photochemical bond dissociation : C=C, C-H, C-N...	Proven efficiency with ArF laser	Complex and expensive	Fluence and number of shots can be adapted[21]

Main compound	Additives	Principle	Advantages	Drawbacks	Comments
Nd_3 + Yttrium Aluminium Garnet, $Y_3Al_5O_{12}$ (YAG) (532 nm) (visible laser)[24]	None	Thermal ablation		HMDS removal from Si not proven	
H_2O (scrubber spray)[21]	None	Mechanic abrasion		Wear	
H_2O + gaz (soft spray)[21]	None	Mechanic abrasion with droplets		Wear	
UV + O_3	None				
Supercritical CO_2[21,23,25–27]	$TMAHCO_3$ + MethOH Acetone DMSO[19]	Unique properties of diffusion and solvatation	Very efficient	Complex and expensive	

Table A.3 – Dry processes for surface cleaning (removal of organic residues after lithography).

19. Dimethyl sulfoxide

A.1.2.3 Summary on cleaning processes

As evidenced by Tables A.2 and A.3, removal of organic contamination from microfabrication processes is an active research topic with many possible answers. Although a relatively standard cleaning procedure with acetone + alcohol + water is often used, this may not result in optimum cleaning of the surface, specially when the latter has been previously coated with PMMA.[18] Other wet cleaning procedures may be used either in acidic environments (HF, piranha) or basic environments[20–22] (ammonia, KOH). The former are known to be very efficient but may result in delamination or dissolution of the surface, whereas the latter are reported not to be better than standard organic solvents.

Dry processes can be used instead or in addition to wet cleaning procedures. Among the different options presented in Table A.3, O_2 plasma ashing appears as a very good candidate both for its efficiency and ease of use. However, it must be noted that this procedure may lead to metal oxidation. In the case of gold surfaces, it has been reported that exposure to O_2 plasma leads to Au_2O_3.[28,29] However, this oxide is unstable at normal temperature and pressure.[28] The characteristic dissociation time (oxide half-life) at 20°C is reported to be 22h and can be accelerated when rinsing with ethanol[29,30] and/or heating.[28]

A.2 Materials and methods used during this work

This section presents the protocols used for the top-down substrate patterning and cleaning. It must be noted that some of these processes were conducted partly or exclusively by others as specified below :

- Processes exclusively conducted by myself :
  - Gold evaporation (plain substrate).
  - Cleaning processes.

- Processes done partly by others :
  - Photolithography with subsequent gold deposition and lift-off, when not done by myself was done by Bertrand Vilquin or Pedro Rojo Romeo at INL.
  - E-beam lithography and subsequent gold evaporation and lift-off was mostly done by Pedro Rojo Romeo or Céline Chevalier at INL.

- Processes exclusively done by others :
  - Silica sputtering, when needed, was carried out by Bertrand Vilquin or Pedro Rojo Romeo at INL.
  - Institut d'Électronique Fondamentale (IEF) partners also provided "macro-patterned" (see Fig. 1.17) gold on glass surfaces.

A.2.1 Lithography

A.2.1.1 Photolithography

The protocol used for photolithography was the following :

1. Spin-coat the HMDS primer followed by AZ 5214 (negative) resist at 5500 rpm for 30s.

2. Bake at 110°C for 1min.
3. Expose to UV through mask for 4s.
4. Bake at 120°C from 2min.
5. Expose whole sample (flood exposure) to UV for 20s.
6. Develop in TMAH (Metal-Ion Free (MIF) 726) for 1min under constant agitation.
7. Stop development by soaking in ultrapure water.

A.2.1.2 E-beam lithography

The protocol used for e-beam lithography was the following :

1. Spin-coat Methyl methacrylate (MMA) at 3000 rpm
2. Bake at 150°C for 1,30min.
3. Spin-coat PMMA at 2000 rpm
4. Bake at 180°C for 1,30min.
5. Expose to e-beam.
6. Develop in MIBK-IPA.
7. Rinse with DCM.

A.2.2 Silica sputtering

For the investigation of silanization and orthogonal functionalizations the substrate was either : (a) a glass microscope slide, (b) a silicon wafer with a 2µm layer of SiO_2 (commercial), (c) a silicon wafer onto which silica was deposited by Bertrand Vilquin at INL or (d) a glass slide covered by a first layer of gold onto which silica was further deposited by Bernard Bartenlian and co-workers at IEF.

A.2.3 Gold e-beam evaporation

Gold e-beam evaporation on different samples was conducted at INL (either by myself or Pedro Rojo Romeo) and IEF (by Bernard Bartenlian and co-workers).

Protocol at INL :

1. Introduce sample in evaporation chamber and pump to a pressure of 1.5 10^{-6} Torr (temperature set at 27K).
2. Switch on the cooling system.
3. Deposition of chromium adhesion layer
   (a) Set voltage to 6kV.
   (b) Increase current until the deposition rate, monitored by a QCM, reaches ca. 1Å/s (a cache is "hiding" the substrate so far so that no deposition occurs on it)
   (c) Remove cache and wait until the deposited layer reaches 2-3nm thickness.
   (d) Place cache back, decrease current slowly to 0, switch off voltage and wait for the socket containing the chromium to cool down.

(e) Change socket to the one containing the gold.

4. Deposition of gold layer
   (a) Set voltage to 6kV.
   (b) Increase current until the deposition rate, monitored by a QCM, reaches ca. 2Å/s (a cache is "hiding" the substrate so far so that no deposition occurs on it)
   (c) Remove cache and wait until the deposited layer reaches 45-50nm thickness.
   (d) Place cache back, decrease current slowly to 0, switch off voltage and wait for the socket to cool down.

This process was conducted in a Leybold© e-beam evaporator.

A.2.4 Substrate cleaning

A.2.4.1 Organic solvents

When cleaned only with organic solvents (typically when no resist residues from lithography were expected) samples were cleaned with the following procedure :

1. Immerse in acetone under sonication for ca. 10min
2. Immerse in ethanol or isopropanol for ca. 5min
3. Immerse in ultrapure water for ca. 5min
4. Dry with nitrogen flow

Alternatively other organic solvents were used such as DCM and heating was also applied though this procedures were quickly abandoned in favor of a simpler and more efficient O_2 plasma, as is detailed in section 3.1.1.

A.2.4.2 O_2 Plasma

Oxygen plasma was found to be the most efficient, thus most used cleaning process. Samples were cleaned by O_2 plasma with the following parameters :

– Applied (forward) power = 350W (typical reflected power was 10W)
– Oxygen flow = 400 sccm
– Pressure = 90Pa
– Time = 5min

This was conducted in an Anatech© chamber where only oxygen and nitrogen are introduced. When this process was conducted in an etching chamber with input lines of different fluorinated gases (SF_6, CHF_3) fluor contamination was detected afterwards by XPS analysis.

Appendix B

DLVO and colloid stabilization

NB : The following paragraphs are adapted from our previous publication.[31]

Before examining the means for globally placing individual particles on pre-defined regions of a substrate, we must ensure that these particles are stabilized, ie : not aggregated to one another or to the walls of the container. Different forces control the particle/particle (or particle/wall) interaction. These can be summarized in what is called Derjaguin, Landau, Verwey, Overbeek (DLVO) theory. In its most basic form, DLVO theory deals with two interaction forces : Van der Waals (attractive) and electric double-layer effects (repulsive)[32,33].

B.1 Van der Waals attraction

Van der Waals forces, and more precisely London dispersion forces, are attractive forces arising from the spontaneous polarization of molecules. This polarization effect is enhanced when dealing with nano and microparticles. Indeed, the Van der Waals potential energy is proportional to the inverse sixth power of the distance ($\propto D^{-6}$) when considering two atoms but the energy per unit area is proportional to the inverse of the distance ($\propto D^{-1}$) for colloidal particles[34] :

$$U_{sphere/sphere} = -\frac{A}{6\pi D} \times \frac{R_1 R_2}{R_1 + R_2}$$

R_1 and R_2 being the radii of the spheres, D the distance between them and A the so-called Hamaker constant which depends on the materials.

The derived attractive force will lead the particles to aggregate to each other and to the walls. Therefore one needs repulsive forces to separate (stabilize) the colloidal dispersion. The main repulsive force in colloidal solutions is linked to surface charge, through what is called the electric double layer.

B.2 Electric double layer repulsion

Surfaces can be charged in polar and non-polar solvents[35] by different phenomena that will not be discussed here. This surface charge induces an electrostatic potential that decays exponentially when moving away from the surface, due to the existence of a double counter-ion layer : a first layer of strongly grafted counter-ions (Stern layer) and a second "diffuse" layer with a majority of counter-ions (Gouy-Chapman layer).

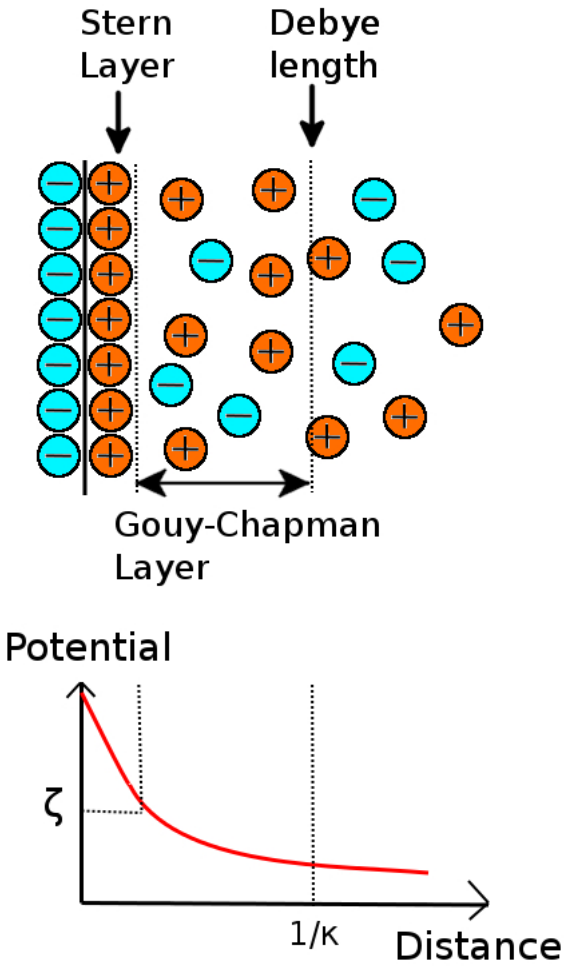

FIGURE B.1 – Electric double layer and corresponding potential for a negatively charged surface.

The mathematical derivation of the electric double layer theory can be found elsewhere[36] and will not be detailed in this review. We shall just introduce two valuable parameters : the potential at the Stern layer (zeta potential, ζ) and the characteristic double layer length (Debye length, κ^{-1} or λ_D) (See Fig. B.1).

When two equally charged surfaces are brought together ($D \ll \lambda_D$, D being the distance between the particles), their electric diffuse layers overlap and a repulsive interaction energy arises from the excess of counterions. Thus for two spheres, we have[36] :

$$U_{sphere/sphere} = 64\pi RkTc^0\Gamma^2 \times e^{-\frac{D}{\lambda_D}}$$

Where R is the particle radius, Γ is the so-called reduced surface potential, k is the Boltzmann constant, T is the temperature and c^0 is the ionic concentration in the bulk.

B.3 DLVO, extensions and practical considerations

In its simplest form, DLVO just adds the interaction energies due to Van der Waals and electric double layer, which for two identical spheres separated by a distance D gives :

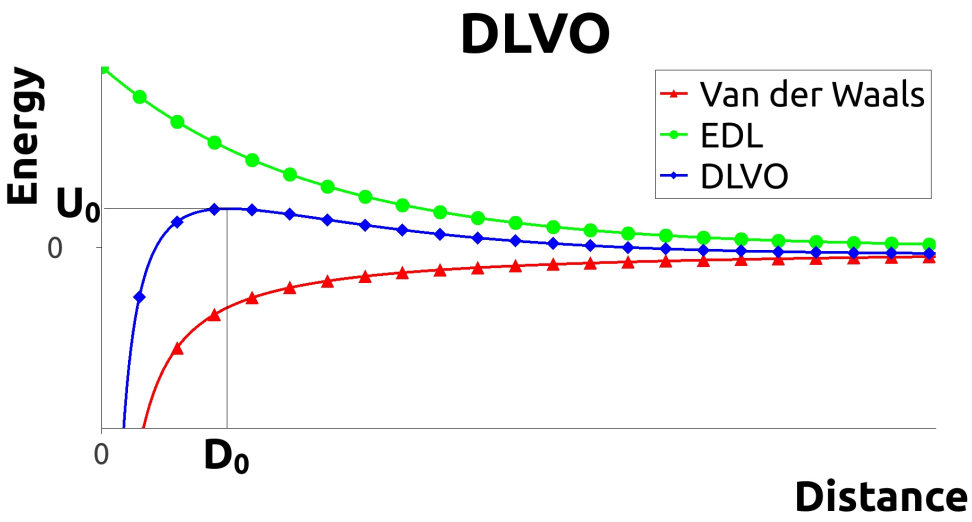

FIGURE B.2 – DLVO energy vs separation distance. EDL stands for electrical double layer repulsion, VdW stands for Van der Waals attractive interaction and DLVO is the sum of both contributions.

$$U_{DLVO} = U_{EDL} + U_{VdW} = 64\pi RkTc^0\Gamma^2 \times e^{-\frac{D}{\lambda_D}} - \frac{A}{6\pi D} \times \frac{R}{2}$$

U_{EDL} and U_{VdW} being the energetic contributions of electric double layer and Van der Waals interactions. A typical shape of U_{DLVO} vs D is shown in Fig. B.2.

In Fig. B.2 we can see that the potential interaction energy between particles reaches its maximum value U_0 at a given separation distance D_0 ($\frac{dU}{dD}|_{D_0} = 0$ and $U(D_0) = U_0$). Moreover, for $D < D_0$ the total interaction is attractive ($\frac{dU}{dD} > 0$) while it is repulsive for $D > D_0$ ($\frac{dU}{dD} < 0$). Physically, this means that for two particles far from each other ($D >> D_0$) if the thermal energy kT is higher than U_0, then the particles can overcome this energy barrier and aggregate due to the short-range dominating Van der Waals attractive forces. If $U_0 > kT$ instead, then the colloids can be well stabilized by the electrostatic repulsion. Nevertheless, other phenomena can play a role in colloidal stabilization and are not taken into account in DLVO theory such as acid/base interactions[37,38], hydration forces[39], steric hindrance[37] or viscous drag divergence near a wall.[40–42] Thus, we can add other terms to U_{DLVO} (the "new theory" is sometimes referred to as "extended DLVO").

In practice, to stabilize a colloidal dispersion, one can fix the ionic strength to change Debye's length. Indeed, as a rule of thumb, at 25°C in aqueous solution, we can estimate :

$$\lambda_D = \frac{0,304\ (\text{nm})}{\sqrt{I}\ (\text{mol/L})}$$

Where I is the ionic strength of the solution in moles per liter.

As an example, λ_D is around 1nm in PBS[43] while it can almost reach 1µm in ultrapure water[44].

Another common method for stabilizing colloids is to graft polymers onto the particles' surfaces to ensure steric hindrance when particles come close together[37].

Appendix C

Characterization tools

C.1 PM-IRRAS

Polarization-Modulation InfraRed Reflection Absorbtion Spectroscopy (PM-IRRAS) can be seen as a refinement of "conventional" Infrared Reflection Absorption Spectroscopy (IRRAS), itself being a special mode of infrared spectroscopy. Let us thus briefly recall the basic principles of Infrared (IR) spectroscopy, followed by IRRAS and eventually describe the PM-IRRAS setup.

C.1.1 FTIR

Infrared spectroscopy is based on the fact that molecular orbitals (chemical bonds) can vibrate at specific resonant frequencies (or wavenumbers : $\frac{1}{\lambda}$; where λ is the wavelength) in the infrared spectrum. Thus, when a sample is on the optical pathway of an infrared beam, it will absorb part of the incident light at specific wavenumbers. By plotting the absorbtion of the sample versus the wavenumber of the light beam one obtains the infrared spectrum of the surface with characteristic peaks of the different molecular bonds in the sample. Most fundamental vibration and rotation modes of chemical bonds can be found in the mid-infrared region (ca. 4000cm^{-1}-400cm^{-1}) as schematically shown in Fig. C.1.

Different vibration modes can be classified and noted as follows :

- ν = stretch (possible for 2 atoms A-B ; and for three A-B-A with symmetric and assymetric modes)
- δ = bending (possible only for more than two atoms) with different modes :
  - Symmetric, in plane (scissoring)
  - Assymmetric, out of plane (twisting)

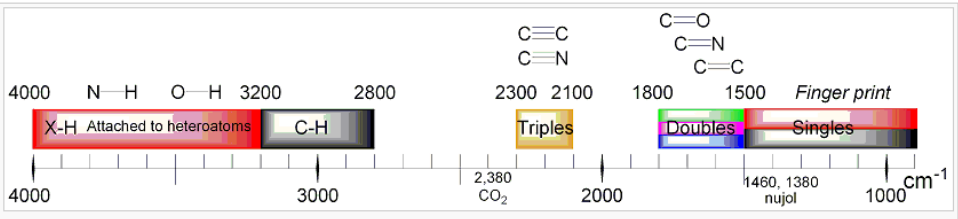

FIGURE C.1 – Schematic representation of IR absorbtion bands (source : wikipedia).

  - Assymetric, in plane (rocking)
  - Symetric, out of plane (wagging)
- Fermi resonance (mixing modes) can occur, shifting some peaks or creating doublets from one mode.

In order to probe the absorbtion of a sample at different wavenumbers, it is possible to shine the sample with a changing monochromatic light beam (through a dispersive spectrometer) thus probing one by one every wavenumber. Dispersive spectrometers are however rarely used anymore for infrared characterization.

Instead, most infrared spectrometers are based on Fourier-Transform Infrared Spectrosocpy (FTIR). Without going into too much detail about FTIR itself, let us say that in this configuration, a "white" light containing the whole spectrum is used. Before reaching the sample, the light beam is split through a Michelson interferometer which induces a retardation on one of the two "halves" of the beam, creating thus constructive and destructive interferences on the beam that reaches the sample. Thus, the raw data obtained by the detector is an interferogram, that is, the intensity as a function of the retardation. This interferogram is later translated into a spectrum by a Fourier Transformation, hence the name of the technique.

The spectral resolution is dependent on the amplitude of the moving mirror in the Michelson Interferometer.

C.1.2 IRRAS

IRRAS is specially suited to probe the chemistry of a highly reflective (specially metallic) surface. In an IRRAS set-up, the infrared light beam is specularly reflected at a grazing incidence onto the metallic surface to be probed. At the surface, only the p-polarized light is non-equal to zero, so that only dipoles having a component perpendicular to the surface can absorb light. However, as far from the surface the light is not polarized, isotropic absorptions due to the environment occur and alter the spectrum (requiring thus the acquisition of a background spectrum prior to probing the sample). This remark is the basis for the PM-IRRAS implementation.

C.1.3 PM-IRRAS

C.1.3.1 PM-IRRAS principle, in short

In a PM-IRRAS setup, the incident beam is polarized prior to reaching the surface. Its polarization is switched from p to s at a high frequency by a PhotoElastic Modulator (PEM). Simply put, this allows the acquisition of two different signals simultaneously : the sum (R(p) + R(s)) and difference (|R(p)-R(s)|) reflectivities. By taking the ratio of these two signals : $\frac{|R_p - R_s|}{R_p + R_s} = \frac{\Delta R}{R}$ one obtains a spectrum of the surface without the contribution of isotropic absorptions from the environment, having thus a better surface-sensitivity without the need of acquiring a background spectrum.

C.1.3.2 The PEM

The PEM is responsible for the **polarization modulation** of the light beam. It is composed of a **controller** connected to an **electronic head** driving an **optical head**. The optical head is a piece of piezoelectronic isotropic material which can change the polarization of a light beam going through it (becomes a birefringent material when stretched). This optical head is driven by a sinusoidal voltage applied by the electronic head. The controller lets the user define the wavelength of the light beam and the desired retardation (such as 0.5 λ or 0.25 λ ; ie : half-wave or quarter-wave) at that wavelength.

*NB : In a PM-IRRAS experiment, the retardation is set to 0.5λ (the optical head acts as an **oscillating half-wave plate**). The light beam is not monochromatic so the retardation of 0.5λ will only occur at a given wavelength (or wavenumber) set by the user on the PEM-controller. This will be the wavenumber of optimum sensitivity.*

The controller also shows the frequency of the electronic head (fixed).

The PEM electronic head drives the optical head with a sinusoidal voltage $V_0 \cos \omega_m t$ which induces a modulation between linear p and s polarizations (half-wave plate ; retardation : 0.5 λ) at a frequency of

$$2\frac{\omega_m}{2\pi}$$

for one particular wavenumber λ_0^{-1}, determined by V_0. For the other wavenumbers, the polarization is not perfectly linear (p and s) but elliptical.[45]

λ_0^{-1} can be manually tuned on the PEM-controller by chosing the wavenumber while indicating a retardation of 0.5 λ. $\frac{\omega_m}{2\pi}$ is fixed by the electronic head.

C.1.3.3 PM-IRRAS signal

The light reaching the detector is modulated twice : first in intensity by the interferometer and second in polarization by the PEM with different efficiencies at different wavelengths depending on V_0.

After electronic treatment (demodulation, filtering... etc)[45] two signals can be acquired on the computer. **If the selected unit on the software is % Transmittance**, then the two signals are :

$$A = |(R_p + R_s) + J_0(\Phi_0)(R_p - R_s)|$$

$$B = |J_2(\Phi_0)(R_p - R_s)|$$

Where R_p and R_s are the reflectivies of p and s polarizations and J_n is an n order Bessel function translating the inefficiency of the PEM at all wavelengths. Φ_0 "is the maximum dephasing introduced by the PEM between the i and j electric field components (Φ_0 is a function of the maximum voltage V_0 apllied to the PEM)"[45].

NB : Because of the Bessel function superimposition, the spectra will be in arbitrary units, although the reflectivity is in % Transmission.[46]

For a metallic substrate, these expressions can be simplified :

$$A = R_p + R_s$$

$$B = |J_2(\Phi_0)(R_p - R_s)|$$

The PM-IRRAS signal can be obtained by ratioing both :

$$S_{PMIRRAS} = \frac{B}{A} = |J_2(\Phi_0)|\frac{|R_p - R_s|}{R_p + R_s} = |J_2(\Phi_0)|\frac{\Delta R}{R}$$

NB : For simplicity we have omitted from the equations the electronic gains that can be applied to channels A and B, as well as the possible different responses of the optical elements (PEM, detector... etc) for p and s polarized light.[45]

C.1.3.4 Baseline correction and units

In order to obtain the final spectrum $\frac{\Delta R}{R}$ one needs to normalize the obtained spectrum to remove the $J_2(\Phi_0)$ contribution. This can be done by different methods :

- A **manual baseline correction dividing the spectrum by a spline function**[46] fitted to the regions of the spectrum where no peak is expected is often performed.[47] This correction gives the correct relative intensities of the peaks (whereas substracting the baseline does not).[46] However this leads to arbitrary units on the Y-axis and the results are user-dependant.

- A **"background" spectrum** with a bare substrate can be collected for **proper normalization**. However, this requires to have a good reference sample (identical to the test sample without the organic layer of interest). Furthermore, it takes away one of the main interests of the PM-IRRAS technique versus conventional IRRAS.

- A **mathematically modelled Bessel function** can be used. However, the superimposed function on the experimental $\frac{\Delta R}{R}$ spectrum may not exactly correspond to a Bessel function, as it may include experimental biases such as an absorbing layer onto a mirror or imperfect behaviour of the PEM (eg : residual birefringence).[45]

It is possible to convert the data to absorbance units which enables the comparison of the absolute intensities of the peaks. However, this is not straightforward.[46]

C.2 XPS

X-ray Photoelectron Spectroscopy (XPS) is a method that probes the energy of electrons present in atoms on a surface (ca. 10nm depth). In an XPS experiment, the sample surface is exposed to photons in the X-ray range (typical incident energy of photons of 1486.6eV for an aluminium source -AlK_α radiation-). These photons interact with core-level electrons that are thus expelled from the surface with a given kinetic energy that depends on their binding energy. A simple energy equality can be written for an elastic collision : $|E_{input}| = |E_{output}| = |E_{binding}| + |E_{kinetic}|$. This translates the fact that the energy of the incoming photons is converted first to overcome the binding energy of the electron (ie : bringing the electron to the vacuum

level, in other words ionisation energy of the atom) and the remaining energy is translated into kinetic energy of the expelled electron. $|E_{input}|$ is known and fixed by the source (eg : 1486.6eV), $|E_{kinetic}|$ is measured, so that the binding energy can be simply deduced $|E_{binding}| = |E_{input}| - |E_{kinetic}|$.

The XPS analyzer counts the number of electrons (per unit time) reaching the detector with a given kinetic energy (translated into binding energy with the aforementioned relation). Thus a typical XPS spectrum shows an intensity (in "counts per second") versus binding energy with peaks associated to the energy of electrons in atoms present at the surface. Obviously, only electrons whose binding energy is inferior to the energy of the input X-ray photons can be detected.

Most importantly, XPS is sensitive to the so-called "chemical shift". This refers to the fact that electrons at the same quantic state (same orbital) of the same element (eg : C1s orbital of a carbon atom) have slightly different binding energies depending on the chemical environment of the given atom. This means that a carbon atom participating in a carboxylic acid chemical group O=*C*-OH has a different XPS spectrum (C1s peak around 289.0eV) than a carbon atom in an alkyl chain CH2-*C*H2-CH2 (C1s peak around 285.0eV). Thus, XPS which is sometimes referred to as ESCA (Electron Spectroscopy for Chemical Analysis) is not only an elemental analysis method but also a chemical one.

C.3 ToF-SIMS

Time-of-Flight Secondary Ion Mass Spectroscopy (ToF-SIMS) is another surface sensitive (typically around 1-2nm depth) analysis method. ToF-SIMS is based on the detection of ionized molecular fragments of the molecules present at the surface sample.

A source is used to bombard the sample with a -primary- ion beam (eg : ionized gold clusters or fullerenes), thus liberating ionized fragments of the present molecules. These -secondary- ions are then accelerated with a constant voltage onto a time-of-flight mass spectrometer that separates the different species according to their mass-to-charge ratio (m/z) which can be determined by computing the "time of flight", that is the time between the generation of the secondary ion and its reaching the detector. Indeed, by equating the potential energy induced by the fixed voltage $E_{electric} = zV$ where z is the charge and V is the voltage, to the kinetic energy of the ion $E_{kinetic} = \frac{mv^2}{2}$, where m and v are the mass and velocity of the secondary ion, it can easily be determined that $t = \alpha\sqrt{m/z}$, where t is the time of flight and α is a proportionality constant that can be determined with well known ion species response (usually hydrocarbons). This technique requires that the ions have a ballistic trajectory, without collision with other species. In other words the mean free path of the ions should be large compared to the distance between the sample and the detector. Thus, it is required to operate in vacuum (ca. 10Pa).

Obviously, depending on the polarization set between the sample and analyzer only positive or negative ions can be detected simultaneously.

C.4 Contact angle goniometry

Contact angle goniometry is based on the measure of the angle θ_C formed by a liquid onto a solid surface in contact with a gas environment (see Fig. C.2).

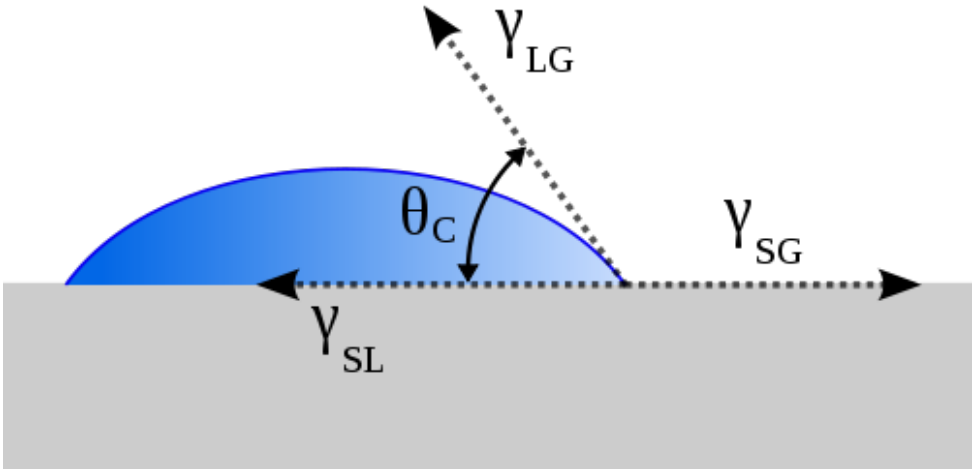

Figure C.2 – Contact angle principle (source : wikipedia).

If γ_{LG}, γ_{SL} and γ_{SG} are the interfacial energies between the liquid and gas, solid and liquid and solid and gas respectively, Young's equation reads as follows :

$$\gamma_{SG} = \gamma_{SL} + \gamma_{LG} \cos\theta_C$$

The liquid used in a contact angle experiment is often ultrapure water which interacts with the surface mostly by hydrogen binding. In this case, the smaller θ_C is, the more hydrophilic the surface is. More generally, the use of distinct liquids may be useful to probe different interactions such as ionic or van der waals forces.

A simple setup for a contact angle experiment consists of a syringe to deposit a droplet (ca. 1µL) onto the surface and a camera to take an image of the droplet and measure the contact angle. This is known as the sessile drop technique.

C.5 AFM

Atomic Force Microscopy (AFM) is one kind of scanning probe microscopy where a nanoscale tip (usually made of silicon, silicon oxide or silicon nitride ; curvature radius of a few nanometers) is attached at the edge of a cantilever whose height is controlled by piezoelectric materials and whose deflection is monitored by a laser beam and photodiode (see Fig. C.3).

The AFM can be used in contact or tapping mode. In contact mode, the tip touches the surface at all times. In tapping mode, the tip is set to oscillate near its resonant frequency above the surface. In both cases, when the surface height changes either the deflection (in contact mode) or the amplitude of the oscillations (in tapping mode) of the cantilever change. Instead of measuring directly the deflection or change in amplitude of the oscillations, the AFM experiment is usually set-up to maintain these parameters constant by a feedback loop, so that it is the signal necessary to maintain them that, indirectly, gives the topography of the surface.

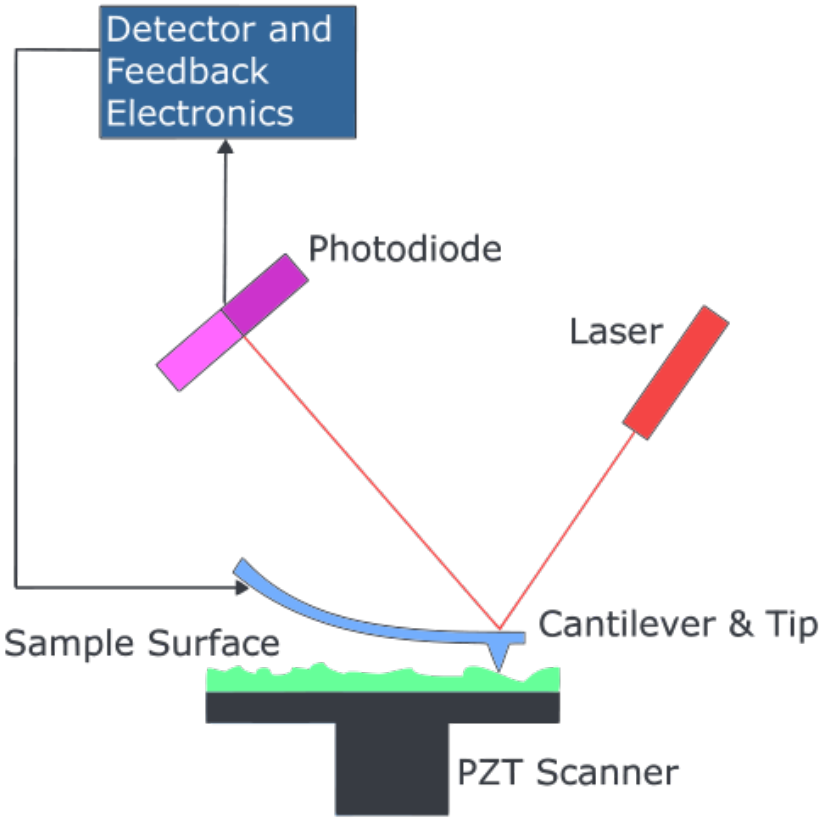

FIGURE C.3 – Atomic force microscopy (source : wikipedia).

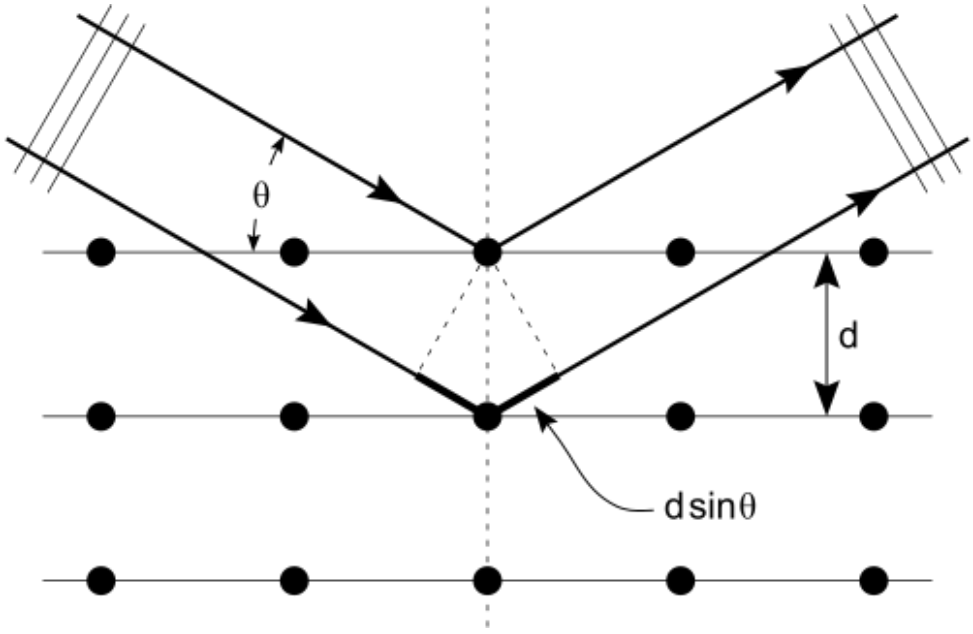

Figure C.4 – X-Ray Diffraction (source : wikipedia).

Furthermore, a chemical difference on a surface can also be detected as it will translate into a lateral deflection of the cantilever (contact mode) or a change in the phase of the oscillations (tapping mode). This is specially interesting to probe inhomogeneities in self-assembled monolayers at a surface.
Eventually, besides imaging of the surface topography and chemical changes, AFM can also be used to conduct force spectroscopy measurements where the tip is brought in contact to the surface and released, which allows plotting the interaction between the surface and the tip vs distance (force-distance curve). These curves usually show a hysteresis translating the adhesion energy between the tip and the sample.

Because of its very high resolution and versatility (operating on different materials and environments) many derivatives of the "standard" AFM which we have described so far exist. These derivatives are linked to the use of AFM tips with added properties (conductive, magnetic... etc) to probe different interactions. For the evaluation of SAMs, specially for biosensing properties, the so-called Chemical Force Microscopy (CFM)[48,49] is an interesting method in which the tip is functionalized with a probe molecule complementary to the one on the surface sample. However, specially for biological interactions, these measurements should be done in the appropriate medium which is often an aqueous buffer and not air.

C.6 XRD

X-Ray Diffraction (XRD) is a method that allows the determination of the crystallinity (crystalline orientation as well as grain size) of a material. This method is based on the elastic scattering of X-rays by the regularly arranged atoms of the sample as shown in Fig. C.4.

For a given crystallinity (distance d between atom planes), scattered waves outcoming from the sample interfere destructively except for given values of θ obeying Bragg's Law :

$$2d \sin\theta = n\lambda$$

where n is an integer and λ is the wavelength of the X-rays.

Thus, in an XRD experiment θ is varied and the intensity of the scattered X-ray beam is measured at each angle. The obtained peaks relate to the different crystalline orientations (computed from the spacings d between atom planes) of the sample.

Moreover, the average grain size δ for a given orientation can be deduced from the corresponding diffraction peak with Scherrer's formula :

$$\delta = \frac{K\lambda}{\beta \cos\theta}$$

where K is shape factor parameter (usually equal to 0.9) and β is the full width at half maximum of the diffraction peak.

C.7 SEM

In scanning electron microscopy, an electron beam is focused on the sample. This beam "scans" the surface generating secondary electrons among others. These can be driven to a detector which is sensitive to the amount of electrons reaching it. Thus, an intensity can be obtained for each "point" on the surface. The Scanning Electron Microscopy (SEM) image represents thus the mapping of this intensity as the input beam scans the sample.
Contrast in an SEM image translates a difference in topography and/or material (elements with higher atomic number give more backscattered electrons, thus a brighter signal).

Appendix D

All the things that did not work (well enough)

This appendix deals briefly with a number of experiments, ideas or side-projects that unfortunately did not bring significant results to be presented in the core of the manuscript. The "failed" experiments are quickly described and different personal hypothesis are evoked hereafter. No data is presented to keep this appendix as light as possible.

D.1 Gold functionalization

Gold functionalization is probably the most important part of this PhD. Though functionalization of plain and micropatterned substrates has been demonstrated by PM-IRRAS, XPS and ToF-SIMS and functionalization of nanopatterned substrates by colloid trapping (indirect characterization), some issues concerning the functionalization could not be clearly elucidated.

D.1.1 Where is the sulfur ?

The XPS spectra of thiolated gold surfaces should reveal the presence of sulfur with a peak at ca. 162 eV (S2p). Furthermore, different contributions could be expected translating the degree of bonding of the thiols on the gold surface.[50] Unfortunately, we were not able to detect the sulfur contribution despite the co-addition of several tens of scans of the S2p region. We can only conclude that under our experimental conditions, the XPS we used is not sensitive enough to detect the (relatively low) amount of sulfur present on the surface.

D.1.2 Mixed-SAMs

The topic of mixed-SAMs would deserve a full review paper with several pages, extensive references and detailed discussions. We will do no such thing here. A brief summary of the literature reports on this topic can be found in paragraph 1.2.1.1.4. To put it simply, in the field of biosensors, many papers claim that mixed-SAMs (including thiols with an "active" headgroup like biotin and thiols with a "diluting" headgroup like alcohol) are better at capturing a target molecule (e.g., streptavidin) than monofuctional SAMs (e.g., only biotinylated thiols). I could never confirm this hypothesis.

The case of biotinylated thiols is, in my opinion, especially striking. In the words of Haussling et al. : *"It was found that the higher the packing density of the biotin labels in the monolayers was, the less effective was their binding ability."*[51] In other words, for a maximum target-binding efficiency one should dilute the biotinylated thiols with a non-reactive thiol as much as possible, which is coherent with the data presented by Kim et al.[52]

When I first conducted colloid trapping based on biotin-streptavidin interactions (see section 3.4.1) I was aware of this literature and thus expected very poor results from a monofunctional biotynilated SAM. To my surprise, the 100% biotin-terminated SAM worked at least as well as a diluted 1/9 biotin/alcohol mixed-SAM.

Furthermore, the "steric hindrance" argument is often evoked in terms like the following : the close-packing of reactive headgroups leads to steric hindrance which reduces the target-binding capabilities of the layer. In my own personal opinion, if this is indeed an entropic effect, it would be valuable to move from this handwaving argument to a more solid proof. Because protein immobilization seems like a very complex matter, experimental measurements on the amount of immobilized proteins may not be the best suited method to address this fundamental issue on SAMs. Maybe statistical mechanics and/or numeric simulations can inform us better on what "steric hindrance" really is or is not in this case.

D.1.3 Gold oxide silanization

We have seen (section 3.1.1) that oxygen plasma on gold surfaces leads to the formation of gold oxide and oxides can in principle be silanized. I have tried building a SAM of PEG-silane on oxidized gold but XPS revealed the absence of the PEG at the end of the process. This was a "one shot" test which I had no time to investigate further. If such a silanization of gold oxide is possible it could be very interesting from a material science point of view, especially if it could contribute to the stabilization of this oxide layer. To investigate this, it would certainly be interesting to better characterize the oxide layer, especially to know the amount of Au-OH surface groups (if any). It would also be interesting to find an environment which stabilizes the oxide during the silanization.

D.2 Colloid trapping

D.2.1 Covalent coupling

I presented colloid trapping based on bio-affinity and electrostatic interactions (section 3.4.1). In all honesty, I did not think that electrostatic binding would resist washing steps and I expected to use the electrostatic-based samples as a sort of "control" or "reference" to evaluate covalent coupling (carboxylatex beads being previously activated into NHS-ester). However, when conducting the NHS-activation on the bead solution the colloidal particles aggregated. This is not surprising since the colloids are stabilized by their negative charge, COO^-. What this means is that NHS-activation of carboxylatex has to be undertaken with extra care (as opposed to activation of a COOH SAM on a flat macroscopic surface). Because electrostatic coupling worked much better than expected and due to the lack of available time, the covalent coupling scheme was not studied further.

If covalent trapping of colloids on a surface through amide bonds is to be further investigated, it might be a good idea to inverse the chemical headgroups : that is, have a COOH-SAM on the flat surface and NH_2-latex. Thus, the NHS activation can be carried on flat surface independently of the colloid dispersion (avoiding aggregation problems).

Eventually, it is not sure that covalent coupling should lead to a stronger binding than electrostatic interactions. Indeed though a covalent amide bond is probably stronger than an a single electrostatic interaction between facing COO^- and NH_3^+ groups, one should also consider the total number of bonds that can be created between the bead and the surface. Knowing the dimensions of the bead and the spacing between adjacent chemical groups, it should be possible to theoretically compute the overall interaction energy. The idea is that electrostatic bonds are present even between chemical groups that are "far" from each other, while chemical coupling can only occur on a few facing headgroups.

D.2.2 Electrostatic trapping as a function of ionic strength

I conducted electrostatic trapping in PBS 10X, PBS 1X and ultrapure water at different times (30min, 1h, 2h, 24h, 72h). The idea behind this was to demonstrate the effect of the ionic strength (i.e., Debye length) on the electrostatic trapping efficiency. I expected different trapping rates as a function of ionic strength, with aggregation occurring on extreme cases. This would enable to start drawing a diagram to find optimum conditions for trapping (as a function of ionic strength and time). However, the results (assessed by SEM) did not show a very clear trend in surface coverage. As this was done only once on a single set of samples (again a "one shot" experiment due to lack of time and samples) it was difficult to make any conclusion on the experiment.

D.2.3 Combination with physical approaches

D.2.3.1 Magnetic

The beads used on the bio-affinity method are magnetic latex. I tried to use the magnetic properties to enhance the trapping (surface coverage) of these beads by attracting them towards the sample surface (from the bulk liquid phase) with a macroscopic neodymium magnet. In this experiment, the sample patterned surface was placed in the center of a liquid millimetric "cell", immersed in the bead solution (few millilitres). The magnet was placed below the cell. The idea was not to rely on diffusion alone to make the beads reach the surface. However, the attraction by the magnet was stronger than expected and the beads ended up moving to the edges of the cell (i.e., far from the sample surface which was placed at the center of the cell) because they were preferentially attracted to the edges of the macroscopic magnet (border effect).

If magnetic trapping is desired it must certainly be done in a smarter and less naive way with patterned micro-magnets for instance.

D.2.3.2 Capillary Force Assembly

In a collaboration with CEA-LITEN we also tried combining the trapping of colloids based on surface chemistry and capillary force assembly (CFA). The idea was to create a dense colloid monolayer by CFA (dip-coating) and then wash the surface so that only the beads that were on a trapping region (with a matching surface chemistry) would stay on the surface while the other beads (remaining only by Van der Waals adsorption forces) would be washed away. This did not work. It is unclear if the surface functionalization was really efficient at that time. Furthermore, it is probably not a good idea to rely on building a dense particle layer first and wash away later. Indeed, it would be better to ensure that particles only "stick" to the trapping regions *during* the CFA (dip-coating).

D.3 Applications beyond trapping

D.3.1 Plasmonics

The title of this PhD explicitly deals with plasmonics (LSPR biosensors). However, we could unfortunately never demonstrate a plasmonic application. The "nano-antennas" presented in section 3.4.2 were tested in vain for an enhanced Raman signal (SERS). It seems that the geometry of these nanostructures (gap size of the dimers especially) does not correspond to the desired geometry for an enhancement of the electric field, due to poor lithography results. Furthermore the Piranex project for which most of this work was developed aims at developing a combined SERS/LSPR imaging biosensor with nanopatterned gold on silica samples (different from the nano-antennas mentioned above). From a photonic point of view, this has been validated by simulation but not yet with a real sample. We can only hope that when real photonic-efficient samples do come, the orthogonal chemistry developed in this PhD can be applied to direct the biomolecules onto the photonic hot-spots and lead to an enhancement of the biosensor sensitivity.

D.3.2 Recursive colloidal lithography

Colloidal or nanosphere lithography (NSL) is based on using a dense monolayer of nanoparticles on a surface as a mask for nanopatterning. Indeed, if a material is deposited on this surface and the beads are then "lifted-off", the material will remain only on the spaces between the beads. My idea was to :

1. Use nanosphere lithography to build nanopatterned gold on silica surfaces (something fairly common in the literature).
2. Functionalize this patterned surfaces in order to allow the selective trapping of a second set of beads only on the gold regions (just as I did with the nanostructures in section 3.4.2).
3. Use the selectively-immobilized beads as a mask for a second patterning (e.g., with silver) and lift-off the beads.

Unfortunately, I had this idea at the very end of my PhD with no more than a week to test it. In a sense I could say I tested this with a protocol that was the opposite of "optimized". As could be expected I failed at the very first step (could not build a monolayer of polystyrene particles on a silica surface by dip coating or spin-coating). Nonetheless I believe that with some optimization this process can be efficiently carried out.

If it were successful, other than being "fun", it could be interesting as a way to create multi-material nanopatterning. The "strength" of this process would be that it relies only on self-assembly whereas if you were to do such a multi-material nanopatterning based on other techniques like imprint lithography, you would need to have a nanometric lateral resolution to match the first and second steps (levels) which I doubt is feasible.

References

[1] G. E. Moore. *Proceedings of the IEEE*, 86,82–85 **(1998)**.

[2] A. Belarouci, T. Benyattou, X. Letartre, and P. Viktorovitch. *Optics express*, 18,381–94 **(2010)**.

[3] J.-P. Cloarec, Y. Chevolot, E. Laurenceau, M. Phaner-Goutorbe, and E. Souteyrand. *ITBM-RBM*, 29,105–127 **(2008)**.

[4] Y. Chevolot, C. Bouillon, A. Meyer, J.-P. Cloarec, A. Jochum, J.-p. Praly, J.-J. Vasseur, and E. Souteyrand. *Angew. Chem. Int. Ed.*, 46,2398–2402 **(2007)**.

[5] A. Duval, A. Laisné, D. Pompon, S. Held, A. Bellemain, J. J. Moreau, M. M. Canva, J. Moreau, and M. Canva. *Optics letters*, 34,3634–3636 **(2009)**.

[6] G. O'Sullivan, D. Kilbane, and R. D'Arcy. *Journal of Modern Optics*, 59,855–872 **(2012)**.

[7] J. Adams, G. Tizazu, S. Janusz, S. R. J. Brueck, G. P. Lopez, and G. J. Leggett. *Langmuir*, 26,13600–13606 **(2010)**.

[8] H. Liu, B. Wang, L. Ke, J. Deng, C. C. Chum, S. L. Teo, L. Shen, S. a. Maier, and J. Teng. *Nano letters*, 12,1549–54 **(2012)**.

[9] J. Dong, J. Liu, X. Zhao, P. Liu, J. Xie, and Y. Wang. *EPL (Europhysics Letters)*, 102,24002 **(2013)**.

[10] L. Y. M. Tobing, L. Tjahjana, and D. H. Zhang. *Nanotechnology*, 24,075303 **(2013)**.

[11] V. R. Manfrinato, L. Zhang, D. Su, H. Duan, R. G. Hobbs, E. a. Stach, and K. K. Berggren. *Nano letters*, 13,1555–8 **(2013)**.

[12] C. Vieu, F. Carcenac, A. Pepin, Y. Chen, M. Mejias, A. Lebib, L. Couraud, and H. Launois. *Applied Surface Science*, 164,111–117 **(2000)**.

[13] V. R. Manfrinato, L. L. Cheong, H. Duan, D. Winston, H. I. Smith, and K. K. Berggren. *Microelectronic Engineering*, 88,3070–3074 **(2011)**.

[14] A. Pimpin and W. Srituravanich. *Engineering Journal*, 16,37–56 **(2012)**.

[15] J. Gong, D. J. Lipomi, J. Deng, Z. Nie, X. Chen, N. X. Randall, R. Nair, and G. M. Whitesides. *Nano Letters*, 10,2702–2708 **(2010)**.

[16] J. Zhang, Y. Li, X. Zhang, and B. Yang. *Advanced materials*, 22,4249–69 **(2010)**.

[17] F. Huo, G. Zheng, X. Liao, and L. R. Giam. *Nature nanotechnology*, 5 **(2010)**.

[18] D. S. Macintyre, O. Ignatova, S. Thoms, and I. G. Thayne. *Journal of Vacuum Science & Technology B : Microelectronics and Nanometer Structures*, 27,2597 **(2009)**.

[19] J. Yang, K. Im, and S. Lim. *Applied Surface Science*, 257,5476–5479 **(2011)**.

[20] J. Petit and J. Moore. Eliminating Solvents in Resist Removal Processes Using Low-Cost Detergents. In *ASMC (Advanced Semiconductor Manufacturing Conference) Proceedings*, pages 301–306 **(2010)**.

[21] D. Grojo. *Mécanismes d'enlèvement de particules par laser impulsionnel : application au nettoyage pour la microélectronique*. PhD thesis, Université de la Méditérranée, Aix-Marseille II **(2006)**.

[22] T. Kamal and D. W. Hess. *Journal of Vacuum Science & Technology B : Microelectronics and Nanometer Structures*, 19,461 **(2001)**.

[23] S. Myneni and D. W. Hess. *Journal of The Electrochemical Society*, 152,G757 **(2005)**.

[24] H. Horibe, M. Fujita, I. Nishiyama, and A. Yoshikado. *Japanese Journal of Applied Physics*, 44,8673–8675 **(2005)**.

[25] S. Zhang, X.-W. Zhao, H. Xu, R. Zhu, and Z.-Z. Gu. *Journal of Colloid and Interface Science*, 316,168 **(2007)**.

[26] X. Zhang and K. P. Johnston. *Chinese Science Bulletin*, 52,27–33 **(2007)**.

[27] S. Kim, H. Yuvaraj, Y. Jeong, C. Park, and K. Lim. *Microelectronic Engineering*, 86,171–175 **(2009)**.

[28] H. Tsai. *Surface Science*, 537,L447–L450 **(2003)**.

[29] H. Ron, S. Matlis, and I. Rubinstein. *Langmuir*, 14,1116–1121 **(1998)**.

[30] K. M. Cook and G. S. Ferguson. *Chemical communications (Cambridge, England)*, 47,12550–2 **(2011)**.

[31] F. Palazon, V. Monnier, Y. Chevolot, J.-P. Cloarec, and E. Souteyrand. *Journal of Colloid Science and Biotechnology*, 2,1–14 **(2013)**.

[32] B. V. Derjaguin and L. Landau. *Acta Physicochim. URSS*, 14,633–662 **(1941)**.

[33] E. J. W. Verwey and J. T. G. Overbeek. *Theory of the Stability of Lyophobic Colloids* **(1948)**.

[34] B. Derjaguin. *Kolloid-Zeitschrift*, 69,155–164 **(1934)**.

[35] C. E. Espinosa, Q. Guo, V. Singh, and S. H. Behrens. *Langmuir*, 26,16941–16948 **(2010)**.

[36] S. Bhattacharjee, M. Elimelech, and M. Borkovec. *Croatica Chemica Acta*, 71,5–8 **(1998)**.

[37] C. J. van Oss. *Journal of molecular recognition : JMR*, 16,177–190 **(2003)**.

[38] J. A. Brant and A. E. Childress. *Journal of membrane science*, 203,257–273 **(2002)**.

[39] J. Sabín, G. Prieto, J. M. Ruso, R. Hidalgo-Alvarez, and F. Sarmiento. *The European physical journal. E, Soft matter*, 20,401–8 **(2006)**.

[40] A. D. Maude. *British Journal of Applied Physics*, 293,4–7 **(1961)**.

[41] C. Cottin-Bizonne, A. Steinberger, B. Cross, O. Raccurt, and E. Charlaix. *Langmuir*, 24,1165–1172 **(2008)**.

[42] A. Despeyroux and A. Ambari. *Journal of Non-Newtonian Fluid Mechanics*, 167-168,38–45 **(2012)**.

[43] E. Stern, R. Wagner, and F. J. Sigworth. *Nano Letters*, 7,3405–3409 **(2007)**.

[44] E. Thormann, A. C. Simonsen, P. L. Hansen, and O. G. Mouritsen. *Langmuir*, 24,7278–7284 **(2008)**.

[45] T. Buffeteau, B. Desbat, J. M. Turlet, and C. D. P. Moleculaire. *Applied Spectroscopy*, 45,380–389 **(1991)**.

[46] B. L. Frey, R. M. Corn, and S. C. Weibel. *Handbook of Vibrational Spectroscopy*, 2,1042–1056 **(2001)**.

[47] C. Methivier, B. Beccard, and C. M. Pradier. *Langmuir*, 19,8807–8812 **(2003)**.

[48] D. Vezenov, A. Noy, and P. Ashby. *Journal of adhesion science and technology*, 19,37–41 **(2005)**.

[49] A. Noy. *Surface and interface analysis*, 38,1429–1441 **(2006)**.

[50] V. Lebec, J. Landoulsi, S. Boujday, C. Poleunis, C.-M. Pradier, and a. Delcorte. *The Journal of Physical Chemistry C*, 117,11569–11577 **(2013)**.

[51] L. Haussling, H. Ringsdorf, F.-J. Schmitt, and W. Knoll. *Langmuir*, 7,1837–1840 **(1991)**.

[52] D.-J. Kim and K.-K. Koo. *J. Ind. Eng. Chem.*, 10,920–926 **(2004)**.

Francisco Palazon

98, Rue Chevreul
69007 Lyon, France
+33 (0)781394778
francisco.palazon@ec-lyon.fr

Education

2011–2014 **PhD student**, *Université de Lyon, École Centrale de Lyon (ECL), Institut des Nanotechnologies de Lyon (INL)*, Lyon.

2010–2011 **Master of Science: Nanoscale Engineering**, *ECL, INSA, UCBL*, Lyon, International Master in English.

2008–2011 **Graduate degree in engineering, major in Micro-Nano-Biotechnology**, *École Centrale de Lyon*, Lyon.

Research experience

2011–2014 **PhD Thesis: Surface functionalization of heterogeneous gold/silica substrates for the directed targetting of biomolecules and colloïds onto LSPR biosensors**, *Université de Lyon, École Centrale de Lyon, Institut des Nanotechnologies de Lyon*.

2011 **Master Thesis**, *UMI-LN2, Université de Sherbrooke*, Sherbrooke, Québec, Canada.
SPR and Metal-Clad Waveguides for Biosensing

2010 **Research Internship**, *Tohoku University*, Sendai, Japan.
Development of nanocomposite tungsten-DLC coating for biomedical applications

Languages

Native (bilingual) in **French** and **Spanish**, *fluent* in **English**, *intermediate* in **German** and *beginner* in **Japanese**. Several long stays (3 months to 3 years) in Australia, Germany, Japan and Canada.

PhD-related activities

Teaching Chemistry tutorials and lab work for undergraduate and graduate students **(192h)** and internship supervisor **(2 months)**.

Administration Member of the board of Ecole Centrale de Lyon's PhD association in charge of cultural and scientific activities, including visits of scientific sites (eg: CERN, Geneva, Switzerland) and industrial sites (eg: Nuclear plant at St Alban, France). Member of the organizing committee of INL PhD Days 2012.

Other skills

Martial arts Black belt in aikido with over 10 years experience.

Photography Several international publications at prestigious online curated gallery 1x.com and international book "Passion" (ISBN: 978-91-979184-3-5).

Publications

F. Palazon, C. Montenegro Benavides, É. Souteyrand, Y. Chevolot, and J.-P. Cloarec. Carbodiimide/NHS derivatization of COOH-terminated SAMs: activation or byproduct formation? *Langmuir*, 30:4545–4550, 2014.

F. Palazon, P. Rojo Romeo, A. Belarouci, C. Chevalier, H. Chamas, É. Souteyrand, A. Souifi, Y. Chevolot, and J.-P. Cloarec. Site-selective self-assembly of nano-objects on a planar substrate based on surface chemical functionalization. In Christian Joachim, editor, *Advances in Atom and Single Molecule Machines*. Springer, (accepted), 2014.

F. Palazon, V. Monnier, É. Souteyrand, Y. Chevolot, and J.-P. Cloarec. NANOTRAPS: different approaches for the precise placement of micro and nano-objects from a colloidal dispersion into nanometric scale sites of a patterned macroscopic surface. *Journal of Colloid Science and Biotechnology*, 2:249–262, 2013.

F. Palazon, A. Garnier, T. Géhin, D. Ferrah, C. Botella, G. Grenet, É. Souteyrand, J.-P. Cloarec, and Y. Chevolot. Poly(ethylene glycol) degradation by X-rays during XPS measurements of PEGylated gold and silica surfaces, and loss of anti-fouling properties. *Langmuir*, (submitted).

F. Palazon, P. Rojo Romeo, C. Chevalier, T. Géhin, É. Souteyrand, Y. Chevolot, and J.-P. Cloarec. Nanoparticles selectively immobilized onto large arrays of gold micro and nanostructures through surface chemical functionalizations: a route towards plasmonic nanoantennas coupling to fluorescent nanobeads. *J. of Coll. and Interf. Sci.*, (submitted).

Oral presentations at international conferences

F. Palazon, P. Rojo Romeo, V. Monnier, F. Zuttion, M. Phaner-Goutorbe, É. Souteyrand, Y. Chevolot, and J.-P. Cloarec. Colloids' selective deposition on a micropatterned gold/silica substrate based on surface chemical functionalization via self-assembled monolayers. *4th International Colloids Conference, Madrid, Spain, 2014*.

F. Palazon, H. Chamas, P. Rojo-Romeo, D. Ferrah, Y. Chevolot, C. Chevalier, G. Grenet, A. Belarouci, V. Monnier, T. Baron, E. Souteyrand, A. Souifi, and J.-P. Cloarec. Sorting, placing and anchoring nano-objects on a large scale with nanometric precision. *LETI Innovation Days: 1st International Workshop on Nanopackaging, Grenoble, France, 2013 (Invited talk)*.

J.P. Cloarec, **F. Palazon**, H. Chamas, D. Ferrah, P. Rojo-Romeo, Y. Chevolot, C.Chevalier, V. Monnier, G. Grenet, T. Baron, E. Souteyrand, and A. Souifi. Collective addressing of nano-objects on supports with surface functionalization and physico-chemistry of interfaces. *CMOS-Emerging Technology Symposium. Whistler, Canada, 2013 (Invited talk)*.

Poster presentations at international conferences

F. Palazon, P. Rojo Romeo, A. Belaroucci, V. Monnier, C. Chevalier, Y. Chevolot, and J.-P. Cloarec. Combining top-down and bottom-up: Surface functionalization of nanopatterned substrates. *5eme Colloque LN2 / UMI-3463, 2012*.

A. Garnier, F. Zuttion, **F. Palazon**, Y. Chevolot, E. Laurenceau, G. Grenet, C. Botella, E. Souteyrand, and M. Phaner-Goutorbe. Surface characterization of pegylated self-assembled monolayers on gold for biosensors applications. *Fuerzas y tunel, San Sebastian, Spain, 2014*.

F. Palazon, T. Takeno, H. Miki, and T. Takagi. Evaluation of adhesive strength of tungsten-containing diamond-like carbon films on NiTi shape memory alloy using film-cracking technique. *7th International Conference on Flow Dynamics, Sendai, Japan, 2010*.

dernière page de la thèse

AUTORISATION DE SOUTENANCE

Vu les dispositions de l'arrêté du 7 août 2006,

Vu la demande des Directeurs de Thèse

Monsieur J-P. CLOAREC et Monsieur Y. CHEVOLOT

et les rapports de

Monsieur L. VELLUTINI
Maître de Conférences HDR - Université de Bordeaux - Institut des Sciences Moléculaires (UMR 5255)
Bâtiment A12 - Groupe Chimie Moléculaire et Matériaux - C2M - 351 Cours de la Libération - CS 10004
33405 TALENCE cedex

Et de

Monsieur G. CECCONE
Docteur - European Commission - DG JRC - Unit Nanobiosciences - Via E. Fermi 2749 TP203 - I21027
Ispra (VA) - ITALIE

Monsieur PALAZON Francisco

est autorisé à soutenir une thèse pour l'obtention du grade de **DOCTEUR**

Ecole doctorale MATERIAUX

Fait à Ecully, le 2 septembre 2014

P/Le directeur de l'E.C.L.
La directrice des Etudes

ECOLE CENTRALE Service Scolarité ECULLY

M-A. GALLAND

Summary - Résumé

Orthogonal surface chemical functionalization is an efficient method for the selective trapping of different targets (biomolecules or nano-objects) onto predefined regions of a patterned substrate. This is specially interesting in the field of localized surface plasmon resonance (LSPR) biosensors, where transduction only occurs on metallic nanostructures. The aim is thus to ensure that the target molecules can be selectively anchored onto these nanostructres and not adsorbed on the surrounding dielectric surface. Thus, we have developped during this PhD different orthogonal functionalizations of micro and nanopatterned gold on silica surfaces with thiols and silanes. In regards to the state of the art in this topic, we have proposed a single-step protocol and demonstrated the good orthogonality of such functionalizations by extensive surface chemical characterization including PM-IRRAS, XPS and ToF-SIMS analysis. Furthermore, these functionalizations have been used for the selective anchoring of different latex nanoparticles onto micro and nanopatterns of gold surrounded by silica, as shown by SEM. At the moment, this methodology is being applied in two different photonic devices where we expect on the one hand a coupling between fluorescent nanobeads and plasmonic nano-antennas and, on the other hand, the increase in sensitivity of an LSPR biosensor for detecting different biomolecules.

La fonctionnalisation chimique de surfaces hétérogènes (fonctionnalisation orthogonale) est une méthode efficace pour diriger l'ancrage de diverses cibles (biomolécues ou nano-objets) sur des zones précises prédéfinies sur un substrat. Ceci est particulièrement intéressant dans le domaine des biocapteurs à plasmons localisés (LSPR) où la transduction ne peut se faire que sur des nanostructures métalliques. L'enjeu est alors d'assurer que les molécules à détecter se fixent spécifiquement sur ces nanostructures et ne s'adsorbent pas sur la surface diélectrique environnante. Dans ce but, nous avons développé dans cette thèse des fonctionnalisations orthogonales de surfaces micro et nanostructurées d'or sur silice à l'aide de divers thiols et silanes. Par rapport à l'état de l'art dans ce domaine, nous avons notamment proposé un protocole en une seule étape et démontré la bonne orthogonalité de ces fonctionnalisations par différentes méthodes de caractérisation chimique de surface (notamment PM-IRRAS, XPS et ToF-SIMS). De plus, ces fonctionnalisations sélectives ont permis l'ancrage spécifique de diverses nanoparticules de latex sur des micro et nanostructures d'or entourées de silice, démontré par MEB. Actuellement, cette méthodologie est en cours d'application dans deux composants photoniques différents où l'on attend d'une part des effets d'exaltation de fluorescence par couplage de nano-antennes et nanobilles marquées et d'autre part un gain en sensibilité d'un biocapteur LSPR pour la détection de différentes biomolécules.